



**Novel Intranasal GNRs-DNA Vaccines against Human  
Papillomavirus Infection**

**Wenqin Li**

**A thesis submitted in fulfilment of the requirements for the award of  
the degree of Doctor of Philosophy**

**Strathclyde Institute of Pharmacy and Biomedical Sciences**

**The University of Strathclyde**

**2015**

## **Declaration of Authenticity and Rights**

I hereby declare that this thesis is the result of my original research. It has been composed by myself and has not been previously submitted for examination which has led to the award of a degree.

The copyright of this thesis belongs to the author under the terms of the United Kingdom Copyright Acts as qualified by University of Strathclyde Regulation 3.50.

Due acknowledgement must always be made of the use of any material contained in, or derived from, this thesis.

Signed:

Date:

## **Acknowledgements**

First of all, I'd like to thank my family. I am able to complete the four years of my PhD studies and my thesis writing because of their constant help and encouragement. In the last year, I've experienced many partings and losses, including the passing of my grandmother, which was a sorrowful time for me. Even though I was in China for three months for animal experiments, I did not get the opportunity to say goodbye to her. Consolation and understanding from my family became my greatest motivation to finish my studies.

I am thankful that within the past four years, I've experienced countless blessings and was able to grow and mature through many obstacles. Many thanks to my supervisors Dr. Jun Yu and Dr. Yu Chen, who accompanied me throughout the difficulties that I had to face during my PhD. They were my guide in academic research, guiding my path towards every breakthrough and helping me in finding my own direction. Special thanks to my first supervisor, who had always been a patient support whenever I was lost and discouraged during all these years. I thank him for being tolerant of my work style, as I am generally more spontaneous than I am logical. Being his student and assistant, I was able to gain a variety of knowledge and technical skills, which in turn further encourage and help me. I also thank him for his endless patience and trust.

I would also like to specially thank one of my colleagues – Rasha, who was another student of my supervisor. In the two years during which we worked together, we had the chance to collaborate and help each other out. Whether it was during times of frustration or joy, we were by each other's side. She was the one who taught me to believe in my own efforts and that they will reap great rewards in the end. Because of her encouragements, even though there were failures and errors in my experiments I was always able to persevere till the end, toward the finish line.

Finally, I would like to thank every person who have reached out and helped me during my PhD. Many thanks to my colleague Muattaz Hussain from Dr Katharine Carter's group for the bone marrow derived macrophages used in my project. I thank my group in Xi'an Jiaotong University, with whom we held collaborations. Thanks to Professor Wang, who provided help and support in our HPV animal experimentation. Thanks to Depu Wang for helping me complete the three months of animal studies, and it was also him with whom I conducted in vivo experimentation, preparation of PsV, and SEAP experimentation. I would also like to thank Dr. Dan Xu who, when I was facing great challenges in the animal experimentation in Xi'an, provided me with technical and emotional support.

I thank in the end my institute, the University of Strathclyde, and my faculty. There are too many people to whom I cannot express my thankfulness individually here. Thanks to my good friends Annie and Tikon for their continuous support. May my Lord, whom I love, be eternally with you.

The significant problems we face can never be solved at the level of thinking that created them. – Albert Einstein

I thank my Lord Jesus Christ for teaching me that “[there is] a time to plant, and a time to uproot what was planted”. (Ecclesiastes 3:2)

## Abstract

Currently licensed HPV vaccines, Cervarix and Gardasil, have been successful in preventing HPV infection and high-graded cervical intraepithelial neoplasia (CIN2, 3) in school girls in the UK and other developed countries. However, their high costs have hindered their wider use in preventing HPV infection and CIN 2/3 associated with HPV type -16 and -18. This project aims to produce cheap and effective GNRs-DNA vaccines. The vaccines were composed of two parts, gold nanorods and circular plasmid DNA that carries codon-optimized HPV type 16 L1 gene for expression of the viral capsid-like particles in host cells. GNRs were functionalized with either PEI or PDDAC cationic polymers for high affinity to negatively charged DNAs. The DNA is constructed in the backbone of a mammalian expression vector, plasmid pcDNA3 YFP of which YFP offered a fluorescent indicator. The HPV type -16 L1 was either expressed alone or together with *E. coli* heat labile toxin B subunit, a well-known nasal adjuvant that enhances immunogenicity. In total, four GNRs-DNA were produced: PEI-GNRs-pcDNA3 YFP L1 (PE-G-L), PEI-GNRs-pcDNA3 YFP L1-ELT (PE-G-EL), PDDAC-GNRs-pcDNA3 YFP L1 (PD-G-L), and PDDAC-GNRs-pcDNA3 YFP L1-ELT (PD-G-EL).

The GNRs-DNA internalization led to expression of VLP in HEK293, HeLa and the murine bone marrow-derived macrophages cell. Intranasal immunization of BALB/c mice with GNRs-DNA resulted in YFP expression in nasal and lung tissues in one day. Three doses ( $3 \times 480\text{ng}$  plasmid DNA per mouse) elicited neutralizing antibodies in the serum and antibody secreting cells in spleen lymphocytes specific to HPV16 L1 protein. PDG-YL appeared to be most potent and comparable to

purified VLP protein in eliciting Nabs and ASCs.

My work has demonstrated the feasibility of using GNRs-DNA as vaccine platforms. GNRs-DNA is cheap to produce, easy to administer and stable at room temperature. These characteristics make GNRs-DNA attractive candidates for future HPV vaccine development. The optimised concentration ratio of GNRs and DNA, T-cell immune-response, IgA secretion require further assessment before the clinical trial.

## List of Figures

Figure 1 – Epidemiological study of Global cervical cancer events.....	3
Figure 2 - The genomic organization of HPV type 16.....	7
Figure 3 - Scheme of carcinogenic progress mediated by high-risk HPV.....	20
Figure 4 - Significance of HR-HPV integration events detected in cervical carcinomas.....	22
Figure 5 - Size index of a rat macrophage comparing micron- to nano-scale..	42
Figure 6 - An absorption spectrum of GNRs exhibits two distinct surface plasmon modes according to the transverse and longitudinal lengths.....	48
Figure 7 - A scheme illustration of the synthesis process of PEI-GNRs (PE-G), and PDDAC-GNRs (PD-G).....	61
Figure 8 - Schematic presentation of construction of pcDNA3 YFP-L1 and pcDNA3 YFP-L1-ELTB and linear structure for digestion..	71
Figure 9 - Schematic presentation of GNRs-DNA assembly.....	72
Figure 10 - Spectrum change of GNRs after coating of each layer..	75
Figure 11 - Spectrum evaluation of the stability of GNRs at room temperature..	77
Figure 12 - Colour indicated the stability of the surface-modified GNRs.....	80
Figure 13 - Gel evidence of L1 and ELT insertion in recombinant DNA by PCR and Digestion. ....	82
Figure 14 - Absorption spectrum plots of fresh prepared GNRs-DNA complexes..	85
Figure 15 - Agarose gel analysis of DNAs conjugation to GNRs... ..	87
Figure 16 - DNA affinity test in accordance with DNA immobilization upon fabricated GNRs.....	89
Figure 17 - MTT assay for cytotoxicity of GNRs with different surface coatings... ..	122
Figure 18 - Flow cytometry analysis of cytotoxicity by GNRs or GNR with PEI/PDDAC surface coatings.. ..	124
Figure 19 - Confocal images of macrophage-like MΦ cells harbouring internalized GNRs or GNRs-DNA.. ..	<b>Error! Bookmark not defined.</b>
Figure 20 - The expression of recombinant YFP plasmid DNAs.. ..	129



Figure 21 - Confocal microscopy for expression of HPV L1 capsid protein from GNRs-DNA in HeLa cells.. .....	132
Figure 22 - Confocal microscopy for expression of HPV L1 capsid protein from GNRs-DNA in BMD MΦ. ....	133
Figure 23 - Western blot for detection of L1 protein extracted from 10% GNRs-DNA treated HeLa (A) and HEK293 cells (B) for 3 days and 2 days respectively.. .....	135
Figure 24 – Time-related L1 expression in HEK293 cells by flow cytometry. ....	138
Figure 25 - Schematic illustration of Bac-to-Bac® expression system for generating recombinant baculoviruses.....	148
Figure 26 - Expression of mucosal IgA immune responses after different routes of vaccination. ....	153
Figure 27 - Flow chart of vaccination and evaluation of immune responses.....	155
Figure 28 - Micrograph of Sf9 cells. Cells were infected with recombinant baculovirus AcHPV16 L1 and grown to monolayer after 2-day post-infection.. ....	169
Figure 29 - Quantitative measurement of VLP concentration by Bradford protein assay.....	170
Figure 30 - Detection of purified His-tagged L1 protein from transfected Sf9 cells.. .....	171
Figure 31 - Fluorescent histological images of tissues from nasal mucosa and lung.. .....	172
Figure 32 - Detection of IgG antibody secreting cells after intranasal immunization with GNRs-DNA.....	174
Figure 33 - Detection of HPV16L1 neutralizing antibody by SEAP assay.. .....	177

## List of Tables

Table 1 - Overview of HPV proteins and their functions. ....	7
Table 2 - Bacterial strains and plasmids .....	65
Table 3 - Oligonucleotides used in this project.....	66
Table 4- Reagents and recipes used in cell experiments.....	111
Table 5 - Reagents used in this animal work .....	156

## Abbreviation

anti-EGFP, anti-epidermal growth factor receptor

AP-1, protein 1

ADC, adenocarcinoma

ASCs, antibody secreting cells

BSC, biological safety cabinet

BMD M $\phi$ , bone marrow derived macrophage

CDK, cyclin-dependent kinase

CIN, intraepithelial neoplasia

CTAB, cetyltrimethylammonium bromide

CtxB, cholera enterotoxin B subunit

CpG DNA, bacterial/viral DNA and synthetic ODN containing unmethylated CpG-dinucleotide

DAPI, 4',6-Diamidino-2-Phenylindole, Di-hydrochloride

DCs, dendritic cells

dH<sub>2</sub>O, distilled water

DMEM, Dulbecco's modified eagle medium

dsRNA, double-stranded RNA

*e.coli*, *Escherichia coli*

*EltB/ELT*, E.coli heat labile toxin B subunit

FDA, US Food and Drug Administration

gDMEM, Growth medium

GNPs, gold nanoparticles

GNRs, gold nanorods

GNSs, gold nanospheres

HPV, Human Papillomavirus

IFN, interferon

IgG, Immunoglobulin G

IgA, Immunoglobulin A

IL, interleukin

i.m., intra-muscular

ISGs, IFN-stimulated genes

LCs, Langerhans cells

LPs, lipopolysaccharide

N/P, nitrogen to phosphate ratio

NPs, nanoparticles

Mabs, monoclonal antibodies

M-CSF, macrophage colony stimulating factor

MDCs, myeloid DCs

MHC, major histocompatibility complex

MyD88, myeloid differentiation primary response gene 88

Nabs, neutralizing antibodies

NKs, natural killer cells

NIR, near-infrared region

O-MALT, organized mucosa-associated lymphoid tissue

OD, optical density

ODN, oligodeoxynucleotides

RT, room temperature

PEI, polyethylenimine

PDDAC, poly (diallyldimethyl ammoniumchloride)

PDG, PDDAC-GNRs

PD-G-Y/PDY, PDDAC-GNRs-pcDNA3 YFP

PD-G-L/PDL, PDDAC-GNRs-pcDNA3 YFP L1 or PDDAC-GNRs-pcDNA3 CFP L1

PD-G-EL/PDL, PDDAC-GNRs-pcDNA3 YFP L1-ElkB or PDDAC-GNRs-pcDNA3 CFP L1-ElkB

PeG, polyethylene glycol

PE-G, PEI-GNRs

PE-G-Y/PEY, PEI-GNRs-pcDNA3 YFP

PE-G-L/PEL, PEI-GNRs-pcDNA3 YFP L1 or PEI-GNRs-pcDNA3 CFP L1

PE-G-EL/PEEL, PEI-GNRs-pcDNA3 YFP L1-ElkB or PEI-GNRs-pcDNA3 CFP L1-ElkB

PFA, paraformaldehyde  
PI, propidium iodide  
Poly(A), polyadenylation  
PRRs, pattern recognition receptors  
PS, phosphatidylserine  
RSV, respiratory syncytial virus  
SEAP, secreted embryonic alkaline phosphatase  
siRNA, delivering small interference RNA  
SNAs, spherical nucleic acids  
ssRNA, single-stranded RNA  
Tc cell, cytotoxic T-lymphocytes  
TGF- $\beta$ , transforming growth factor beta  
Th1, T helper-type 1 cells  
TLR, Toll-like receptors  
TZ, transformation zone  
TNF, tumor necrosis factor  
URR, upstream regulatory region  
VLP, virus capsid-like particle  
YEL, pcDNA3 YFP-HPV16 L1  
YL, pcDNA3 YFP-HPV16 L1-ELT

# Contents

Declaration of Authenticity and Rights .....	ii
Acknowledgements.....	iii
Abstract.....	vi
List of Figures .....	viii
List of Tables .....	x
Abbreviation .....	xi
Contents.....	xiv
1. General Information.....	1
1.1. The importance of HPV infection to public health worldwide.....	1
1.2. HPV Infection-Induced Cervical Cancer .....	2
1.2.1. Worldwide prevalence of HPV-induced cancer .....	2
1.2.2. The Epidemiology of Cervical Cancer Raised by HPV Infection .....	4
1.2.3. Overview of HPV genome and the gene functions .....	6
1.3. Immune responses to HPV infections.....	8
1.3.1. General Information .....	8
1.3.2. HPV Pathogenesis v.s. Epithelial Immune System .....	12
1.3.3. Cervical carcinogenic progression .....	20
1.4. Preventive and therapeutic HPV vaccines .....	25
1.4.1. Current prophylactic HPV vaccines.....	26
1.4.2. Perspectives for therapeutic vaccine targets.....	33
1.5. DNA vaccination .....	35
1.5.1. What is a DNA vaccine?.....	35
1.5.2. Application of gold particles in DNA vaccination .....	37
1.6. Aims of the project.....	40
2. Synthesis of DNA-Gold Nanorods.....	41
2.1. Abstract.....	41
2.2. Introduction .....	42
2.2.1. Nanoparticles (NPs).....	42
2.2.2. Physical properties of gold nanorods (GNR) .....	44
2.2.3. Bio-application of GNPs.....	51
2.2.4. NPs as drug adjuvant .....	54
2.3. Aim .....	58

2.4.	Material and Methodology .....	59
2.4.1.	Synthesis of Gold Nanorods .....	59
2.4.2.	Purification of plasmid DNA from <i>E. coli</i> .....	62
2.4.3.	Agarose gel electrophoresis .....	63
2.4.4.	Polymer Coated GNRs Conjugate with Plasmid DNA.....	71
2.4.5.	Characteristics of coated GNRs .....	72
2.4.6.	Statistical Analysis .....	74
2.5.	Result .....	75
2.5.1.	Successful production of surface-modified GNRs demonstrated by spectrum analysis .....	75
2.5.2.	Spectrum analysis for GNRs stability after half-year room-temperature shelf-storage .....	76
2.5.3.	Colour and morphology assessment related GNRs Stability.....	78
2.5.4.	PCR gels for DNA recombination cloning.....	81
2.5.5.	DNA Affinity to GNRs with different surface coatings .....	84
2.6.	Discussion.....	91
2.7.	Conclusion.....	95
3.	<i>In vitro</i> studies of HPV GNRs-DNA complexes.....	96
3.1.	Abstract .....	96
3.2.	Introduction .....	98
3.2.1.	From cell uptake to GNP distribution .....	98
3.2.2.	Biocompatibility of NPs based delivery system .....	107
3.3.	Materials and Methods for In Vitro Experiments .....	111
3.3.1.	Cell culture .....	112
3.3.2.	Cellular uptake & Cell viability assay .....	113
3.3.3.	Gene expression analysis of GNRs-DNA complexes.....	116
3.3.4.	Statistical analysis.....	120
3.4.	Results.....	121
3.4.1.	Cell Viability Assay .....	121
3.4.2.	Confocal microscopy for HPV L1 intracellular.....	129
3.4.3.	Time related GNRs-DNA intracellular expression observed within different incubation time .....	133
3.5.	Conclusion.....	140
4.	Nasal immunization of BALB/c mice with GNRs-DNA.....	142
4.1.	Abstract .....	142

4.2.	Introduction .....	144
4.2.1.	VLP Properties .....	144
4.2.2.	VLP based immunogenicity analysis .....	147
4.2.3.	VLP-based techniques in this <i>in vivo</i> work.....	148
4.2.4.	Mucosal immunization and HPV vaccination.....	151
4.3.	Aim .....	155
4.4.	Material and Methods.....	156
4.4.1.	Animal preparation .....	158
4.4.2.	Production of HPV16 L1 Viral-like Particles (VLPs) .....	161
4.4.3.	Detection of antibody specific to HPV16 VLPs.....	165
4.4.4.	Statistical Analysis .....	168
4.5.	Result .....	169
4.5.1.	Successful expression of VLPs in Sf-9 infected with recombinant baculovirus for His-tagged VLP preparation. ....	169
4.5.2.	Measuring protein concentration by Bradford Assay .....	170
4.5.3.	Histological imaging to detect YFP protein expression.....	172
4.5.4.	Immunological Assays after intranasal immunization of PEI/PDDAC-GNRs-HPV16 L1 vaccine .....	173
4.6.	Discussion.....	179
4.7.	Conclusion.....	184
5.	Conclusion and Future perspectives.....	185
	Bibliography.....	191



# **1. General Information**

## **1.1. The importance of HPV infection to public health worldwide**

Human papillomaviruses (HPVs) are non-enveloped icosahedron viruses <sup>1</sup>. Belonging to the *Papovaviridae* family, the viral genome is double-stranded circular DNA. HPV infections are transmitted through skin contact and mainly during sexual intercourse. There are over 120 genotypes of HPVs that have been isolated, classified according to the sequence variation in the major capsid gene L1 <sup>2,3</sup>. HPVs induce cervical cancer, which is the second most common cancer in women with an 80% incidence rate in developing countries, published by data-based study GLOBOCAN 2000 <sup>4</sup>. A subset of high-risk human papillomavirus (HR-HPV) plays a major causative role in not only cervical cancer, but also other anogenital, like vulvar, vaginal, anal and penile cancers. Up to 99.7% of cervical squamous cell carcinomas (SCCs) and 94-100% of cervical adeno- and adenosquamous carcinomas was reported to be associated with HR-HPV infection <sup>5,6</sup>. Besides, HR-HPV has been detected in a group of head and neck cancers <sup>7</sup>.

It is well-documented that HPVs only keep as low as approximately 10 to 100 virus copies per infected cell in the initial infection site <sup>8</sup>. Among the 120 genotypes, the majority only cause asymptomatic subclinical infection, whereas some patients could have productive infections in keratinocytes of skin or/and mucous membranes. In the latter cases, the infections usually exhibit self-limiting lesions, which are cleared within 1-2 years in most cases, despite there being no particular treatment for HPV

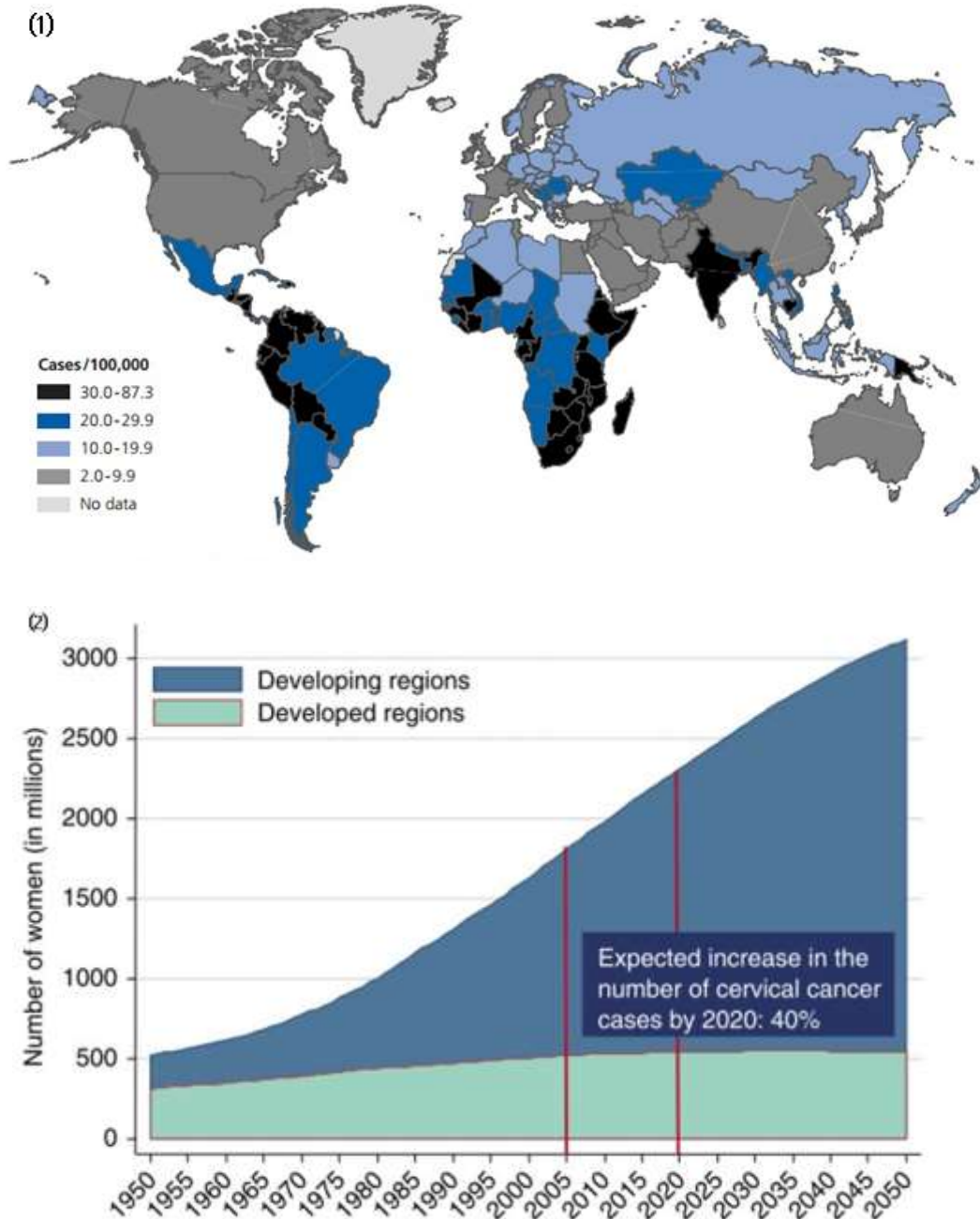
infections <sup>9</sup>. However, more than 30 types of HPV viruses are detected in the anogenital tract, of which a few are defined as high-risk subtypes that cause cancer <sup>10</sup>. These high-risk types may infect the epithelial tissue of the cervix, vagina, rectum, anus, penis, and oropharynx <sup>11</sup>. Infections by high-risk subtypes result in pathological changes in the tissues. Thus, they are also called cancer-causing (oncogenic) types. The disease burden raised by HPVs will be described in the following sections.

## **1.2. HPV Infection-Induced Cervical Cancer**

### **1.2.1. Worldwide prevalence of HPV-induced cancer**

Genital HPVs affect the genital squamous epithelium of the uterine cervix, vaginal wall, vulva, and penis. HPVs induce 99.7% of anogenital intraepithelial neoplasia, especially cervical carcinoma <sup>10</sup>, although there is a proportional variation of data partly caused by variant analysis methods across studies and geographic issues <sup>12</sup>. HPV infections in oropharyngeal and genital cancer have remarkable effects. Reis and Cruz have highlighted that HPV infection contributes to 90%–93% of anal cancers, 40%–64% of vaginal cancers, 40%–51% of vulvar cancers, 36%–46.9% of penile cancers, and 12%–63% of oropharyngeal cancers <sup>13</sup>. Due to the distinguishing vaccination and screening strategies, health education by different medical authorities, the ratio varies substantially according to the level of country development <sup>14</sup>, and even in the same country <sup>15</sup>. Meanwhile, various methods applied in causal studies based either on population or molecular or epidemiologic analysis formed data evidence, attribute the data variation <sup>12</sup>. These striking local

variations also influenced by disease development level and HR-HPV type <sup>16</sup>. A comprehensive meta-analysis of 85 studies also demonstrated the type varies significantly between SCC and adenocarcinoma (ADC) <sup>17</sup>.



**Figure 1 – Epidemiological study of Global cervical cancer events.** (1) International Variation in Cervical Cancer Incidence Rates; 1(2) World population prospects for women  $\geq$  15 years.(Bosch et al., 2008)

The “GLOBOCAN project”, managed by International Agency for Research on Cancer Registries (IARC), has predicted a higher steady creep-up by 40% globally for 15 years till 2020 (Figure 1). Developing countries in Asia, Latin America and Africa are estimated to increase by 50-55% in case number, comparing with a 23% increase in North America and 6% in Europe. In a numerical sense, 90% of worldwide deaths in 2012 consisted of 144,400 in Asia including India, 60,100 in Africa, and 28,600 in Latin America plus the Caribbean. As reported, cervical cancer not only inhabits the second top incidence of cancer in women with a high lethality performance, typically in Africa and Southwest Pacific <sup>18</sup>.

### **1.2.2. The Epidemiology of Cervical Cancer Raised by HPV Infection**

Cervical carcinoma is a type of common cancer affecting women worldwide and is responsible for second most common women’s cancer and multiple epithelial infections. It is a major type of epithelial keratinocyte-derived tumour. Epidemiological studies show that about 30-40 genital HPV types are carcinogenic types and highly associated with cervical cancer. Current epidemiologic classification varied among different studies. Pooled data from 11 studies of cervical cancer from 1985 to 1997 covering Africa, South America, Asia and Spain have shown a reliable epidemiologic classification <sup>4</sup>. Through geographical widespread data associated with HPV type-distribution in past three decades, precancerous lesions or cancers were reported to be highly associated with genotypes 16, 18, 31,

33, 35, 39, 45, 51, 52, 56, 58, and 59. Recent studies classify type 66 and type 68<sup>19,20</sup> into the oncogenic group.

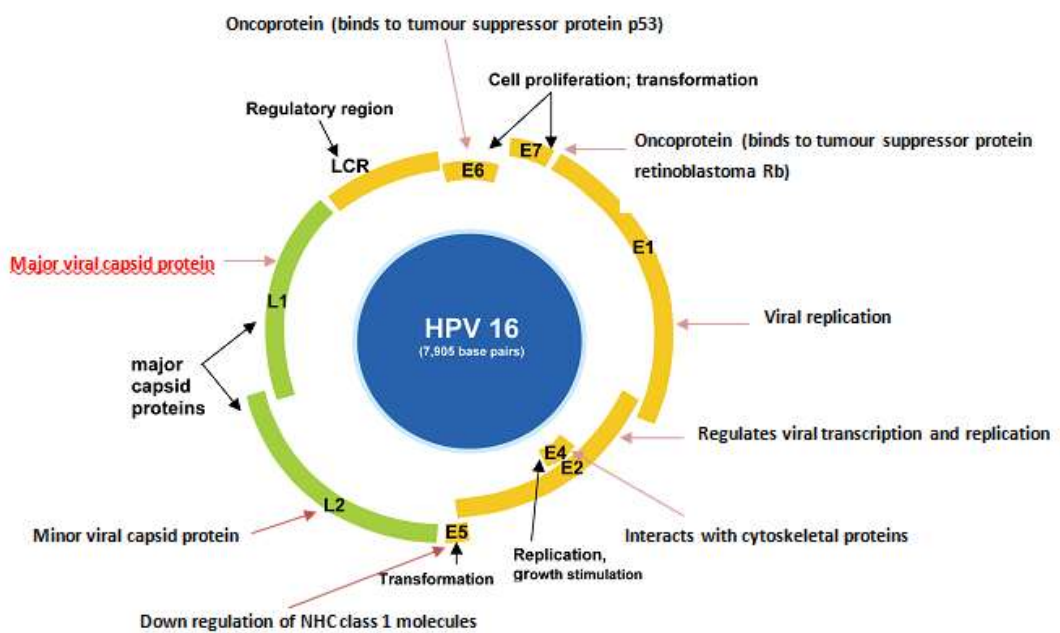
Although HPV acquisition is all-pervading during sexual behaviours particularly among young adults, HR-HPV appears a higher prevalence than the incidence of non-oncogenic infectious type<sup>21</sup>. Oncogenic types are defined according to their high odds ratios (ORs). The determination of high OR is based on  $\geq$  ten cervical cancer cases positive for the genotype being examined<sup>22</sup>. Types 26, 53, 66, 68, 73 and 82 were classified as a probable high-risk group with an OR value  $\leq$  nine cervical cancer cases positive. In contrast, those non-oncogenic types, like HPV 6,11 26, 40, 42, 53, 54, 55, 61, 62, 64, 67, 68, 69, 70, 71, 72, 73, 81, 82, 83, 84, IS39 and CP6108 dominantly cause only non-oncogenic HPV infection, like hyperplastic lesions - warts<sup>23</sup>. The type-distribution of oncogenic and non-oncogenic HPVs varies slightly among different regions.

According to epidemiological studies, cervical cancers including squamous cell carcinoma and adenocarcinoma/adenosquamous carcinoma are mainly caused by alpha HPV subtypes<sup>4</sup>. Types 16 and 18 are responsible for about 70% of cervical cancers in Africa<sup>24</sup>, and 50% of the cases are caused by type 16. The prevalence of HPV types 16 and 18 is consistent with the worldwide epidemiological estimate. In sub-Saharan Africa, the distribution of the top five HPV types frequently associated with invasive cervical cancer involves type 16, 18, 33, 35 and 55, similar to the worldwide ranking (HPV Information Center, 2009). It is noticeable that approximately 80% of cervical cancer occurs in developing countries. Besides, the

predominant type 16, 58, 52 and 33 are also HR-HPVs among Chinese women<sup>25-28</sup>. Data collected for ten most frequent HPV oncogenic types in China from cytological tests and screening indicated 38% cases of type 16, 18% of type 52 and 16% of type 58 in Chinese women with high-grade lesions. The ratio changed into 16.2% of type 16, 16.1% of type 52 and 13% of type 58 for those with low-grade lesions<sup>26</sup>. While HPV type 52 and type 58 are relatively uncommonly detected in invasive cervical cancers in America, Europe, Africa and Southeast Asia<sup>29</sup>. In the global analysis and estimate, HPV16 and 18 attribute a higher risk of progression to pre-cancerous malignant lesions compared with the other HPV subtypes<sup>24</sup>.

### 1.2.3. Overview of HPV genome and the gene functions

The genome of HPV is approximately 8 kilo-base-pair (kbp), which encodes eight major proteins. Figure 2 illustrates the high-risk type 16, which accounts for about 50% of cervical cancers worldwide<sup>29</sup>.



**Figure 2 - The genomic organization of HPV type 16**, modified from Villa's image (Villa, 2006).

As shown in the (Figure 2), the HPV genes are divided into early (E) and late (L) genes, depending upon the time of expression during viral replication. Table 1 summarizes the primary functions of the eight viral genes.

**Table 1 - Overview of HPV proteins and their functions**, modified (Boulet et al., 2007).

<b>Protein</b>	<b>Group</b>	<b>Function</b>
<b>L1</b>	Late	Major structure capsid protein
<b>L2</b>	Late	Minor capsid protein, role in recruiting viral genomes for encapsidation, involvement in nuclear transport of viral DNA
<b>E1</b>	Early	Helicase function; essential for viral replication and control of gene transcription
<b>E2</b>	Early	Interaction with cytoskeleton proteins; viral assembly
<b>E4</b>	Late	Interaction with cytoskeleton proteins; viral assembly
<b>E5</b>	Early	Growth stimulation by interaction with growth factor receptors; Prevents cell differentiation
<b>E6</b>	Intermediate	Prevents cell differentiation; cell immortalization; p53-degradation; anti-apoptotic effect; telomerase activation; induction of genomic instability
<b>E7</b>	Intermediate	Cell immortalization; interaction with pRb and pRb-associated pocket proteins; prevents cell-growth arrest/differentiation – inhibits inhibitor of E2F transcription factor

Early genes E1, E2, and E5 manipulate viral DNA replication, transcription and cellular transformation and viral assembly and release. E4 is considered to be another late gene due to its late expression during viral replication. E6 and E7 are two oncogenes, described as intermediate proteins in the period of the HPV infection cycle<sup>30</sup>, because they directly interact with components of the interferon signalling

pathways and down-regulate IFN- $\alpha$  inducible gene expression<sup>1,31</sup>. HPV infection is initiated from the primary entry of viruses through micro abrasion of the squamous epithelium causing epithelial denudation<sup>32</sup>. L1 and L2 are two late genes expressing the structural capsid protein of HPVs. The major capsid protein L1 is capable of mediating internalization in the basal lamina<sup>33</sup>, although the viral genome and mature virus are released from the uppermost layers after the proliferation at the end of their lifespan. The expression of L2 capsids proceeds to L1 assembly in the outermost cornified layer<sup>34</sup>. More details will be introduced in the pathogenesis and immune section.

### **1.3. Immune responses to HPV infections**

#### **1.3.1. General Information**

In response to viral infection, immunocompetent hosts deploy innate immunity (phagocytes, soluble cytokines like cytokines, complement and epithelial barriers) and activate adaptive immunity to generate specific humoral and cellular immune. When the local inflammation is presented after activation of innate immunity by cell injury or cell death, soluble and cellular innate immune effectors recruited and local parenchymal cells and phagocytes are initiated to secrete inflammatory cytokines and other defence molecules. Then the adaptive immunity is activated by naïve T lymphocytes after the active response of APCs, which are dendritic cells (DCs) predominantly<sup>35</sup>.



Sex hormonal regulation of the female reproductive tract is an essential and distinguishing protection feature in contrast to other mucosal sites. Cytokines, chemokines, and antimicrobial products contribute to the protective mechanisms in the cervical mucosal immune system. However, rather than the Immunoglobulin (Ig) A and IgG secreted in local cervicovaginal infection site, systemic IgG mediates predominate protection, which is able to transude across the cervical epithelium via the squamocolumnar junction <sup>36,37</sup>. The infection site of HPV at keratinocytes in the basal layer of the epithelium is possible to achieve more direct access to systemic IgG, which is likely the reason for a high-enough concentration of systemic IgG levels for local mucosal protection in contrast with the level in cervical secretions <sup>38,39</sup>. Furthermore, keratinocyte migrates along the basement membrane to repair the initial micro-wounds over 1-2 day duration. Recent studies have shown that HPVs were probably blocked by a type of primary receptors to the infected basement membrane before conformational distortion to enter the keratinocyte, which are presumably different from serum Nabs <sup>32</sup>.

Pathogen recognition receptors like Toll-like receptors (TLRs) are mediated via different adaptor molecules to trigger host signalling pathways in both innate and adaptive immune responses by stimulating myeloid differentiation primary response gene 88 (MyD88) in the case of HPV infection <sup>39,40</sup>. In adaptive immunity, cellular immunity induced by mucosal infection due to intracellular pathogens HPV plays a crucial role against HPV infection <sup>41</sup>. T lymphocytes act as a crucial role in both cell-mediated and humoral immunity, which recognise peptide antigens. Peptides bond to the major histocompatibility complex (MHC) proteins presented as a membrane-

bound receptor complex on the cell surface of others cells, like nucleated cells, macrophages, B cells and DCs <sup>35</sup>. As part of the cellular immunity, CD8+ cytotoxic T-lymphocytes (Tc cells) recognise antigen presented by MHC I as MHC/peptide complex after endogenous antigen HPV broken down into small peptides and delivered onto cell surface <sup>35</sup>. Meanwhile, CD4+ T helper-type 1 cells (Th1) to initiate the defence and secret a group of cellular cytokines (IL-2, IL-12, IL-18, IFN- $\gamma$ , TNF- $\alpha$ , TGF- $\beta$  et al.) to generate cell-mediated immunity <sup>31,42-44</sup>. In humoral response, macrophages and B cells initiate an antibody response against pathogens utilising TLR4/MyD88-dependent signalling pathway in the endolysosomes <sup>64, 65</sup>. MHC II presented on the surface of DCs and macrophages mainly interact with exogenous antigen broken down in the endosome of the APCs to form MHC II/peptide complex <sup>35</sup>. TLR activation and signalling stimulate DCs for antigen presentation to naïve T cells, activate B cells and the differentiation of DCs and naïve T cells into antibody-secreting plasma cells via Th2 path by IL4, 5, 6, 10, and 13 <sup>39</sup>.

HPV infection leads to permissive or persistent pathological changes of infected skin or mucosa. Only a limited proportion of infections develop persistently to trigger cancerous lesions <sup>45</sup>. Phagocytes and soluble proteins of innate immunity play as the first-line barrier in host defence, following with the initiated clearance by activated antibody and cytotoxic effector cells in adaptive immunity <sup>35</sup>. HPV clearance is defined by two consecutive negative results after a positive test in the epidermis layer of a patient. An intact mucosal immune system plays a pivotal role in HPV clearance <sup>19</sup>. Additionally, cytological studies have shown that not all infected women develop neoplasms. Since cervical cancer only happens to a small percentage of HR-HPV

infected women after a long-term development. Plenty of cofactors provides the opportune milieu for the progression of persistent cervical infection, like long-term use of hormonal contraceptive<sup>46</sup>. Factors like age, several sexual partner, multiparity, smoking, immunosuppression, overweight or physical inactivity, micronutrient depletion, use of contraceptive drugs, and in particular retinoid deficiency can influence viral clearance<sup>5,18,19,46,47</sup>. In the review by Gariglio et al. the synergic effect of estrogens, retinoid deficiency, nutritional status and HPV viral types leads to the progression and final persistent infection<sup>46</sup>.

Variations in pathological features have been observed among HPV types. The cytological study demonstrates reduced clearance rate in infectious cases caused by high-risk virus types (16, 31, 33, 35, 52, 58) compared with low-risk types<sup>5</sup>. In non-oncogenic-type infections, young women aged below 35-years-old require a longer clearance period<sup>48</sup>. However, no correlation was found between age and clearance time in oncogenic infections. A productive HPV lifecycle is determined possibly also by these external multi-factors. For example, low levels of estrogens were found to influence the development of cervical cancer<sup>46</sup>.

Immune cell organization and hormonal control in the lower reproductive tract, which vary in different stages of the menstrual cycle, may lead to different immune responses upon HPV invasion; the precise underlying mechanisms remain to be elucidated. The outcome is the result of dynamic conflict between the host epithelial immunological responses and the mechanism of viral pathogenesis. During pregnancy, the increasing levels of estrogen and progesterone are eminently possible

to raise the risk of persistent or progressive infection <sup>49</sup>. Estrogen or progestagens is able to stimulate the hormone response elements in HPV16 LCR, and result in the development of cervical cancer <sup>50</sup>. Thus, hormonal contraceptives are highly possible to contribute the development of cervical cancer because of enhancing HPV gene-expression in the cervix <sup>22</sup>. Besides, the most estrogen- and retinoid-sensitive region of the cervix is the transformation zone (TZ), where the HPV infection occurs primarily <sup>46</sup>. Multiparity is likely to stimulate TZ and increase exposure chances to HR-HPV and other cofactors <sup>51</sup>.

### **1.3.2. HPV Pathogenesis v.s. Epithelial Immune System**

#### **1.3.2.1. Viral Pathogenesis**

Host defence in the epithelium involves both innate (phagocytes, soluble proteins like cytokines, complement, and epithelial barriers) and adaptive (antibody, cytotoxic effector cells) immune response. Poor immunogenicity of the HPV viruses is due to the lack of cytolytic infectious process and dsRNA intermediate, which compromise eliciting strong innate immunity and specific adaptive immune response. Hence, systemic antigen presentation does not occur during HPV infection <sup>30</sup>.

HPVs encode non-secreted nucleoproteins which are non-structural viral proteins expressed at low levels. Lipopolysaccharides (LPs) as a critical integral component of the outer membranes of Gram-negative bacteria stimulates macrophages to secrete TNF- $\alpha$ , IL-1, IL-6, IL-10, macrophage inflammatory protein-1 $\alpha/\beta$  (MIP-1 $\alpha/\beta$ ), and

other inflammatory effector substances as a causative agent of endotoxic shock <sup>52</sup>. Unlike other viruses with the ability to trigger host immunity, HPVs interfere with viral antigen processing to avoid host immune responses. During natural HPV evolution, viral oncogenesis occurs as the result of viral replication and viral immune evasion. The happen of progressive infection requires an HPV genome intergrading into the DNA of the host cell <sup>53</sup>. In initial infection, HPVs are only produced in undifferentiated keratinocytes in the basal layers of stratified epithelium. In this stage, infected keratinocytes replicate solely accompanied by their differentiation program without sufficient immune recognition in circulation <sup>54</sup>. The subsequent particle formation is not in primary infected site, but in external differentiated epithelial cells as a low profile <sup>1</sup>. Thus it can be kept hidden from the immune system during initial viral infection.

Seropositivity detected in patients with genital warts exhibits only sufficient quantities of late capsid protein but not early viral proteins. Studies demonstrated that early viral proteins of HPVs localize in the cell nucleus without sufficient quantity to be recognized by immune cells and molecules <sup>54</sup>. In terms of genome organization, the major protein L1 is also an antigenic capsid protein that accounts for 80% of the viral particle weight, and L2 is the infectivity-enhancing protein <sup>55</sup>. Usually, capsid proteins located outside of viral nucleus leads a specific high immunogenicity of natural immune responses. However, the non-lytic HPV does not elicit any pro-inflammatory signals during life-cycle to initiate immune-response in squamous epithelia and activate the DCs. The production of the highly immunogenic capsid proteins takes place in the terminally differentiated outer layer without blood-borne

phase life cycle <sup>56-58</sup>. All measurable antibody against the L1 major capsid could only be readily detected after a long time from initial infection, varying from four months to five years in a limited number of patients <sup>59</sup>. Additionally, sharing of epitopes of HPV16 E7 with several human proteins (xeroderma pigmentosum group G complementing protein and retinoblastoma binding protein 1) is possible to evade functional antigen-specific immune recognition by human T-cells <sup>1</sup>.

### **1.3.2.2. Epithelial Innate Immune System vs. HPV Infection**

A permeability immune barrier of epithelial cells lining mucosal surfaces is associated with its dynamic communication with cell types comprising the mucosal immune system. Keratinocytes play a pivotal role in early detection and host clearance of mucosal HPV infections. Significant increased endosomal TLR3, TLR7, TLR8 and TLR9 associated with highly secreted IFN- $\alpha$ 2 are responsible for detecting danger sensing of viral nucleic acids via pattern recognition receptors (PRRs) to clear the infection after incident infection <sup>60</sup>. TLR3 senses double-stranded RNA (dsRNA), TLR-7 and TLR-8 recognize single-stranded RNA (ssRNA), and TLR-9 in keratinocytes sense CpG ODN to promote the production of TNF- $\alpha$ , IL-8, CCL2, CCL20, CXCL9 and type 1 IFN <sup>44</sup>. Epithelial inflammatory microenvironment created by chemokines are recruited by different cell types including monocytes, NK cells, memory T cells, DC/LC, activated Th1 cells and other innate immune cells reviewed by Moerman-Herzog <sup>61</sup>. CCL20 potentially induces immature LC to migrate and attracts CCR6-positive memory B and T cells. Following the migration of activated LCs, keratinocytes recruit LCs and secrete cytokines and chemokines including CCL20 to activate LC and T cells <sup>62,63</sup>. Despite

CXCL9 and CXCL10 responding TLR3 and TLR9 induce recruitment of activated Th1 cells to establish further local adaptive immune response <sup>64</sup>, HPV16 oncogenes are potent to reduce both the cytokine-stimulated chemokine expression in keratinocytes <sup>65,66</sup>.

The HPV life cycle begins exclusively in the intra-epithelial microenvironment. Thus there is no viraemic phase to trigger the immune cells in circulation <sup>67</sup>. This mucosal system connects with systemic immunity, metabolism, organ function, and molecules and microbes involved between outside space and inner microenvironment <sup>68</sup>. Epithelial cells are the constituent of the mucosal immune system to resist the invasion of pathogens and the random uptake of antigen. Additionally, they are capable of regulating the associated immune cells, and permit the regulated sampling of antigenic materials by various factors, in particular chemokine receptor signalling, in either peripheral lymph node or organized mucosa-associated lymphoid tissue (O-MALT) <sup>69</sup>. O-MALT is type I mucosal epithelia having specific B cell and T cell zones in tissue structure. The initial HPV infection stimulates more non-specific immune responses, including neutrophil chemo-attraction and series of cellular mediated activities involving not only keratinocytes, macrophages and DCs, but also natural killer cells (NKs), and Langerhans cells (LCs). At the same time, T-cell response appears also involved in the early-stage of viral clearance <sup>70</sup>.

Cytokines measured in cervical secretions indicate local cytokine production in the cervix rather than circulating cytokines. Studies for local cervical cytokines in both infected and non-infected women with carcinogenic HPV types demonstrated an

inflated Th1 cytokine profile, associated with positive IFN- $\gamma$  and TNF, negative IL-4, and variable IL-12 expression capable to enhance HPV clearance <sup>71</sup>. Cytokines including type I IFNs, TNF- $\alpha$ , IL-1 $\alpha$ , IL-4, IL-13, and TGF- $\beta$  inhibit the expression of HPV early genes and suppress the growth of normal or non-tumorigenic HPV transformed keratinocytes <sup>72-74</sup>. Type I IFNs produced by those front-line defensive cells to react to viral infection in both infected cells and prevent the infection spreading to neighbouring cells. Initial danger sensing stimulates the expression and activation of IFN-stimulated genes (ISGs) through intracellular nucleic acid-sensing PRRs and autocrine and paracrine signalling pathways depending on signal transducers and transcription factors <sup>75,76</sup>.

However, studies have demonstrated cancerous infection with ongoing HPV evasion. There is a lack of cytolysis or cytopathic death after virus replication and assembly <sup>77</sup>. The LCs in CIN play important role in antigen presentation. Nevertheless immune system is hard to detect HPVs because the viruses are exclusive in the epithelium. As a subset of key lymphocytes in the innate immune system, NKs cells chase viral-infected cells and tumour cells that lack MHC I expression<sup>31</sup>. They are in sub-epithelial layers as LCs and are more efficient in killing infected cells once the late viral capsids are expressed <sup>78</sup>. The trigger of antigen-presenting cells (APCs) requires the immune surveillance for damaged cells. Reduced NK cell activity could be observed in patients with active HPV 16 neoplastic disease. Poor neutrophil trafficking linked with losing or inoperative chemokine receptor CXCR4 and IFN released by NK cells reportedly leads to further virus evasion <sup>42,79</sup>. Further



observations about LC demonstrated that interfered recruitment of functional LCs and decreased E-cadherin expression positively relate to grades of CIN<sup>80</sup>.

On one side, apoptosis of initially infected cells occurs in the superficial epithelium (deeper connective layer), where there is a lack of patrolling leukocytes and LCs<sup>39</sup>. In contrast, the apical layers of the mucosa with abundant LCs are not involved in HPV initial infection<sup>67</sup>. On the other side, infected cells appear not to undergo lysis process, which would otherwise cause inflammation and signals to immune systems<sup>31,81</sup>. The delayed expression of highly immunogenic capsids in differentiated epithelium provides the ability to avoid LCs dwelling in the proximal epithelial layers<sup>54</sup>. These dramatic immune-evasion mechanisms provide viral avoidance or subvert the host immune response. This evasion mechanism includes interference with the interferon (INF) pathway, modulation of antigen presentation, inhibition of interleukin-18 (IL-18) activity and down-regulation of major histocompatibility class I (MHC I) on infected cells<sup>82</sup>. Non-existing or incomplete eradication results in HPV persistence<sup>82</sup>.

### **1.3.2.3. HPV Evasion vs. Adaptive Immune Response in HPV Infection**

Systemic humoral immunity contributes to adaptive immune responses by assisting with cellular immunity against HPV infection. In HPV humoral immune response, B cells activated by CD4 helper T cells, APCs, and Th2 cytokine pattern produce antibodies – mainly IgG1 to neutralize and opsonize HPVs<sup>83</sup>. Antibodies move to lymph nodes for targeting extracellular capsid protein L1 to avoid further

keratinocytes uptake, restrict cell surface binding and emit signals for macrophage ingesting viruses. This process releases inflammatory cytokines like IFN- $\gamma$ , TNF, IL-2 and IL-12 from Th1 and Th2 cells <sup>72</sup>.

In both natural infection and vaccine-induced immune response, HPV-specific neutralizing antibodies are the core for reliable protection against HPV infection <sup>84,85</sup>. The low level and late appearance of HPV neutralizing antibodies is the main feature after natural HPV infections <sup>59</sup>. Serological studies have shown the type-specific antibody against the major viral coat protein L1 rather than minor viral coat protein L2 detectable in natural HPV infection events in animals or humans <sup>86</sup>. Another important feature of HPV antibodies was described as no cross-protection among different HPV subtypes several years ago <sup>39</sup>. However, in the current decade, studies demonstrated conflicting results in the existence of partial cross-protection <sup>87</sup>. Several cross-neutralizing monoclonal antibodies (MAbs) groups were discussed in neutralizing activity investigations with L1 virus-like particles (VLPs). HPV16.J4, HPV16 I23, and HPV33.E12 was identified with cross-neutralizing MAbs <sup>87</sup>. For the currently licensed vaccine, a certain level of cross-protection between HPV type16 and 31, as well as type 18 and 45 <sup>88</sup>. These properties extend the understanding of HPV prevention for further therapy strategies.

Apart from B cells secreted MAbs, which are responsible for neutralising viruses, cellular immunity comprises part of the adaptive immune system by stimulating T cells to kill the virus-infected cells. Healthy cervical epithelial cells present positive MHC I comprising numbers of major human leukocyte antigens (HLA) with

negative MHC II. MHC class I molecules express cytoplasmic proteins as endogenous antigens to cytotoxic CD8+ T cells typically on all nucleated cells, while MHC II express exogenous antigens outside the APCs, like DCs and macrophages to helper CD4+ cells <sup>89</sup>.

However, viral immune evasion led by invading HPVs will not express MHC class I on all nucleated cells. Besides no cytolytic or ‘programmed death signal’, the key antiviral defence troops, IFNs are mandatorily suppressed by HR-HPV oncogenes. E6 and E7 inhibits the IFN receptor signalling pathway and downregulate IFN response genes and TLR9 to evade effective innate immune response and delay the activated adaptive immunity <sup>1,52,90</sup>. Active parts of mucosa-associated lymphoid tissue (MALT) inductor exist in the lymphoid follicles of the female genital tract <sup>91</sup>, which is capable to stimulate the expression of MHC II molecule in LCs, macrophages and lymphoid <sup>92,93</sup>.

In the majority of cervical carcinogenesis events, high-risk HPV genes integrate into the host genome and keep transcriptionally silent <sup>94</sup>. These multistep processes mediated by episome-derived E2 protein, which deregulates the expression of the HPV oncogenes E6 and E7. Moreover, E5 as a minor oncoprotein is able to inhibit the expression of MHC molecules on the cell surface and restrict the adaptive immune response <sup>95</sup>. Consequently, local APCs, like DCs fail to detect the virus. HR-HPV escapes from clearance of host innate and adaptive immunity to progress into cervical carcinogenesis.

### 1.3.3. Cervical carcinogenic progression

Malignant progression of HPV infected cells perform as a stepwise process including the integration of viral genes into host cell chromosome following silencing of two viral replication proteins E1 and E2, and upregulating oncoprotein expression to alter cell functions towards cell immortalization <sup>96</sup>. The scheme in Figure 3 modified by Hausen's study has summarized the irreversible process of carcinogenesis and malignant maintenance after the initial infection (Figure 3). Genomic mutation, estrogenic derivatives, and chromosomal instability could accelerate the progress.

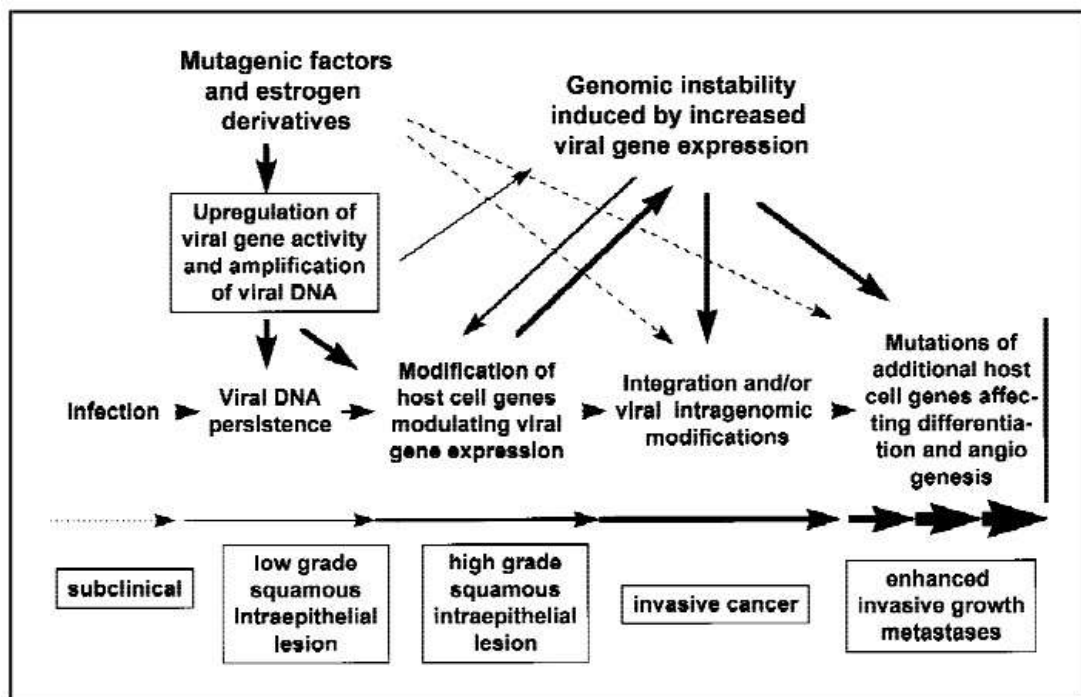


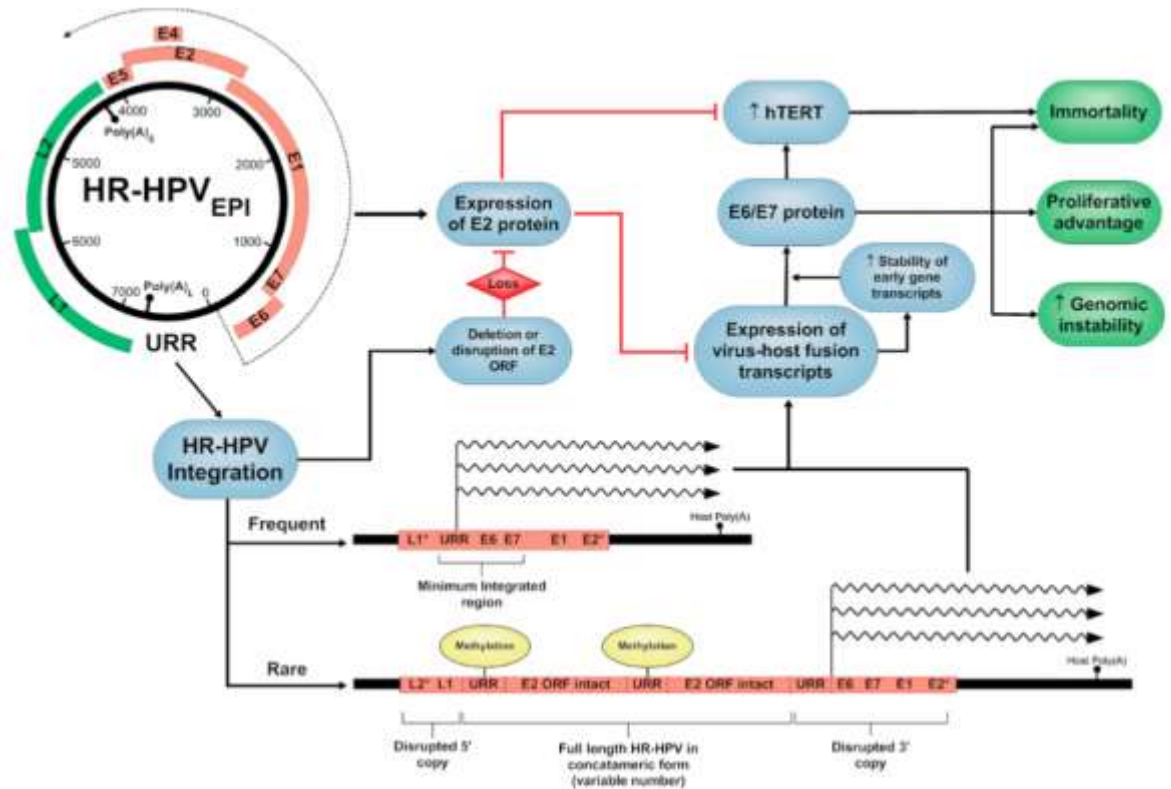
Figure 3 - Scheme of carcinogenic progress mediated by high-risk HPV, referred from (Zur Hausen, 2000).

Integration of viral genome of HR-HPV is an essential process progression to the invasive phenotype, which results in the loss of expression of the viral regulatory

protein E2 (Figure 4). HPV integration enables infected cells to retain oncogene expression, resist host clearance and avoid cell death <sup>94</sup>. Observations demonstrated that E2 regulates the expression of the viral oncogenes E6 and E7 by repressing the promoters of HR-HPVs against the expression of E6 and E7 gene products<sup>97-99</sup>, inhibits immortalization capacity in primary keratinocytes <sup>99</sup>, restrains growth and cell cycle arrest <sup>98,99</sup>. HR-HPV integration happens with a vital cellular presence of episomal virus expressing the inhibitory E2 proteins E2 (episome-derived E2 protein). The activation of innate immune pathways leads to episome loss <sup>94</sup>. Spontaneous rapid loss of transcriptionally active episome-derived E2 is required for the selection of intracellular mixtures of episomes and integrants contained cells expressing the viral oncogenes at a high level regulated by activated type I interferon (IFN)-inducible antiviral genes <sup>90,100</sup>.

Integrants majorly deriving from the insertion of HR-HPV episomes into the host genome maintain at low copy number with the coexistence of E6, E7 oncogenes, and viral upstream regulatory region (URR) <sup>101,102</sup>. The increase of integrant copy number occurs during the viral amplification and flanking host DNA <sup>103</sup>. Normally E2 protein regulates viral replication and inhibits expression from integrated virus and virus-host fusion transcripts by the binding site in URR <sup>99</sup>, which are completely or partially disrupted by integrants at E2 ORF in HR-HPV integration events <sup>102,104,105</sup>. Disruption of the viral genome displays as the transcription dissociation of viral early gene from the early polyadenylation (poly(A)) signals associated with a prolonged half-life of the transcription activities of virus-host fusion transcripts subsequently <sup>106</sup>. In the last decade, studies revealed transcriptionally silent HR-HPV

integrants concomitant with viral episomes in infected cells present in the intermediate stage of cervical carcinogenesis. Thus, the lack of E2 consequently promotes transcriptional imitation, increases expression of virus-host fusion transcripts, and deregulates E6 and E7<sup>107</sup>, leading to cellular immortalization, deregulated proliferation, and increased genomic instability as Figure 4 illustrated<sup>94</sup>.



**Figure 4 - Significance of HR-HPV integration events detected in cervical carcinomas,** referred from Pett' diagram (Pett & Coleman, 2007)

Structural chromosomal changes and numerical chromosome imbalances present in cervical carcinomas and HPV-immortalized cell lines, which derive chromosomal translocations, deletions, amplifications of certain chromosomal regions or other changes<sup>108</sup>. Structural chromosome instability of HPV oncoprotein expressing cells manifests as impaired ability to respond to DNA damage presumably resulting from

loss of p53 or pRB function<sup>109-112</sup>. The pleiotropic functions of oncoprotein E6 and E7 listed in Hausen's review demonstrated that the host gene mutational consequences triggered by E6 and E7 include viral to host cell genome integration. The binding-deficient mutants of cyclin-dependent kinase (CDK) as transformation defective and the degradation blockage by E6 and E7, causatively stimulate the massive growth of these oncoproteins in high-risk HPV infection events<sup>56,113</sup>. High-risk E7 gene is one key to genomic stability and the final centriole amplification in the infected region. Cell division abnormality in suprabasal epithelial layers with abnormal centrosome numbers subverted by HR-HPV E7 oncoprotein<sup>114,115</sup>, forms multipolar mitotic spindles in asymmetric cell divisions with inclined chromosome gains or losses<sup>116,117</sup>. Aneuploidy in gene replication, as described in the previous section, results in centrosome-related mitotic defects and aberrant cellular DNA<sup>115</sup>, which induces cell tumorigenesis<sup>118</sup>.

Furthermore, The alteration in the host genome restrains viral transcriptional silencing in integrated cells and interferes cellular immunity following remained expression ability of viral oncogenes and initiated grafting in basal layers<sup>56,94</sup>. Macrophage-derived cytokines were involved in compromised cellular immunity<sup>74</sup>. In non-tumorigenic HPV-infected cells, JE (MCP-1) gene triggers an intracellular pathway and plays a pivotal role in negative interference of viral transcription, and protein 1 (AP-1) transcription factor complex regulate viral gene expression<sup>74,119</sup>. However, systematic inflammatory cytokines like TNF $\alpha$ , interleukin 1 and cell functional cytokine transforming growth factor beta (TGF- $\beta$ ) inhibit viral gene expression in genomic mutated host cells like HR-HPV-immortalized keratinocytes

due to mutations of relevant regulatory genes in these tumorigenic cells<sup>73,120,121</sup>. Furthermore, RNA splicing and polyadenylation regulate HPV viral gene expression initially<sup>122–124</sup>.

Although the fundamental role of methylated papillomavirus DNA in carcinogenesis is still unclear, consequently efficient DNA methylation of integrated HPV DNA and cellular cap-dependent splicing of the E6E7 pre-mRNA might highly associate with dysregulated gene expression program for cervical cancer development<sup>124,125</sup>. Bacterial/viral DNA and synthetic oligodeoxynucleotides (ODN) containing unmethylated CpG-dinucleotide (CpG DNA) are capable of stimulating B cell proliferation and activating macrophages and DCs. TLR9-mediated CpG DNA activates the intracytoplasmic signalling molecules like IRAK, TRAF6, NF- $\kappa$ B and MAP kinase and stimulates Th1 immune responses<sup>52,126</sup>. The immune-stimulatory activity of bacterial DNA repressing the growth of various syngeneic animal tumours and allergy, enhancing NK cell activity and inducing production of IL-6, IL-12, IFN $\alpha/\beta$  and IFN- $\gamma$  from mouse spleen cells and human PBL was initially reported by Tokunaga's group in 1984<sup>127</sup>. Host genome mutation at CpG dinucleotide region including adjacent regions, like inversion to CpG or methylation could abrogate its immune-stimulatory potentials<sup>128</sup>. Thus, CpG methylation in HPV 16 and 18 genomes mainly in LCR regions and part of L1 ORF regions, where locate upstream of the P97 promoter, will not be transcribed during HPV DNA integration. Additionally, the frequency of DNA hypermethylation of host genome affects the severity of neoplasia<sup>124</sup>.



#### **1.4. Preventive and therapeutic HPV vaccines**

HPVs express early genes in immature basal epithelial cells, but viruses transcribe late genes and assemble new virions away from the submucosa, the site of epithelial immune surveillance at the differentiation stage <sup>129</sup>. HPV pathogenesis, immune evasion mechanism and tumorigenesis reviewed in the last section have facilitated the baseline of vaccine development. In contrast with non-tumorigenic HPV infected cells, mutations in invasive HR-HPV integrated cells also cause certain deletions of early genes and late genes associated with upregulated transcription of E6 and E7 after the loss of E2. Inactivated tumour suppressors p53 and retinoblastoma (Rb) genes induce the host genomic instability and apoptosis repression <sup>129</sup>.

Therefore, the viral mechanism of effective evasion of innate immunity and delayed adaptive immunity becomes the obstacle in achieving high immunogenicity of HPV vaccination. Lack of inflammation during viral replication, assembly and release and down-regulation of IFN secretion cause the prolonged “silence” of epithelial cell-mediated response with low-level of serum neutralizing antibody in animal models <sup>31</sup>. Unlike the natural infection, vaccines must be able to stimulate both innate and adaptive immunity, differentiating B and T cells into long-lived memory cells, which would prompt strong and instant reactions to clear the virus when HPV infection occurs <sup>130,131</sup>.

The aim of prophylactic vaccines is to generate high L1 neutralizing antibody to block initial HPV infection in epithelial cells, while therapeutic vaccines require

executing T-cell activation to eliminate integrants. The challenge of therapeutic vaccines is to operate and regulate HPV antigen-specific effector cells in the non-inflammatory milieu to be recruited to the infected site, which takes a protracted idle period without local immune response. The deregulation but high expression of HR-HPV oncogenes in a persistent HR-HPV infection is possible to induce dominance of T regulatory cells rather than the effective cell-mediated immune response to dispel invasive carcinogenesis<sup>132,133</sup>. Another criterion for successful immunisation is immune memory generated after vaccination in the performance of antibody persistence and robust recall from the VLPs as a standard of duration measurement for vaccine-induced protection<sup>134</sup>.

#### **1.4.1. Current prophylactic HPV vaccines**

L1 and L2 capsid proteins are required for the virus to penetrate the epithelial cells during the early stage of infection<sup>135</sup>. The envelope L1 protein is highly immunogenic in natural animal infections and is able to elicit neutralizing antiviral antibodies<sup>84</sup>. Two epitopes on L1 are responsible for eliciting the host humoral immune response<sup>136</sup>, offering the basis for the prophylactic vaccination strategy<sup>137</sup>. The L2 protein exhibits a linear epitope cross-neutralizing infection with many HPV types. Use of L2 as a candidate for type-common protection is challenging due to its low antigenicity compared with L1 protein<sup>138</sup>. An adequate adjuvant is required to enhance L2's antigenicity.

L1 VLP studied using a 22-multiplex cytokine bead assay indicated significantly increased production of Th1-type (IL-2, IFN- $\gamma$ ), Th2-type (IL-4, IL-10, IL-13), and inflammatory (IL-1 $\alpha$ , IP-10) cytokines/chemokines in PBMCs after vaccination <sup>139</sup>. HPV L1 VLPs are able to generate high immunogenicity even without any adjuvant by their strong potentials to stimulate both innate and adaptive immunity, accompanied with rapidly recognition and coalescence by myeloid DCs (MDCs) and B lymphocytes. A potent Th1 response associated with activated NF- $\kappa$ B/AP-1 mediated inflammatory response signalling via MyD88-dependent TLR4 triggers both high-titer Nabs and cell-mediated immune responses <sup>140</sup>. Further VLP potentials will be reviewed in the animal model chapter.

Currently licensed vaccines include Cervarix<sup>TM</sup>, a bivalent HPV 16/18 L1 vaccine developed by GlaxoSmithKline (GlaxoSmithKline Biologicals, Rixensart, Belgium) and Gardasil<sup>®</sup>, which is a quadrivalent vaccine against HPV 16/18/6/11 ( Merck and Co. Inc., West Point, Pennsylvania, USA) <sup>39</sup>. Gardasil has already been licensed in more than 50 countries in late 2006 <sup>129</sup>. HPV 6 and HPV 11 are known as the two major types found in more than 90% of anogenital warts <sup>141</sup>. These prophylactic VLP vaccines are delivered intra-muscular (i.m.), by which vaccines are able to circumvent the intraepithelial immune evasion by means of rapid access of antigen to the local lymph nodes <sup>142</sup>. After 3 shot i.m. schedule, HPV L1 viral-like particles are able to elicit high titers and long-term anti-L1 neutralizing antibody to the infectious site of mucosa <sup>85,143–146</sup>.

VLP-based prophylactic vaccines are delivered to women before exposure to the virus, because up to 63% of girls reported having HPV infection within 4 years after first-time sexual behaviour <sup>147</sup>. In America, the FDA licensed the quadrivalent VLP vaccine for women age between 9 to 26 <sup>148</sup>. Although early vaccination is worth consideration, possible break-through infections due to early vaccination without boosters in a more effective age should be concerned <sup>149</sup>. The HPV vaccination among homosexual and bisexual men confronts with the low knowledge of potential health consequences of HPV infection in the male <sup>150</sup>. Acceptability of HPV vaccines among men, especially among homosexual and bisexual males grows, with the increasing incidence of HPV induced anal and oral cancers in men <sup>150-152</sup>. From 2013, the Commonwealth Department of Health and Aging launched national HPV immunisation program for males aged from 12-13 in a 3-dose course in Australia <sup>153</sup>. American Cancer Society's 2016 recommendations for HPV vaccination also recommends HPV vaccination for male aged 13-26 and homosexual or bisexual males with weakened immunity though aged 26 <sup>154,155</sup>. However, the approval of HPV programme to boys is keeping delay in the UK <sup>156</sup>.

As mentioned previously, VLPs are rapidly bound by MDCs and B lymphocytes via MyD88-dependent TLR4 and NF- $\kappa$ B mediated signalling pathway moderated by TGF- $\beta$  <sup>157,158</sup>. Current prophylactic HPV VLP vaccines have demonstrated a high immunogenicity by B cell activation and antibody generation. After the approval of quadrivalent and bivalent vaccines by the US Food and Drug Administration (FDA) in 2006 and 2009 respectively to prevent initial HPV infection, studies have shown an impressive recall response initiated by Gardasil<sup>®</sup> to antigen challenge as 5-year

post-immunisation, and Cervarix<sup>TM</sup> capable to circulate HPV-specific B memory cells 1 month after the final immunisation with persistent B and T cell stimulated antibody secretion <sup>159,160</sup>. Currently, the best assumption is that the mechanism of protection elicited by VLPs is serum antibodies. Part of the fundamental immunization mechanism of VLP vaccination against high viral challenge is based on the persistent level of serum IgG, which was testified in animal model <sup>85,161,162</sup>. Distinct from serum IgG, another type of noticeable Nabs highly considered according to presumable ability with a low level of Nabs to intercept high concentration of virus capsid proteins before their episome-conformational distortion essential for viral entry into keratinocytes, is speculated to be blocking Abs <sup>32</sup>.

Previous clinical data showed that pre-teenage girls and young adolescents obtained good or even better immune response than older females after completion of the three-dose vaccination course <sup>163,164</sup>. Although preventive vaccines were believed without any therapeutic effects on pre-existing HPV infections and HPV-associated lesions due to probably insufficient cell-mediated immune response to infected cells <sup>129</sup>, a new randomized cohort analysis shows that the bivalent HPV 16/18 VLP vaccine was not only effective against HPV infection, but also protected infected women from progressing to persistent cervical infection or cytological abnormalities associated with HPV 16/18 <sup>165</sup>.

Besides, the prophylactic quadrivalent HPV vaccine has been shown efficacious in preventing not only high-grade cervical intraepithelial neoplasia and precancerous lesions of the cervix, vulva and vagina infected by HPV type 6,11,16 or 18, but also

efficacious in men against related external genital infections <sup>151,166-168</sup>. High efficacy (>96%) of the Gardasil<sup>®</sup> HPV 16/18/6/11 vaccine was shown against vulvar and vaginal intra-epithelial neoplasia and external genital warts. It's efficacy remained to be more than 86% against external genital warts in heterosexual men and 70% against anal intra-epithelial neoplasia in homosexual/bisexual men aged between 16-26 years old <sup>151,167</sup>. These findings indicate the great potential of the licensed VLP vaccine. The potential benefits of the vaccination include a low probability of HPV infection, low recurrence rate, and less severity of the diseases. These potentials require further large-scale trials and long-term follow-up studies to assess for confirmation. However, long-lasting anti-L1 Nabs were detected in vaccinated subjects at least over 5 years in most vaccines but inapplicable to HPV 18 Abs in about 20% of subjects after the Gardasil<sup>®</sup> vaccination <sup>169</sup>.

The adjuvant of Cervarix<sup>™</sup> is aluminium hydroxide and MPL (AS04) while Gardasil<sup>®</sup> is based on aluminium hydroxyphosphate sulphate. Clinical trials indicated that the adverse reactions from local injections could be mainly related to AS04 <sup>170</sup>. However, there are several advantages of the AS04-based formulations combined the TLR4 agonist MPL. They include a consistently enhanced high and sustained stimulation to CD4+ T or B lymphocytes, prolonged cytokine responses at the injection site, and especially an increased ratio of HPV specific memory B-cells profile in contrast with aluminium salts alone <sup>171</sup>. Thus, AS04 formulated Cervarix<sup>™</sup> was observed achieving a stronger, faster and longer Ab response than VLPs with alum alone <sup>129</sup>. The adjuvant benefits could also be demonstrated in data as a higher frequency of HPV-specific memory B-cells and HPV-16/18 neutralizing antibody

levels of Cervarix™ versus Gardasil®<sup>170</sup>. A new question is raised as to whether the broad-spectrum-targeted V503 has the similar long-term immune memory as Cervarix™ without any adjuvants.

In natural HPV infections, the detectable neutralizing antibody is heterogeneous, but HPV L1 VLP vaccines testified by two commercial vaccines generate cross-reactive and cross-neutralizing Nabs<sup>172</sup>. In a Scottish programme of national surveillance in the catch-up cohort survey for three-dose uptake of bivalent vaccine Cervarix™ started from 2008, combined data for vaccination, screening and HPV testing records indicated cross-protection against HPV 31, 33 and 45<sup>173</sup>, with 94.2% efficacy against HPV 45 induced infection and 54.5% efficacy against HPV 31 caused incidence<sup>129</sup>. L1 VLPs are complex multiple-overlapping epitopes recognized by B cells. Although these immunodominant Abs are type-specific epitopes, but possible a subpopulation of other types of antibodies sharing same epitopes as polyclonal Abs<sup>31</sup>. Low concentration of detectable Nabs generated in natural infections presents type-specific immunization, while Nabs secreted after VLP immunization are speculated to comprise a small but effective portion of cross-reactive and cross-neutralizing serum Nabs in a higher concentrated Abs<sup>172,174</sup>. Finally, the efficacious populations of either polyclonal or heterogeneous Nabs induced via HPV VLP vaccination depend on the output of individuals' stimulated B cells<sup>31</sup>.

Due to the broad-spectrum neutralization epitopes of L2, chimeric VLP contained L2 induces more efficacious cross-neutralizing antibodies than L1-VLP only<sup>175</sup>. The cross-protective vaccine is a chimeric HPV 16 VLPs containing E7 protein fused to

the C-terminus of truncated L1/L2 proteins, which is manufactured with Sf-9 or High Five<sup>TM</sup> insect cells. Any adjuvant is not included in this chimeric vaccine <sup>176</sup>. Another new 9-valent HPV vaccine for cross-protection, called V503, is in phase III trials among aged 16-26 year old young women in U.S. It could be safer than currently commercialized ones together with high immunogenicity (Reference: <https://clinicaltrials.gov/ct2/show/NCT01984697>). This vaccine is manufactured by Merck Company, which is developed to extend the coverage by use of VLPs from HPV type 6, 11, 16, 18, 31, 33, 45, 52, 58. Several clinical trials in the US are ongoing to analyse the immunogenicity and tolerability of multivalent V503 in naïve young adolescents with a 2-dose regimen to compare with *Gardasil*. This V503 vaccine could be highly impressive regarding its broad spectrum coverage of HPV types <sup>177</sup>.

The disadvantages of preventive vaccination are current concerns. The first and most intensive discussion is regarding the expensive expense for worldwide application of current licensed prophylactic vaccines. The fact is that anogenital infections and cancers overwhelmingly affect women in developing countries, where screening is not available. These two main protein-based vaccines, are unaffordable and undeliverable in the existing health programs of developing countries. The high costs of vaccination is caused by several reasons: 1. protein-based formulation; 2. refrigeration is required for storage; 3. large size population in developing countries; 4. lack of governmental and social economic support in developing area; 5. broad-aged immunisation targets among both male and female. 6 need for continued screening after the introduction of a prophylactic HPV vaccine, especially in



developing countries <sup>178,179</sup>. The cost becomes the major burden for extending vaccination worldwide. Fortunately, a vaccine alliance called GAvi started HPV vaccination projects for the middle-income countries since 2013 with a sustainable supply of HPV vaccines for about US\$ 4.5/dose compared with US\$ 100/dose previously <sup>180</sup>. It is a public-private global health partnership committed to increasing access to immunisation, but their effort still only covers limited population in middle-income countries <sup>18</sup>.

#### **1.4.2. Perspectives for therapeutic vaccine targets**

The urgent attention on HPV therapeutic vaccines is increasing on account of the vast number of HPV infected diseases in both men and women over the recent decade. Varied attempts from fusion protein/peptide formulas, chimeric VLPs, recombinant live-vector vaccines to DNA vaccines, as well as whole cell vaccines like DC-based vaccines and tumour cell-based ones, were failed to efficaciously dispel established HPV infection and lesions via current poor adjuvants and immunisation strategies <sup>129,181</sup>. Therapeutic HPV vaccines require prompting cell-mediated immunity rather than Nabs to eliminate HPVs before gene integration <sup>182</sup>. Beyond impressive immunogenicity inducible by the first-generation VLP vaccines Gardasil and Cervarix, the development of second-generation prophylactic vaccines is working to elicit more wide and active responses as a both prophylactic and therapeutic mucosal vaccine.

For some therapeutic vaccine targets, the E7 protein induces genotype-specific antibodies after the onset of invasive cervical cancer, which is not due to the immune response of host protective. Antibodies specific for the non-structural protein E7 could only be detectable in cases of invasive cervical cancer, after undergoing one to two decades of progression from chronic to invasive malignancy<sup>183</sup>. Besides, the E7 protein could induce protective cellular immunity associated with clinical and cytological resolution of HPV-induced cervical intraepithelial neoplasia (CIN)<sup>184</sup>. Activated E7 provokes the cell cycle actively even during the cell differentiation as long as undergoing viral genome replication<sup>185</sup>.

There is only evidence supporting the natural Ab response unique to E7 but not E6, whereas, the joint function of E6 and E7 is more efficient than their separated cell immortalization function<sup>56</sup>. Considering the co-function of E2, E6, and E7 in viral pathogenesis, they were highly targeted in therapeutic vaccine design to intervene cell immortalization and malignant conversion of infected cells<sup>30,186</sup>. Early replication proteins E1 and E2 are responsible for viral replication within keratinocytes before the viral-host gene integration, which are examined by some researchers for the clearance of low-grade HPV-infected diseases, like genital warts and low-grade dysplasia<sup>187</sup>. Recently E5 is also considered for vaccine design. Researchers noticed that E5 could stimulate cellular DNA synthesis in primary human keratinocytes while the proliferation and transformation caused by the activation of E6 and E7. Meanwhile, it can improve HPV activity and control viral persistence by inducing loss of surface major histocompatibility complex (MHC) I expression in the infected basal cells to avoid T-cell hunting, reduce inflammation

and escape from the other host immune <sup>188</sup>. Therefore, a novel chimeric VLP is highly possible to be applied as both prophylactic and therapeutic HPV vaccine associated with the promising induced cytotoxic T cell reactions and Nabs by fusing viral oncogenes in mice <sup>176</sup>. These Overall studies of vaccine targets, novel adjuvants and administration strategies, and tumorigenesis will benefit both preventive and therapeutic intervention synergistically.

## **1.5. DNA vaccination**

### **1.5.1. What is a DNA vaccine?**

Recombinant DNA technology refined “naked” DNA to produce small circular DNAs as “plasmids” in bacteria. Viral DNA is able to mediate certain cellular immunoresponse after internalisation into the host cells. Subsequent transcription and translation lead to viral protein expression via the endogenous MHC class I pathway. Interests in DNA vaccines began in the early 1990s, during this period ‘gene gun’ was invented and used for producing human growth hormone in mouse <sup>189</sup>. In the past 15 years, four DNA vaccine have been approved in veterinary medicine, targeting like horses, salmon, dogs and so on <sup>190</sup>. The pharmaceutical company, Merck, inject ‘naked’ plasmid DNAs i.m. to prevent influenza infection in mouse <sup>191</sup>. The use of plasmid vector for DNA vaccines possess impressive potentials to because various viral genes can be expressed from the vector.

The prime advantage of DNA vaccines is their persistent induced humoral and cellular-mediated immunity (Davies 2005, Ling 2000). The plasmid DNA vaccine could lead to expression of antigens from pathogens or tumors, which mimics natural antigen presentation after the endogenous process. Cell co-expressing MHC-I and the foreign/tumor antigens would be recognised and killed by macrophages, DCs and Tc cells. Subsequently, cytotoxic CD8+ and CD4+ lymphocytes are activated through MHC-I and MHC-II pathways, leading to strong cellular as well as humoral immunoresponses developed as a result of activation of T and B cells <sup>190</sup>. This efficacious immunogenicity could be induced by a low dosage (micrograms) of DNA vaccine. Commendable properties of DNA vaccines furtherly manifest in its safety, flexible engineering and manufacture, stability, long shelf-life and easy transport <sup>192</sup>.

The shortcoming of DNA vaccines identified through preclinical and clinical trials against various infection include the inconsistency, and unstable immunogenicity is due to the poor uptake of 'naked' plasmid DNAs by APCs following rapid DNA degradation of 'successfully-uptaken' consequence <sup>193</sup>. Therefore, adjuvants, formulations and more rational design of the plasmid vector have been all be considered in developing DNA vaccines <sup>194</sup>.

Plasmid DNA is cheaper and easier to produce and distribute <sup>182,195</sup>. Besides, pharmaceutical authorities claim that DNA vaccines are safer than live recombinant vaccines. Whereas the concern of injected viral DNA is about the possible integration of viral-host genes either activating oncogenes or inactivating tumour suppressor genes <sup>195-197</sup>. Therefore, a need of improved immunization strategies and

mutated viral genes to both maintain the critical epitope structure and eliminate the potential for integration or oncogenic transformation <sup>196</sup>.

To lessen the limited potency of DNA vaccine lays emphasis on prime-boost strategies like adjuvant improvement. In the last decade, HPV L1 DNA vaccine studied in South Korea fused a chemokine and secretory signal peptide as DNA encoding immunostimulator <sup>198</sup>. Tobery's study comparing various prophylactic HPV DNA vaccines in monkeys showed a better cell-mediated response than Nab elicitation, which indicate the higher potentials of HPV DNA vaccines in therapeutic treatment rather than prevention <sup>199</sup>. Recombinant live vector was applied to delivery and stimulate DNA antigen expression in other studies <sup>200</sup>. Apart from adjuvants application, researchers have tried different targeting strategies to enhance the effectiveness, especially for therapeutic purposes. For example, Johns Hopkins University commenced a preclinical research before consisting of intracellular targeting strategies, intracellular spreading strategy and targeting co-administering antiapoptotic factors, to enhance the expressing and survival of APCs and DC <sup>201</sup>.

### **1.5.2. Application of gold particles in DNA vaccination**

One of the earliest DNA vaccination involved in the injection of genetically engineered plasmid DNA carrying the human growth hormone. Injection of this naked DNA into the ears of 5-8 week-old mice resulted in the production of specific antibodies against human growth hormone <sup>189</sup>. Further application derived from this

“gene gun” idea is needle-free vaccination using gold particles against various type of infections. But this technique only achieved significant immunogenicity with a whole profile including binding antibody, neutralizing antibody, CD8 and CD4 with HIV-2 DNA vaccines in nonhuman primates <sup>202</sup>. An intriguing recent development is the use of particle-mediated epidermal delivery (PMED) of DNA vaccine <sup>203</sup>. It involves in the use of needle free “gene gun” to deliver gold particles coated with DNA plasmids encoding vaccine antigens into the epidermal layer of the skin. The PMED has been demonstrated as a safe and well-tolerated immunization platform with mild dermal reactions in clinical trials. The antigen delivered by PMED include SIV and SIV antigens. It has further merits in inducing immunoresponse without boost or adjuvants, and remains stable for storage at room temperature (RT) after gold particle precipitation.

Since the DNA vaccine requires a nuclear localisation before expression of the antigen, the delivery role of functionalized GNRs gives consideration to the DNA release occasion. Size and coating layers will influence both the cellular uptake and expression of DNA. GNPs sized 30 nm provide impressive cell-membrane penetration by endocytosis and micropinocytosis and affinity for DNA, RNA and endoplasmic reticulum in the cells <sup>204</sup>. Studies revealed endosomal trapping and cytoplasmic localisation of small GNPs disrupting the DNA vaccination <sup>205</sup>. However, after internalization of functionalised GNPs, GNPs mainly localized in the cytoplasm and perinuclear region, which produced accumulated vacuoles near the nucleus with no-toxic up to hundreds  $\mu\text{g/ml}$  <sup>206</sup>. Delivery of functionalised GNPs

shift from nucleus to endoplasmic reticulum is highly influenced by the diameter of engineered particles and the density of biomolecules<sup>204</sup>.

There are two promising DNA vaccines based on gold nanorods (GNRs) delivery system studied in this decade to prevent HIV infection and respiratory syncytial virus (RSV). Surface modified GNRs as adjuvants for HIV/AIDS vaccines promoted significant cellular and Nabs –mediated immunity with inflated T cell proliferation via APC activation<sup>207</sup>. Cationic polymer coating surface of GNRs, like polyethyleneimine (PEI) or poly(diallyldimethylammonium chloride) (PDDAC), assessed in this study, is potent to reduce the cytotoxicity of nanomaterials<sup>208</sup> and enhance DNA transfection and release<sup>209,210</sup>. The properties of these GNRs will be furtherly discovered in the next chapter. Their promising and reliable features as vaccine adjuvants include boosted antigen-specific IFN- $\gamma$  induced cellular immunity, the proliferation of CD3+CD4+ T helper cells, and especially pronounced DC maturation (CD11c<sup>+</sup> MHCII<sup>+</sup>CD86<sup>+</sup>CD80<sup>+</sup>) stimulated by PDDAC<sup>207</sup>. PEI without GNRs conjugated with TianTian viral DNA expressing HIV-1 delivered via intranasal priming, demonstrated the potent induction of both strong T-cell mediated and striking Nabs responses in the early year<sup>211</sup>. Therefore, there are profound synergistic adjuvant effects between surface coating and GNRs delivery system. Like the RSV DNA vaccine, which using glycoproteins as GNRs covalent coating surface is capable of achieving a dispersed particle population to enhance significant T-cell activation in *in vitro* study<sup>212</sup>.

## **1.6. Aims of the project**

The high cost of current VLP vaccine is the major obstacle in promoting worldwide vaccination against HPV infection. Developing an innovative cost-effective and convenient HPV vaccine platform the entire goal of this project.

The pioneer HIV-PMED development has established the feasibility of using nano-sized gold particle as a carrier, which exhibited enhanced cellular uptake and expression of HIV-1 plasmid DNA, significantly improved immunogenicity and increased DC maturation in mice model <sup>207</sup>. The immunisation strategy is delivering DNA vaccine through intranasal immunisation additional to a further assessment of remarkable mucosal adjuvant cholera toxin B subunits <sup>213</sup>. The specific goals include: 1) Genetic engineering of the plasmid vector for expressing HPV type 16 L1 protein; 2) Demonstration of L1 protein expression in transfected cells; 3) Demonstration of the safety via intranasal immunisation using mice; 4) Demonstration of the immune responses from immunised mice.



## 2. Synthesis of DNA-Gold Nanorods

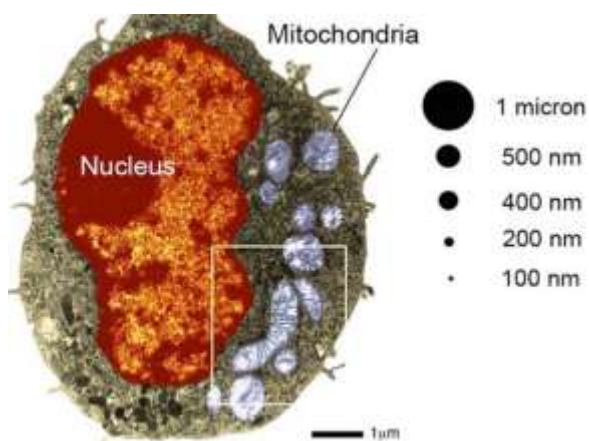
### 2.1. Abstract

DNA-GNR base vaccines has been reported for development of HIV vaccines<sup>207</sup>. In this study, I took similar strategy and functionalized surface-coated GNRs with circular plasmid DNA that carried entire coding sequence of HPV 16 L1, which is optimized for expression in human cells. By coating GNRs with either of the two cationic polymer: poly-(diallyldimethylammonium chloride) (PDDAC) or polyethyleneimine (PEI), the negatively charged plasmid DNAs were firmly conjugated to surfaces of the GNRs. The plasmids were constructed in the backbone of pcDNA3 YFP. The expression of HPV 16 L1 gene is driven by the promoter pCMV. A second version of the plasmid also carried the *E. coli* heat labile enterotoxin B subunit (*ELtB/ELT*) gene down-stream to the L1 gene. ELT gene is a known potent immune-stimulator for mucosal immunity. The work of this chapter includes: 1, surface modification of GNRs; 2, cloning HPV 16 L1 gene or 16 L1 and *eltB* into pcDNA3 YFP; 3, surface-functionalization of GNRs with engineered plasmid DNA. The end products were: PEI-GNRs-pcDNA3 Y/CFP L1 (PE-G-L); PEI-GNRs-pcDNA3 Y/CFP L1-ELT (PE-G-EL); PDDAC-GNRs-pcDNA3 Y/CFP L1 (PD-G-L); and PDDAC-GNRs-pcDNA3 Y/CFP L1-ELT (PD-G-EL). These products were tested *in vitro* and *in vivo* in following chapters.

## 2.2. Introduction

### 2.2.1. Nanoparticles (NPs)

Nanotechnology has brought the more in-depth discussion about matters onto a scale of 1 to 100 nanometers (nm). It covers a broad range from atomic to molecular and supramolecular level, which has significantly advanced modern molecular biology. Figure 5 illustrates size comparison of nano-scale particles in respect to the size of organelles in a rat macrophage, which is usually larger than 1  $\mu\text{m}$ . The diameter of human red blood cell is generally around 10  $\mu\text{m}$ . In microbial world, bacteria are around 0.8 microns; a Vaccinia virus is about 200nm, and most viruses are about 50nm. The thickness of a cell wall is in a smaller scale around 12.9 nm. Particles smaller than 12nm in diameter could pass the blood-brain barrier<sup>214</sup>. The majority of the organic matter are on the nano-scales: antibodies are roughly 10nm in diameter, DNA strand is about 2nm wide, glucose is about 1nm in diameter.



**Figure 5 - Size index of a rat macrophage comparing micron- to nano-scale.** The rat macrophages are half size of human macrophages. This TEM image was produced by Environmental Health Perspectives, and reproduced by (Buzea et al., 2007).

The atom measurement is  $10^{-10}$  meters, the nanometer equivalent to  $10^{-9}$  meter-scale could be applied to investigate the molecule functions across atom level. Interestingly, the physio-chemical properties of nanoparticles (ranging 1-100nm), do not restrict to the original definition of the material but exhibit unique feature according to the size and shape of the composition of nanoparticles-molecule. This feature is due to specific atom positions of materials on nano-scale <sup>215</sup>.

Modern technology allows synthesizing particles in nanoscale. Nanoparticles (NPs) are solid colloidal particles with nano-size in diameters. NP techniques complement the traditional research insight about the application of small-scale single cellular molecules, like enzymes, proteins, and nucleotides <sup>216,217</sup>. One example is the intracellular delivery of nucleic acids for gene regulation. The use of spherical nucleic acids (SNAs) for delivering small interference RNA (siRNA) has enabled practically gene regulation. Densely packed oligonucleotides increase cell endocytosis uptake, leading to knockdown the expression of particular genes and prevent the construction of main disease proteins. NPs of this kind of packed arrangement of single molecules may boost the bio-application and life-science discovery by structure change into a 3D architecture <sup>218</sup>. In short, the engineered nanomaterials are suitable for broad applications ranging from gene therapy and drug discovery to fundamental research.

Moreover, modified NPs take advantage of certain physio-chemistry properties, including photo-physical properties suitable for bio-imaging and thermal-therapy. Research shows that the photo-physical properties of nano-materials are highly

dependent on their size and shape, which is usually not the case for matters in a larger scale (> 100 nm) or as a single organic molecule. Therefore, nanoparticles made of different materials with distinctive shapes and size could compose with various complex objects for distinct purposes <sup>219</sup>.

### **2.2.2. Physical properties of gold nanorods (GNR)**

Gold nanoparticles (GNPs) are gold colloid in nano-scale between 1nm to 100nm. One can synthesize GNPs in diverse structures with various traits in the forms of capsules, tubes, dots, rods, spherical-shaped, wires and fibres, which may be used in experiments of physical chemistry and biochemistry <sup>220-221</sup>. Electrochemical method and seed-mediated synthesis are the two primary methods to synthesize gold nanorods (GNRs) <sup>222</sup>. The approach of adding silver nitrate into the growth solutions was designed by Jana and co-workers <sup>223</sup>, and improved by Nikoobakht and El-Sayed <sup>224</sup> for massive GNRs yields with desirable monodispersity and finely tuned aspect ratios of rod shape <sup>225</sup>. Adjusting the concentration of silver ions and cetyltrimethylammonium bromide (CTAB) in the growth solution is one quick and convenient way to obtain desired optimal length-to-width aspect ratio <sup>226,227</sup>, which optimizes the required optical properties and enhances application potential <sup>228-230</sup>. Polar headgroup attached CTAB was reported as a stabilising surfactant as a bilayer surrounding the gold nanocrystal to create aqueous dispersibility <sup>231</sup>. Iodide concentration in the CTAB growth solution mediates nanorod formation as an inhibitor to adjust the aspect ratio <sup>232</sup>. The iodide impurity in CTAB is variable with the supplier.

Additionally, there are appealing chemical properties of GNPs. GNPs obtain lower melting point and resistance to electricity. At the beginning of the current decade, control of shape and size in the synthesis of monodisperse nanoparticles with large quantities was the primary challenge. The experimental conditions of temperature, reaction time, the concentration of reagents, and the molar ratio between capping reagent and reducing agent became main obstacles in synthesising GNPs with required the geometric shape and dimensions of the product <sup>233</sup>.

#### **2.2.2.1. Mie scattering theory and special surface plasmon resonances of GNRs**

Particle responses to emitted light by setting discrete electric charges (electrons and protons) in oscillation induced by an interacting electromagnetic field with emitted lower secondary radiation as scattering. The extinguished scattering between the incident light beam and incident radiation is absorbed by the particle, which is termed extinction. Metal gold nanoparticles, the gold nano-sized colloidal solution as a prominent inorganic luminescent material have a long life-time and high intensity of absorption and scattering due to the surface plasmon resonance (SPR) <sup>215</sup>. The resonances of collective oscillation of the free conduction electrons are manifested as SPR <sup>228</sup>.

The most important fundamental formulation theory of particle-light interaction applied in this work is based on Mie theory developed by Gustav Mie in 1908 based on the study of spherical particles<sup>234</sup>. Mie theory quantifies the SPR by simplifying Maxwell's equations theoretically of all electric and magnetic multipole oscillations on particle surface by the total light extinction cross section resulted in absorption and scattering<sup>235,236</sup>. According to the mathematical calculation based on the emission of the light beam and light path, the particle geometrical morphology, and radius associated with surrounding medium could be analysed<sup>237</sup>. For the small NPs sized smaller than 20nm and  $\lambda$  wavelength of the exciting light smaller more than 25nm<sup>228</sup>, SPR is quantitatively described as following equation:

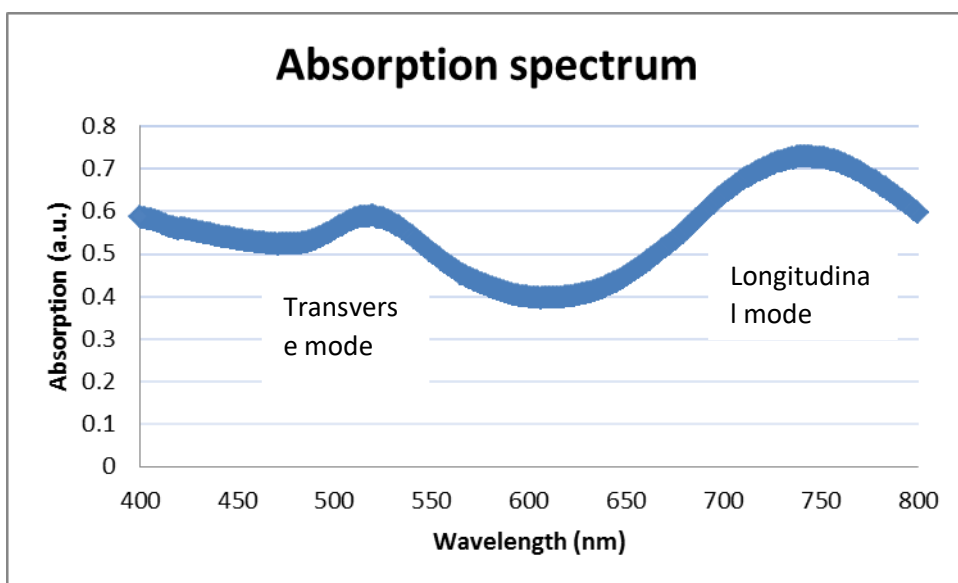
$$(2.1) \quad C_{\text{ext}} = \frac{24\pi^2 R^3 \varepsilon_m^{3/2}}{\lambda} \frac{\varepsilon_i}{(\varepsilon_r + 2\varepsilon_m)^2 + \varepsilon_i^2}$$

Where  $C_{\text{ext}}$  is the cross-sectional extinction,  $\lambda$  denotes the wavelength of the incident light. Symbols  $\varepsilon_r(\omega)$  and  $\varepsilon_i(\omega)$ , where total  $\varepsilon = \varepsilon_r(\omega) + i\varepsilon_i(\omega)$ , describe the real part and the imagery part of the dielectric function of the metal material,  $R$  is the diameter of the sphere, and the  $\varepsilon_m$  depicts the dielectric constant of the surrounding medium, related to the refractive index of the medium by  $\varepsilon_m = n_m^2$ . The occurrence of SPR resonance takes place when  $\varepsilon_r(\omega) + 2\varepsilon_m = 0$  with the maximum extinction  $C_{\text{ext}}$ , which means the change of surrounding medium resulted in variation of both  $\varepsilon_m$  and  $\varepsilon_r$ .

Thus a slight change of particle size distribution and radius causes dramatically quantitative fluctuation in light spectrum of extinction, absorption, and scattering.

The UV-vis absorption spectrophotometer is able to analyse the plasmon absorption on NPs corresponding to extrinsic size effect, which calculates the homogeneous size distribution of GNP samples as a plasmon bandwidth with absorbance referred particle density <sup>228</sup>. Studies explicitly demonstrated the shift of plasmon absorption maximum towards longer wavelength with the increasing radii of NPs <sup>228,238</sup>. Based on the findings of NP size-change providing more spectra shift of scattering to the total extinction, researchers also have illustrated the thickness of chemical or biomolecular layer contributes similar but more sensitive influence of scattering peak shifts than absorption and extinction <sup>238</sup>, which conduct a further application of metal NPs as advanced optical biosensors.

For an optical biosensor, SPR determines the property of metallic nano-structured materials, according to the change in refractive index of the metal surface to adjacent transmitter/medium. SPR is essentially influenced by the distance and position between the receptor molecules and transmitter <sup>239</sup>. SPR spectroscopy generates a sensitive detection to exploit the images based on the specific absorption spectra of size/shape dependent metal nanoparticles and the applied ambient circumstance <sup>240</sup>. GNPs with one diameter, like gold nanospheres (GNSs) exhibit a peak value of particles' optical extinction with plasmon resonant frequency, which varies according to size, shape and surrounding medium of the materials.



**Figure 6 - An absorption spectrum of GNRs exhibits two distinct surface plasmon modes according to the transverse and longitudinal lengths.**

GNS solution due to its SPR generated in the visible spectral region at approximately 520nm displays as a red liquid. GNRs could provide two distinct surface plasmon resonances, depending crucially on their specific aspect ratio (Figure 6). The free electrons oscillated along the long and short axis of GNRs provide an intensive SPR band in both near-infrared region (NIR) and a weak band in the visible region<sup>228,241</sup>. Overlapped frequency of GNRs' longitudinal surface plasmon resonance with the laser excitation wavelength, exhibit a peak value of electromagnetic enhancement in absorption spectrum<sup>241</sup>.

#### **2.2.2.2. Synthesis process and adjustable properties of GNPs**



The GNPs could be prepared with flexible nanostructures, size, composition, assembly and encapsulation through chemical reactions. The production of GNRs is a growth solution adjusted seed-mediated approach. In wet chemical methods of GNP synthesis, the presence of CTAB plays the critical role as a cationic surfactant to help the growth of sphere-shaped GNPs toward rod-like shape by facet-sensitive surface adsorption, and prevent the aggregation of GNRs<sup>242</sup>. A mixture of gold salt, silver nitrate, ascorbic acid and CTAB is added to spherical seed nanoparticles, through which silver nitrate adjusts the length leading to under-potential deposition of silver on the GNR surface<sup>243</sup>. Furthermore, the use of aqueous H<sub>2</sub>AuCl<sub>4</sub> solution that reacts with silver templates in synthesising GNPs has resulted in the production of pure GNPs with distinct morphologies<sup>233,244</sup>. Increasing the silver concentration aids to adjust the aspect ratio (ratio of the longitudinal length of GNRs over transverse length up to 4.5<sup>224</sup>). Precision in time control and the reaction medium during the synthesis process allow production of GNPs from spherical to rod-shape with different size of gold, which was mentioned earlier<sup>225,245</sup>.

Meanwhile, the longitudinal surface plasmon resonance of GNRs could be finely tuned by adjusting the concentration of silver ions as mentioned before. Previous observations demonstrated that functionalized gold nanorods exhibited a higher potential to improve the detecting intensive efficiency than gold nanospheres (GNSs). Modification of the concentration of GNRs could also tailor the extent of red-shift of the longitudinal plasmon band to the ideal peak for bio-application<sup>225</sup>. The biological tissue has high penetration in the NIR-spectral region between 650-900nm. The

water and biomolecules have minimal absorption in this region. In contrast, longitudinal plasmon mode of GNRs above 600 nm is tuneable. Additionally, GNRs have strong electric fields, and maintain lowest energy loss at the wavelength near 700nm. The anisotropic shape of nanoparticles creates distinctive chemical affinities for different crystallographic assembly faces<sup>222,246</sup>, which provides GNRs prefer to an end-to-end packing rather than side assembly<sup>247</sup>. Simple dipole-dipole “selection rules” for the plasmon coupling was described by Jain et al. to explain the optical change of plasmon modes with a slight change in GNP geometry after assembly. Moreover, the tunability of GNRs plasmon exhibits as a more detectable red-shift in the longitudinal mode with end-to-end assembly morphology, and a blue-shift of side-by-side geometry<sup>248,249</sup>. The structural control of the conformational transition of surface coating provides distinctive properties in GNP bio-application.

Another coating polymers I am introducing here are polymer-(polystyrenesulfonate (PSS) and poly (diallyldimethylammonium chloride) (PDDAC). Negative-charged PSS has been used in the medium coating for multilayer coating system<sup>250</sup>. This kind of layer-by-layer polyelectrolyte coating could modify the surface charge and condition of GNPs, making it suitable as functionalized probes in biomedical research<sup>251</sup>. It is noteworthy that embedded organic PSS will cause an observable blue shift of absorption bands due to a possible effect of quantum confinement revealed by some previous studies, and the size change could be estimated via the values of the blue-shift plasmon mode<sup>252,253</sup>. Since GNP is positive-charged due to CTAB, cationic PEI/PDDAC polymer requires another negative-charged surface

layer for electrostatic interaction, these coating methods produce a layer-by-layer functionalized GNPs.

In conclusion, the gold material can be easily synthesized by simple chemical reactions. This metal material causes low oxidation, which has an absolute advantage as a bioengineered material. With a change of size, shape, length-width ratio and reaction solution, the phenomenon of surface plasmon resonance (SPR) allows the adaptive and controllable optical properties of gold nanoparticles<sup>230</sup>. The variability of size and shape of GNPs results in distinct optical resonances referring to the intensity of scattering. The high-scattering cross-sections of GNPs own the high potentials to improve the study of bioimaging and photothermal therapy (Ling et al., 2009; Huang et al., 2006; Huang et al., 2008).

### **2.2.3. Bio-application of GNPs**

The promising extensive application of GNRs due to their significant physical advantages comparing to GNSs<sup>220</sup>. Their optical extinction dropped in NIR offers a better optimal light penetration in NIR (650-900nm), where tissue absorption is minimal. Seed-mediated growth approach was well-developed for easily size-manipulated GNRs with stable structure, tuneable longitudinal plasmon mode, large oscillator strength, high yield and monodispersed morphology. The asymmetrically structured nanorods can assemble into numbers of alternatively aligned configurations providing optical anisotropy properties for bio--photonic application.

### **2.2.3.1. Imaging benefits of GNP**

Optical observation is one of the most important strategies to understand the mechanism of biology. Sapsford has reviewed several benefits of imaging-applied nanoparticles, in particular, high fluorescence intensity, cost effectiveness, and convenient synthesis procedure<sup>257</sup>. In physics, the optimal NPs have peak absorption in the NIR, which could obtain deep light transmissivity<sup>258</sup>. Therefore, the initial application of NPs in bio-imaging is to increase the NIR contrast of targeted organelles<sup>259</sup>.

Through application of nano-biochemical and molecular methods, nanoparticles open up a new era for drug delivery, biosensor study, gene therapy and enhanced electromagnetic fields in medical diagnostics<sup>215, 260</sup>. The capability of imaging and contrast agents is the backbone to achieve bio-imaging between different cellular or sub-cellular organelles. The conventional imaging agents represented by lanthanide chelates and organic fluorophores have defects and restriction. NPs have advantages to overcome the obstacles of traditional agents including high cost, complex producing process, photobleaching and broad emission window.

Metallic NPs like GNPs are inexpensive and simple nanofabricated optical sensing materials, which can be substitutive for fluorescence imaging. GNPs provide intensive real-time fluorescence detection, which has been used in transcriptomic and proteomics<sup>261</sup>. For imaging purpose, the absorption of a gold nanostructure, which

depend on its scattering property, broadly cover both the visible region of spectrum and the near-infrared region, which results in a sharper imaging contrast,<sup>215</sup>. Therefore, due to the intensively enhanced scattering in the NIR, conjugated GNRs-antibodies complex provided a clear cell imaging when it was used as a contrast agent by conventional dark-field microscopy<sup>255</sup>. In conclusion, GNPs have become an increasingly popular bio-imaging tool in past two decades with different shapes (tubes, spheres, cages, shells, and rods) in nanoscale size to produce a stable light effluence and surface enhanced fluorescence.

For NIR imaging, GNRs are more ideal than GNSs as mentioned in previous section<sup>226</sup>. Especially, the short axis of GNRs provides a transverse resonance, and the long axis elicits a longitudinal resonance towards infrared wavelength. This property makes GNRs extremely attractive for biomedical optical imaging to cover the low-energy visible to near-infrared wavelength regions<sup>225</sup>. Besides, NIR imaging may exploit the utilization of two-photon luminescence microscope which enhances luminescence detection<sup>262-267</sup>. Furthermore, due to the photo-thermal effect, GNPs were practiced in photoacoustic imaging study<sup>258</sup>.

#### **2.2.3.2. GNPs application in photo-thermal therapy**

For clinical studies, a significant advantage of GNP in the targeted photo-thermal therapy for cancers depends on their unique and tunable optical properties, i.e. intense surface plasmon absorption and rapid photo-thermal change. Light energy transforms into heat during surface plasmon resonance<sup>268</sup>. Benefitted from the

enhanced scattering of GNRs caused by strong SPR with narrower bandwidth, cancer cells could be separated from the healthy cells by a conventional light-scattering microscopy under dark-field. Apart from the photothermal properties of NPs, drug-containing NPs provide very promising intracellular delivery systems for noble therapies, including gene therapy<sup>204,269,270</sup>

#### **2.2.4. NPs as drug adjuvant**

##### **2.2.4.1. GNPs functionalized DNA complexes**

Using nucleic acid, protein and polymer to modify the surface of GNPs could improve the biocompatibility of living material. The bio-conjugation of GNRs to biological molecules could achieve advanced imaging functions. Researchers modify GNPs using variant proteins, such as bovine serum albumin<sup>225,271,272</sup>, monoclonal antibody<sup>225</sup> and peptides<sup>273</sup> by electrostatic and hydrophobic methods. Coated GNPs conjugated with peptides not only enhance the uptake of proteins, but also enhance immune responses by improving the recognition of distinct proteins by APCs<sup>273</sup>. The conformational change after GNP conjugated peptides improves the cell recognition and response in the immune system to provoke the induction of pro-inflammatory cytokines. The type of biochemical reaction corresponds to both of peptide morphology and the assembly structure of the peptide-coated GNPs rather than peptides or GNPs alone<sup>274</sup>. The coated protein can be analytic molecules or antigens for intracellular interactions analysis in drug discovery<sup>216,239</sup>. DNA-GNPs conjunctions (including oligonucleotide-GNPs) increase the detection and interaction between functional oligonucleotide, DNA/RNA base pairing<sup>207,275</sup>. The optimal size

of colloidal gold also enhances its binding affinity with bio-coating molecules. In one study evaluated GNPs (with several different sizes including 30nm and 50nm), have demonstrated more proteins conjugated with 30nm GNPs but not the ones more than 50 nm <sup>276</sup>. The adjuvants above 12nm and below 50nm are ideal for maintaining a high transfection ability without permeabilization of the blood-brain barrier. Size-dependent GNP bio-application will be furtherly illustrated in the *in vitro* study.

#### **2.2.4.2. Polymer-functionalized DNA complexes**

Polyethylene glycol (PeG) is another common organic coating polycations, which can avoid macrophage recognition and phagocytosis with a prolonged circulation and enhanced permeability in cell experiments <sup>277-279</sup>. PDDAC-coated GNRs obtain higher positive surface charge than PeG coating, the higher affinity and uptake efficiency provided by PDDAC is able to enhance its adjuvant ability in drug delivery and antigen presentation <sup>280</sup>. PDDAC and PEI modified GNRs driven HIV-1 plasmid DNA significantly elicit both cellular and humoral immunity in contrast with the naked DNA <sup>207</sup>.

Foreign naked DNA or RNA is degraded by endogenous enzymes quickly after internalization. Therefore, limited naked nucleic acids will be internalized in the cell and expressed. NPs provide new ways for intracellular-targeted drug delivery, which exploit variant strategies intracellularly to an achieve successful delivery outcome. It can be further introduced in the section of intracellular investigations. NPs include VLPs, liposomes, polymers, non-degradable NPs and other immune-stimulating

complexes (ISCOMs) that modulate the immune responses by stabilizing vaccine constructs and delivering genetic materials to APCs by distinct pathways<sup>281</sup>.

One widely used polymeric delivery system for gene therapy and vaccination is PEI-DNA/RNA complexes<sup>211</sup>. Polyethylenimine (PEI) represented polycations are formed into a nanoscaled complex containing DNA or RNA. It is able to elicit immune responses for balanced Th1/Th2 immunostimulatory functions, CD4+ and CD8+ T cells<sup>282</sup>. This polycation enhances the production of high levels of antibody against the encoded protein<sup>283</sup>. Obviously, different adjuvant-antigen complexes elicit distinct different systemic immune-response profiles, which would also be affected by the immunization route<sup>284</sup>.

Despite the high-charge density PEI provides successful gene delivery with high transfection efficiency. Some experiments demonstrate noticeable cytotoxicity caused by polycationic<sup>285</sup>. High-dose free PEI can cause the death of mice and several adverse reactions, including a possibility of dysfunction in Alzheimer's disease due to inappropriate membrane permeabilization by free polycations with high molecular weight<sup>286</sup>. However, several experiments demonstrated that the conjugated PEI with other adjuvants or DNAs shows highly reduced cytotoxicity by highly reducing the free poly-dispersed PEI without changes in surface charge concentration or eliminating its outstanding buffering capacity<sup>282,287</sup>.

#### **2.2.4.3. *Escherichia coli* heat-labile enterotoxin B subunit (ELT/EltB) as DNA adjuvant**



A well-known protein adjuvant is *Escherichia coli* (*e.coli*) heat-labile enterotoxin B subunit ELT, which is genetically and functionally related to cholera enterotoxin B subunit (CtxB) from *Vibrio cholerae*<sup>288,289</sup>. ELT can enhance immunogenicity of attenuated live bacterial vaccines (like recombinant *Salmonella*-HIV and *Shigella*-HPV), and DNA vaccine against viral infections and tumour, especially when it was given at the prime stage in mice model<sup>290-292</sup>. Plasmid expressed CtxB has been used as an adjuvant for intradermally administering DNA vaccines, which not only enhance mucosal immune responses but also improve Th1-mediated cellular responses, as well as mucosal tolerance for prophylactic vaccines against autoimmune diseases<sup>293-295</sup>.

### **2.3. Aim**

Taken information above, two cationic polymers (PEI/PDDAC) has been used in synthesizing GNRs, and *eltB* gene has been cloned in one version of the HPV 16 L1 expression plasmid. The resultant vaccine constructs were tested *in vitro* and the mouse model for cell uptake, protein expression, and immunogenicity.

## **2.4. Material and Methodology**

### **2.4.1. Synthesis of Gold Nanorods**

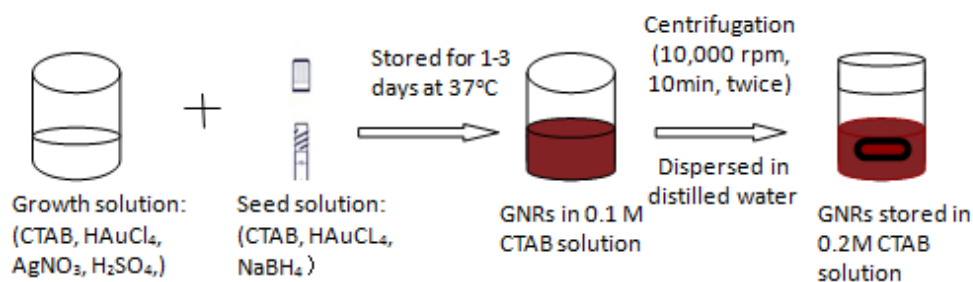
The Gold nanorods (GNR) was produced according to seed-mediated synthesis<sup>296</sup>. Size adjusted between a ratio from GNSs to GNRs by changing the concentration of Au<sup>+</sup> ions and the cetyl trimethyl ammonium bromide (CTAB) surfactant (Sigma-Aldrich, UK).

The GNRs synthesis procedure was modified according to a previously established protocol in our group to obtain GNRs with a length at 40nm and an aspect ratio about 1:3 (transverse/longitudinal)<sup>297</sup>. The synthesis procedure for the PDDAC/PEI surface-functionalized GNRs illustrated in Figure 7 was comprised of two pivotal steps: 1: Synthesis of GNRs using seed-mediated growth approach; 2: Polymer coating to produce functional saturated assembled surface layers. The seed-mediated synthesis of GNRs required to prepare seed solution first and add a certain amount of seed solution into the growth solution. The concentration of these two solutions was dependent on the final size of GNRs willing to be produced.

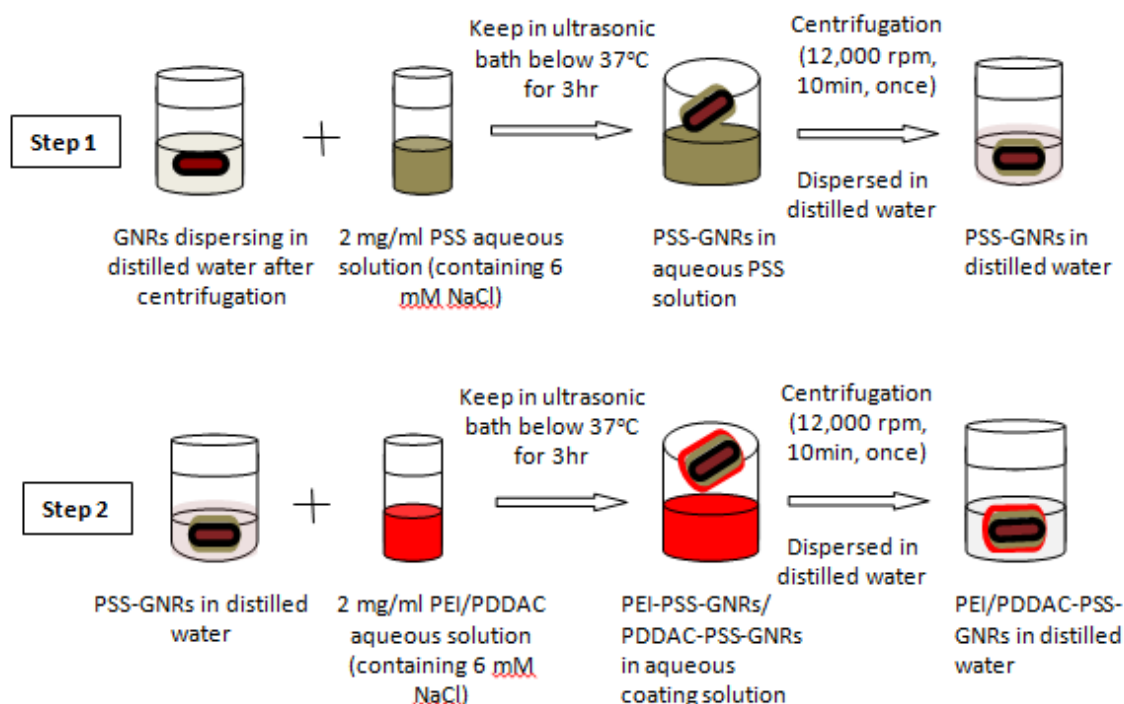
For seed solution (Figure 7), 7.5ml of 0.2M CTAB were stirred with 2.5 ml of 0.01M HAuCl<sub>4</sub> for 5 minutes. Then 0.6ml of 0.01M ice cold NaBH<sub>4</sub> were added into the seed solution slowly and kept stirring for 2 minutes till the solution turned a brownish colour. The second step was for the preparation of growth solution. 50ml of

0.2M CTAB mixed with 50ml of 0.01M H<sub>2</sub>AuCl<sub>4</sub> and was stirred till the colour changed from yellow to orange. For synthesizing GNRs with a longitudinal wavelength near 830nm, 2ml of 0.04M AgNO<sub>3</sub> were added together with 700µl ascorbic acid (0.0778M) into the growth solution. After the mixture turned colourless, 80µl seed solution was added into the growth solution. The GNRs solution was kept in 37°C until particles obtained the optimized wavelength. The final concentration of GNRs was estimated by optical density (OD) with as absorbance reading value, which was adjusted into approximate 1.0 with a wavelength between 800-830 nm<sup>297</sup>. Except for the cytotoxicity analysis, other batches of GNRs alone applied *in vitro* and *in vivo* study were centrifuged twice before the experiment.

### Synthesis of GNRs:



### Polymer coating:



**Figure 7 - A scheme illustration of the synthesis process of PEI-GNRs (PE-G), and PDDAC-GNRs (PD-G).** The colours are for coding not presenting the real colours of the solutions. GNRs were produced by a mixed incubation of seed solution into growth solution at 37°C for 1-3 days to obtain size-specific GNRs with a 1:4 transversal/longitudinal length ratio and near 800nm absorption spectrum. The final operation time and concentration were modified according to two previous protocols and the quality of reagents provided by chemical manufacturers<sup>207,250</sup>. (10,000 rpm - 9,600g; 12,000rpm- 13,900g)

Further coating work was proceeded via electrostatic layer-by-layer growth using PSS and PEI/PDDAC<sup>207</sup>. Negatively charged PSS provided an intermediate coating layer for cationic PEI or PDDAC electrostatic assembly. All particles were centrifuged at 12,000 rpm (13,900 g, Thermo Scientific Heraeus Fresco 17) for 10 min to remove the excess CTAB/polymers and re-dispersed in deionized/distilled water with a final concentration around 10M. The second layer was assembled on the surface of GNRs after removing the excess CTAB by centrifugation. GNRs precipitation was dispersed into 2mg/ml PSS aqueous solution containing 6mM NaCl in a concentration of OD equivalent to 1.0. The solution was stirred for 3 h in an ultrasonic bath at 37°C. The third layer is PDDAC (Sigma-Aldrich, 409014) or PEI (Sigma-Aldrich, 408727) coating, which was processed same as PSS coating. OD of GNRs was adjusted using distilled water according to the absorption value according to spectrum estimates after each process. Spectrum analysis was assessed after each coating step by an absorption spectrometer (V-660 Spectrophotometer, JASCO).

#### **2.4.2. Purification of plasmid DNA from *E. coli***

This step was carried out using QIAprep Spin Miniprep (QIAGEN). Bacteria from L-broth culture were collected in 1.5ml Eppendorf tubes by centrifugation at 13,000 rpm (16,200 g) for 3 min at room temperature, and the supernatant was discarded. Bacteria were re-suspended in the 250 µl Buffer P1 by a pipette, and 250 µl of buffer P2 was added to lyse the bacteria for 5 min. 350 µl Buffer N3 was used to neutralize the pH by inverting the tube several times. The mixture was centrifuged for 10 min at 13,000 rpm (16,200 g). Clear supernatant from above step was applied to a QIAprep

spin column, centrifuged for 1 min. Flow-through was discarded, and the column was washed by 0.5ml buffer PB, followed with 0.75ml buffer PE. DNA was eluted by addition of 50  $\mu$ l dH<sub>2</sub>O on the column and centrifugation. The DNA concentration was measured using Nanodrop, 2000C (Thermo Scientific). Buffers obtained from QIAGEN following general formulas of P1 (50 mM Tris-HCl pH 8.0, 10 mM EDTA, 100  $\mu$ g/ml RNaseA), P2 (200 mM NaOH, 1% SDS), N3 (4.2 M Gu-HCl, 0.9 M potassium acetate, pH 4.8), and PB (5 M Gu-HCl, 30% isopropanol).

### **2.4.3. Agarose gel electrophoresis**

Agarose gels (1%, w/v) were prepared at concentrations in 1X TAE buffer and 0.05  $\mu$ l/ml gel stain (SYBR, 10,000X, in DMSO). The DNA samples were mixed with a 20% volume of DNA loading dye (30% glycerol and 0.25% Br-phenol Blue), and loaded on the gel. DNA bands were separated at 100V, 79mA 30 mins. DNA bands were visualized by UV illumination ( $\lambda = 260$  nm) and the images were recorded with a gel documentation system (DigiGenius, Gel-Doc, Syngene).

#### **2.4.3.1 DNA recombination**

*E. coli* strain DH5 $\alpha$  and JM109 were routinely grown on Luria-Bertani agar (L-agar) plates at 37°C overnight. Colonies were picked to grow in nutrient broth in at 37 °C with shaking (250 rpm) to the early stationary phase for competent cell preparation.

Ampicillin (Sigma-Aldrich) was added to reach a final concentration of 100 µg/ml for the maintenance of plasmids.

#### **2.4.3.2 Competent cells preparation**

Bacteria from mid-log phase were chilled on ice and harvested by centrifugation followed by 2X washes with chilled sterilized distilled water and 2X washes with cold sterilized 10% glycerol. All the procedures were completed at 4°C. Cell suspension 10% glycerol was aliquoted (70µl per aliquot) and stored in -80°C or used immediately for electroporation using Gene Pulse (BioRad). Cells were recovered after electroporation with 1ml SOC medium and incubated for 1 h at 37 °C with shaking 250 rpm. The components of SOC medium include 0.5% Yeast Extract, 2% Tryptone, 10 mM NaCl, 2.5 mM KCl, 10mM MgCl<sub>2</sub>, 10mM MgSO<sub>4</sub> and 20 mM Glucose.

#### **2.4.3.3 DNA manipulation (Construction of plasmid, pcDNA3 YFP-HPV16 L1 and pcDNA3 CFP-HPV16 L1)**

Plasmid DNAs were extracted from O/N cultures using a QIApre Spin Miniprep Kit (Qiagen) following the manufacturer's instruction. Strains and plasmids used for the recombinant cloning work were listed in Table 2. Primers used for PCR are listed in Table 3. Ordinary polymerase chain reaction (PCR) was performed in a PCR machine (Bio-Rad) using a MyTaq Kit (Bioline).



**Table 2 - Bacterial strains and plasmids**

Name	Description	Source
<b>Strain</b>		
<b>DH5<math>\alpha</math></b>		Promega
<b>JM109</b>		Promega
<b>DH5<math>\alpha</math>@T-easy-L1</b>	pGEM®-T Easy vector with ampicillin marker containing HindIII - HPV16 L1- BamHI insert	This work
<b>DH5<math>\alpha</math>@T-easy-ELT</b>	pGEM®-T Easy vector with ampicillin marker containing EcoRV-ELTB-EcoRV insert	This work
<b>JM109@pcDNA3 YFP/CFP-L1</b>	pcDNA3 YFP or CFP plasmids with ampicillin marker containing HindIII-L1-EcoRI insertion	This work
<b>JM109@pcDNA3 YFP/CFP-L1-ELT</b>	pcDNA3 YFP or CFP plasmids with ampicillin marker containing HindIII-L1-EcoRI insertion and EcoRV-ELTB-EcoRV	
<b>pcDNA3-YFP</b>	DH5 $\alpha$ with pcDNA3 plasmid carrying with YFP marked with ampicillin gene	<b>Addgene</b>
<b>pcDNA3-CFP</b>	DH5 $\alpha$ with pcDNA3 plasmid carrying with CFP marked with ampicillin gene	
<b>Plasmid</b>		
<b>pJCB12-icsA-L1</b>	<b>4168-bp fragment, including icsA gene with HPV 16 L1 in transcriptional-fusion ORFs, in pJCB12</b>	<b>Xu's<sup>298</sup></b>
<b>pcDNA3.1-L1</b>		<b>1*</b>
<b>pET28 mCherry/EGFP</b>		<b>This work</b>
<b>pMMB68</b>	<b>A plasmid carrying ELTB gene</b>	<b>2*</b>

\*1 was a kind gift from professor Wang (Xi'an Jiaotong University, China)

\*2 was obtained from NASHAR et al., (1996. PNAS 93:226-230)

**Table 3 - Oligonucleotides used in this project**

Name	Sequence	Targeted product
P2F_HindIII	5' – GGG <u>AAG CTT</u> AAT TAC AGG AAA CAG GT – 3'	HindIII - HPV16 L1 (Outframe) - BamHI
P2R_BamHI	5' – TTT <u>GGA TCC</u> CTC CTT ACT TCA TTT AAC – 3'	HindIII - HPV16 L1 (Inframe) - BamHI (without stop codon)
P2R_2_BamHI	5' – TTT <u>GGA TCC</u> CTC CTT ACT TCA TTT AATC – 3'	HindIII - HPV16 L1 (Inframe) - BamHI (with stop codon)
L1 LF	5' – GGG <u>AAG CTT</u> ATG AGC CTG TGG CTG CCC – 3'	HindIII - HPV16 L1 - EcoRI
L1 LR	5' – <u>GGA ATT CTC</u> ACA GCT TCC TCT TCT TCC TC -3'	HindIII - HPV16 L1 - EcoRI
SP1F_rev	5'- CAA CAA GAT CCT GGT GCC CA – 3'	HPV16 L1
SPIR_rev	5' – GTT CAC CTC CCA GAA GGT GT – 3'	HPV16 L1
Elt_F	5' – GGT TTG <u>ATA TCG</u> AGG AAT GAA TTA TGA – 3'	EcoRV-ELT- EcoRV
Elt_R	5' – GGT TTG <u>ATA TCC</u> TAG TTT TCC ATA CTG – 3'	EcoRV-ELT- EcoRV
16L1_F2_ HindIII	5' – GGG <u>AAG CTT</u> ATG TCT CTT TGG CTG CCT – 3'	HindIII-HPV16 L1- XhoI
16L1_R_XhoI	5' – GGG <u>CTC GAG</u> TTA CAG CTT ACG TTT TTT – 3'	HindIII-HPV16 L1- XhoI

\*Restriction sites are underlined.

There are two versions HPV16 L1 genes kindly supplied by Professor Wang. One version is the original HPV 16 L1 gene and the other one is optimised for expression in mammalian cells. Plasmids carrying HPV 16 L1 genes were used as templates for PCR to amplify full-length. Primers for un-optimized 16 L1 genes are 16L1\_F2\_

HindIII and 16L1\_R\_XhoI, and primers for optimized sequence are P2F-HindIII/P2R\_2\_BamHI set and L1 LF/R pair. P2R\_2\_BamHI (Table 3) contains a stop codon. DNA sequencing service was used (Eurofins Genomics, Germany) to confirm the PCR products. The whole procedure is schematically illustrated in

Figure 8.

### **i. PCR for HPV 16 L1 and ELT**

To construct the recombinant plasmid DNA, PCR products of HPV16 L1 and ELT were amplified using MyTaq<sup>TM</sup> DNA Polymerase Kit. For a 20 $\mu$ l reaction, 1  $\mu$ l HPV16 L1 or LTB template required 2 $\mu$ l from 10 $\mu$ M concentration of each primer. The annealing temperatures for HPV16 L1 and ELT are 59 $^{\circ}$ C and 55 $^{\circ}$ C respectively.

The procedure is as follow:

1. 95 $^{\circ}$ C for 5 mins
  2. 95 $^{\circ}$ C for 1min
  3. 59/55 $^{\circ}$ C for 1 min
  4. 72 $^{\circ}$ C for 45 sec
  5. 72 $^{\circ}$ C for 10 mins
  6. 4 $^{\circ}$ C for 1hr
- } 30 cycles

### **ii Enzyme digestion**

Restriction enzymes used were HindIII, BamHI, EcoRI, and EcoRV, (New England BioLabs, USA) during the recombinant DNA production (Figure 8). During DNA manipulation, two version of recombinant DNA were produced: pcDNA3 YFP-L1 and pcDNA3 YFP-L1-ELT. To synthesize pcDNA3 YFP-L1, pcDNA3YFP plasmids were digested with HindIII and BamHI for the PCR insertion HindIII-L1- BamHI. The second version of recombinant plasmid DNA was designed for co-expressing L1-ELT genes in the same plasmid. To produce pcDNA3 YFP-L1-ELT, the vector pcDNA3 YFP was firstly digested by EcoRV enzymes for the ligation with ELT PCR product to obtain pcDNA3 YFP-ELTB. This ELTB encoded recombinant plasmid was further digested by HindIII and EcoRI/ BamHI to ligate HindIII-L1-EcoRI PCR product (Figure 8 No.1) or HindIII-L1-BamHI (Figure 8 No.2).

These two ligation work obtained a recombinant pDNA encoding HPV16 L1 and ELT genes as a pcDNA3 YFP-L1-ELTB (YEL) plasmid. To confirm the successful cloning work, pcDNA3 YEL plasmids (No.2 & 3) were digested were BamHI and EcoRV; pcDNA3 YL (No.1) plasmid was digested with HindIII and EcoRV. Right sizes of digested bands are listed beside each construct. However, For No.2 and No.3, HindIII was added into digestion mixture by mistake. So the final enzymes for YEL digestion are HindIII, BamHI and EcoRV.

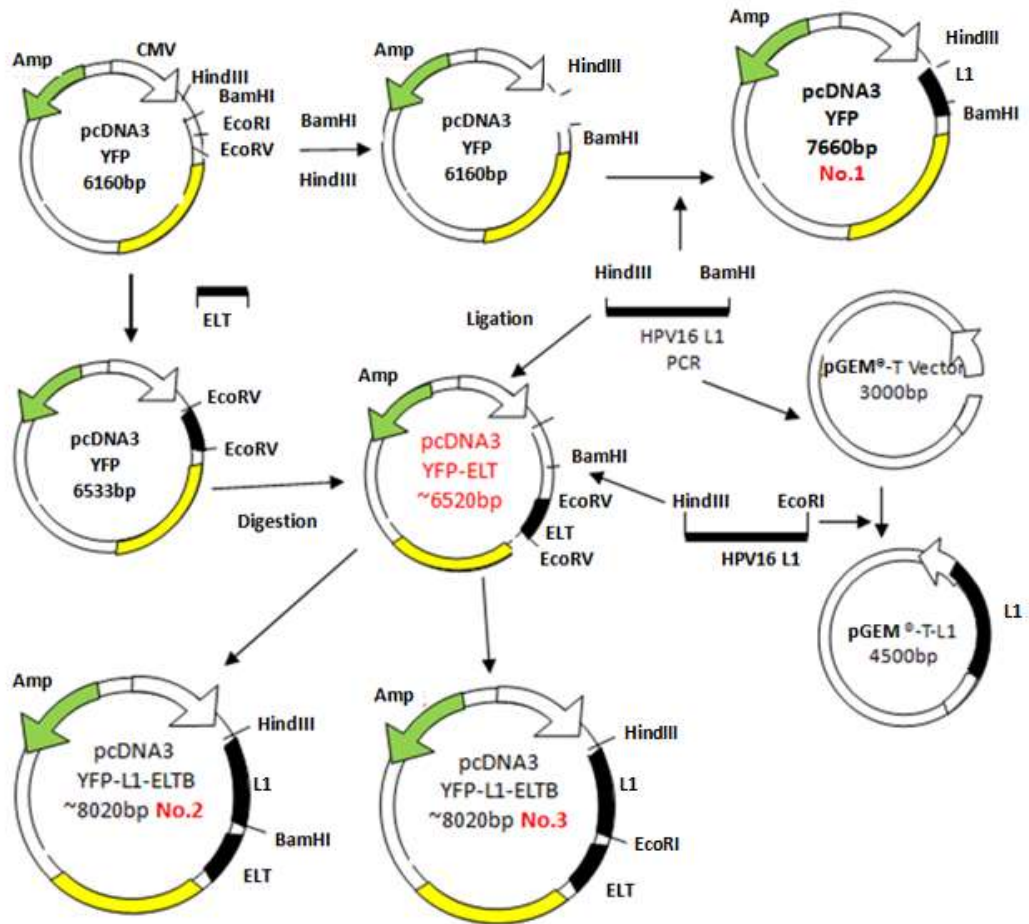
### **iii PCR and gel purification**

PCR products and DNA samples after restriction were gel purified using QIAquick® PCR purification kit & QIAquick® gel extraction kit (Qiagen), and final purified product was suspended in sterilized distilled water.

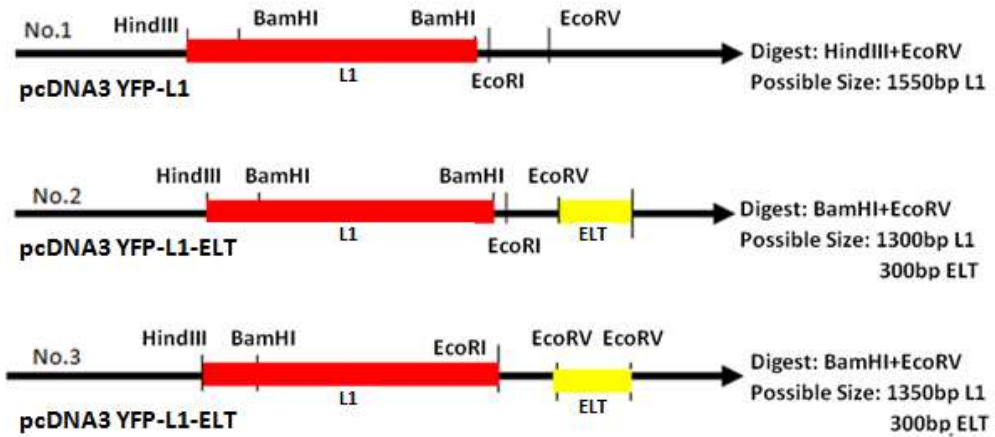
#### **iv Molecular cloning**

Ligation prepared with pGEM®-T Easy ligation kit (Promega) and T4 DNA ligase (BioLabs) using T Easy vector and pcDNA3 YFP/CFP respectively. The pcDNA3 YFP/CFP is mammalian based expressing vector. These recombinant constructs including pcDNA3 YFP/CFP were driven by CMV promoter. L1 PCR product was inserted into it for the expressing of HPV major capsid protein. The conditions and procedures followed the manufacturers' manuals. PCR product of HindIII - HPV16 L1- BamHI amplified by P2F-HindIII/ P2R\_2\_BamHI set were ligated into pcDNA3 Y/CFP to generate pcDNA3 YFP/CFP HindIII-L1-BamHI. The PCR product of HindIII-HPV16 L1-EcoRI amplified by L1 LF/R pair was applied in the pcDNA3 YFP/CFP ELTB ligation to produce pcDNA3 YFP/CFP L1-ELTB. For pGEM®-T Easy-L1, 7 µl IPTG (20mg/ml stock, Sigma) and 20 µl X-Gal (50mg/ml, Promega) were mixed with the culture on Ampicillin plate for antibiotics selection.

**A**

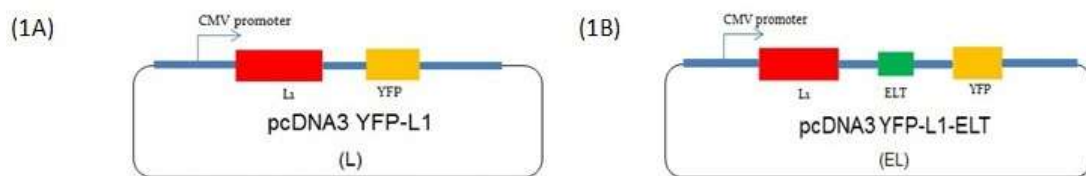


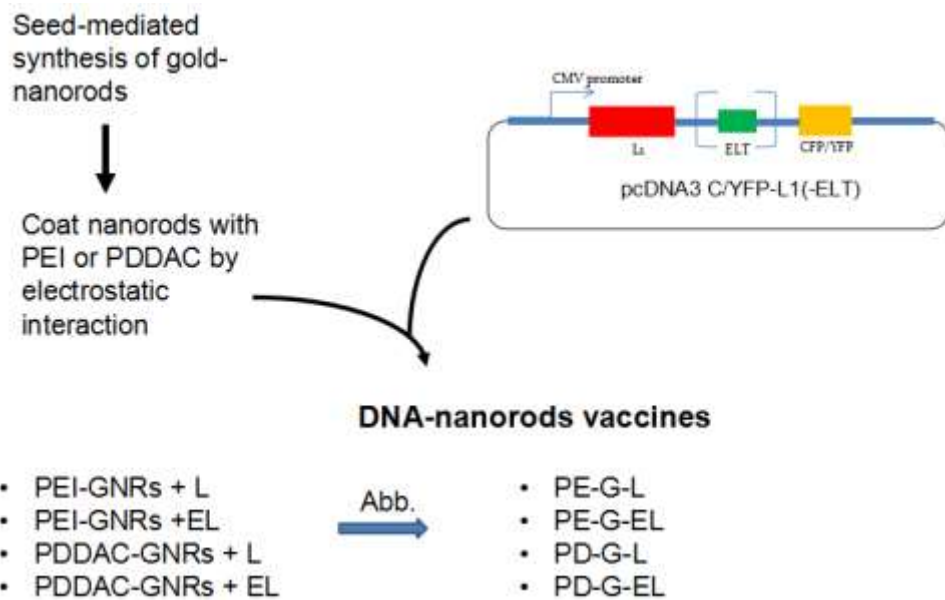
**B**



**Figure 8 - Schematic presentation of construction of pcDNA3 YFP-L1 and pcDNA3 YFP-L1-ELTB and linear structure for digestion (not to scale).** A: Production of recombinant plasmid DNAs; B: Digestion for cloning confirmation of L1 insert and ELT insert. The plasmid harbouring L1 with or without ELT gene was constructed by insertion of L1 and ELT. Purified PCR products were amplified using pJCB12-icsA-L1 plasmid DNA<sup>298</sup> as template with two pairs of primers (P2F-HindIII/ P2R\_2\_BamHI set and L1 LF-HindIII/R-EcoRI pair). This step harvested two sets of L1 PCR products with different digestion codes for the following experiment. ELT gene has EcoRV codon at two sides. The final constructs contained HPV16 L1 (L) in pcDNA3YFP or HPV16L1-ELT (EL) in pcDNA3YFP. No.1: pcDNA3 YFP-L1 with HindIII \_L1\_BamHI PCR insert; No.2: pcDNA3 YFP-L1-ELT with HindIII\_L1\_BamHI; No. 3: pcDNA3 YFP-L1-ELT with HindIII\_L1\_ EcoRI. The labels of pcDNA3 YFP-L1 and pcDNA3 YFP-L1-ELT were simplified into YL and YEL to denote the recombinant plasmid DNAs. In B: the digestion enzymes for pcDNA3 YFP-L1-ELT (YEL, No.2 & 3) were BamHI and EcoRV; enzymes for pcDNA3 YFP-L1 (YL, No.1) were HindIII and EcoRV. Speculated appropriate sizes of successful recombinant DNAs after digestion are listed beside each construct.

#### 2.4.4. Polymer Coated GNRs Conjugate with Plasmid DNA





**Figure 9 - Schematic presentation of GNRs-DNA assembly** (plasmid draws not to scale). 1A, carries L1 gene alone, and 1B is carries L1 and ELT genes. YFP indicated yellow fluorescence protein. The coated GNRs labelled as PEI-G and PDDAC-G were mixed with recombinant plasmid DNAs pcDNA3YFP-L1 (YL) and pcDNA3YFP-L1-ELT (YEL) with a concentration as 1.6µg/ml in cell work and 16µg/ml in animal study by electrostatic interaction. The concentrations applied in *in vitro* and *in vivo* study following the previous GNRs-DNA study against HIV infection<sup>207</sup>. Therefore, the final vaccine preps together with adjuvants are PE-G-L, PE-G-EL, PD-G-L and PD-G-EL. They are furtherly simplified and labelled as PEL, PEEL, PDL, and PDEL in some following figures.

## 2.4.5. Characteristics of coated GNRs

### 2.4.5.1 Spectrum analysis of GNRs-DNA complexes



After the spectrums of GNRs were measured by an absorption spectrometer (V-660 Spectrophotometer, JASCO), the concentration were adjusted into OD/absorbance = 1.0. GNRs with an absorbance (optical density) in 1.0 is equivalent to a concentration of 10 µg/ml speculated in accordance with equations based on Mie theory introduced before<sup>299300</sup>. 1.6µl/ml of plasmid DNA were added into each of the GNRs solutions and incubated 30 to 60 min at RT for DNA immobilization upon GNRs surface. The adsorption efficiency means the ability of functionalised GNRs to conjugate DNAs. The incubation of DNAs and GNRs will provide polymer-coated GNRs with another DNA coating layer on the top. Following the DNA adsorption efficiency test for GNRs-DNA vaccine<sup>207</sup>, the absorption spectrum of each solution was measured using a UV/VIS spectrometer (Lambda 25, PerkinElmer), and the analysis were graphed using a spectrum software Spekwin32 (version 1.72.0).

#### **2.4.5.2 DNA affinity test**

In order to test the proper incubation approach, different incubation periods (5mins/30mins) were applied to estimate the aggregation status of GNRs by spectrometer. Same samples prepared in the spectrum analysis were centrifuged at 13,000 rpm (16,200 g) for 15 min. Except the extracted supernatant, same amount of distilled water was added to resuspend the precipitant. Agarose electrophoresis described in previous section were used for the an agarose gel retardation assay. Electrophoresis were running at 80V, 3A for 40 min with Tri-Acetate-EDTA (TAE) running buffer, and images were taken by a GelDoc (Ingenius, Syngene). DNA/Polymer modified GNRs complexes were formed by adding 32µl/ml of

plasmid DNA into 10  $\mu$ l/ml of GNRs solution. 'Fresh GNRs' named in this test means the newly prepared GNRs from the 1-year GNRs stock in 0.2M CTAB, which was dispensed in distilled water before test. Samples centrifuged for 10 min at 13,000 rpm (16,200 g) were prepared into supernatant samples for gel analysis. Samples were measured by DNA concentration analysis before and after 2-minute centrifugation at 13,000 rpm (16,200 g) with the absorbance at 260nm using Nanodrop 2000c (Thermo Scientific). All samples were measured at least 3 times for mean value. The DNA affinity described as adsorption efficiency is calculated based on following formula:

$$(2.2) \quad \text{Affinity/Adsorption efficiency ratio} = \frac{(\text{total DNA} - \text{free DNA})}{\text{totalDNA}}$$

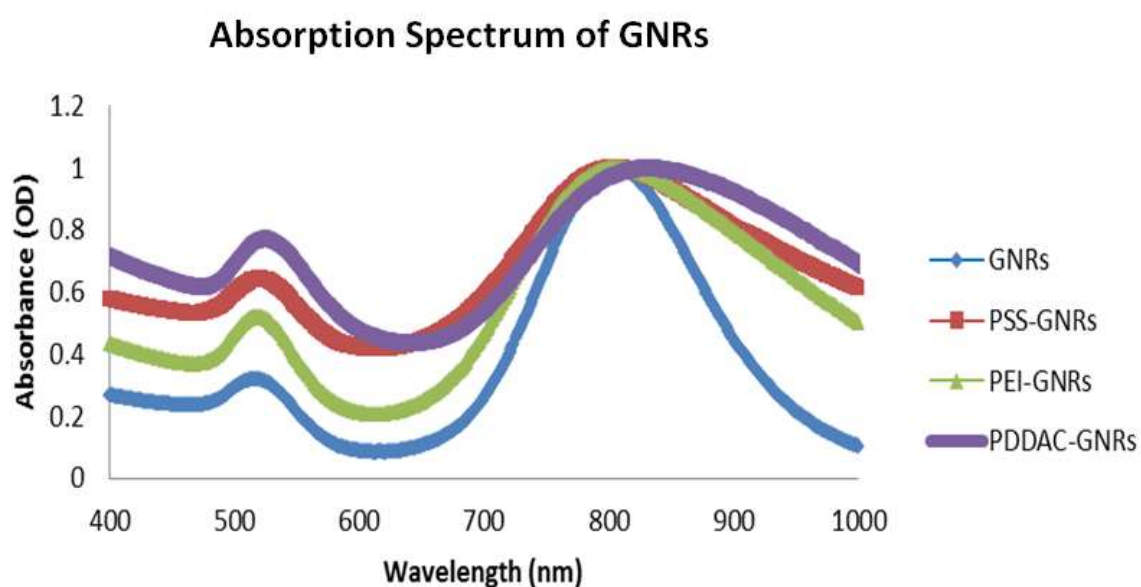
#### **2.4.6. Statistical Analysis**

All the samples were prepared in triplicate for analyzed and all experiments were repeated at least three times. One-way ANOVA and Tukey test were applied for statistical comparison.  $p$  value less than 0.05 is considered statistical significance.

## 2.5. Result

### 2.5.1. Successful production of surface-modified GNRs demonstrated by spectrum analysis

In order to evaluate the physical properties of surface functionalised GNRs, absorption spectrum provides an estimation of the size and morphology of GNRs. As the physical features of GNRs SPR discussed in the Introduction section, GNRs produced via seed-mediated growth method showed two peaks in SPR wavelength with a higher longitudinal peak near 800nm. Successful surface coating generated a small band shift, which is more observable in the longitudinal SPR.



**Figure 10 - Spectrum change of GNRs after coating of each layer.** Concentrations of DNRs were adjusted into 10  $\mu\text{l/ml}$  (optical density=1.0). Following the protocol, the GNRs achieved a longitudinal (second peak) wavelength above 800nm. Spectrum data was measured between 200nm to 1000nm. The value of absorption detected by GNRs scattering,

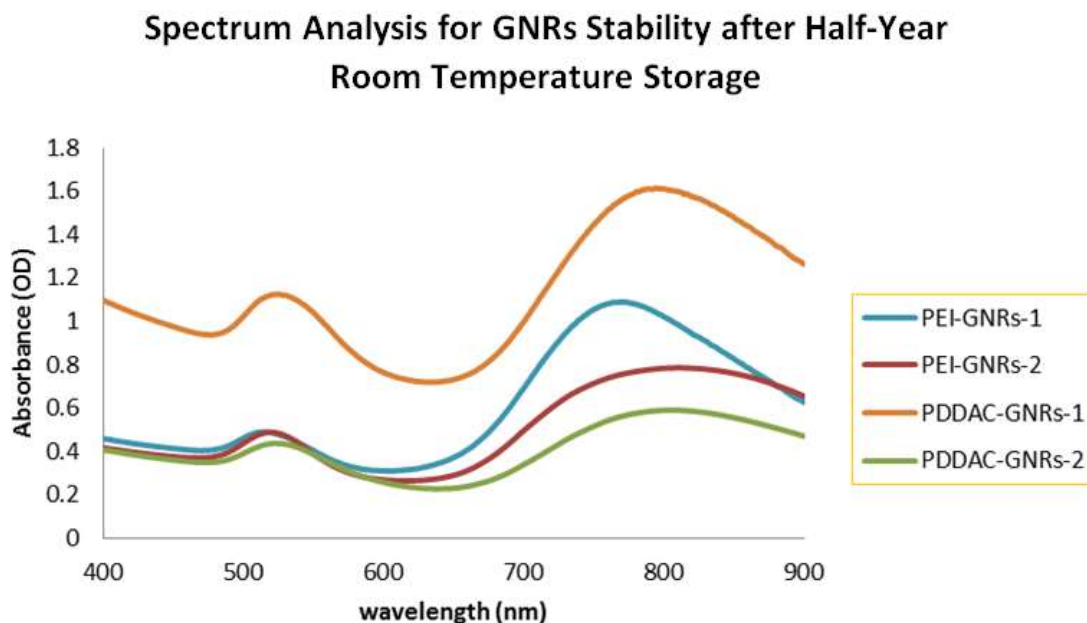
proportionate to the value of GNRs concentration. The absorption of GNRs is equivalent to their optical density (OD) based on Mie' theory of metal materials.

As shown in Figure 10, during the coating process, the optical wavelength of GNRs was changed after coating at the longitudinal scattering. The change of the optical density (OD) means the change of concentration, which was affected by the suspension and centrifugation steps are adjustable by distilled water. The PSS-coating will lead to a slight blue shift (< 5nm) in wavelength. The slight red-shift of longitudinal wavelength indicated the morphology change of GNRs after coating with PEI and PDDAC, which didn't influence the aseptic ratio in a concerned variation<sup>301</sup>. The final PEI-GNRs and PDDAC-GNRs still maintain rod shape as the spectrum demonstrated.

### **2.5.2. Spectrum analysis for GNRs stability after half-year room-temperature shelf-storage**

Absorptions of applied surface-engineered GNRs were investigated after half-year RT storage to measure the stability of GNRs in size and structure. OD represented particle density was adjustable by water. The study concerned about the further application of GNRs as an appropriate and convenient adjuvant for delivering DNA vaccines with a minimal administration and longer shelf life. If there was a shift of the wavelength and changed the distance of two peaks, it means the change of sample size and aspect ratio. The obvious peak shift means the size distribution of GNRs changed, which will cause the loss of vaccine efficiency due to the change of

the DNA binding ability. This study also revealed the stability of GNRs morphology after surface modified by polymers.



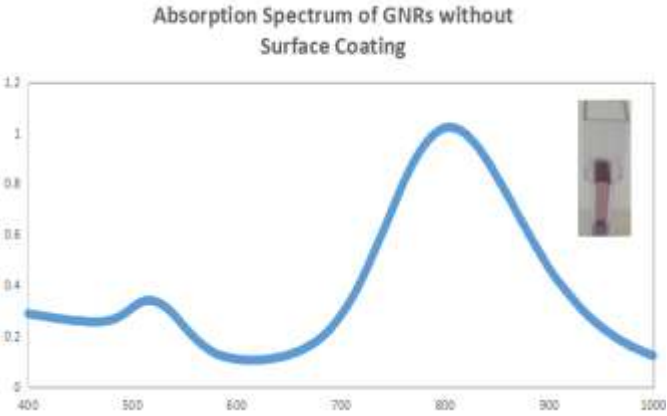
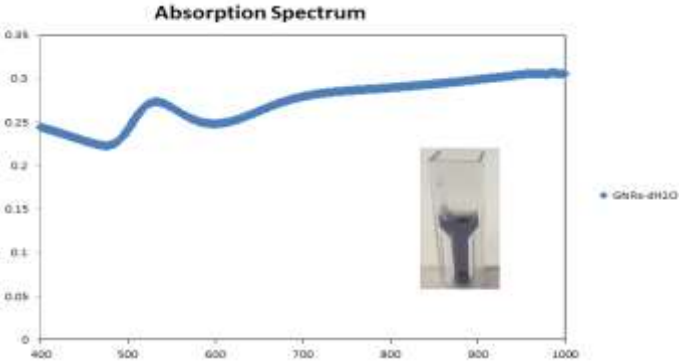
**Figure 11 - Spectrum evaluation of the stability of GNRs at room temperature.** All GNRs samples were stored in distilled waters at RT. The original products of PE-G and PD-G were labelled with number '1' after their names, while the No.2 labelled samples are stored on the shelf after half-year.

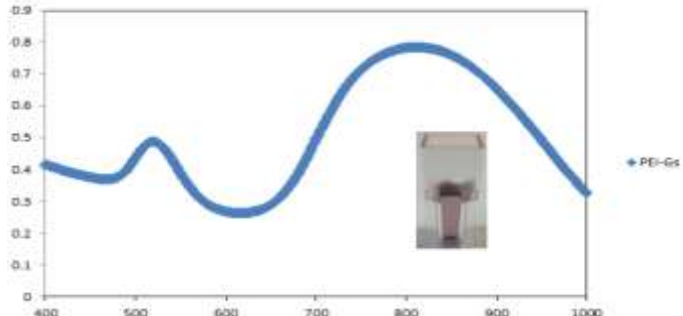
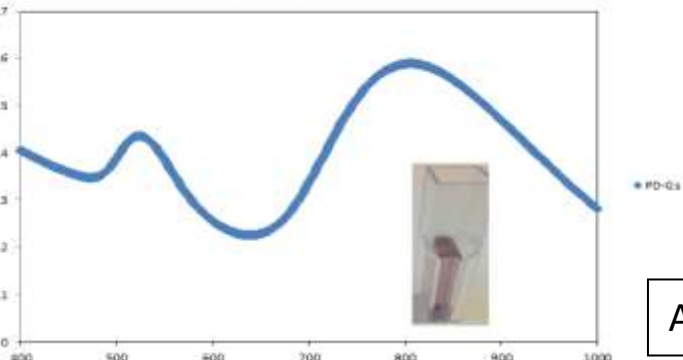

For half-year storage, the aspect ratio of either PE-Gs or PD-Gs didn't change too much according to the distance of two peaks in each curve. It means without any DNA binding, the surface-coated GNRs with these two types of polymers remained their transverse/longitudinal ratio. However, the spectrums show a red-shift across two coating samples, which means more GNPs, obtained an increased length. However, the free reagents were moved and all samples remained in the distilled

water. Therefore, a highly possible explanation is the aggregation appeared after half-year storage.


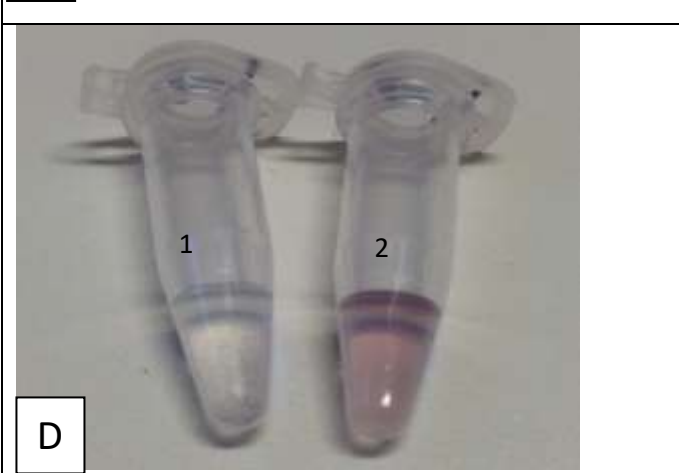
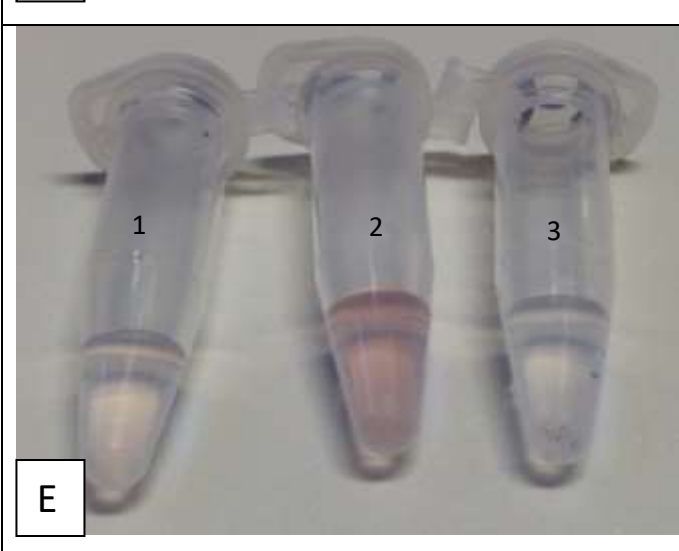
### 2.5.3. Colour and morphology assessment related GNRs Stability

Pictures of surface-modified GNRs along the RT shelf storage were taken for the colorimetric assay to detect the colour change indicated morphologic alteration of metal NPs. The purpose to record the sample images during storage was similar to absorption spectrum analysis. Besides, images provided direct observation of sample quality, like dispersity, which could highly affect the actual vaccine dosage during administration.

Pictures	Description
<p>1.  The graph shows the absorption spectrum of GNRs without surface coating. The x-axis represents wavelength in nm, ranging from 400 to 1000. The y-axis represents absorbance, ranging from 0 to 1.2. The curve shows a small peak at approximately 520 nm and a large, sharp surface plasmon resonance (SPR) peak at approximately 820 nm. An inset image shows a test tube containing a red suspension.</p> <p>2.  The graph shows the absorption spectrum of GNRs in distilled water after half-year storage. The x-axis represents wavelength in nm, ranging from 400 to 1000. The y-axis represents absorbance, ranging from 0 to 0.35. The curve shows a broad SPR peak centered around 800 nm. An inset image shows a test tube containing a blue suspension. A legend indicates 'GNRs-dH2O'.</p>	<p>Samples were prepared half-year before the stability assay based on the original GNRs. The spectrum of original GNRs was measured after twice wash and resuspension in distilled water. After spectrum confirmation, which were shown in figure 10, all samples (GNRs, PE-Gs and PD-Gs) were kept at RT for half year. All samples were centrifuged and diluted with distilled water for an OD equivalent to 1.0 before the storage. Due to a low amount of samples left after half-year, they were diluted again with distilled water before the spectrum measurement to observe the stability of rod structure and size distribution:</p> <ol style="list-style-type: none"> <li>1. Original GNRs</li> <li>2. GNRs in distilled water after half-years</li> </ol>

<p style="text-align: center;"><b>Absorption Spectrum</b></p>  <p>3. PEI-Gs after half-years</p> <p>4. PD-Gs after half-years</p> <p style="text-align: center;"><b>Absorption Spectrum</b></p>  <p style="text-align: right; border: 1px solid black; padding: 2px;">A</p>	<p>3. PEI-Gs after half-years</p> <p>4. PD-Gs after half-years</p>
 <p style="text-align: center; border: 1px solid black; padding: 2px;">B</p>	<p>1-year old GNRs solution at RT:</p> <ol style="list-style-type: none"> <li>1. GNRs (in distilled water)</li> <li>2. GNRs (in 0.2M CTAB)</li> <li>3. PE-Gs</li> <li>4. PD-Gs</li> </ol>

B

 <p data-bbox="288 573 363 651">C</p>	<p data-bbox="1050 147 1410 248">GNRs after 2-years RT storage GNRs after ultrasonic resuspension:</p> <ol data-bbox="1150 383 1278 472" style="list-style-type: none"> <li>1. GNRs</li> <li>2. PE-Gs</li> <li>3. PD-Gs</li> </ol>
 <p data-bbox="288 1043 363 1122">D</p>	<p data-bbox="1050 651 1410 797">Vaccine preps after one-year storage at RT. PEI-GNRs aggregated and precipitated at the bottom of tubes)</p> <ol data-bbox="1150 887 1342 943" style="list-style-type: none"> <li>1. PE-G-pDNA</li> <li>2. PD-G-pDNA</li> </ol>
 <p data-bbox="288 1581 363 1659">E</p>	<p data-bbox="1050 1122 1410 1335">Vaccine preps after two-year storage at RT (The colour of GNRs sample became lighter; PEI-GNRs aggregated and precipitated at the bottom of tube)</p> <ol data-bbox="1150 1424 1358 1514" style="list-style-type: none"> <li>1. GNRs-pDNA</li> <li>2. PSS-G-pDNA</li> <li>3. PE-G-pDNA</li> </ol>

**Figure 12 - Colour indicated the stability of the surface-modified GNRs.** The left column shows pictures of GNRs solutions in different conditions, which are described in the right column.

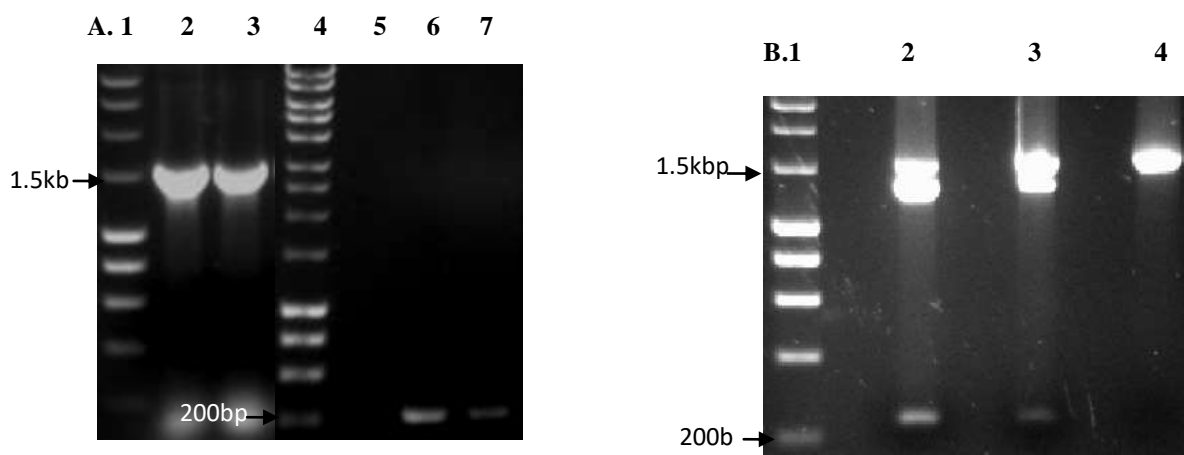


Pictures and spectrums in Figure 12 indicated that GNRs could keep their infrared plasmon modes for at least 1 year with the saturated coating but not in distilled water only. The long-time RT stored GNRs in distilled water led to a change of colour with a loss of rod structure illustrated in the spectrum. The missing longitudinal peak suggested that the substantial rods were shortened into sphere structure. A concomitant colour changed from brownish red into dark greyish hue after half-year (Figure 12, A2). The colour of uncoated GNRs finally faded into colourless after 2 year RT shelf storage (Figure 12, C1), even with the existence of a low concentration of DNA (E1).

In contrast, coated GNR stored at the same condition remained original colour except for precipitation and aggregation of PE-G samples after long-term shelf storage (B3, D1, E3). It is noticeable that Figure 12B showed that PEI-GNRs solution became colourless after 1 year storage, due to aggregation of the PE-Gs which settled to the side and the bottom of the tubes. Incubation of aggregated PEI-GNRs with DNA did not reverse the aggregates; the solution remained colourless (E3). The aggregates stacked on the container walls could be re-suspended using ultrasonic bath, and the colour of re-suspended PE-Gs still maintain light red colour (Figure 12, C2). Nevertheless, PSS-GNRs and PDDAC-GNRs did not have aggregation with or without carrying DNA as photos demonstrated.

#### **2.5.4. PCR gels for DNA recombination cloning**

The correction of recombination plasmid DNAs was evaluated according to the digestion strategy described in Figure 8B. Work processed via different sets of digestion enzymes. As the schematic presentation of YL and YEL structures listed in Figure 8A, successful production of recombinant YL plasmid would provide a band of L1 gene near 1.5kbp, after digested with HindIII and EcoRV. While YEL constructed as No.2 in Figure 8A would show a 1.3 kbp band representing L1 insertion and 300 bp one for ELT gene. Cloned No.3 would present bands of L1 and ELT similar as No.2.



**Figure 13 - Gel evidence of L1 and ELT insertion in recombinant DNA by PCR and Digestion.** The DNA ladder used in the gel analysis is HyperLadderI (Bioline). ImageA is the PCR and B is the digestion work. A: Lane1: HyperLadderI; Lane2: YL; Lane3: YEL; Lane4: 1kb Ladder; Lane5: ELT test for YL construction (No.1 Plasmid: HindIII\_L1\_BamHI); Line6: YEL (No.2 plasmid: HindIII\_L1\_BamHI) and YEL (No.3 plasmid: HindIII\_L1\_EcoRI). In B: the digestion enzymes for pcDNA3 YEL (No.2 & 3) were HindIII, BamHI and EcoRV; enzymes for YL (No.1) were HindIII and EcoRV. Lane1: HyperLadderI; Lane2: No.2 plasmid; Lane3: No.3 plasmid; Lane4: No.1 plasmid.

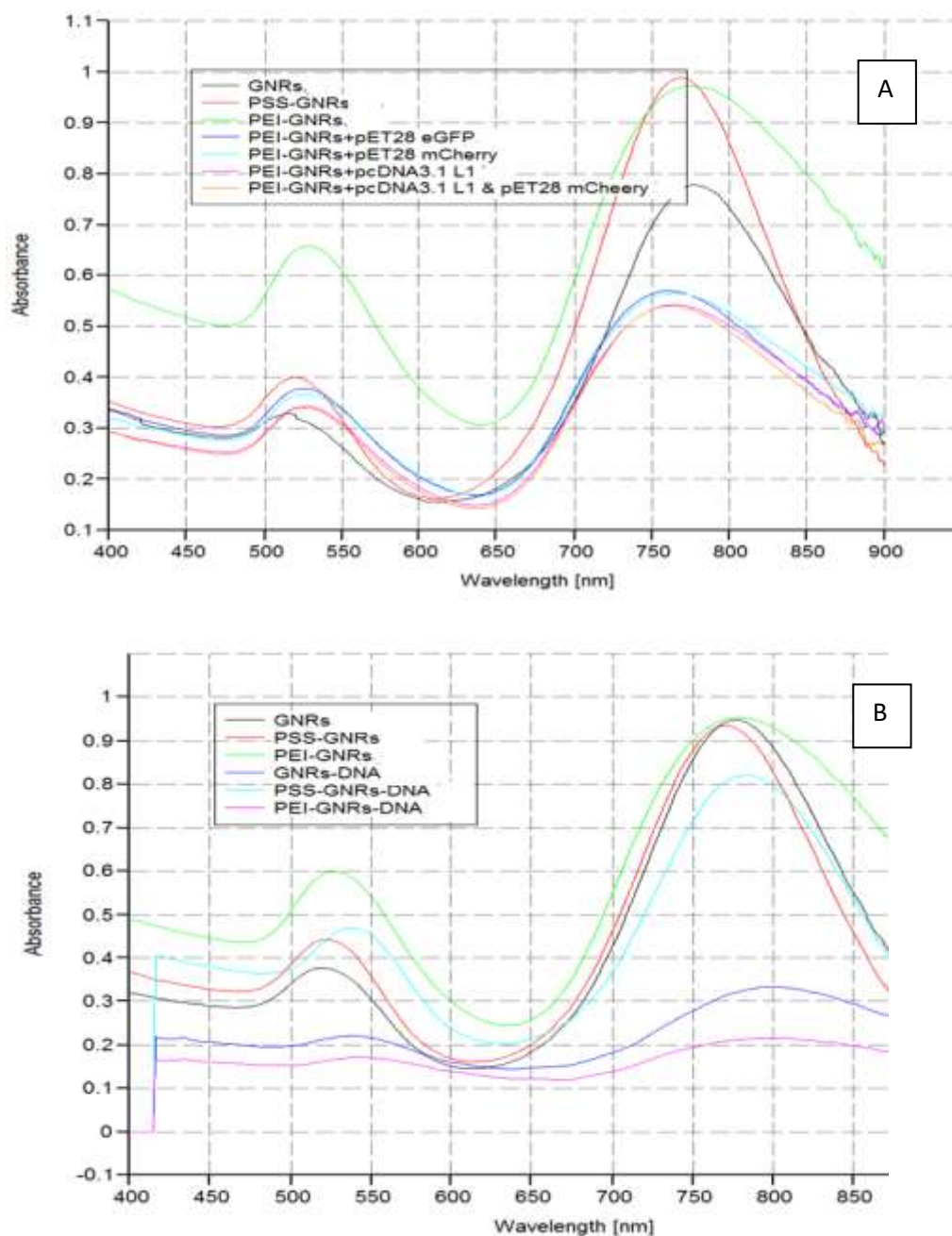
Figure 13 shows the PCR products amplified from the final constructs pcDNA3 YEL and pcDNA3 YL. Note that the ELTB coding sequence is ~370bp and 1% (w/v) agarose is not sensitive to detect such small size change between L1 and L1-ELTB. In 13-A: for the L1 PCR, the two construct pcDNA3 YL and PE-G-L was amplified with L1 primers. The products site at 1.5kbp compared with the hyperladder 1kb marker. ELT PCR confirmed the bands between 200bp and 400bp were not primer dimmer in contrast to the pcDNA3 YL in Line A-5 without any product illustrated on the gel by elt primers.

For the digestion analysis, the sizes of ideal bands were illustrated in previous methodology part (Figure 8B). BamHI and EcoRV were applied to digest two pcDNA3 YEL versions, which have different L1 PCR inserts. According to the digestion scheme on Figure 7B, pcDNA3 YEL with HindIII\_L1\_EcoRV will have a slightly larger product (50bps more). Both of these two plasmids were digested with three enzymes (HindIII ,BamHI and EcoRV). Gel image demonstrated a slightly smaller band of No.2 plasmid (Lane2) than No.3 plasmid (Lane3). Both of them were provided a digested band in between 200bp to 400bp, which should be the ELT cut out by EcoRV. Recombinant plasmid pcDNA3 YL (No.1) were digested by HindIII and EcoRV (Lane4). It provided a band slightly higher than 1.5kb and without ELT presence. All plasmids were sent to sequencing for further confirmation. All the inserts were proved by the sequencing analysis by DNA sequencing company (Eurofins Genomics, Germany).

## **2.5.5. DNA Affinity to GNRs with different surface coatings**

### **2.5.5.1. Spectrum analysis of GNRs-DNA complex**

Following previous observation, this test was to examine the adsorption and aggregation after the GNRs-DNA incubation. As articulated in the previous Introduction, the morphology of conjugated GNRs-DNA by spectrum depends on the GNRs rather than DNAs, due to unobservable scattering and absorption of DNAs. Following the concentration adopted by Xu's group for HIV vaccination to mingle DNAs into GNRs solution <sup>207</sup>, the purpose of this assay was to trace the impact of factors in vaccine preparation for a well-distributed conjugated preps. In this section, the change of O.D. only means the loss of sample concentration, which was adjustable during preparation by distilled water.

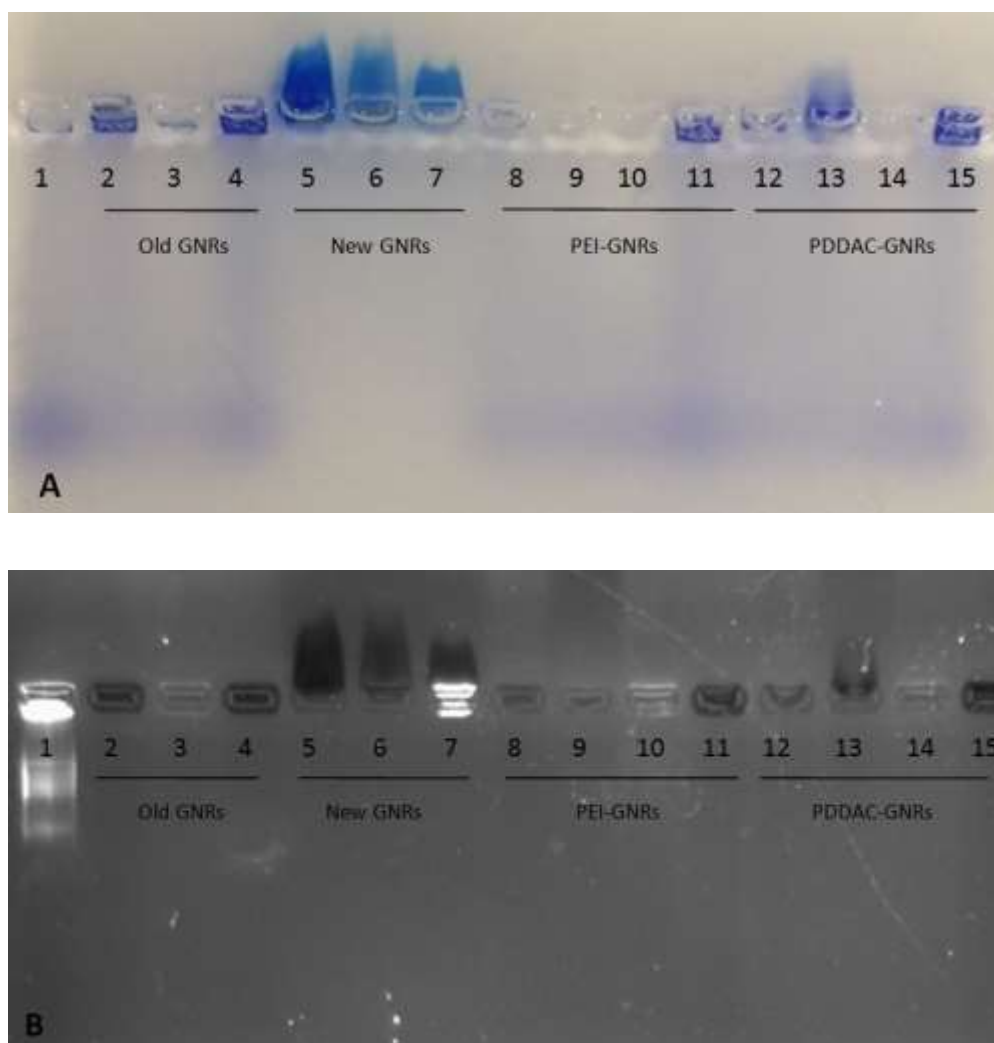


**Figure 14 - Absorption spectrum plots of fresh prepared GNRs-DNA complexes.** UV-vis spectrophotometry analysis of the spectrum change in accordance with a polymer coating. A: DNAs (1.6ng/ $\mu$ l) in different sizes was added into the PEI-GNRs solution, the concentration of which was adjusted to be OD=1.0. Samples were incubated on a bench shaker (500 rpm, Thermo) for 30 mins. Spectra were measured after centrifugation at 13,000 rpm for 10 mins and resuspension. B: Same DNAs were added into GNRs solutions with

different surface layers for 5 minutes without using a shaker. Following procedures were same as samples in A.

In Figure 14A, incubation with different sized DNAs didn't show a remarkable spectrum alteration of GNRs, which means that the distribution and adsorption of GNRs were not influenced by the size of DNAs as long as samples were well-mixed in 30 mins. This figure demonstrated that the DNA combination would not influence the GNRs morphology and size, because DNA doesn't provide detectable light scattering. The decreased density of GNRs was observed in all the centrifuged samples. The non-shifted wavelength indicated that adjuvant PEI-GNRs still has an intact and stable structure after DNA conjugation. Thus, the widened peak bands of GNRs spectra after short-time (5 mins) incubation, particularly in cationic GNRs and PE-GNRs in contrast with anionic PSS-GNRs, illustrated the possible aggregation of GNRs and higher affinity of cationic surface-engineered GNRs. The combination ability of PE-Gs was stronger than GNRs without coating. However, the dispersity of PE-Gs is weaker than other tested samples without constant shaking procedure.

### 2.5.5.2. Agarose gel retardation assay

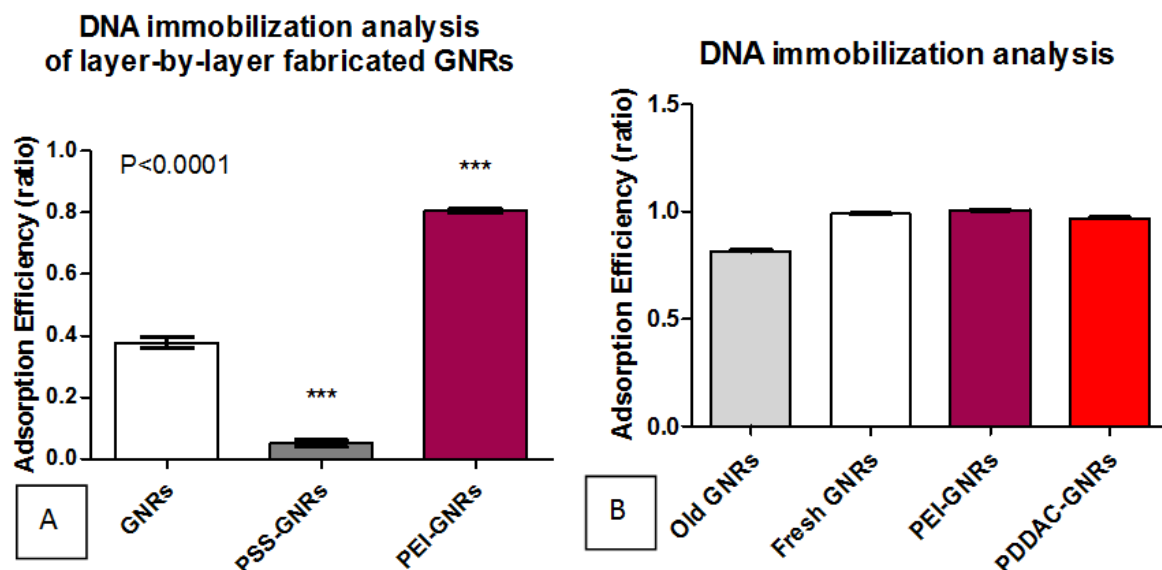


**Figure 15 - Agarose gel analysis of DNAs conjugation to GNRs.** A plasmid control was applied in the first loading lane. The image of agarose gel (1% w/v) after electrophoresis. For both A and B, from No.1 to No.15, samples arrangement is as follow: 1: Plasmid DNA control; 2: Old GNRs; 3: Old GNRs-DNA conjugates; 4: Supernatant of Old GNRs-DNA conjugates; 5: Fresh GNRs; 6: Fresh GNRs-DNA conjugates; 7: Supernatant of Fresh GNRs-DNA conjugates; 8: PEI-GNRs; 9: PEI-DNA mixture 10: PEI-GNRs-DNA conjugates; 11: Supernatant of PEI-GNRs-DNA; 12: PDDAC-GNRs; 13: PDDAC-DNA mixture 14: PDDAC-GNRs-DNA conjugates; 15: Supernatant of PDDAC-GNRs-DNA. Sample preparation was described in method section. B: Gel UV-vise image of GNRs-DNA complexes for A. DNA loading dye is the intercalating agent, which was prior added into the GNRs-DNA conjugates before the agarose gel retardation assay. Images were taken by a gel doc (Ingenius, Syngene).

The electrophoresis image demonstrates the higher DNA affinity of cationic GNRs and PEI-GNRs in contrast to negative-charged PSS-GNRs (Figure 15). PEI-GNRs-DNA complexes were found to be the strongest binding formulation. Moreover, the supernatant of PSS-GNRs-DNA contained more free DNAs than other samples. It means the binding between DNA and positive-charged GNRs is more stable and reliable than negative-charged GNRs. It is noticeable that the dye staining with CTAB-GNRs samples remained in the loading holes. However, the final sample for CTAB-GNRs-DNA left less dye in the loading well. This loose binding ability of GNRs without coating was further proved in Figure 15A. Comparing the conjugates prepared with the old GNRs sample, which was remained in distilled water than 1 year at room temperature, the loading dye mixed with fresh made GNRs was failed to conjugate DNAs, which left a retardation strip in opposite of DNA running direction. Therefore, for the agarose gel retardation assay, data validate a highest binding ability of PEI-coated GNRs and a dissociated issue of negative-charged PSS-GNRs and positive-charged GNRs without coating. PEI-GNRs bound to DNA tighter than PDDAC-GNRs. Figure 15A indicated an intermediate binding strength between polymer PDDAC and DNA, which obtained a stronger effect possible affecting the polymer-GNRs binding of PDDAC-GNRs, in contrast to PEI-GNRs (A9). Figure 15B shows the free PEI-GNRs and PDDAC-GNRs samples without DNA conjugation remained in the supernatant of centrifuged GNRs-DNA complexes (Lanes 11 and 15 in Figure 15B).



Meanwhile, the DNA immobilization is another features suggested the affinity of DNA upon fabricated gold nanostructure modified adjuvant surface. It described the adsorption efficiency of DNAs on the layer-by-layer coated GNRs, which demonstrated the DNA loading ability of the vaccine adjuvants.



**Figure 16 - DNA affinity test in accordance with DNA immobilization upon fabricated GNRs.** Data were generated by UV spectrometry (OD 260nm) using Nanodrop 2000c (absorption at 260 nm, Thermo) before and after incubation and centrifugation of DNA with GNRs. Sample preparation processes were described in Materials and Methods. A and B were two trials. GNRs with the same name were from a different batch of GNRs. A: DNA Adsorption efficiency comparison between negative-charged GNRs coating and positive-charged GNRs coating. B: DNA adsorption efficiency comparison between PEI/PDDAC-GNRs. 32 ng/μl of plasmid DNA was incubated with GNRs. The incubation time for experiments was half h for A and 1h for B. Data was pooled from independent experiments for each test. Statistical analysis was applied to all data using one-way ANOVA method,  $p > 0.05$ . The DNA affinity of GNRs-DNA complexes was calculated according to the following

equation:

$$\text{Adsorption efficiency} = \frac{(\text{total DNA} - \text{free DNA})}{\text{totalDNA}}$$

Double-stranded plasmid DNA generated stable concentration values in distilled water during measurement time. Layer-by-layer coating means more than two coating layers on the GNRs, which obtained opposite electric charge. In accordance with the gel images in Figure 15, the loading ability of PEI-GNRs is significantly higher than GNRs and PSS-GNRs (Figure 16A). Newly prepared GNRs from the 1-year 0.2M CTAB maintained GNRs still have a significant high DNA affinity, with increased adsorption efficiency after increased the incubation time. All supernatants after PE-Gs incubation with plasmid DNA obtained OD260nm absorption values of 0 as measured by Nanodrop, indicating that all DNA was attached to PE-Gs. In agreement with Figure 14, PEI-GNRs had significantly stronger DNA immobilization than PD-Gs.

## 2.6. Discussion

In this project, due to lack of a zeta-potential analyser and high resolution scanning electron microscopy (SEM), the surface modification of GNRs could only be evaluated by absorption spectrum, which might neglect the distribution of polymer coating structure. Zeta potential illustrates the electrostatic potential on the particle surface, which was measured by the electrophoretic mobility of GNRs using dynamic light scattering<sup>302</sup>. Studies demonstrated the change of zeta potential after GNP immobilised with DNA aptamers, giving a distinctive electrostatic potential and structure on the particle surface<sup>207,302</sup>. As the efficacy and stabilisation of vaccine samples were discovered in work, the changed structure and aggregation status of GNRs-DNA could highly affect the final immunisation result causing reduced and variable immunogenicity.

Moreover, due to the strong affinity of cationic polymers to negative charged DNA, GNRs coated with positive-charged PEI and PDDAC enhance the DNA conjugation remarkably (Figure 16). Figure 15B demonstrated the affinity benefits of PE-Gs and PD-Gs than raw GNRs by a lower amount of free DNA in their supernatant after centrifugation. However, data and pictures shown in Figure 12 & 14 also exhibited a strong aggregation trait of PE-Gs even after mixing with 1.6 ng/ $\mu$ l DNAs, which might cause the heterogeneity of vaccine samples. Furthermore, in Wang's study, the zeta potentials on the surface of GNRs changed in associated with both size of gold nanoparticles and concentration of DNA conjugates<sup>302</sup>. Therefore, the immobilisation ability of DNAs on the GNP surface strongly depends on the

electrostatic potential of surface-engineered particles, which could furtherly determine the cellular uptake<sup>303</sup>. As previously described, studies have demonstrated more internalization of proteins conjugated with 30 nm GNPs but not 50 nm ones<sup>276</sup>. GNRs with shortened length than our optimized nano-size (30-40nm) and likely symmetrical morphology caused by long-term storage in distilled water, could possibly reduce conjugation of DNAs to GNRs. This hypothesis was revealed by the affinity analysis of GNRs after long-term RT storage (see Figure 16) and the distribution of length-reduced GNRs was displayed in Figure 12A. Therefore, short-term storage and proper surface coating significantly benefited DNA immobilization, which can be validated in the affinity test. Aggregation formed in PEI coated GNRs (Figure 11 & 12), whereas PDDAC modified GNRs seemed more stable, which is a more suitable to formulate final vaccines. Longer incubation time resulted in increased DNA immobilization to the fabricated GNRs, which indicated a prior mixture of GNRs to DNA samples would significantly increase of DNA-GNR complex. Although the increase of nitrogen to phosphate ratio (N/P), which indicates PEI/DNA ratio, increases the toxicity of complexes, this ratio does not cause significant harm in mice study through intranasal immunization<sup>211</sup>. However, further investigations of appropriate N/P for the application of surface-engineered GNPs need to be discussed in the future.

There is one possibility to estimate the molecules of the saturated coating layer. The saturated DNA loading ratio has not been evaluated in this project. However it is worth discovering for a promising potential to apply maximal amino-groups of polymer PEI for DNA conjugation in the future. The discussion of saturated DNA-

polymer coated GNRs will boost the vaccine efficiency and maintain its dispersity with a long-time shelf life.

According to the equation reckoned by Lopatynskiy's work, developed from the symmetrical Bruggeman effective medium theory, the possible surface concentration of saturated monolayer coating on the NP surface with different radii is equal to:

$$(2.3) \quad N_s = \frac{(R+r)^2}{4r^2 R^2}$$

The radius (nm) of NP and the outside monolayer were represented by R and r respectively. This equation (2.3) is able to estimate the number of coating molecules on the NP surface calculated based on the measurements of the LSPR extinction peak shift after the thickness change of coating layers. Through the scattering spectrum of surface-engineered GNPs, the parameters of coating layer size are able to be adjusted for further discussion of appropriate DNA loading ability.

DNA recombinants contained optimized HPV16 L1 gene and constructed with and without ELTB gene in a pcDNA3 plasmid. Two L1 PCR products were prepared for this project, to ensure the success of digestion and ligation in plasmids. The codon optimised L1 gene contains a BamHI digestion site on its up-stream. Two L1 PCRs are HindIII\_L1\_BamHI and HindIII\_L1\_EcoRI (Figure 8). Both of them was successfully inserted into the vector pcDNA3 YFP/CFP (Figure 13). The digestion work proved that the entire viral gene was ligated into YFP vector. Two recombinant DNA structures were generated, which were pcDNA3 YFP L1 and pcDNA3 YFP-L1-ELT. Abbreviations YL and YEL were applied in the following work to indicate

these two plasmid DNA products. Both versions of pcDNA3 L1-ELT plasmids with different enzyme codons at the 5' and 3' sites after L1 insertion (Figure 8) were successfully cloned into the vector backbone. Since the selection of digestion enzymes was to benefit cloning procedure, either of them (Figure 8 No.2 or No.3) was utilized during the whole study.

CFP is another fluorescence protein, which can be excited by 405nm laser and detected at 485 nm. In contrast, the excitation and emission peaks of YFP are 514 nm and 527 nm respectively. Considering the fluorescence techniques require special YFP filter to enhance the detection and distinguish its fluorescence from other red-fluorescence staining (like Propidium iodide, PI) used in the in vitro study, L1 gene and ELT gene were also ligated into pcDNA3 CFP plasmid to achieve broader selection of fluorescent dye.

## 2.7. Conclusion

For vaccine preparation work, I successfully fabricated the layer-by-layer coated GNRs, and demonstrated the enhanced stability of surface-engineered DNA in contrast to the raw GNRs. Assays illustrated in Figure 11 & 12 proved that the 1-year shelf storage of PE-Gs and PD-Gs either with or without DNAs remained the morphology and binding ability of GNRs compared with the GNRs stored in distilled water. Although PE-Gs aggregated along the storage period in current DNA: GNRs ratio, PD-Gs conjugants remained better dispersity. This observation provided further evidence to prove the simplicity to manufacture the GNR-DNA vaccines with a different coating layer for long term storage.

To evaluate the effect of full ELTB gene as an additional adjuvant to improve the delivery and expression of DNA vaccine, this pcDNA3 YFP -L1-ELTB was still applied in the cell and animal work for preliminary evaluation. However, the pcDNA3 YFP -L1 were successfully cloned, which will transcribe and translate both L1 protein and indicator protein YFP. The following two chapters will narrate the *in vitro* and *in vivo* expression efficiency of these GNRs-DNA complexes in details.

### **3. *In vitro* studies of HPV GNRs-DNA complexes**

#### **3.1. Abstract**

The first assessment of vaccine in the biological system was *in vitro* analysis based on primary epithelial cell lines and immune cells for evaluation of expression and cell viability. Owing to the finite time, excretion profile of cytokines, integrins and chemokines has not been completely investigated in this project. However, I demonstrated the successful internalization of DNA-GNP vaccines and enhanced expression of L1 genes and fluorescent indicator genes when HeLa, HEK293, and murine macrophages were incubated with 5% (v/v) vaccine solution. Based on the previous study of the surface modification improved GNP cytotoxicity, MTT and apoptosis study indicated the dose-dependent cellular cytotoxicity of raw GNRs in similar size with a high dosage as 10% (v/v) induced intensive activation of caspases. Aspect ratio alteration up to 5 caused limitedly low effects to GNR induced cellular cytotoxicity. Vaccine dosage calculated according to our previous estimated volume percentage as 1% (v/v) is approximately  $10^{-12}$  M (0.05  $\mu\text{g}/\text{ml}$ ) GNRs based on the absorption coefficient of different sized GNPs, was inferred by a hypothetical cellular dispersion rate of 300 particles per cell in 96-well plates with  $1 \times 10^4$  cells<sup>250</sup>. It suggested a reasonable GNRs concentration of 10% (v/v) surface-modified GNRs in cell application with a cell density seeded from  $1 \times 10^6$  cells/well. Excluding the cytotoxic possibility of CTAB and polymer substrate by re-suspending GNRs in distilled water after twice wash, moderate cytotoxicity due to increased cell apoptosis



was observed with an improved cell viability and remained apoptosis effect after GNRs surface modification were observed in several assays. In the presence of surface-modified GNRs adjuvants, the expression of viral genes along with plasmid indicator fluorescent gene was highly enhanced even without the supplementary ELT gene.

## **3.2. Introduction**

For the application of DNA-nanorods vaccination, there are several questions concerning the interaction between GNPs and cells. How do the cells internalize GNRs-DNA complexes? Where will the GNPs stay in the cell and what are the cellular trafficking mechanisms related to different size, surface composition, molecular weight, surface charge and hydrophilicity? Is DNA-nanorods complex toxic to the cell? What is the final fate of the GNPs?

Several physicochemical parameters can affect the application of ordinary biodegradable polyelectrolytes, such as layer assembly sequence, micro-patterning, thickness, surface charge, pH changes, the salt concentration of polymer, roughness, biodegradability and biocompatibility<sup>304-311</sup>. These factors presumably influence the DNA-nanorods uptake, distribution, cytotoxicity and release of DNA for gene expression.

### **3.2.1. From cell uptake to GNP distribution**

#### **3.2.1.1. GNPs internalization**

Previous studies have clearly demonstrated that the uptake, toxicity, aggregation and distribution of GNPs are in size-dependent manner<sup>312,313</sup>. It is known that small nanoparticles (less than 30 nm) are able to cross the cell membrane through

energetically unfavourable endocytosis process<sup>314</sup>. The GNPs in a range of 30-50 nm were tracked in the endosome vehicles (sized 300-500 nm), and form nanoaggregates in lysosomes of various cell lines, which were revealed by transmission electron microscopy (TEM) in several studies<sup>315-320</sup>. As the scattering signal of GNPs smaller than 30nm is difficult to be identified, researchers defined the optimal diameter for GNPs to investigate cellular uptake in the reasonable range of 40-60 nm<sup>302</sup>.

However, cells internalize objects with a size ranged from 100nm to 500nm via phagocytosis pathway to form larger cargoes. Cargoes travel routes is from early endosome to the late endosomes and finally reach lysosomes for degradation. The whole process is based on specific sorting mechanisms mediated by a group of Rab proteins<sup>321</sup>. Rab5 regulated by endosomal autoantigen EEA1 for endosomal fusion mainly appear in early endosomal trafficking, while Rab4 and Rab11 mediate the recycling mechanism<sup>322</sup>. Rab7/Rab9 present in late endosome stage and deliver substrates together with phagocytosis and autophagy to the primary degradative compartments of the cells. This compartment for degradation maintained by integral membrane protein LAMP is called lysosome<sup>323,324</sup>. The endosomal pathway is highly integrated with the autophagosomal and lysosomal pathways involving in both early and late-endosomal fusion<sup>325</sup>.

For receptor-mediated endocytosis, requires a cluster of NPs clumps together to produce enough energy for completely wrapping the NPs on the cell membrane with

long diffusion time. Comparing GNRs with different particle sizes for drug delivery, increasing particle size attenuates cellular uptake through endocytosis<sup>302</sup>. Since the uptake speed and ability of receptor-mediated endocytosis of NPs are influenced by the binding energy of ligands to receptors and the diffusion kinetics for the recruitment of receptors to the binding site, as well as the thermodynamic driving force for wrapping the NPs. Particles larger than 80 nm cannot be completely wrapped into membrane with a full curvature. Size range of GNRs between 40 to 60 nm is more optimal to achieve membrane bending rigidity and ligand-receptor binding energy<sup>326-328</sup>. Therefore, larger or smaller sized GNRs beyond this range, exhibited a movement to the top of extracellular cells and bound to the cell membrane rather than cellular entrance<sup>302</sup>. The longer of the size, the faster and stronger movement for immobilization of GNRs on the top outside of the cells observed<sup>302</sup>. Additionally, the larger colloid particles are less stable to keep monodisperse morphology, but resulting in large aggregates. Interestingly, GNRs aggregates not only appear an extracellular adhesion on the surface, but also stimulate the cell growth<sup>329</sup>.

Efficient trafficking of endocytosed intracellular GNPs are influenced by not only particle size, but also determined by surface properties, aspect ratio, nanoconstruct geometry and concentration<sup>330,331</sup>. The internalization of high aspect-ratio particles in micro-particles was much faster than the more symmetric low-aspect-ratio particles. GNPs with high aspect ratios also demonstrated negligible phagocytosis coated with IgG compared with spherical particles with equal volume<sup>332</sup>. In the diameter range of 30 to 90 nm, GNSs in a size of 50 nm were more efficiently

internalized by cell lines like prostate cancer cell<sup>330 333</sup>. Small sized NPs with high aspect ratio were internalized faster than cubic and cylindrical NPs via multiple endocytosis pathways<sup>334</sup>.

Moreover, the modified surface coating could enhance the cellular uptake and speed up intracellular transport of GNPs. The unmodified GNP surface performs as the glass substrate, which is hard to interact with cells<sup>335</sup>. In biological system, the self-assembly of organic, inorganic, soft and hard, polymers and lipids, lipids and proteins for functional bio-NPs is due to utilization of hydrophilic nature of materials to modify the hydrophobic inert substance gold colloid<sup>336</sup>. The hydration repulsion between NPs promote their colloidal stabilization in water solution<sup>337</sup>. Aggregation was slow at low ionic strength and practically absent at ionic strength volume fraction less than 0.03, due to stabilizing effect of the electrostatic repulsion of the intervening medium<sup>338</sup>.

Beside liposome hybridised particles targeting special protein receptor, other biocompatible protein-based nanosystems, like recombinant self-assembled VLPs derived from HPV as multivalent vaccine carriers have been explored for cervical cancer<sup>339</sup>. For gene delivery, cationic liposomes and polymers combine anionic nucleic acids facilitate a high degree of DNA immobilization.

One critical role of adjuvant is to protect DNA from degradation and enhance the uptake and expression of vaccines. The pH, charge and molecular weight of the

coating surface will further affect the endocytosis type and efficiency, and facilitate transport of carried materials into different delivery targets. Usually GNRs were predominantly trapped within endocytic vesicles without nuclear presentation. Typical uptake pathway of NPs is endo-lysosomal pathway, which transports the particles in to lysosome for degradation or exocytosis out of the cells. The drug and gene release from the endosomes by different means is dictated by the properties of delivery particles. The pH from the endosomes to final lysosomes changes from 6 to 4, which impacts the structure and physical status of surface coated NPs to destabilize the membrane of the vesicle. This observation was applied to developing acidic nanoparticles to restore lysosomal acidic environment and improve its degradative function to degrade materials delivered by autophagy or phagocytosis <sup>340</sup>.

Previous studies have revealed that GNP-liposomes resulted in 1000-fold higher cellular uptake compared to bare GNPs. In contrast, similar to the cationic lipid-based delivery systems <sup>193</sup>, the cationic polymer-DNA complexes studies in the last decade, demonstrated that compacting DNA into particles through electrostatic interactions was able to protect the DNA from enzymatic degradation and the positive charge of polymer-DNA complexes facilitate the cellular uptake <sup>341</sup>. One of the well-evaluated polycationics is PEI <sup>282,302,342</sup>. As a promising DNA delivery material, PEI provide the DNA access to the cytoplasm because of its capacity to permeabilize the endosomal membranes<sup>343</sup>. Evidences demonstrated the penetration of PEI-GNRs into cells by caveolin-dependent and lipid raft-mediated endocytosis and enhance the accumulation in endosomal and nuclear localization of PEI-DNA complexes than other cationic lipids <sup>341,344</sup>. During endocytosis penetration, PEI

induces osmotic swelling of endosome and subsequently raise the burst of endosome through protonation, an influx of chloride ions caused by their large numbers of amine groups<sup>345</sup>. This ‘proton-sponge effect’ provide DNAs with an effective endosomal escape and increased cytoplasmic release. Especially increasing amino groups with more branching polymer promotes more sufficient cellular uptake <sup>346</sup>.

Other polyelectrolytes, like PDDA, were also well-studied to fabricate the surface of NPs for biocompatible layer-by-layer biosensing probes and delivery system <sup>347–349</sup>. Studies have shown that PDDAC fabricated GNRs generated higher cellular internalization than PeG coated samples <sup>280</sup>. The PDDA coated layer performs not only as a dispersant, but also provides an electrostatically organized coating layer with controllable thickness and positive charge. An aspect ratio of 4 shaped PDDAC coated GNRs presented higher and more efficient cellular uptake than negative-charged GNRs <sup>350</sup>. The quaternary ammonium groups structured PDDAC is able to destabilize the activity of endosome, and disrupt the endosomal or lysosomal membrane to provide sufficient endosomal escape of DNAs <sup>207,351</sup>. The endosomal escape and ultimate localization of GNRs assist GNRs-DNA to improve DNA delivery and subsequent exogenous gene expression <sup>205</sup>.

The peaks of two-photon luminescence matched bright-field peak perfectly during the GNRs aggregation in cell experiments, which provide GNRs sized with a NIR emission observable in normal bright-field imaging during aggregation <sup>350</sup>.

### 3.2.1.2. GNRs intracellular delivery

As mentioned earlier, the interaction between NPs components and endosomes will affect the cellular location of NPs. Desired cellular location can be tuned by decorating NPs with various conjugants that are recognizable by the endogenous intracellular trafficking machinery<sup>321</sup>. The functionalized GNRs with different surface chemistry and tuneable physical properties generate various delivery approaches to escape the final degradation from lysosome<sup>352</sup>. Two major functions revealed in endosomal escaping for organelle targeting<sup>321</sup>. Some NPs can interact directly with the endosomal membrane depending on the surface charge under acidic conditions<sup>353,354</sup>. Others escape from the degradative compartments by fusion with other vesicles towards final destination without lysis<sup>355</sup>. PEIs could permeabilise plasma membrane by disrupting the outer membrane of vesicles<sup>356</sup>.

The influence of PEI coating in GNRs-DNA combination indicated remarkable result in endocytosis procedure and final delivery. The outer layer of PEI reduces the aggregation of GNPs-DNA complexes and presents GNRs cargo within endocytic vesicles. In contrast, the final outer layer designed with DNA in PEI coated GNRs caused the aggregation into larger clusters in endocytic vesicles. This observation implied that the internalization of GNRs-DNA complexes is highly dictated by the type of the outer coating layer<sup>357</sup>. This formation of layer-by-layer coated GNRs is critical for the final fate of GNRs-DNA complexes, because data demonstrated the



top-layer coating will consequently influence the proper delivery for the final release and presentation of drug including functionalized genes.

GNPs are able to distribute to living organs <sup>312214</sup>. It increases the potentials to exploit drug delivery, imaging investigation and gene therapy. The organ distribution differ according to the size, incorporated components, diffusion, agglomeration, surface charges and administration route of NPs complexes. PEI with an average molecular weight of 22 kDa formulated DNA complexes are found in lung, spleen, liver, heart and kidney via intravenous administration, together with a prolonged organ retention <sup>358</sup>. In a recent *in vivo* study PeG-GNPs were mainly found in Kupffer cells in the liver and in macrophages in the spleen which resulted in acute inflammation in the mice livers after intravenous injection <sup>359</sup>. Another *in vivo* study demonstrated smallest samples (10nm) GNSs distributed to more organs in mice than larger sized ones at 50, 100 and 250nm <sup>360</sup>. Blood, liver and spleen are the more frequently presented sites of their vast samples. However, the possible organ burden is negligible in this project due to the low-dosed intra-nasal vaccination selected rather than intravenous injection of GNRs-DNA.

There are more observations that smaller GNSs could appear in multiple organs involving heart, lung, thymus, brain and reproductive organs. Semmler-Behnke have compared the bio-distribution of 1.4 nm with 18 nm GNPs after intravenous injection in rats, and demonstrated that the 18nm GNPs are almost completely disappeared from the blood within 24 h and consequently accumulated predominantly in liver and

spleen. But the ones in size 1.4 nm had a small amount of residue in liver and spleen, and majority are excreted through the kidneys and hepatobiliary system <sup>361</sup>. On the other hand, 1.4nm GNPs more readily translocated through the air-blood barrier of the respiratory tract than the 18nm GNPs.

This well-developed GNPs delivery platform applied for selective delivery target by manipulating the surface with specific conjunction. Functional peptide modified GNPs complexes provide high penetration efficiency to nuclear membrane <sup>362</sup>. Size-influenced selective uptake of GNPs is furtherly applied in the tumour treatment, because the GNPs in 20 – 100nm are possible to diffuse into the tumour interstitium as the leaky vasculature of the tumour blood vessels passively <sup>256,363</sup>. Proteins like anti-epidermal growth factor receptor (anti-EGFP) antibodies and tumor necrosis factor- $\alpha$  (TNF $\alpha$ ) has been successfully grafted upon GNPs surface and achieved efficient growth inhibition of various tumours in clinical trials assisting thermal-therapy <sup>279,363-365</sup>.

The VLPs act as one kind of NPs in several studies. HPV-1 based VLP incorporating HPV-16 E7 protein was reported to elicit strong specific CD8+ cytotoxic T lymphocytes to protect mice against tumours <sup>366</sup>. The anti-E6 antibody conjugated into tri-calcium phosphate modified NPs displayed stronger anti-sensing efficiency with enhanced binding with complementary E6 mRNA <sup>367</sup>. In previous evaluation about NPs-DNA complexes, researchers developed an oligomannose liposome based HPV16 E6/E7 DNA vaccine, which evoked HPV16 E6-specific cytotoxic T

lymphocytes effectively. Therefore, the delivery of the HPV viral gene coated layer-by-layer fabricated GNRs is highly possible to achieve a cross-protective and genotype-specific prevention and treatment against HPV infection induced malignant tumours.

### 3.2.2. Biocompatibility of NPs based delivery system

There are possible toxicity effects of nanoparticles to cause cellular irreversible damages due to oxidative stress or organelle injury. The acute adverse side effects of some dose/size-dependent GNPs are mainly caused by the free binding reagents rather than the inert GNPs, or a large sized GNP aggregates<sup>206,329,368,369</sup>. Higher concentration could cause apoptosis and upregulation of pro-inflammatory genes<sup>370</sup>. In one *in vivo* assessment, the unfit detoxication system will influence its toxic reaction to GNPs. The administration of GNPs could increase the inflammatory response, hepatotoxicity and stress-induced apoptosis of damaged liver<sup>371</sup>. Smaller positively charged NPs were more toxic than bare and larger sized NPs, which has been observed *in vitro* and *in vivo*<sup>329,371,372</sup>. In an *in vitro* studies, 1.4nm GNPs cause cytotoxicity via oxidative stress and mitochondrial damage, and finally resulted in necrosis for cell death<sup>373</sup>. GNPs with in size of 3.7nm penetrate nucleus and cause no cytotoxicity<sup>374,375</sup>. In an *in vivo* studies the smaller sized NPs induced cell death and dysfunction in mice due to inappropriate membrane permeabilization raised higher risk of Alzheimer's disease<sup>356,376</sup>. Additionally, comparing with anionic particles, cationic NPs tend to generate certain toxicity due to cell lysis rather than receptor-mediated endocytosis<sup>377</sup>.

Data collected from *in vitro* and *in vivo* studies have been consistent that the bare GNRs do not elicit severe cytotoxicity or elicit strong immune responses, especially when GNRs have stably bonded coatings<sup>330,368</sup>. CTAB-fabricated GNPs platform does not cause serious cytotoxicity, but free CTAB are highly toxic<sup>250,378</sup>. Thus, the cytotoxicity GNPs could be minimised by changing the physical properties, such as size, shape, surface charge, surface chemistry, and agglomeration<sup>224379380</sup>. GNR becomes instable when CTAB is removed. Hence, several polymers have been used to functionalize the GNRs surface. These include poly-(acrylic acid) (PAA), poly-(diethylammonium chloride)-poly(4-styrenesulfonic acid) (PDADMAC-PSS), PEG, PDDAC and PEI<sup>381-384</sup>.

Toxic effect could be observed in other cationic free coating reagent, like PEI<sup>286</sup>. Furthermore, although the deposition of cationic PEI onto coated surface demonstrated highly efficient gene delivery, free PEI is cytotoxicity due to high molecular weight which hinders its biocompatibility for clinical application<sup>385</sup>. This risk can be minimised by removing unbounded polycations from the transfection solution, or replacing the high molecular weight branched PEI (which is greater than 2kDa) with a smaller-molecular weight 600Da nanogram<sup>211,344,386</sup> (Fischer et al. 2003). However, the polymers with lower molecular weight usually do not have enough cationic charges for a stable polycation complex formation to delivery materials efficiently into the cell<sup>387</sup>. Therefore, the optimisation must be balanced to obtain relative higher molecular-weighted polycations to maintain strong electrostatic interaction with nucleic acids.

Fabricating the outer-layer with other bio-materials, such as BSA, oligo/polypeptides, oligonucleotides, antisense RNA, antibodies, reduces cytotoxic as well <sup>204,287,350,388–390</sup>. Moreover, although no effects on cell viability at a low concentration, PDDAC or PSS coated GNRs are found to have cell-specific effects on expression of certain genes <sup>280</sup>. Up-regulation of heme oxygenase-1 specifically occurs in mouse embryo fibroblast cell-line but not in other cell-lines.

Interestingly, GNRs show useful antiseptic and disinfectant function. The quaternary ammonium groups, which are the main component of PDDAC polymer, are able to disrupt the endosomal membrane <sup>391,392</sup>. Both degradable and non-degradable polymers have been applied in developing delivery systems for drug release, which obtained different properties <sup>393</sup>. The biodegradability of polymeric materials depends on the chemical structure, functional group stability, reactivity, hydrophilicity, and swelling behaviours. In addition, the physico-mechanical properties such as molecular weight, porosity, elasticity and morphology are responsible for the biodegradation as well <sup>394,395</sup>. The drug release from the non-degradable materials remains relatively constant, which is more linked to the thickness and permeability <sup>396</sup>.

In contrast, there are other potential advantages of biodegradable polymers carrying reducing toxicity and the preventing polymer accumulation in the cells after repeated administration. Furthermore, the degradation of the polymers can be applied as a tool

to release the plasmid DNA into the cytosol <sup>287</sup>. This release ability requires the unstable polyion complex formation of polycations inside cells for efficient biological activity with low cytotoxicity after degradation, in accordance with efficient selective endosomal escape.

The acidic pH-responsive polycations generate highly buffering capacity at pH 5.0-7.4 to disrupt endosomes when the endosomal maturation induced decreased pH to near 5 in later-endosome <sup>397-399</sup>. The buffering effect induces an extensive influx of proton and increases chloride ion during endosomal maturation, leading to disruption of the endosome by the influx of water with hypo-osmotic pressure. <sup>387</sup>. Due to high buffering ability, PEI forms a pH-sensitive delivery system for preventing the cleavage of the acid-labile linkable in antisense conjugates and delivering nucleic acids <sup>207,400,401</sup>.

In the GNRs-DNA synthesis work, four types of vaccine formulation developed. Two recombinant plasmid DNAs YL and YEL (pcDNA3 YFP-L1 and pcDNA3 YFP-L1-ELT) were synthesised, which were furtherly conjugated with two surface-coated GNRs separately. The outstanding capacity of this platform to promote proton sponge-mediated endosomal escape of DNA enhanced the sufficient expression of HIV-1 proteins intracellularly <sup>207</sup>. In this project, I'll investigate the following: 1, the internalisation and cellular location of GNRs and GNRs-DNA; 2: cell cytotoxicity by GNRs-DNA; 3: L1 capsid protein expression after GNRs-DNA internalisation.

### 3.3. Materials and Methods for In Vitro Experiments

**Table 4- Reagents and recipes used in cell experiments**

Name	Description	Conditions
DMEM complete medium	Dulbecco's Modified Eagle Medium (DMEM), fetal bovine serum, 110 mg/L sodium pyruvate, 10 ml/L of 100x non-essential amino acids, 100 units/ml penicillin and 20 µg/ml streptomycin	pH: 6.1-6.2, biological safety cabinet (BSC) of class II
Growth medium (gDMEM)	DMEM, 20% heat-inactivated foetal calf serum (HI-FCS), 30% of L-cell conditioned medium, 5 mM L-glutamine, 100 U/ml Penicillin and 100 µg/ml Streptomycin	Freshly prepared in a BSC
Completed RPMI-1640	10% FBS, supplement with 0.3 g/L L-glutamine, 125 µg/ml 100 U/ml Penicillin and Streptomycin	4°C, Sigma
HeLa	Human cervical cancer cells, ATCC® CCL-2™	37°C, 5% CO <sub>2</sub>
HEK293	Human embryonic kidney cells, ATCC® CRL-1573™	37°C, 5% CO <sub>2</sub>
Broad-range protein ladder	Biolabs	-20°C
Flow-check Pro Fluorospheres	Beckman Coulter	4°C
Calbrite™ 3 beads	BD Calibrite™	4°C
DNA Transfection reagent	X-tremeGENE9, Roche	4°C
Anti-HPV16 L1	Ms, mAb, ab 30908, Abcam	-20°C
Anti-mouse-TRICT	Goat, anti-mouse, ab6786	-20°C
Alexa Fluor®680	Goat, anti-rabbit, IgG (H+L), life technology	-20°C
Vybrant® Apoptosis Assay	Kit # 6-V23200, Molecular Probes™, Invitrogen	
Biotin-X annexin V (Component A)	250 µl of a solution in 25 mM HEPES, 140 mM NaCl, 1mM EDTA	pH 7.4
Propidium iodide (Component C)	100 µl of a 1 mg/ml (1.5 mM) solution in dH <sub>2</sub> O	
5X annexin-binding buffer (Component D)	28ml of 50 mM HEPES, 700mM NaCl, 12.5 mM CaCl <sub>2</sub>	pH 7.4
10 × TBS (1L)	24.2g Tris, 84 g NaCl	pH 7.6
1 × T-TBS	1 mL of Tween 20 / 1L of 1 × TBS	
10 × SDS Running buffer	144 g Glycine, 36.3g Tris Base, 50ml 20% SDS	1 L
10 × Towbin buffer	144 g Glycine, 30.3 g Tris	1 L
Resolving gel buffer (1.5 M Tris HCl, pH 8.9)	Tris Base 18.1 g (Trizma base, sigma), Dissolve in 40 ml H <sub>2</sub> O and make up to 100 ml	pH 8.9 4°C
10% resolving gel (1.5mm)	6.25 distilled water, 3.75 LGB-resolving buffer, 5ml ACE, 10% APS 60µl, TEMED 20 µl	
Stacking gel buffer (0.5 M Tris HCl, pH 6.8)	Tris Base 6.06 g (Trizma base, sigma), Dissolve in 40 ml H <sub>2</sub> O and make up to 100 ml	pH 6.8, 4°C
10% stacking gel	Upper gel buffer 3.75ml, dH <sub>2</sub> O 9.25ml, ACIYL 2ml, 150 µl aps, 15 µl TEMED	
SDS-PAGE Coomassie staining solution	0.25 g Biorad Coomassie R-250, 200 ml methanol, 50 ml glacial acetic acid, dH <sub>2</sub> O upto 500 ml	
SDS-PAGE destaining solution	200 ml methanol, 100ml acetic acid, 700 ml dH <sub>2</sub> O	1 L

### 3.3.1. Cell culture

HeLa and HEK293 were routinely cultured at 37 °C under 5% CO<sub>2</sub> with completed Dulbecco's Modified Eagle Medium (DMEM). Completed DMEM contains 10% heat-inactivated fetal bovine serum, 110 mg/L sodium pyruvate, 10 ml/L of 100x non-essential amino acids, 100 units/ml penicillin and 20 µg/ml streptomycin. Cells were passage into separate flask when the culture was confluent. For routine culture, medium was replaced 2-3 times a week. During cell passage, the culture was collected and centrifuged at 1500 rpm (rotor: 11.5cm) for 5 minutes at room temperature. All cell work was completed in sterilized biological safety cabinets (BSC).

Macrophage study based on sacrificed BALB/c mice was processed following the schedule 1 procedure ordinarily assisted by Muattaz Hussain. Mature murine bone marrow-derived macrophage (BMD M $\phi$ ), cultured from the femurs of 7-8 weeks-old male BALB/c mice. In this project, BMD M $\phi$  was applied to study the potential responses of macrophages during in vivo immunization. Intact and clean murine bones stripped from sacrificed BALB/c mice were immersed in 70% ethanol few minutes for sterilisation. BMD stem M $\phi$  Cells were flushed from the femur with 5ml gDMEM from the stripped bones maintained in pre-washed by sterile gDMEM and singled passing through a sterile BD falcon 40 µm cell strainers (Becton and Dickinson Company, Ireland). Stem cells were cultured in gDMEM for 8 days with medium substitution at the 4th day, added with L-cell conditioned medium extracted



from the metabolised upper medium from L-929 culture. This type of murine fibroblastic cell line secretes macrophage colony stimulating factor (M-CSF) into the culture, which becomes a necessary conditioned supplementary for the growth and differentiation of BMD stem M $\phi$ . Matured M $\phi$ s were harvested by centrifugation at 1500 rpm for 5 mins and seeded into 24-well plates ( $1 \times 10^6$  cells/well) with completed RPMI-1640 (Sigma, 10% FBS, supplement with 0.3 g/L L-glutamine).

### **3.3.2. Cellular uptake & Cell viability assay**

#### **3.3.2.1. Cellular uptake**

The assessment of cellular uptake was based on the cellular expression study and apoptosis assay in this project. A dark-field optical part was applied working together with a confocal scanning microscope. Laser scanning confocal microscope (LSM510, Leiss) was equipped with a 60W metal halide light with a hemisphere glass lens. Based on the dark-field imaging study by Wang's group<sup>302</sup>, the uptake of GNRs in this work illustrated a stronger dark scattering intensity. Larger organelles internalizing GNRs aggregates are able to generate more intensive colour with dark-field imaging.

#### **3.3.2.2. MTT assay**

MTT (3-(4,5-Dimethylthiazol-2-yl)-2,5-diphenyltetrazolium bromide) assay was carried out in the following procedure. HEK293 cells were seeded at  $1 \times 10^4$  cells per well in 96-well plates. After 24 h of incubation (37°C, 5% CO<sub>2</sub>), a series of samples including 5% reagents, 5% (v/v) GNRs, 5% (v/v) GNRs-DNA complexes and the same amount of DNA samples as the vaccine complexes (in dH<sub>2</sub>O) were added to each well. The cells were further incubated overnight. In the next day, 20 µl of MTT (4 mg/ml in PBS) was added to each well and incubated for up to 4 h at 37°C, 5% CO<sub>2</sub>. After careful removal of the media, 150 µl of DMSO was added to each well to solubilise the purple crystals. After being incubated at 37°C for 10 min, OD<sub>540nm</sub> was measured with a plate reader (Epoch BioTek).

### **3.3.2.3. Flow cytometry analysis of GNRs cytotoxicity**

Flow cytometry was applied to evaluate the intracellular uptake of surface-coated GNRs. Due to the high population required to performed triplicate measures, each GNR sample was washed twice with distilled water and 5% (v/v) GNR solution in PBS for incubation with HeLa cells for 1 h at 37°C under 5% CO<sub>2</sub>. HeLa cells were seeded in 6-well plates with a population as  $10^6$  cells/well. After 2 days, 5% GNRs samples (OD was adjusted around 1.0) were added to the cell culture for 1 h. Medium was not changed. After 1 h incubation, cells were washed with PBS, then harvested and fixed in 4% paraformaldehyde (PFA) for 15 minutes. Propidium iodide (PI) is impermeant to live cells and apoptotic cells, and only provide a red-fluorescence through binding to the nucleic acids. Triplicate samples were sorted in each experiment, 10,000 events per sample. The distribution was determined using a

MoFlo Cell Sorter (Beckman Coulter). PE-A depict PI stained dead/dying HeLa cells. The excitation and emission were 535/617 nm for PI. A population was gated according to the PE-A parameter by fluorescence beads calibration for the positive signal. Data acquisition and analysis was performed using Kaluza™ software (Beckman Coulter, UK).

#### **3.3.2.4. Apoptosis assay**

Cells were maintained in RPMI-1640 (Sigma) supplemented with 0.3 g/L L-glutamine and 10% FBS (Fetal Bovine Serum). Cells were grown for 5 days. Reagents were prepared according to manufacturer's manual (Vybrant® Apoptosis Assay Kit # 6-V23200, Molecular Probes™, Invitrogen). After 5-day culture, except the control sample, tested cells were treated with 10% GNRs for 1 day. High GNRs dosage (10%, v/v) was applied in the apoptosis assay, because proved dose-dependent cellular cytotoxicity of raw GNRs in this high concentration inducing intensive activation of caspases was observed in our previous investigation<sup>250</sup>. The plate was gently centrifuged at a speed of 90 g for 10 minutes at room temperature. The supernatant was moved completely. Then cells were rinsed with 1×PBS gently to remove extra GNPs without causing the cell detachment. Add 100 µL of 1×annexin – binding buffer and 5 µL of Biotin –X annexin V (Component A) to each well and incubate the cells at room temperature for 15 minutes. Centrifuge the plates with a same slow speed, and discard the supernatant. Repeat wash with 0.5ml 1×annexin-binding buffer and centrifuge again before adding another 100µL of 1×annexin-

binding buffer. Annexin V is a calcium-dependent phospholipid-binding protein, which has a high affinity for the phosphatidylserine (PS). The apoptosis will cause PS translocation to be detected by Annexin V. Add 1  $\mu$ L of 1mg/ml Alexa Fluor dye, listed in the table (Table4), and incubated the plates on ice for half hour binding process. Half hour later, after another binding buffer wash, 1  $\mu$ L of 1mg/mL PI stock solution was added to the culture. Cells were stained with PI on ice for 5-10 minutes, and later with 100  $\mu$ L 4% paraformaldehyde (PFA) for 15 minutes at room temperature. Finally cells were covered with a coverslip for imaging with Confocal Leica LSCM, HCX PL APO CS 20 $\times$ 0.7 IMM.

### **3.3.3. Gene expression analysis of GNRs-DNA complexes**

For the GNRs-DNA expression experiments, there were mainly five techniques involved. 1: cell culture and treating; 2: Immunocytochemistry; 3: Western blotting; 4: Flow cytometry; 5: Imaging.

#### **3.3.3.1. Cell treating**

HEK293, HeLa and M $\Phi$  were pre-cultured in the 24-well plates for imaging work, and 6-well plates for flow cytometry. The growth condition was as previously described. After 2-day culture for HEK293 and HeLa, or 5-day culture for M $\Phi$  cells, 10% GNRs or GNRs-DNA conjugates were added in the culture (medium was not changed). After incubation for a certain experiment time, which was according to the

experiment type, cells were gently washed. For HEK 293 and HeLa, positive controls were the plasmid delivered by a transfection reagent (X-tremeGENE9, Roche), with the same DNA concentration as GNRs-DNA complexes (10%, 1.6ng/  $\mu$ L). After post-infection time (labelled with each figures), cells were rinsed by 1  $\times$  PBS. For imaging, immunochemistry steps were listed in the next section; for flow cytometry, after PBS wash steps, cells were trypsinised, and centrifuged (MULTIFUGE 3 S-R, Heraeus). Steps were similar as apoptosis staining. Annexin V and the dye were replaced by anti-mouse HPV16 L1 (mouse, mAb, ab30908, Abcam) and anti-mouse TRICT (ab6786, goat), and the binding buffer was replaced by 1-2% BSA/PBS, or 1% FCS/PBS.

### **3.3.3.2. Flow cytometry parameters**

For the L1 expression analysis by both confocal imaging and flow cytometry, the first antibody was anti-mouse HPV16 L1 (mouse, mAb, ab30908, Abcam), and the second antibody was anti-mouse TRICT (ab6786, goat). YFP was excited by a blue laser with an excitation at 488nm and detected using FITC channel at 512nm emission; L1 labelled with TRICT was detected by PE channel at 559nm. Final data acquisition for flow cytometry (BD FACSDiva with Software v5.0.3, USA), was analysed by Kaluza™ software (1.02version, © 2009 Beckman Coulter, Inc.)

### **3.3.3.3. Immunochemistry**

After GNRs-DNA treatment and PBS washing, 200  $\mu$ L 4% paraformaldehyde (PFA) fixation 50mM  $\text{NH}_4\text{Cl}$  was applied on the slides for quenching. Wash the slides 5minutes with PBS, 0.1% Triton X-100 /PBS was applied to permeabilise cells for 10 minutes at room temperature. After 3 time wash with PBS, 5% BSA/PBS was applied to block the non-specific binding sites in the cells. The blocking procedure was recommended for 1 hr at room temperature. First-antibody was diluted (1:200) with 1%BSA/PBS overnight at 4°C. After 3 times wash by 1 $\times$  PBST, the second antibody was prepared as 1:500 dilution for 1 hr room-temperature incubation. Cells were a three-time wash again, and dry for staining cell nuclei with one drop of 4',6-Diamidino-2-Phenylindole, Di-hydrochloride (DAPI, ProLong® Gold antifade reagent, molecular probes, life technology). The image was done by LSCM (Leica, HCX PL APO CS 40 $\times$  0.7 IMM) and adjusted using Image J. or Corel Draw X5 software.

#### **3.3.3.4. Western blotting**

After cells were treated with the different GNRs-DNA for 72hrs, cells were washed and the medium was aspirated off for the preparation of cell lysates. An amount of 50  $\mu$ l of TNTE lysis buffer (150mM NaCl, 5mM EDTA, 0.3% TX100) was added into each well and kept on the ice for 5 mins with a fresh 1/25 dilution of protease inhibitor (Roche, 05892791001) added prior to stabilise the proteins. The cell lysate was removed from the well surface using a cell scraper and stored at -80°C in Eppendorf tubes before using. For preparing the fractionated proteins, cell lysate was centrifuged at 15,000  $\times$  g for 2 mins at 4°C. 20  $\mu$ l of each sample was mixed with 10

$\mu\text{l}$  2  $\times$  Laemmli sample buffer (Bio-rad, 1610737), containing 1% 1M Tris-HCl (pH 6.8), 4% SDS, 20% Glycerol, 25%  $\beta$ -mercaptoethanol and 0.05% Bromophenol blue. The mixture was heated at 100°C for 5 mins. A pre-stained broad-range protein ladder (Biolabs) as a molecular marker and 30  $\mu\text{l}$  boiled sample mixture were run together. Cellular proteins were fractionated after 1hr at constant 120 Volts in 1  $\times$  running buffer and transferred from the 10% SDS-PAGE gel onto polyvinylidene difluoride (PVDF) membrane by running the gel sandwiches for 40 mins in 1  $\times$  Towbin buffer at 0.4 Amber. Gel sandwiches prepare in an order as a sponge, 2 pieces of Whatman paper, gel, pre-methanol-soaked PVDF Immobilon membrane, 2 pieces of paper and sponge from the bottom to the top. The pH of transfer buffer requires being more than the protein isoelectric point in order to transfer the negative-charged proteins from cathode gel side to anode membrane side. After rinsing the membrane in the blocking solution (1  $\times$ TBS, 5% skimmed milk) for 1hr at RT, immobilon membranes were bound to primary antibodies HPV16 L1 (1:5000, mouse, mAb, ab30908, Abcam). After a careful triple wash process with 1  $\times$  TBST (5 mins/each time), membrane was bound to the second anti-mouse dye (ALEXA Fluor, 680nm, 1:5000 Invitrogen). Each antibody immunoblotting step was performed with 1  $\times$  TBS (5% skimmed milk) diluted specific antibody for 1 hr at RT by the aid of a bench roller. To clean the excess antibody on the membrane, triple washes with 1  $\times$  TBST (5 mins/each time) were required after each immunoblotting interval. Band images on the membranes were taken by a multi-wavelength scanner at 700nm excitation.

### **3.3.4. Statistical analysis**

Experiments were prepared with triplicate samples and investigated at least two times. For the imaging study, each sample was prepared in triplicate and images were taken from more than three random areas on each slide. Statistical analysis was performed by GraphPad Prism (5.0 version) and tested using one-way ANOVA following Turkey's Multiple Comparison Test, which measured  $p < 0.05$  as a statistically significant difference between samples. The sample size of cytotoxicity analysis by flow cytometry was only 1,000. In order to investigate the result appropriately, based on the results of mean and standard deviation measured by GraphPad, one-way ANOVA power analysis of F tests and to the "A Priori" power analysis was completed using G\*Power Data Analysis (version 3.1.9.2, Germany).

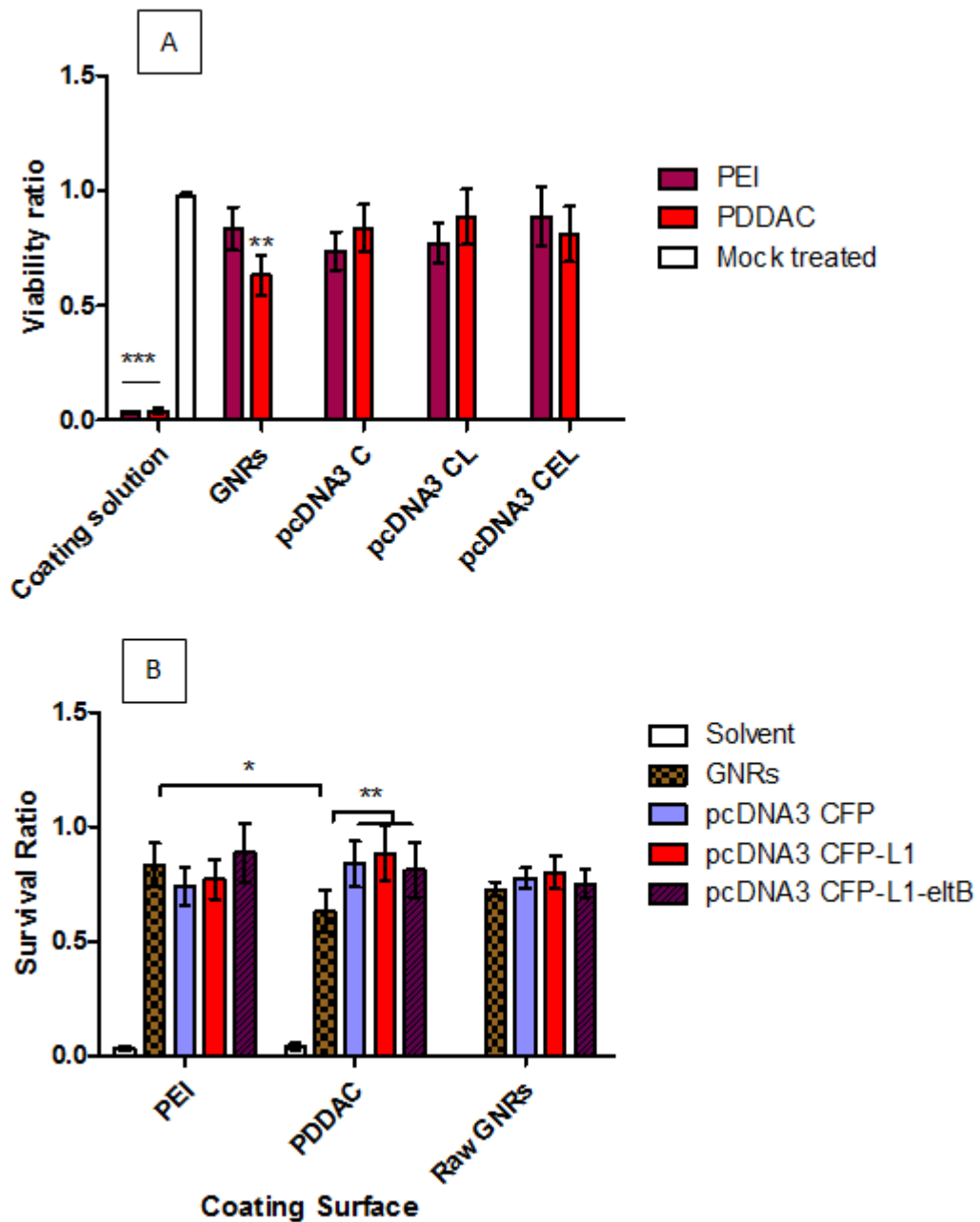


## **3.4. Results**

### **3.4.1. Cell Viability Assay**

#### **3.4.1.1. MTT assays in order to investigate cytotoxicity of GNRs or GNRs-DNA**

In order to study the effect of free polymers to cells, 2mg/ml coating solutions were cultured with HeLa cells. Although the previous study of DNA adsorption demonstrated the high affinity of positive-charged polymers to DNA and the stabilisation of surface-engineered GNRs in RT for 1 year, there is another important question about GNRs driven DNA vaccine, which is the cell viability of vaccine constructs. Meanwhile, since this type of GNRs-DNA structure comprises surface-coated GNRs and extracted plasmid DNA from *E.coli* culture, the cytotoxicity of polymer solution, raw GNRs and plasmids with or without ELT gene insertion was tested. Although an early study of experimental rabies DNA vaccine has already shown the endotoxin-free purification of milligram amounts of DNA based on improved techniques similar as using a commercial kit<sup>402</sup>, the cytotoxicity of extracted plasmid DNAs was also tested by MTT. Data was interpreted in two formats, one of which shows the effect of separated constructs, and the other one focuses on elucidating remained cell viability of the whole GNRs-DNA vaccines based on the previous study and speculated assumptions.



**Figure 17 - MTT assay for cytotoxicity of GNRs with different surface coatings.** Data shown in both A and B were generated from the same group of samples. A: the cytotoxicity effect of pure coating solution and plasmid DNAs. B: Remained cell viability of GNRs-DNA vaccines. HeLa cell viability was tested after an overnight (24h) treatment with samples including PEI- or PDDAC-solutions (2mg/ml), or mock treated with PBS, or treated with 5% PEI-GNRs or PDDAC-GNRs, or DNAs. DNAs tested for cell viability were isolated plasmids: pcDNA3 CFP (pcDNA3 C); pcDNA3 CFP L1 (pcDNA3 CL) and pcDNA3 CFP L1-ELT (pcDNA3 CEL). MTT derived purple precipitates were dissolved by addition of DMSO, and OD540nm was taken using a plate reader (Epoch BioTek). Pooled data from

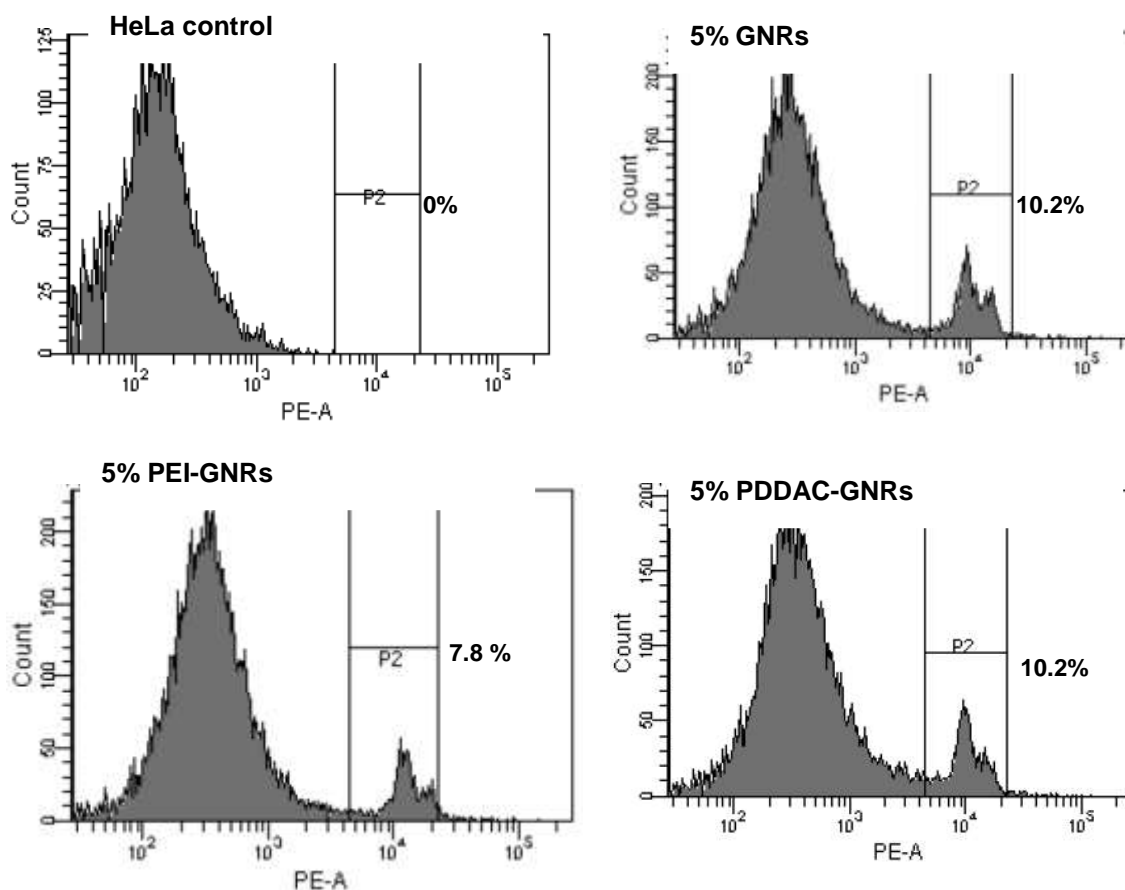
three experiments (triplicate in each experiment) were analysed with one way ANOVA before data re-grouped according to coating surface and expressed as mean + SD. Asterisks depict statistical significance (\*\*  $p < 0.05$ ; \*\*\*  $p < 0.001$ ).

In this assay, the first critical appearance is remained high cell viability after surface-engineered GNRs with cationic polymers. As shown in Figure 17, free PEI or PDDAC coating solutions significantly reduced the viability of HeLa cells, compared to mock treated control cells. In contrast, GNRs coated with PEI or PDDAC were much less toxic to HeLa cells; albeit both coats showed statistical significance (PEI,  $p < 0.05$  and PDDAC  $p < 0.001$ ). Both PE-Gs and PD-Gs were washed twice before applied to cell monolayers. This indicated that twice-wash with PBS was sufficiently to remove free PEI or PDDAC from GNRs and the high affinity of polymer surface to GNRs help to remain the cell viability. The strong adsorptivity of positive-charged PEI and PDDAC observed in this test is coincident with the affinity analysis illustrated in Figure 14, 15 & 16.

The cytotoxicity of GNRs-DNA remained low without significant difference between PE-Gs and PD-Gs adjuvant vaccines. Although PDDAC coating was slightly more toxic than PEI coating (Figure 17), conjugation with plasmid DNA render it less toxic (B, statistic insignificant:  $p > 0.05$ ). PEI and PDDAC gave different surface charge states (PEI is more negatively charged than PDDAC), which was probably the reason why PEI-GNRs were less toxic to HeLa cells. A non-significant variation of survival ratio among GNRs-DNA samples, which gives a better cell viability to PE-G-EL (PEI-GNRs-pcDNA3 CEL) and PD-G-L (PDDAC-

GNRs-pcDNA3 CL). In summary, PBS washes sufficiently removed toxic free PEI or PDDAC, and conjugation PEI or PDDAC coated GNRs with various plasmid DNA did not raise significant concerns in terms of cell cytotoxicity.

### 3.4.1.2. Flow cytometry analysis of cytotoxicity of GNRs



**Figure 18 - Flow cytometry analysis of cytotoxicity by GNRs or GNR with PEI/PDDAC surface coatings.** Each GNR or DNA-GNR sample was washed twice with distilled water and 5% (v/v) GNR solution was prepared in PBS for incubation with HeLa cells for 1 h at 37°C under 5% CO<sub>2</sub>. Cells were stained with propidium iodide (PI) for dead or dying cells. Triplicate samples were sorted in each experiment, 1,000 events per sample, using a MoFlo Cell Sorter (Beckman Coulter). PE-A depict PI stained dead/dying HeLa cells (gate P2). Each sample was prepared in triplicate without repeated test. The percentages of PI+

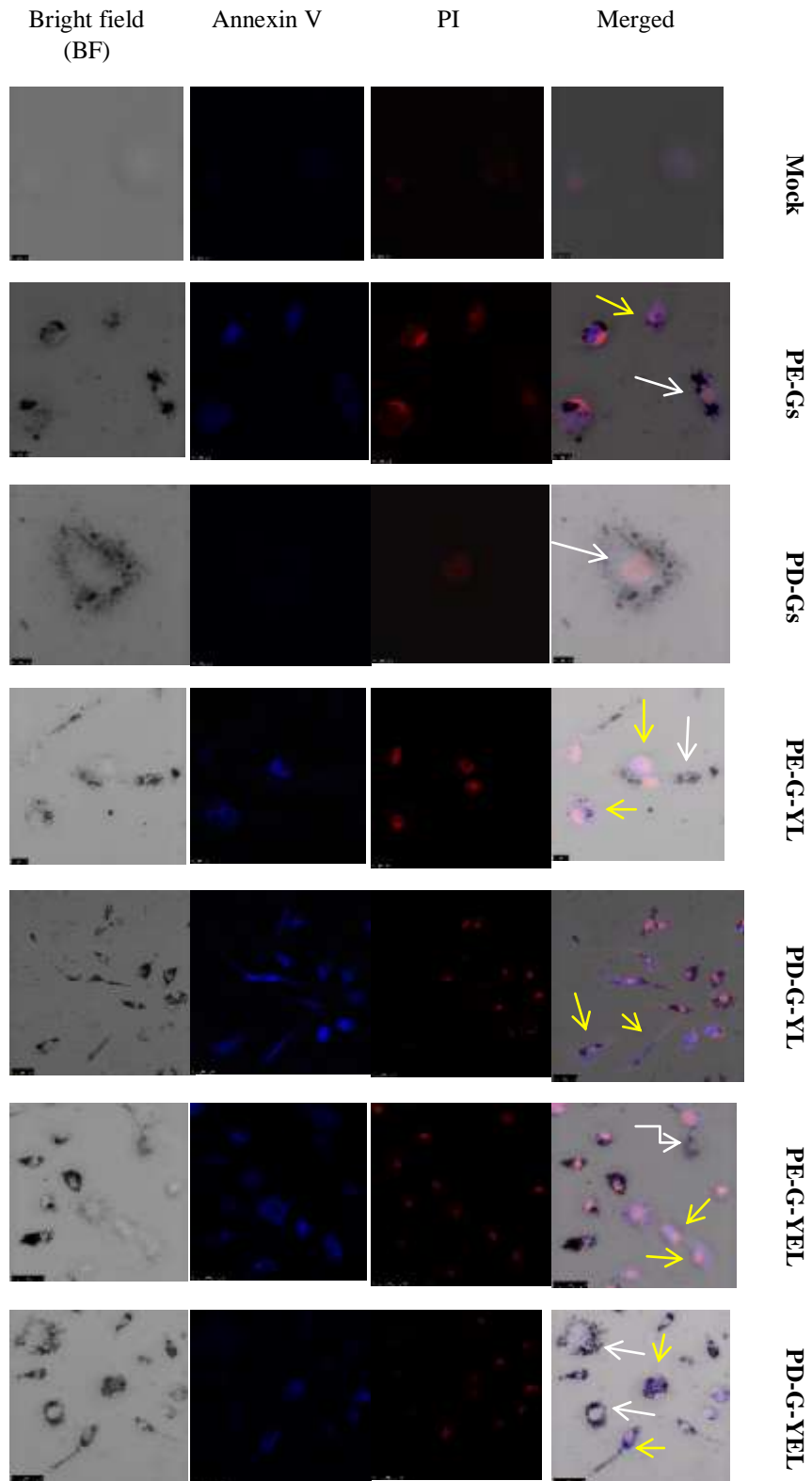
population were illustrated as means over triple measures for each sample. One-way ANOVA with Tukey's Multiple Comparison Test was applied resulting in a  $p$  value  $<0.001$  of tested samples over control. The result of PE-Gs cytotoxicity was significantly different to the others ( $p < 0.0001$ ). To evaluate the sample size, one-way ANOVA power analysis was applied using G\*Power Data Analysis (version 3.0.10) together with Graphpad (5.0) showed that an appropriate set of sample measurement (power=.95 and Alpha=.05) to avoid both type I and type II error require an appropriate sample size (measures/sample)  $>8$ , or a population  $> 3506$ .

Flow cytometry was utilised once in the study of cell viability after 1 h incubation of twice washed GNRs or coated GNRs in cells by a PI staining for dead cells. Corresponding to the previous data in Figure 17, GNRs without free CTAB maintained similar cell viability in contrast with PE-Gs and PD-Gs. Following the similar trend as Figure 17B, PE-Gs provided a lower cytotoxicity of 7.8% cell death compared with a 10.2% percentage of dying cells caused by raw GNRs or PD-Gs. Although the difference level of cell death was statistically significant ( $p < 0.001$ ) consistent with data obtained using MTT assay (Figure 17), a power analysis demonstrate the insufficient sample size for variation comparison. G\*Power estimating minimum sample sizes necessary to avoid given levels of type II errors based on the given levels (power=.95 and Alpha=.05) was a population more than 3506 cell counts or more than 8 repeated measures of each sample.

### **3.4.1.3. Confocal images for apoptosis assay**

As our previous study demonstrated, the higher concentrated (10% v/v) GNPs could cause apoptosis and upregulation of pro-inflammatory genes<sup>370</sup>, inducing intensive

activation of caspases<sup>250</sup>. During early apoptosis, PS translocate from the inside of the plasma membrane to the surface. Annexin V calcium-dependent phospholipid-binding protein will binds to exposed PS specifically on the cell membrane of early apoptotic cells, was analysed using confocal and bright field imaging.



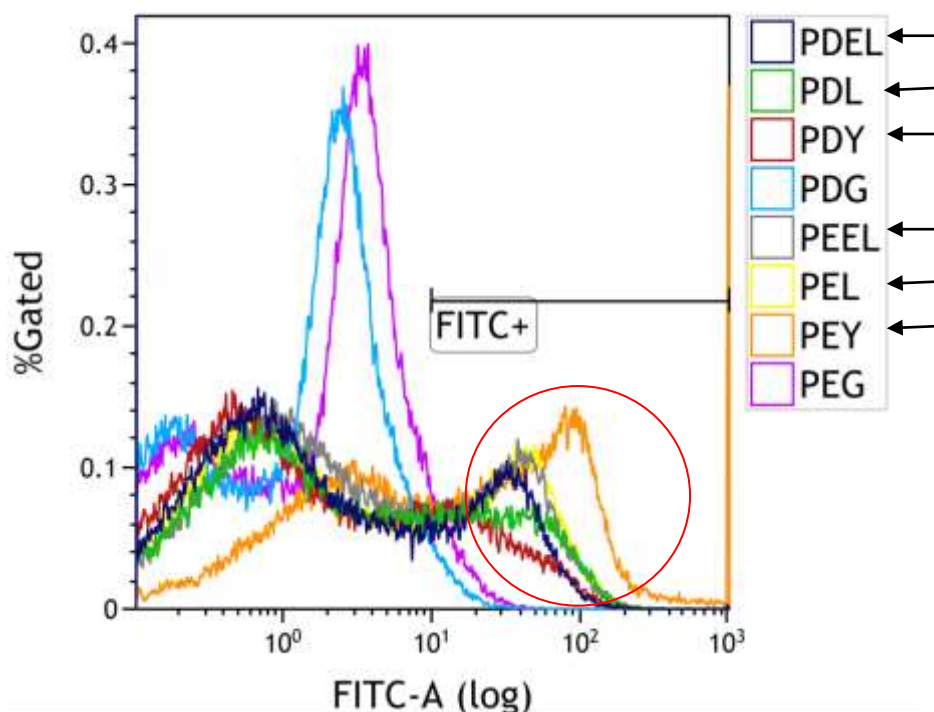
**Figure 19 - Confocal images of macrophage-like M $\Phi$  cells harbouring internalized GNRs or GNRs-DNA.** M $\Phi$  cells were differentiated in RPMI-1640 medium supplemented with 10% fetal bovine serum for 5 days, then incubated with 10% (v/v) GNRs or GNRs-DNA for 1 day at 37°C under 5% CO<sub>2</sub>. Annexin V was used to detect early apoptotic cells and PI was used to stain all dead or dying cells (apoptotic and necrotic). Black dots inside cells under bright-field are internalized GNRs or GNRs-DNA, which are not present in untreated control cells. The white arrows indicate live cells, and yellow arrows indicate the apoptotic cells.

BMD M $\Phi$  cells were active in internalizing GNR or GNRs-DNA; black dots were found inside treated but not untreated cells under a bright-field microscope (Figure 19). Internalized GNRs or GNRs-DNA were either dispersed in the cell cytosol or accumulated surrounding nuclei. After 1 day incubation with either GNRs or GNRs-DNA, nearly all cells harboured GNRs or GNRs-DNA albeit vary in numbers. Approximately 50% of cells with internalized GNRs or GNRs-DNA have undergone apoptosis under the vision field, which was detected by annexin V sensitively (Figure 19, yellow narrow). Plasmid DNA conjugation did not difference to PEI or PDDAC coated GNRs. Noticeably, the cell morphology of PEI-GNRs incubated cells presented with more rounded shape with PI stained damaged nucleus, while the PDDAC-GNRs provided more variant cell sizes and shapes.



### 3.4.2. Confocal microscopy for HPV L1 intracellular

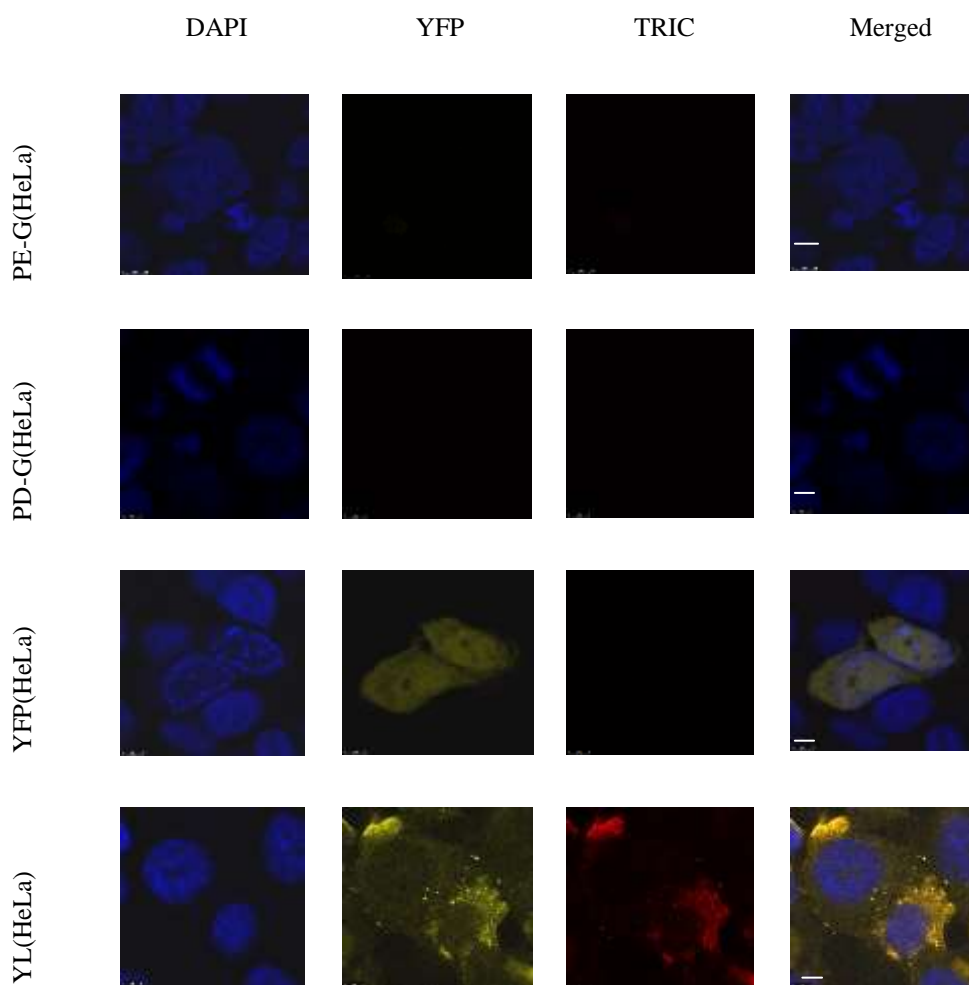
#### 3.4.2.1. Enhanced intracellular GNRs-DNA expression measured by flow cytometry analysis

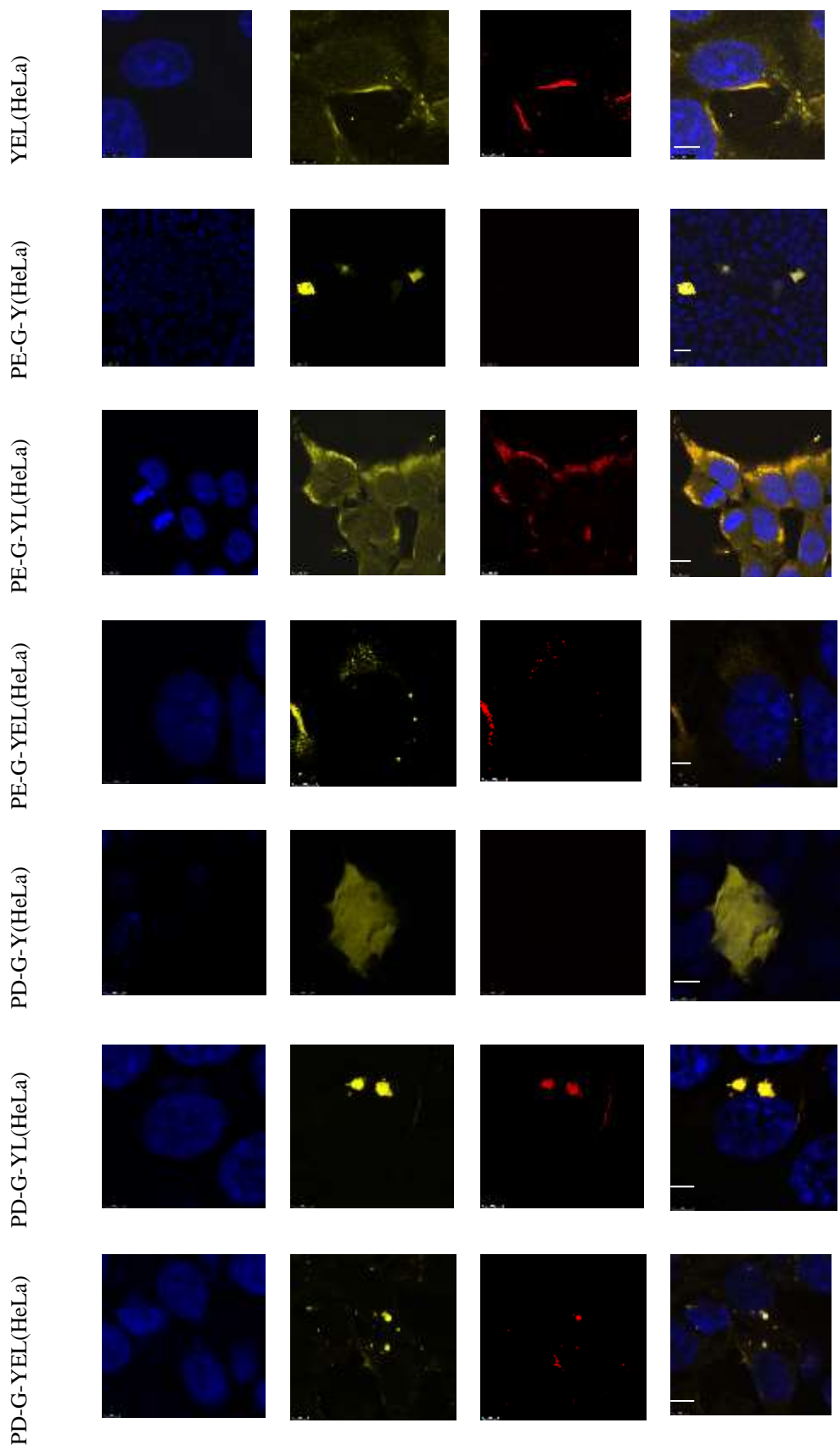


**Figure 20 - The expression of recombinant YFP plasmid DNAs.** HeLa cells were incubated with 10% (v/v) GNRs-DNA for 3 days, and a population of 50,000 cells per samples was analyzed by a flow cytometer (FACS Canto, BD). The plasmids used in this experiment were pcDNA3 YFP (Y), pcDNA3 YFP-L1 (L), and pcDNA3 YFP-L1-eltB (EL). Two negative GNR controls were negative controls and marked as PE-G (PE-Gs) and PD-G (PD-Gs) in the histograms. Calibration and compensation were completed during the measurement and analysis with beads (Calibrite™ 3 beads, BD) and analysis software (Kaluza v1.2). Arrows indicated samples with positive signals circled in the overlaid histograms.

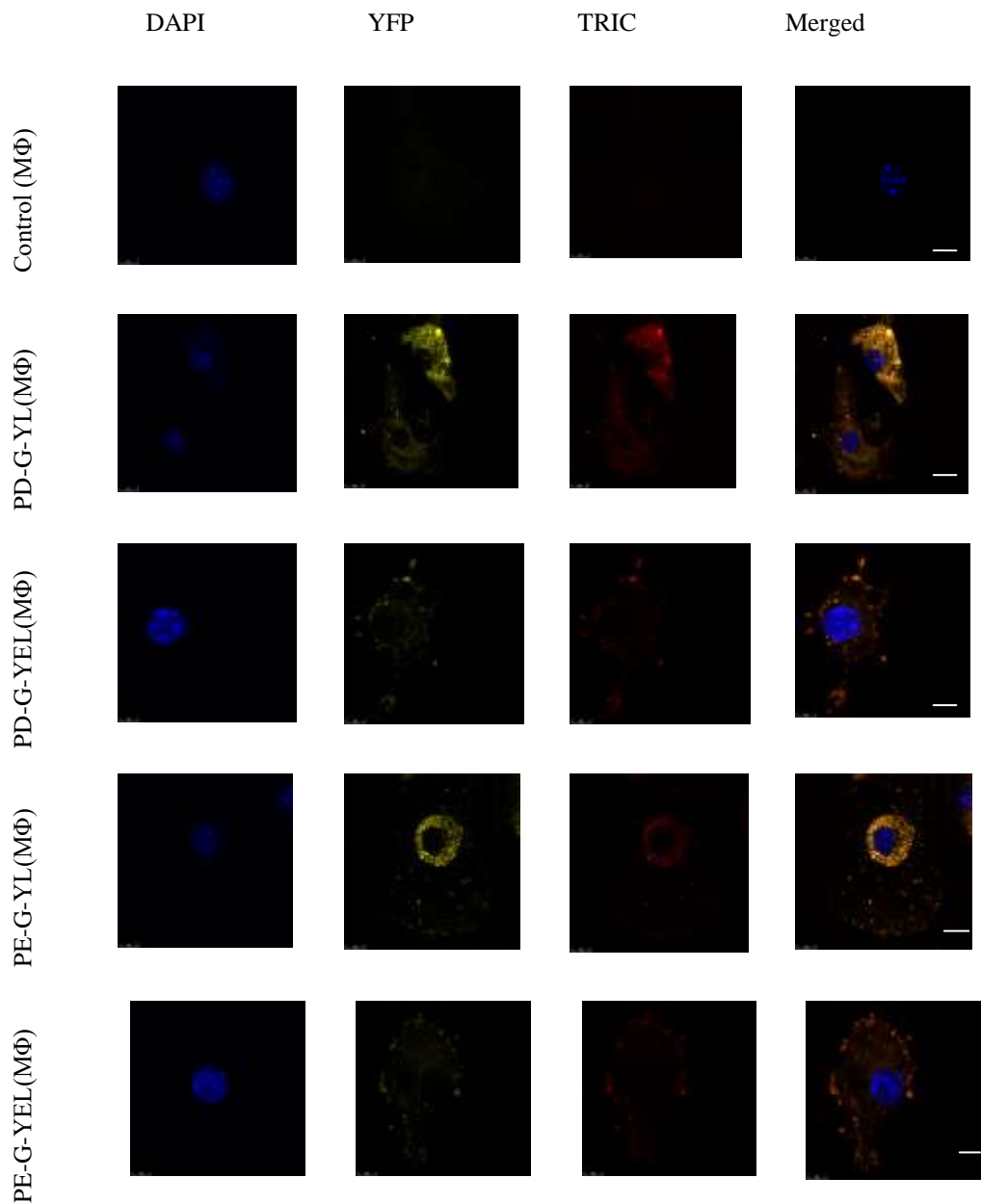
Three days after incubation with GNRs-DNA (either with PEI or PDDAC coat) cells (80% confluence) were positive in the expression of YFP as indicated by a clear fluorescent shift to the right around  $10^2$  (circle in Figure 20).

### 3.4.2.2. Enhanced intracellular expression of GNRs-DNA complexes observed by confocal imaging





**Figure 21 - Confocal microscopy for expression of HPV L1 capsid protein from GNRs-DNA in HeLa cells.** Various plasmid carrying HPV L1 gene were transfected to HeLa cells using transfection reagent (X-tremeGENE9, Roche). This was used to compare the efficiency with GNR-mediated DNA uptake and gene expression. Same DNA (80ng) as that of GNRs-DNA in (B). The DNAs were YFP (pcDNA3 YFP), YL (pcDNA3 YFP-L1), and YEL (pcDNA3 YFP-L1-eltB). B. HeLa cells were incubated with 10% (v/v) GNRs-DNA for 2 days. L1 protein was detected with a monoclonal antibody against L1 protein (abcam,ab30908) followed by goat/rabbit anti-mouse antibody TRICT (abcam, ab6786). Images were taken with laser scanning confocal microscope (Leica LSCM,). Scales bar = 5.5  $\mu$ m.



**Figure 22 - Confocal microscopy for expression of HPV L1 capsid protein from GNRs-DNA in BMD MΦ.** Sample preparation and confocal imaging were processed similarly to the description in Figure 21.

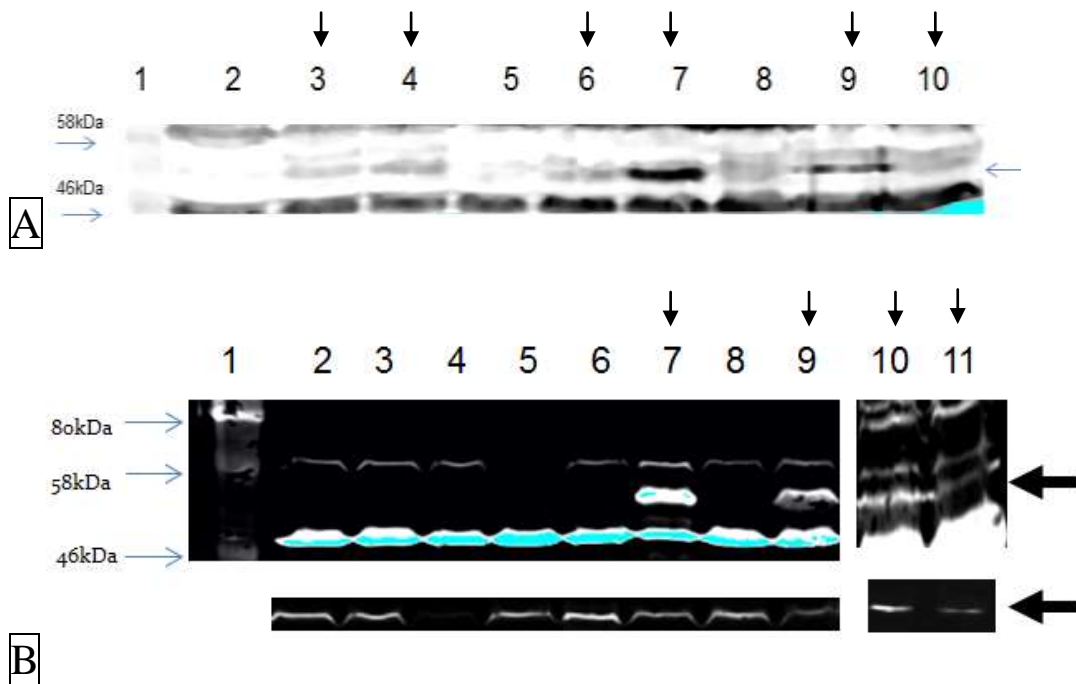
Laser scanning confocal microscopy (LSCM) was applied to investigate the cellular internalization of GNRs-DNA conjugates and the expression of recombinant L1 DNA plasmids in both HeLa cells and BMD MΦ (Figure 21 & 22). In agreement with the previous study, PEI/PDDAC-GNRs showed high efficacy to bring DNAs into cells as Figure 21. Yellow fluorescence protein and Tric-labelled L1 were observed intracellularly in this experiment with 2-day post-transfection, which demonstrated the successful cellular internalization of PEI/PDDAC-GNRs-DNA complexes. The observation of sufficient protein expressed in the cell cytosome indicated that DNAs were effectively brought into cell nucleus after uptake. Both pcDNA3 YL and pcDNA3 YEL achieved an enhanced expression after adjuvant with PE-Gs and PD-Gs.

### **3.4.3. Time-related GNRs-DNA intracellular expression observed within different incubation time**

In order to study the intracellular expression of L1 genes in each sample, both HeLa and HEK293 cells were treated with 10% GNRs-DNA for either 2 days or 3 days.

During the experiments, there was one technique problem due to the fragile attachment of HEK293 to the flask surface, which caused that a certain amount of cells was easily washed off. It was concerned that apoptosis or necrosis might happen to the cells according to confocal imaging after GNRs-DNA uptake (Figure 19). To confirm the enhanced expression of L1 in all GNRs-DNA samples, protein expression of 10% (v/v) GNRs-DNA treated HEK293 and HeLa cells was examined using Western blotting. Due to the weak attachment of HEK293 cells, treatment was only performed in 2 days. A time-related L1 expression in HEK293 cells was analysed by flow cytometry in a time course of either 17 hrs or 24 hrs, and apoptosis-induced cell loss was required to be concerned in the latter time course.

### 3.4.3.1 Testing L1 protein expression using Western blotting



**Figure 23 - Western blot for detection of L1 protein extracted from 10% GNRs-DNA treated HeLa (A) and HEK293 cells (B) for 3 days and 2 days respectively.** A: Line 1: Broad-range protein ladder (Biolabs); 2: 3-day HeLa control; 3: YL plasmid with transfection reagent; 4: YEL plasmid with transfection reagent; 5: PE-G; 6: PE-G-L; 7:PE-G-EL; 8: PD-G; 9: PD-G-L; 10: PD-G-EL. There were some probably leaking proteins at line 8. The blue arrow at right indicated the L1 protein site (55kDa, IgG2a, ab30908, Abcam). B: Cells were incubated with GNRs-DNA for 2 days. L1 protein was detected with a monoclonal antibody (IgG2a, ab30908, Abcam) Lines: 1, Hyperpage prestained marker (Bioline); 2: HEK293 control; 3: PE-G; 4: PD-G; 5: YFP; 6: YL; 7: YEL; 8: PE-G-L; 9 PE-G-EL; 10: PD-G-L; 11: PD-G-EL. The top arrow indicates L1 protein, and the bottom arrow indicates  $\beta$ -actin as the control.

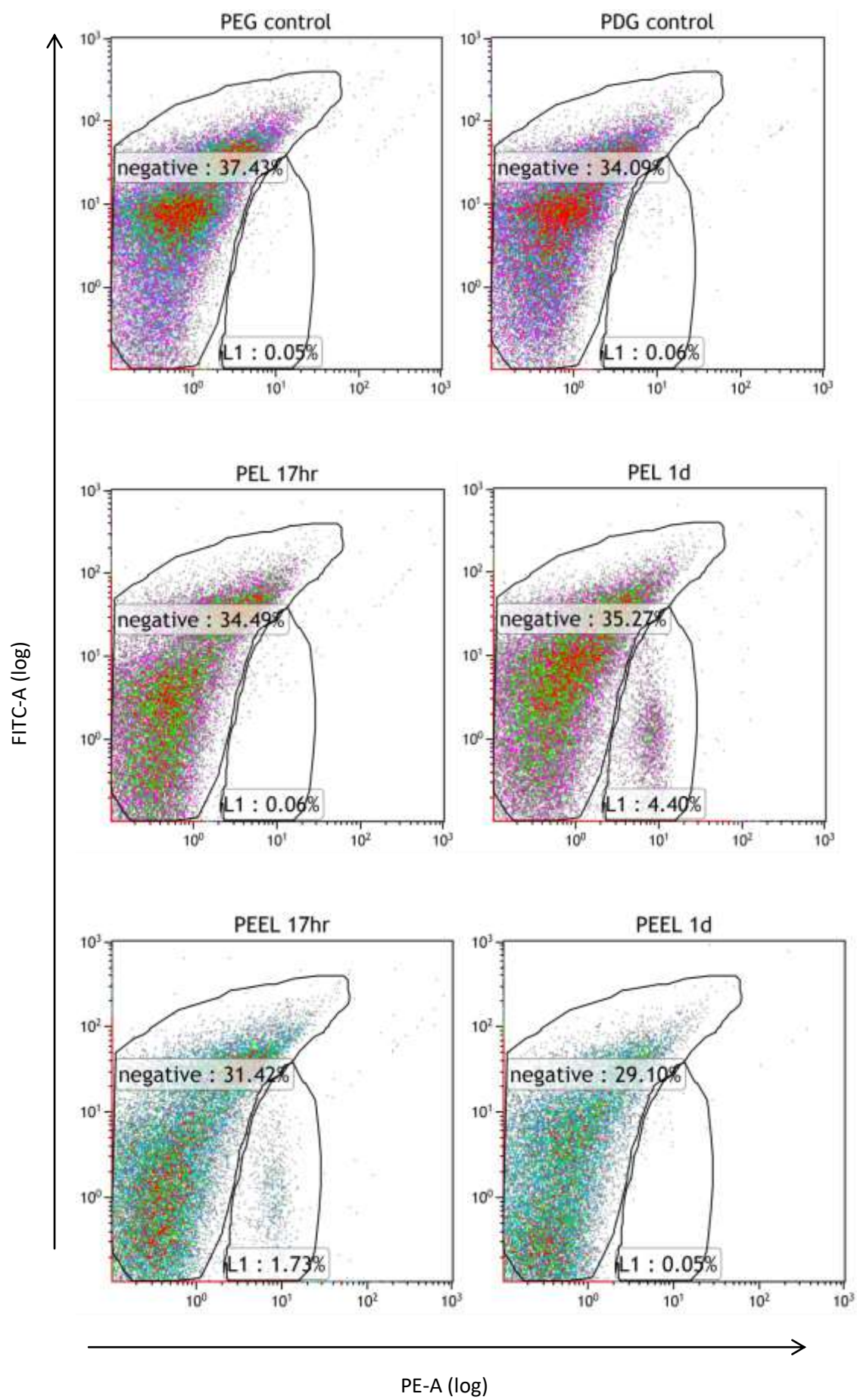
Western blot double-stained with L1 and  $\beta$ -actin was scanned at wavelengths of 700nm and 800nm respectively. L1 proteins were visualized between 46kDa-58kDa, according to the Hyperpage pre-stained marker on Lane2. Near 46kDa, there was a

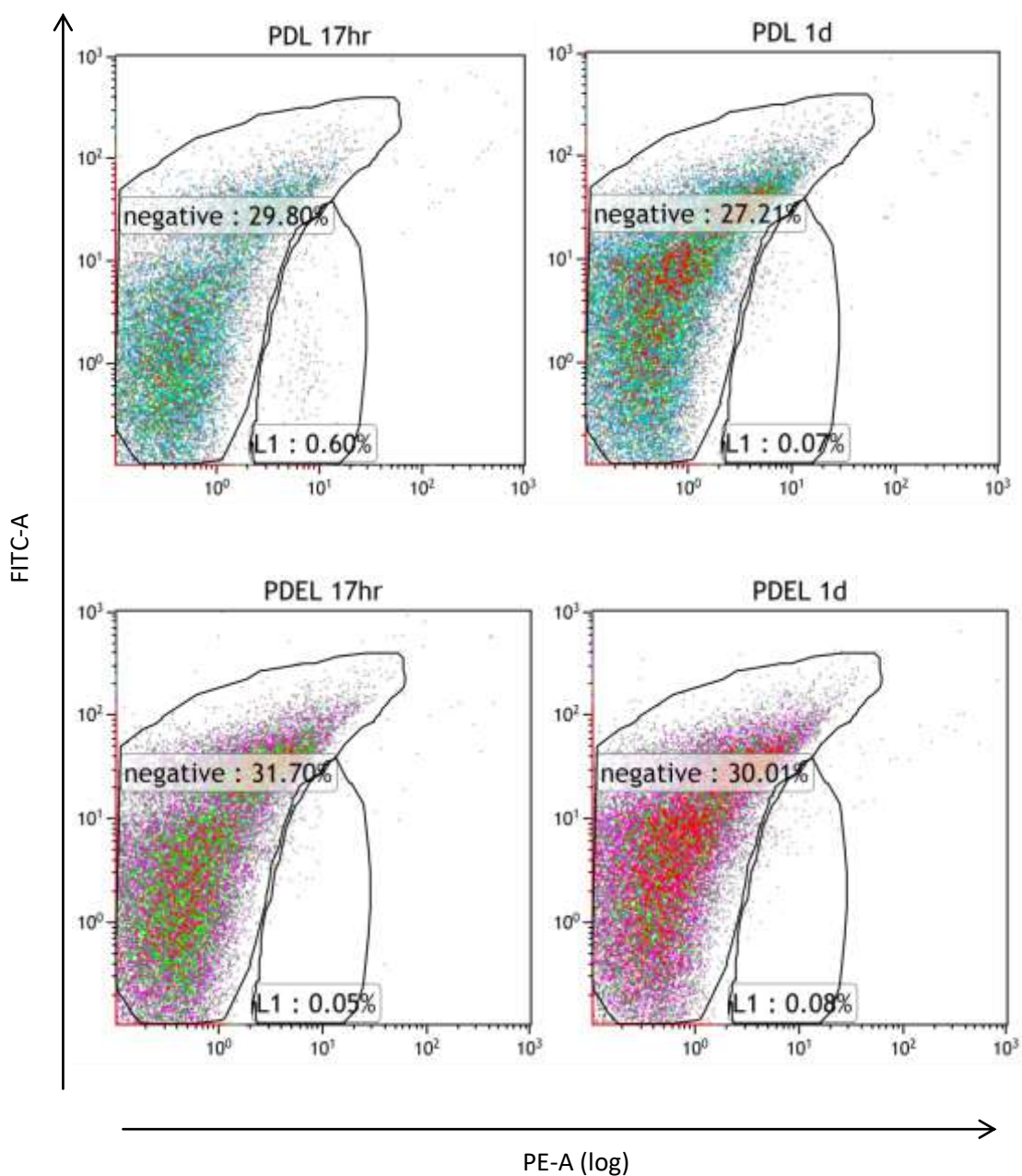
line of false binding caused by the anti-HPV16 L1 antibody (ab30908, abcam). For the two-day transfected HEK293 cells (B), Lane 7, 9, 10 and 11 highlighted by top arrow give a strong L1 signal. Comparing YEL (pcDNA3 YFP-L1-ELT) transfected by reagent in lane 7 (B) with YL (pcDNA3 YFP-L1) in lane 6 (B), which demonstrated an efficient adjuvant ability of Heat-labile enterotoxin. It is noticeable that GNRs-DNA complexes were successfully expressed with L1 protein detected on Western blot, except PEI-GNRs-L1 (PE-G-L) at line 8 for 2-day 10% GNRs-DNA treated HEK293 cells (B). However, corresponding to the data in MTT test (Figure 17), PE-G-EL and PD-G-L referring to lane 9 and 10 in Figure 23B performed a higher cell survival ratio and more remained L1 expressed cells in the Western blotting assay.

On the blot of transferred 3-day GNRs-DNA treated HeLa cells, observable expression of L1 genes was found in lane 3, 4, 6, 7, 9 and 10. The *eltB* gene contained plasmid resulted in a higher expression of L1 gene in lane 4 in contrast with L1 only in lane 3 (Figure 23A). Comparing with reagent transfection, surface-modified GNRs as adjuvant impressively increased the L1 expression in sample PE-G-EL (lane 7, A) and PD-G-L (lane 9, A). It was an affirmative analysis to demonstrate the promising adjuvant ability of PE-Gs and PD-Gs for DNA intracellular expression.

#### **3.4.3.2 Testing L1 expression by flow cytometry**







**Figure 24 – Time-related L1 expression in HEK293 cells by flow cytometry.** Flow cytometry (FAC Canto, BD) analysis of L1 expression 17 or 24 after incubation with 10% Surface-coated GNRs-DNA complexes, followed by anti-mouse TRICT immunochemistry staining (goat, anti-mouse, Abcam, ab6786) detected by PE-channel. In gate FITC, the signals of fluorescent protein CFP to indicate the DNA expression, were hard to be collected by FITC detector. The analysis was done by Flow cytometry software (Kaluza, v1.2). PEL: PE-G-L; PEEL: PE-G-EL; PDL: PD-G-L; PDEL: PD-G-EL

Similar to the result in the Figure 23, the variance of L1 expression after treatment of PE-Gs and PD-Gs in HEK293 cells was observed concordant with flow cytometry data (Figure 24). The Tric-labelled L1 population was gated according to the red fluorescence pattern indicated by a signal intensity of PE-A at  $10^1$ . As compared to the GNRs control, except PD-G-L, the other three complexes PE-G-L, PE-G-EL, PD-G-EL expressed L1 observed at a different time (Figure 24). At the time of 17hrs, PD-G-L and PE-G-EL exhibited a proportion of L1 expressed cells, while PD-G-EL expressed L1 shown at 24h. The expression variance of L1 gene among different GNRs-DNA samples might be caused by the higher loss of cells during wash procedures. The strong apoptosis induced by surface-coated GNRs was observed in confocal imaging (Figure 19). The different level of apoptosis stimulated by PE-Gs and PD-Gs doesn't influence the final expression intensity of GNRs-DNA vaccines.

### 3.5. Conclusion

The *in vitro* study of GNRs-DNA demonstrated a highly enhanced L1 gene expression in two cell lines (HEK293, HeLa) and BMD MΦ cells. The L1 expression of all GNRs-DNA samples was confirmed by a 3-day treatment of HeLa cells (Figure 23). Although the western blot indicated the PE-G-L and PD-G-EL complexes didn't strengthen the plasmid expression in 2-day treated HEK293 cells, the result was concerned to be influenced by the apoptosis or another type of cell death after 1 days. This expression variation was discussed previously and adjustable in both Western blotting and flow cytometry analysis. Although a portion of apoptotic cells was observed after 1-day treatment of GNRs-DNA complexes (Figure 19), there was no significant toxicity of GNRs-DNA detected by both MTT, the statistical analysis proved there was no significant decreased cell viability ( $p > 0.05$ ). Except for PD-Gs without DNAs conjugation generated a higher cytotoxicity, which was significantly reduced after DNA binding (Figure 17). In Figure 17B, PE-G-EL and PD-G-L provided a better cell viability with a higher L1 gene expression shown in Figure 23.

Apoptosis induced by this type of vaccines is able to benefit further *in vivo* immune response as mimicking a microenvironment during viral infection. Caspase I activation during apoptosis leads to the secretion and activation of IL-1 $\beta$  and IL-18 as pro-inflammatory signals<sup>403</sup>. Furthermore, DNA vaccination was reported to primer antigen-specific cytolytic T lymphocytes (CTLs) associated with IgG2a Ab production for an enhanced cellular-mediated immune-response with the assistance

of activated lymphokines and pro-inflammatory factors <sup>192</sup>. In the case of HPV immunisation, due to the non-lytic HPV life-cycle, a low profile of pro-inflammatory signals restricts the activation of DCs and MΦ cells causes virus immune evasion 1. In normal immunity, CD40-expressing ECs ligate with type II membrane protein CD40L (CD154) in both cellular and humoral immune responses activating DCs mature, stimulating production of pro-inflammatory cytokines and chemokines like IL8 (CXCL8) and CCL5, and upregulating MHC II and co-stimulatory molecules like CD80 and CD86 <sup>404</sup>. HR-HPV was observed downregulating the expression and secretion of various pro-inflammatory cytokines in the basal cells. A further discovery of the surface-charge induced apoptosis according to the significantly increased expression of 5 genes related to inflammation in macrophages after GNRs incubation showed stimulated pro-inflammatory effects by negatively charged GNRs but not by neutral or positively charged ones. The positive charge of GNRs surface led to anti-inflammation <sup>384</sup>. Therefore, these results foreshadow the climax of GNRs-DNA vaccines. HPV16 L1 recombinant DNA with adjuvants PEI/PDDAC-GNRs were further assessed in the mouse model.

## 4. Nasal immunization of BALB/c mice with GNRs-DNA

### 4.1. Abstract

Plasmid DNA carrying HPV16 L1 or HPV16 L1-*eltB* conjugated with either PEI or PDDAC surface-coated GNRs were used to immunize BALB/c mice via the intranasal route. GNR-associated pcDNA3 YFP was found to be highly expressed in mouse nasal and lung tissues one day after immunization. Humoral immune responses to GNRs-DNA were assessed by ELISPOT and SEAP assays, which detected ASCs in spleen lymphocytes specific to HPV16L1 capsid protein and neutralizing antibodies in blood plasma, respectively. Compared with purified HPV VLP, DNA-GNR constructs appeared to elicit variable numbers of ASCs, which might be influenced by the slight variation of cytotoxicity dependent on the surface coating and stabilisation and aggregation of surface-modified GNRs. Some individuals produced significantly strong activation of ASCs but some others produced fewer numbers of ASCs referring to the number of HPV 16 L1 specific IgG secreted ASCs stimulated by VLP vaccination. In general, PDDAC-GNR-pcDNA3-YFP-L1 (PD-G-L) was most potent than other DNA-GNR construct in eliciting ASCs. EAP assay showed that PD-G-EL (encoding *E. coli* heat labile toxin B subunit), elicited lowest levels of Nabs, whereas PE-G-L, PE-G-EL and PD-G-L1 elicited highest levels of neutralizing antibody. These data suggested that *eltB* and PDDAC may counteract each other resulting in loss of adjuvant function. Taken together, GNRs-DNA vaccines are potent in inducing immune-responses specifically to HPV type 16 L1 proteins in BALB/c mice. These constructs deserve further

investigation for an overall profile of secretion of the specific cytokines, chemokines and other factors in cellular-mediated immune response and local Nab in the cervix, including the cross-presentation ability of vaccine antigen.

## **4.2. Introduction**

### **4.2.1. VLP Properties**

As described in Chapter 1, the HPV L1 and L2 proteins are the late gene products. They regulate virus transmission, spread and survival in the host <sup>405</sup>. These proteins are also assembled into virion shells – the individual capsomere subunits in the viral capsid. Following viral entry into the suprabasal layers, these two capsid proteins self-assemble to icosahedral capsid shell composed of 72 capsomers assembled by 360 copies of L1 and 36-72 copies of L2 <sup>406</sup>. This structure envelopes viral genome DNA in the host cell cytosol <sup>407</sup>. Capsomers, or so-called pentamers in HPV virions are arranged in an icosahedral T = 7 particle lattice with a diameter of 55nm, including 60 hexavalent and 12 pentavalent pentamers, which were revealed under Cryo-electron microscopy <sup>408</sup>. The sequence variation in the major capsid gene L1 classifies more than 120 genotypes of HPVs <sup>2,3</sup>.

Immunogenicity is the ability of particular antigens to induce desirable immune responses in human or animals. The key immune response that offers protection against HPV infection is the induction of HPV neutralizing antibodies (NAb) in serum <sup>84,85,146</sup>. As a major structural capsid protein, L1 induces a humoral immune response, which is conformation-dependent; neutralizing epitopes accumulate on the surface of the capsid with immunodominance <sup>409,410</sup>. The neutralizing epitopes highly rely on hypervariable loop structures with highly homologous domains extending



outward from the capsid surface; each HPV type has distinct structures<sup>411</sup>. The stability of the type-specific conformation determines the titers of the neutralizing antibodies, and this conformation specific recognition mechanism is the key for the immune system to maintain a long-term conserved immune response against HPV antigens<sup>87,412</sup>. There are also conformation insensitive L1 epitopes, which could offer cross-reactive monoclonal antibodies (MAbs), but the neutralization titers are relatively low<sup>87,413</sup>. Relatively, the modifications of L1 may influence assembly into higher-order structures<sup>414</sup>, and denatured L1 possibly results in failure of the immune responses<sup>415</sup>.

In natural immune response of HPV infection, the small measurable antibody against the L1 major capsid occurs after a long period from the initial infection<sup>59</sup>. Therefore, the development of a prophylactic HPV vaccine requires deploying the virtue of major capsid protein L1 to be self-assembled in an eukaryotic expression system. Virus-like particles (VLPs) are comprised of assembled 72 L1 capsomeres in a shell with roughly similar size as L1 virions<sup>406,411</sup>. This type-specific NAb is the key in humoral immune responses against HPV infection, which has been approved by WHO as the main mechanism of VLP-based vaccines in human<sup>416</sup>.

The neutralization antibodies elicited by VLPs in vaccinated animals are predominantly specific to the immunodominant L1 epitopes<sup>417-419</sup>. Observations indicate that the immunogenicity of HPV VLP is highly conformation-dependent on the surface-exposed L1 loops. A small number of mutations of hypervariable residues in VLP surface-exposed loops led reduced neutralizing antibodies, cross-

neutralizing binding ability, and DNA encapsidation<sup>420</sup>. VLPs elicits a 20 – 40-fold increased humoral responses than capsomere alone<sup>421</sup>. However, rather than an epitope-dependent immunogenicity, studies demonstrated the immune activity of L1 capsomeres and VLPs is highly dependent on its subsequent assembly structure by capsomeres<sup>414,421</sup>. This property is same as naïve L1 virions for all types of papillomavirus derived from different species. No matter L1 capsid protein alone or with L2 co-presence, L1 is capable to self-assemble into VLPs in a recombinant expression system<sup>415</sup>. This property provides VLPs with high immunogenicity to induce IgG and IgA secretion<sup>85,422</sup>.

Evidence indicates that L1 VLPs may elicit long-term high neutralizing antibody responses with a synchronized trend of cytokine profile in peripheral blood mononuclear cells<sup>139</sup>. Strong immune response mediated by Th1 and Th2 polarized cells with a significant stimulus of cytokine and chemokine are critical to the efficacy of prophylactic vaccination. Apparently, VLPs triggers not only the high titers of IgG1 and IgG 2 in addition to Th1-reponse and Th2-response<sup>423</sup>, but also induce phenotypic maturation of murine bone marrow-derived DCs by strengthening their sensing and signaling between innate and adaptive immune responses via TLR4-mediated-MyD88 pathway<sup>140</sup>. Vaccination with HPV 16L1 VLP induced B cell activation including up-regulating the expression of costimulatory molecules by naïve B cells, increasing the B1 B cell subpopulation, and generating various pro-inflammatory factors like IFN $\alpha$ , IL-6, MIP-1 $\alpha$ , RANTES and KC<sup>424</sup>. Their potentials were also observed in other animal work<sup>425,426</sup> and clinical trials, which reveal more promising future not only as antigens for vaccines, but also as adjuvants benefitting

drug delivery, gene therapy and immune therapy<sup>427,428</sup>. VLP assembly can occur in mammalian cells as well as in Vaccinia, baculovirus, and yeast systems, without the assistance of other HPV oncogenes<sup>339,429,430</sup>. Therefore, HPV VLPs are highly immunogenic with self-assembled empty viral capsids without any self-infectivity, which are morphologically and antigenically similar to authentic virions<sup>431</sup>.

#### **4.2.2. VLP based immunogenicity analysis**

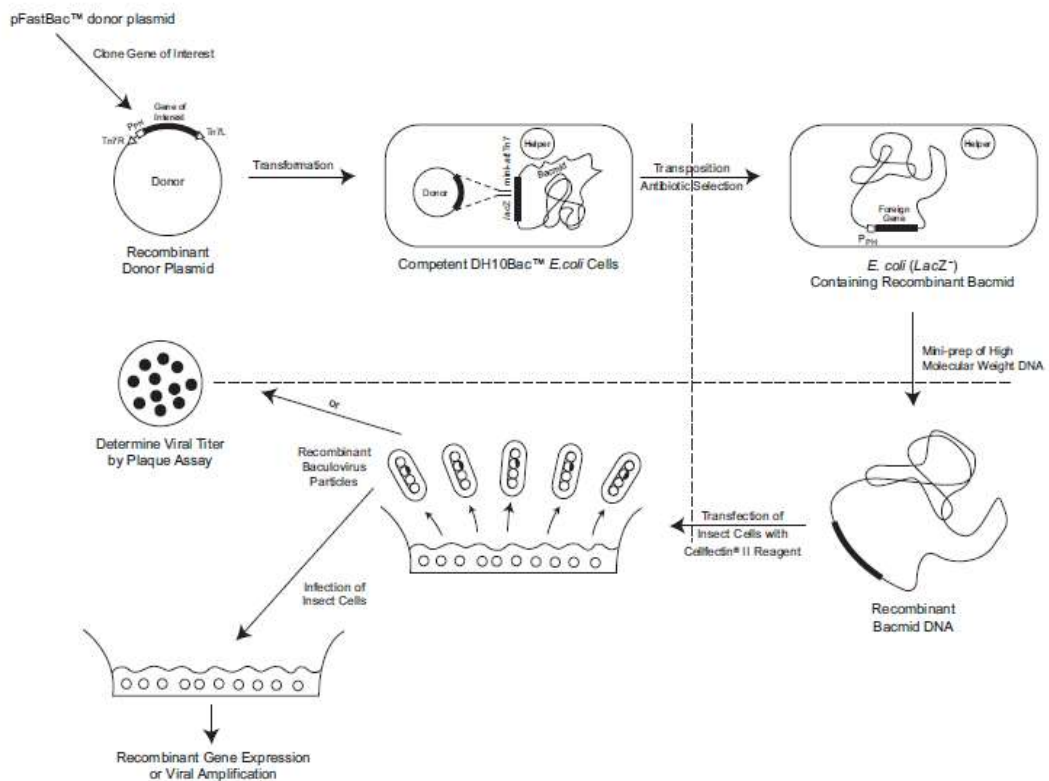
Besides the HPV-specific neutralizing antibodies, systematic immunoglobulin G (IgG) and passive transfer of serum from vaccinated animals are afforded protection against HPV infection<sup>85,161</sup>. A study of cottontail rabbit papillomavirus shows that passive transfer of serum or IgG pooled from pre-immunized rabbits with native CRPV L1-L2 results in protection of  $\frac{3}{4}$  nonimmune rabbit<sup>161</sup>. The pooled fractionated IgG antibodies from 'regressor' beagles, which were prior infected by canine oral papillomavirus (COPV), provide naïve weanling beagles with circulating IgG antibodies against further intraoral infection by high-copies of COPV<sup>162</sup>.

These animal studies have demonstrated the neutralizing IgG activity induced by VLPs in serum is a critical protective barrier. In contrast, local mucosa IgA is less specific and less protective than systematic HPV-11 L1 neutralizing antibodies. Although the cervicovaginal antibody responses have been demonstrated to be induced together with the serum responses for protection from HPV infection, a single dose of VLP vaccine could elicit predominant IgG, whereas a single dose is insufficient to elicit detectable VLP-specific IgA or polymeric secretory

immunoglobulin A (sIgA) in the vaginal wash. These are evidence that the antibodies detected in genital tract were originated from the serum <sup>36</sup>. In contrast with other mucosal immunization, the predominant immunoglobulin isotype secreted in female genital mucosal is IgG, but not sIgA <sup>37</sup>. Therefore, the presence of Nabs at disease-relevant sites (cervicovaginal) is consistent with their resource as systematic secretion of IgG.

### 4.2.3. VLP-based techniques in this *in vivo* work

#### 4.2.3.1. Bac-to-Bac® baculovirus expression system for His-tagged VLP production



**Figure 25 - Schematic illustration of Bac-to-Bac® expression system for generating recombinant baculoviruses (CAT. 10359-016, Life technologies, Invitrogen).**

The insect Sf-9 cells (*Spodoptera frugiperda*) were infected with baculovirus which harbored HPV16 L1. The recombinant bacmid DNA was constructed by Zheng and described in her previous publication <sup>429</sup>. As shown in Figure 25, DH10Bac competent cells containing the bacmid with a mini-attTn7 target site. The mini-Tn7 element is able to transpose to the mini-attTn7 target site in the insect cells genome mediated by transposase expressed from the helper plasmid. The initial recombinant colonies were obtained by blue-white selection in *E. coli*. The DNA was purified from the culture of white colonies. During the post-transfection with these recombinant baculoviruses, self-assembled viral particles were expressed and amplified in the insect cells. The supernatant is harvested from the culture for further infection. Stock used in this project was collected by Zheng in Professor Wang's lab (Xi'an Jiaotong University, China) and the infected insect cells were maintained at -80°C. The chimeric subunits on VLPs were engineered to have six histidine residues (His-tag) at the carboxyl terminus. The Nickel-chelating resin ProBond™ purification system could be used to purify the recombinant L1 protein <sup>432</sup>.

#### **4.2.3.2. Neutralization assay: HPV pseudovirions (PsVs)-based secreted alkaline phosphatase (SEAP) assay**

Neutralization assay is a widely used in detecting the immunogenicity of HPV VLP vaccines. In early decades, antibody-mediated *in vitro* neutralization of HPV pseudovirions (PsVs) was developed to detect HPV-specific antibody responses in the sera. This technique was further modified using PsVs from mammalian cells.

Pseudovirions (PsVs) expression was achieved in the *in vitro* HEK293TT cells which mimics the infection of native HPV virions. The pShell plasmid carried codon-optimized HPV L1 and L2 genes. The report vector pYSEAP expressed secreted alkaline phosphatase <sup>433</sup>. Both plasmids containing an SV40 origin of replication were transfected to HEK293TT cells, which co-express the SV40 large T antigen (TAg) to promote the synchronous replication of cell DNA and viral genome L1 and L2 <sup>434</sup>. This type of VLPs is infective and encapsulates both L1/L2 and a reporter gene – secreted alkaline phosphatase (SEAP) for detection. Self-assembled PsVs encapsulating the reporter plasmid, pYSEAP, which expresses alkaline phosphatase <sup>433</sup>. Transfection of cells with PsVs then leads to cleavage of chromogenic substrates (p-nitrophenyl phosphate), resulting in yellow precipitates which is the readout of SEAP assay. If sera containing the neutralizing antibody, incubation of sera with PsVs would prevent PsVs transfection, resulting in reduced phosphate activity with reduced yellow precipitates <sup>433</sup>. An online protocol was used in this study, “Production of Papillomaviral Vectors” by Dr. John Schiller in 2010 (<http://home.ccr.cancer.gov/lco/pseudovirusproduction.htm>).

Neutralization assay based on PsVs requires pre-incubation with sera with a serial dilution to titrate the neutralization capacity of antibodies specifically against PsVs. The higher efficiency of neutralization activity results in the lower degree of infection with less SEAP expression. As a result, the antibody-mediated neutralization of PsVs is indirectly detected as an inhibition towards SEAP activity by highly sensitive chemiluminescent reporter system <sup>433</sup>. This assay is dependent on multiple epitopes for appropriate assessment of vaccine protective potential including

all the Nab isotypes<sup>435</sup>. The procedure is complicated and required high purity of the PsVs preps.

#### **4.2.4. Mucosal immunization and HPV vaccination**

Mucosal immune responses are fundamentally distinctive from systemic responses. Delivering foreign genes to induce mucosal immunoreponse for epithelial immunity is always challenging in clinical practice despite successful studies using animal models<sup>40</sup>. There are several studies show that after DNA vaccination via the oral route significant levels of specific IgG and IgA and specific cytotoxic T lymphocytes are found in both intestinal mucosal sites and the whole circulation<sup>436</sup>. Intranasal immunization is the common route of animal vaccination, and this route induces significantly higher systemic neutralizing antibodies than orally immunised<sup>437</sup>. Immuno-responses initiated from one specific mucosal location after vaccination could result in immuno-responses in other mucosal sites. Antigen-specific immunoglobulin and inflammatory reactions are remarkably influenced by immunization route.

One study using the mucosal adjuvant cholera toxin has demonstrated that intranasal immunization elicits IgA responses and IgG-associated inflammation in respiratory tract<sup>438</sup>. The route of immunisation is paramount important as illustrated in (Figure 26). For eliciting IgA antibody response in the reproductive tract mucosa, the oral route is relatively inefficient compared with the intranasal route. This conclusion is drawn from a study by use of cholera toxin B subunit in humans through different

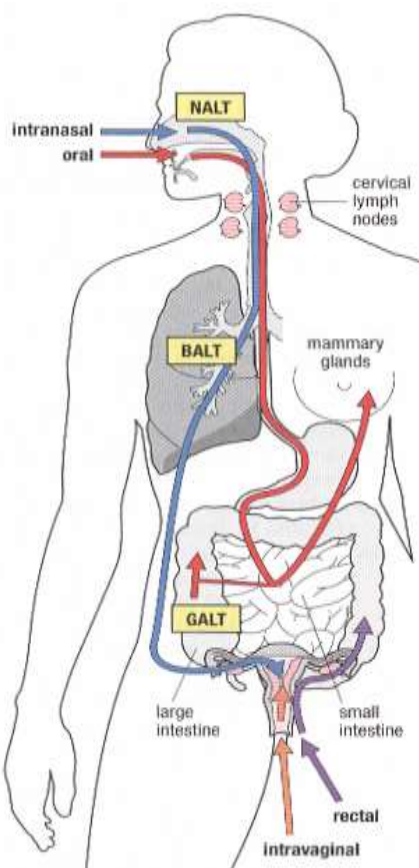
mucosal immunization routes. This study has discovered that strongest response occurs at the directly exposed mucosa site and generates a relatively lower response at adjacent mucosae or specifically interconnected inductive-expression mucosal systems<sup>438</sup>.

However, the challenge for intranasal immunization in human is due to the unpredictable risk of brain influence via blood-brain barrier during the mucosal inoculation in the nasal cavity, which was supplied by several major nerves, including parts of the facial nerve, pharyngeal nerve and ophthalmic nerve. There is an intranasal influenza vaccine testing the first licensed intranasal influenza vaccine in Swiss in 2000 and Scotland in 2013. The increased risk of Bell's Palsy is evident by this inactivated virosomal-subunit influenza vaccine with ELT as mucosal adjuvant (Nasalflu, Berna Biotech, licensed in Switzerland)<sup>439</sup>.

Despite the safety concerns, intranasal vaccination to induce cervicovaginal immune-response remains an attractive option vaccination. Nasal mucosal immunization showed a strengthened immunization potential not only stimulating an immune response in the respiratory tract, but also induce strong genital-vaginal mucosal immune-response<sup>213</sup>. Moreover, vaginal vaccination stimulates stronger genital tract T-cell immunity, which could also be considered as alternative regiment<sup>40</sup>. The enhanced mucosal and systemic immune responses delivered via nasal cavity may exceed in magnitude than oral immunization. Other studies further show that the intranasal route is superior in leading substantial IgA and IgG responses in cervical and vaginal secretions as described earlier in VLP section<sup>440,441</sup>. This superiority of



local secretions of vaginal IgA and IgG merely manifests in intranasal immunization<sup>441</sup>. Compared with this profound feature of intranasal immunization, the local vaginal route is limited with a weak secretion of IgA and IgG antibodies in vaginal fluids of mice<sup>442</sup>. Significantly, considering the lack of professional administrators in resource-poor countries, nasal spray or drops would be more convenient and cost-effective than intramuscular injection.

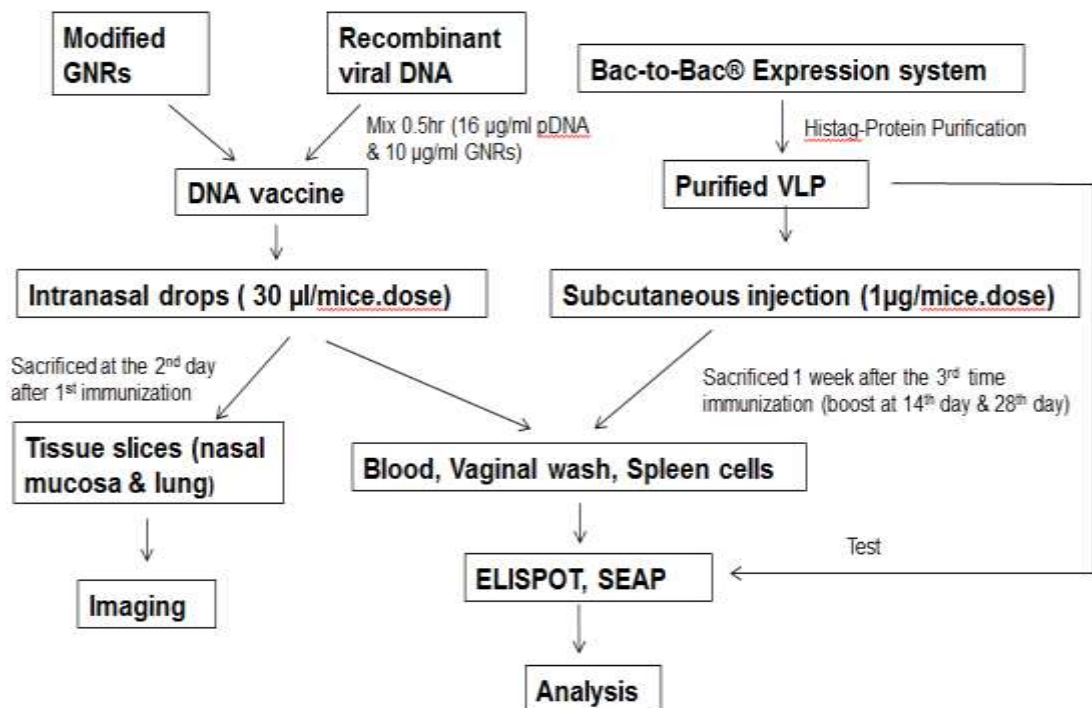


**Figure 26 - Expression of mucosal IgA immune responses after different routes of vaccination**, cited from Holmgren's review (Holmgren and Czerkinsky, 2005). Cholera toxin B subunit studied in humans through different mucosal immunization routes have clearly revealed that the strongest response appears at the directly exposed mucosa site and

generates a relatively lower response at adjacent mucosae or at specifically interconnected inductive-expression mucosal systems. Nasal mucosal immunization showed a strengthened immunization potential not only stimulating an immune response in the respiratory tract, but also induce strong genital-vaginal mucosal immune-response.

### 4.3. Aim

Due to the mechanisms revealed in Figure 27, I have designed vaccination experiments using GNRs-DNA as well as purified AHPV type 16 VLP as illustrated in Figure 27 below:



**Figure 27 - Flow chart of vaccination and evaluation of immune responses.** Measurements were specific (SEAP & ELISPOT) humoral immune responses to GNRs-DNA or to purified HPV 16 L1 VLP. ELISPOT: Enzyme-Linked ImmunoSpot; SEAP: Secreted alkaline phosphatase (SEAP) assay for detecting neutralizing antibodies specific to HPV L1 capsid protein. ELISA: enzyme-linked immunosorbent assay. According to the experiment design of the *in vitro* cellular expression assay, imaging was taken after the 2<sup>nd</sup> day of 1<sup>st</sup> immunisation.

#### 4.4. Material and Methods

**Table 5 - Reagents used in this animal work**

Name	Description	Conditions
Grace stock medium	Grace powder (Gibco), 3.3g/l lactalbumin hydrolysate, 3.3g/l yeast extract, 0.35g/l Na <sub>2</sub> CO <sub>3</sub>	pH: 6.1-6.2 Sterilized
Grace completed medium	Grace stock medium, 10% calf serum	pH: 6.1-6.2
Grace infection medium	Grace stock medium, 2% calf serum	pH: 6.1-6.2
VLP mixture for subcutaneous injection	1:1 (v/v) concentration of His-tagged VLP and Freund's adjuvant (F5881 and F5506, Sigmaaldrich)	Subcutaneously injection
10× stock solution A	200 mM NaH <sub>2</sub> PO <sub>4</sub> , 5M NaCl	-
10× stock solution B	200 mM Na <sub>2</sub> HPO <sub>4</sub> , 5M NaCl	-
Native binding buffer	1 × stock solution A 2.9 ml, 1 × stock solution B 47.1ml	pH: 7.2-7.6 (7.5*)
Native washing buffer	1 × stock solution A 37ml, 1 × stock solution B 13 ml	pH: 6.0 (7.5*)
3M Imidazole stock buffer (10×)	Imidazole 20.6g, stock solution A 8.77 ml, Stock solution B 1.23 ml, Water up to 100 ml	pH: 6.0
Native-Imidazole elution buffer (50mM)	3M Imidazole stock buffer 0.16 ml, Native wash buffer 9.84 ml	pH: 7.5*
Native-Imidazole elution buffers (200ml)	3M Imidazole stock buffer 0.66 ml, Native wash buffer 9.34 ml	pH: 7.5*
Native-Imidazole elution buffer (350mM)	3M Imidazole stock buffer 1.16 ml, Native wash buffer 8.84 ml	pH: 7.5*
Native-Imidazole elution	3M Imidazole stock buffer 1.66 ml, Native wash	pH: 7.5*

buffer (500mM)	buffer 8.34 ml	
1 × PBS buffer (Litter)	8g NaCl <sub>2</sub> ; 0.2g KCl; 1.44g Na <sub>2</sub> HPO <sub>4</sub> ; 0.24g KH <sub>2</sub> PO <sub>4</sub> , water up to 1L	pH: 7.4
1 × PBS buffer (Ca <sup>+</sup> , Mg <sup>+</sup> , 1L)	8g NaCl <sub>2</sub> ; 0.2g KCl; 1.15g Na <sub>2</sub> HPO <sub>4</sub> ; 0.2g KH <sub>2</sub> PO <sub>4</sub> , 0.1g CaCl <sub>2</sub> ; 0.1gm MgCl <sub>2</sub> 6H <sub>2</sub> O; water up to 1L	pH: 7.4
Lysis buffer stock (LBS)	10% Triton X-100/PBS	
Lysis buffer	5% LBS, 0.1% (v/v) Benzonase, 1/40 (v/v) 1M ammonium sulfate, 0.1% Plasmid Safe	pH: 9
Coating buffer stock (CBS)	0.795g Na <sub>2</sub> CO <sub>3</sub> ; 1.465g NaHCO <sub>3</sub> , water up to 500ml	pH 9.6 at 4°C
Coating buffer	500 μl Imidazole mixture (200mM Imidazole + 350mM native-imidazole elution buffer), 25ml CBS	4°C storage
Blocking buffer	5% BSA/PBS	Fresh prepared
ELISPOT Medium	RPMI-1640, 10% FCS, 100U Strepenicillin	
ELISPOT wash buffer	1 × PBST (0.1% Triton-X-100/ PBS)	
Protein inhibitor cocktail tablet	Boehringer Mannheim, Roche	4°C storage
lymphocyte separation medium	LTS1077, TBDscience	
Infection solution	Prof. Wang's lab	
calf serum	Hzsjq company, China	
HEK293TT cells	Invitrogen	
Mab CamVir-1	ab69, Abcam	-20°C storage
embedding medium	O.C.T Compound, Tissue-Tek®	
96-well u-bottom plates	3799, Corning	
RPMI-1640 medium	NYM1034, HyClone	
Probond™ columns	Invitrogen	
bicinchoninic acid	BCA, Beijing Dingguo Changsheng Biotech.	

protein assay kit		
alkaline phosphatase yellow (pNPP) liquid	Sigma-Aldrich	
Optiprep	OptiPrep™ Density Gradient Medium, Sigma-Aldrich	

\*: The condition applied in my experiment

#### 4.4.1. Animal preparation

##### 4.4.1.1. Mice immunization

The experimental animals were 6-8 week-old female BALB/c mice. The experimental protocol has been proved by the Animal Research Ethical Committee of the Xi'an Jiaotong University, and mice were maintained under specific pathogen-free condition according to the guidelines.

For vaccination with DNA-PEI or DNA-PDDAC nanorods, both constructs were prepared in distilled water to a final concentration of 16ng/μl, of which 10ng/μl was surface-modified GNRs. Each of the BALB/c mice was given 30μl (480ng GNRs-DNA in total) as nose drops on the day 1. The dosage was prepared as 10 × dose of *in vitro* test, due to the convenience of delivery and preparation back to China. The same dose was given on the day 7 and day 28 via the same route to boost vaccination. As a positive control, mice were immunized subcutaneously with 2μg His-tagged VLP mixture per dosage/animal at day 1, and boosted at day 7 and day 28. Dosage scheme was administrated according to previous VLP studies<sup>443,444</sup>. The VLP

mixture was 1:1 (v/v) concentration of His-tagged VLP mixed with Freund's adjuvant following manufacturer's instruction to inject complete adjuvant at the first time and incomplete ones for the rest(F5881 & F5506, Sigma-Aldrich). Several mock vaccination control groups were also set up using: 1, PBS; 30µl of PEI-GNRs or PDDAC-GNRs (10ng/µl for both); 3, Two naked plasmids DNA, pcDNA3 YFP-L1 and pcDNA3 YFP-L1-eltB.

#### **4.4.1.2. Histology sample preparation and microscopy**

Nine mice were sacrificed on the second day after receiving the nose drops of pcDNA3 YFP -PEI or pcDNA3 YFP-PDDAC or PBS for histological imaging; three mice for each group. The mucosa membranes were isolated from bones inside nasal cavity, mainly on the two sides of the nasal septum, and the entire lungs were excised. Nasal mucosa and Lung tissues were fixed in formaldehyde for 5 minutes and then mounted to a metal object plate using embedding medium (O.C.T Compound, Tissue-Tek<sup>®</sup>). Tissues were cut by a cryostat (CM 1860, Leica) manually to produce consistent sections of 10µm thickness at -20°C degree and fixed on the coverslips directly at room temperature. Slides were examined under a fluorescent microscope.

Histological images of nasal mucosa and lung tissues were obtained using a laser scanning confocal microscope (LSM510, Leiss) with 10×40 magnification.

#### **4.4.1.3. Collection of the Sera and virginal wash**

Four weeks after immunization, vaginal washes were collected and pooled in each group. Mouse sera were then obtained from orbital sinus by eyeball removal from the socket with a pair of tissue forceps under full anaesthesia. Samples either processed for immediate analysis, or stored in -20°C freezer in 0.02% NaN<sub>3</sub>, a condition that can keep the sample for at least half year. Mouse sera were centrifuged in micro tubes at 4°C 3000 g 15 min. Sera were transferred to fresh tubes for further analysis.

#### **4.4.1.4. Collection of spleen lymphocytes**

To collect the splenocytes, mice were sterilized in 75% ethanol for 2-3 minutes after execution, and spleens were extracted from abdominal cavity in the super clean bench under asepsis condition.

Spleens were soaked in 4ml modified RPMI-1640 (NYM1034, HyClone) per tube. Spleens were cut up into bits and ground by sterilized pestle. By pressing the ground spleen passing through a stainless steel cell sieve, splenocytes dispersed and washed in modified RPMI-1640 medium. Dispersed splenocytes were applied into lymphocyte separation medium carefully (LTS1077, TBD science). The cell suspension was placed on the top of the separation medium. After the centrifugation at 1500-2000 g for 15-18 min, lymphocyte layer was located between the top medium and the lymphocyte, and the cell pellets will be on the bottom. Lymphocytes for each sample, which placed as the white layer in the middle, were carefully taken out and cultured in 5ml new RPMI-1640 with supplemented 1:1000 diluted 100 µg/ml of streptomycin and penicillin. Cell re-centrifuged to obtain the cell pellets. Lymphocytes population was counted after re-suspending cells in fresh RPMI



medium. Finally, after third-time centrifugation, spleen lymphocytes were culture in RPMI medium,  $10^5$  per well in 96-well u-bottom plates (3799, Corning), which were pre-coated with His-tagged VLPs. Cells were grown at 37°C under 5% CO<sub>2</sub> for 4 h before ELISPOT assay, which was described in the following sections.

#### **4.4.1.5. Ethics Statement**

The mice experiments were approved by the Laboratory Animal Administration Committee of Xi'an Jiaotong University under the licence (No XJTU2014-102), and performed according to the guidelines of Animal Experimentation of Xi'an Jiaotong University. The Guideline on the Care and Use of Laboratory Animals issued by the Chinese Council on Animal Research, which was published by the US National Institute of Health (NIH publication No. 85-23, revised 2011). The care and execution of mice were operated carefully to ensure animals suffer from minimal stress during all experiments.

#### **4.4.2. Production of HPV16 L1 Viral-like Particles (VLPs)**

##### **4.4.2.1. Production of His-tagged HPV16 VLPs using baculoviral system**

HPV16 L1 VLPs were produced in insect cells Sf-9 (*Spodoptera frugiperda*) harboring HPV L1-encoding recombinant baculovirus and purified through Ni-NTA resin column (50% slurry in 20% ethanol, Invitrogen), which was described by <sup>429</sup>. Sf9 cells obtained in Wang's lab were recovered using completed Grace Medium for daily culture at 28-30°C without CO<sub>2</sub>.

Sf9 cell cultures were routinely grown at 28°C without CO<sub>2</sub>. Cells were expanded up to 30 flasks (25cm<sup>2</sup>) with confluent monolayers. Cells were pooled for the preparation of self-assembled HPV16 L1 VLPs as following. Cells were adapted to Grace medium containing 2% calf serum (Hzsjq company, China) and then infected with recombinant baculovirus at a multiplicity of infection (MOI) of 20 (100µl of infection stock solution). Sf-9 infected cells were harvested at 72 h post-infection.

After centrifugation at 1200 g for 10 min, a cell-suspension was adjusted to 1X10<sup>8</sup>/ml in PBS for counting, then washed and resuspended in native binding buffer in the same density with one tablet of the protease inhibitor cocktail tablet (cOmplete™, EDTA-free , Boehringer Mannheim, Roche, Germany). The cell lysis was performed by repeated freezing (in -80°C or liquid nitrogen) and thawing method, the following sonication with three 15-s burst at 60 & maximal power (Vibra-cell) for 20 min on ice. Cell lysis was treated with RNase (10 µg/ml) and DNase (5 µg/ml) and kept in -80°C freezer.

#### **4.4.2.2. Purification of His-tagged VLPs by Probond™ purification system**

To purify His-tagged VLPs, Zheng's protocol <sup>429</sup> and the instruction manual of ProBond™ purification system (Novex®, Life technology) was followed under native purification condition.

Probond™ columns or resin contained 1.5ml tubes (Invitrogen) were centrifuged at 800 xg for 2 min to remove the ethanol. The columns were washed three times at 800 xg for 2 min in 700 µl distilled water following 2x wash with the same volume of native binding buffer. The resin then was ready for protein purification.

After centrifugation of cell lysis at 3000 xg for 15min, 800 µl of the supernatant was mixed with 200µl resin and incubated at room temperature 30 min. The mixture was centrifuged at 800 xg for 2 min and the supernatant was discarded. Repeated centrifugation steps were followed three-time wash with 0.5 ml native binding buffer and four-time wash with 0.5 ml native wash buffer. Between each wash, the mixture was allowed for 2 min incubation at room temperature. After a final wash, His-tagged L1 protein was eluted with a serial of buffers that contained native-imidazole from 50mM to 500mM. Each elution was collected and L1 protein concentration was estimated with SEAP analysis and Western blotting (see below).

#### **4.4.2.3. Microscopy evaluation of Sf-9 infection**

Light microscope (Olympus) was applied to monitor the growth condition of cell culture daily. Sf-9 images and the self-assembled intracellular VLPs were taken by inverted light microscope (Nikon) with 40x10 magnifications.

#### **4.4.2.4. Production of HPV pseudovirions (PsV) for SEAP analysis**

Procedure began with a 3-day co-transfection of pYSEAP and HPV16 L1/L2 pShell to HEK293TT cells (Invitrogen). Cells were trypsinised with a lower concentration

(0.05%) than routine work (0.25%). Cell wash was carried out with PBS buffer containing (Ca<sup>+</sup>, Mg<sup>+</sup>), followed by centrifugation at 3000 rpm. After second-time wash, the cell density was adjusted to 1 x 10<sup>8</sup> cells/ml with PBS. Lysis buffer with containing 0.1% butazodine instead of DNase and RNase was mixed with cell suspension to lyse cell for crude lysate. Cells were briefly vortexed several times for complete lysis and the lysate was incubated at 37°C overnight.

Before releasing PsVs from HEK293TT cells by detergent lysis, the PsVs were allowed to mature to a stable conformation, by means of adding sodium chloride (17% (v/v) 5M NaCl) into overnight/1-day crude cell lysate at 37°C. Cells were placed on ice for 5 min before purification. Immediately after maturation, extraction of capsid VLPs was performed using Optiprep (OptiPrep™ Density Gradient Medium, Sigma-Aldrich) purification. After centrifugation at 4°C 5000 xg for 5 min, the supernatant was collected and centrifuged again at 4°C 5000 xg for 5 min. To decrease contamination with cellular proteins, purification was followed by ultracentrifugation through stop gradient with 60% (wt/vol) iodixanol (Optiprep) to harvest pseudovirions. Ultracentrifuge was carried with a rotor SW40.1 Ti at 40,000 g for 4.75 h to obtain the PsVs in middle grey layer. The purity of PsVs was sufficient for SEAP analysis to detect neutralizing antibodies using SEAP assay.

#### **4.4.2.5. Bradford protein assay**

Bradford assay was carried by a bicinchoninic acid protein assay kit (BCA, Beijing Dingguo Changsheng Biotech.). This assay is based on reduction of Cu<sup>2+</sup> to Cu<sup>1+</sup> which results in oxidation of peptide bonds. The concentration of His-tagged VLPs

was calculated based on standard curve generated with a serial dilution of BSA. OD562nm was taken for each of the dilutions to generate the standard curve using a microplate reader (VMax Kinetic ELISA, Molecular Devices, US). The calculation was made with Microsoft Excel 2007.

#### **4.4.2.6. Detection of His-tagged HPV16 VLP and PsV by Western blotting**

To evaluate the quality of HPV16 L1 encoded His-tagged HPV16 VLP and PsV, western blot was applied. The procedure was similar to the description in Chapter 2. A volume of 20µl purified His-tagged VLPs from each of the elution fractions described above, and 20µl PsVs were heated at 95°C for 5 min in a water bath, including a same volume of 2x protein loading buffer (Biorad). Protein was run at 120V for 1hr at 10% SDS-PAGE gel and transfer onto a polyvinylidene difluoride (PVDF) membrane at 0.4Am. A monoclonal antibody specific to HPV16 L1 protein, (ab69, Abcam®), was diluted 1:5000 in blocking solution containing 5% BSA to incubate with the PVDF membrane. An antibody, Mab CamVir-1, was used to detect HPV16 pseudovirions<sup>87</sup>. Mab CamVir-1 is able to bind to the L1 linear epitope GFGAMDF located at aa 230-236, which will not be destroyed by the L2 insertion of HPV 16 pseudovirions<sup>445</sup>. Secondary Ab Alexa Fluor® 680 (1:5000, Anti-mouse IgG, Invitrogen) was anti-mouse polyclonal, providing the fluorescence emission at 700nm. According to the grayscale and protein concentration measured by Bradford Assay, the concentrations of VLPs were estimated.

#### **4.4.3. Detection of antibody specific to HPV16 VLPs**

#### **4.4.3.1. Coating U-bottom 96-well plates with His-tagged VLPs**

According to the protein concentration calculated by Bradford Assay and the degree of purity estimated according to the grayscale of Western blot, 4.0 µg of His-tagged VLPs was coated for each well of 96-well plates, to maintain a concentration of 2.0 µg/well. The VLP proteins were diluted in the Na<sub>2</sub>CO<sub>3</sub> coating solution (2.0 µg/well). The coating solution was replaced by 1x phosphate-buffered saline (PBS, pH 7.4) to achieve a greater surface area binding efficiency for the remaining mice in the second trial.

#### **4.4.3.2. Detection of antibody secreted spleen lymphocytes by ELISPOT**

The technique was based on the method of Czerkinsky et al.,<sup>446</sup>. The frequency of HPV16 L1-specific IgG secreted ASCs in spleen represented as detected by an anti-mouse secondary antibody (Goat, IgG, HRP conjugate, Dako/Invitrogen). Coated plates were washed with PBS, and treated with blocking buffer for 1 h. Before seeding 10<sup>5</sup> spleen lymphocytes per well, plates were washed three times with PBS.

After overnight incubation at 4°C in ELISPOT medium under 5% CO<sub>2</sub> humidity, and plates were washed with 0.1% PBS-T for 4 times and shaken for one minutes gently at each time. Same wash procedures were applied after 1hr incubation with second HRP-labelled anti-mouse Ab (1:30, REAL EnVision-HRP, Dako/Invitrogen). Tetramethyl- benzidine (TMB) solution for chromogen preparation required to preheat the soluble TMB substrate with 1% agarose at 46°C. Plates were dried and added quickly with 100 µl/well TMB solution in 37°C water bath following

immediate storage in a freezer for 1-2 min. The substrate was chromogenic after placing plates in the dark-room for 5-30 min. Blue spots in each well were counted within 4 h to avoid photobleaching. The number of blue ASCs in  $10^5$  lymphocytes was counted under microscope with 10 x magnified objective lens.

#### 4.4.3.3. Neutralization Assay

PsVs which harboured secreted alkaline phosphatase (SEAP) reporter plasmid (pYSEAP) were incubated for 1 h with a serial dilution of pooled plasma from immunized mice. HEK293TT cells were prepared at a concentration of  $3 \times 10^4$ /well, after cells attached to the plate (2-4 h), a 1 h pre-incubated mixture of PsVs and pooled plasma (50  $\mu$ l/each) at 4°C was added into each well. Triplicate samples were prepared for each group. Negative control was triplicate copies of HEK293TT cells with PsVs which were not treated with mouse plasma as 100% infection ratio, while positive controls were the plain cells without PsVs transfection.

EC50 calculation was based on the inhibition ability of HPV16 L1 neutralizing antibody in the plasma against PsVs, the calculation equation below was used.

$$\frac{1 - [\text{sample} - \text{positive}]}{[\text{negative} - \text{positive}]} \times 100\%$$

A positive Nab titer is the diluted ratio which provided an inhibition ability more than 50% inhibition ratio (EC50) for the sample. The chemiluminescent substrate used was p-nitrophenyl phosphate (pNPP) in liquid form (Sigma-Aldrich), which was specific and sensitive to secreted alkaline phosphatase (SEAP). This method was

also developed by Dr Schiller's group with online protocol at <http://home.ccr.cancer.gov/Lco/neutralizationassay.htm>.

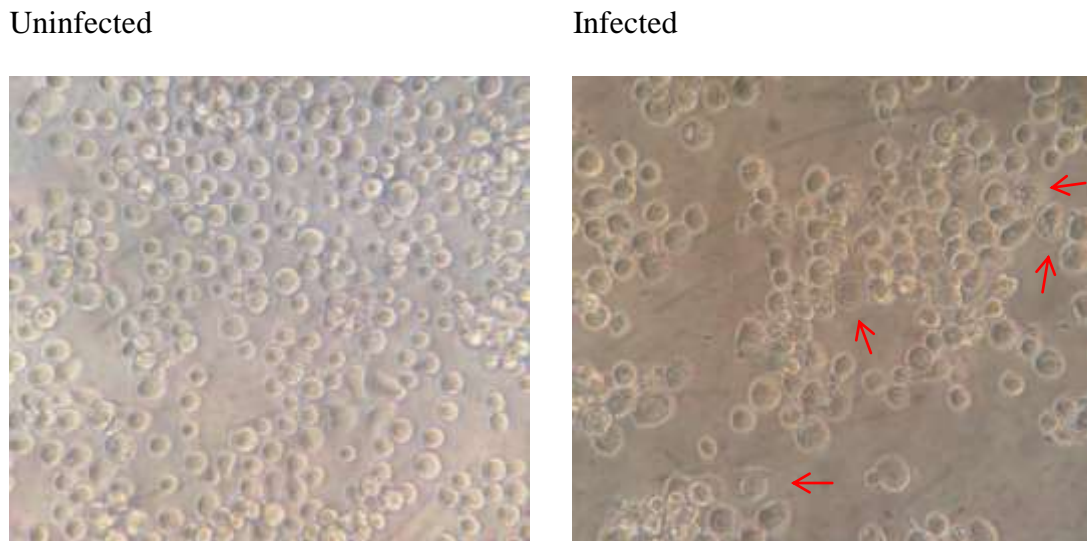
#### **4.4.4. Statistical Analysis**

For statistical analysis, all the sample groups were prepared with more than triple copies, and cell prepared for each pooled samples were more than 3 wells. The study was completed including two trials. The mouse number for each group was increased to 8-10 in order to avoid individual difference among animals, and the protocols for all experiments were modified in the second trial. Data was collected and analysed by Microsoft Excel 2007 and GraphPad Prism (Ver. 5.0) with one or two-way ANOVA assay, following Tukey test. Significant statistical analysis was marked with asterisks (\*:  $p < 0.05$ ; \*\*:  $p < 0.01$ ; \*\*\*:  $p < 0.001$ ).



## 4.5. Result

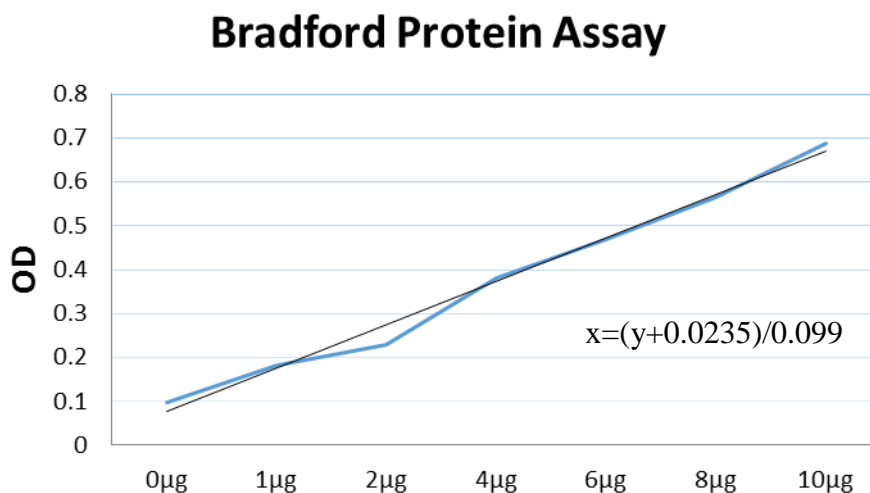
### 4.5.1. Successful expression of VLPs in Sf-9 infected with recombinant baculovirus for His-tagged VLP preparation.



**Figure 28 - Micrograph of Sf9 cells. Cells were infected with recombinant baculovirus AcHPV16 L1 and grown to monolayer after 2-day post-infection. AcHPV16 L1 contained recombinant HPV16 L1 Bacmid DNA. Compared to untransfected cells, the cell expressing His-tagged VLPs HPV 16 L1 became large with expanded cytoplasm. Red arrows depict the cells with such characteristics. Magnification, 10 X 40.**

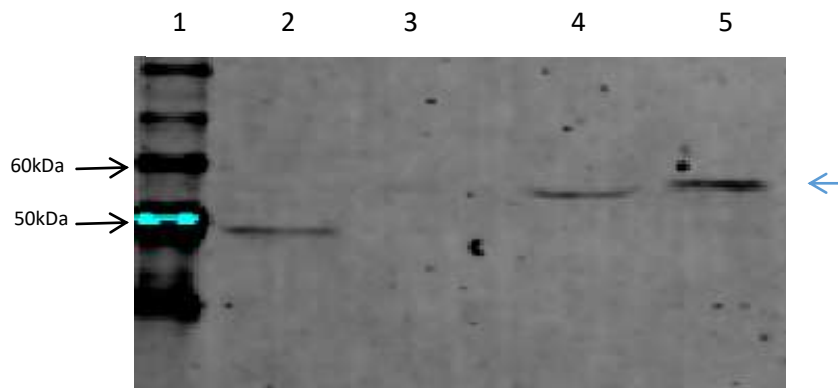
Current authorized vaccine - Cervarix™ (GlaxoSmithKline, Biologicals) are HPV VLP-based. Therefore, the baculovirus system was used to prepare high-yield of recombinant L1 VLPs comparison with GNRs-DNA. Sf9 inset cells showed morphological change which presumably due to expression of L1 protein and self-assembly of VLP in the cell cytoplasm (Figure 28). Indeed, high-yield VLP was demonstrated in the later experiments from Sf-9 cells 3-4 days post-infection.

#### 4.5.2. Measuring protein concentration by Bradford Assay



**Figure 29 - Quantitative measurement of VLP concentration by Bradford protein assay.** According to the OD of a serial diluted BSA controls measured at 562nm, a trendline was generated along the standard curve. Concentration of His-tagged VLPs was calculated according to the trendline equation. OD<sub>562nm</sub> was taken using a microplate reader (VMax Kinetic ELISA, Molecular Devices, US). Calculation was completed with Microsoft Excel 2007.

Protein quantification was done by Bradford protein assay. OD values of a serial dilution of BSA control were measured at 562nm, which formed the blue line in Figure 29. An equation as “ $x = (y + 0.0235) / 0.099$ ” was generated as the trendline based on the standard curve. Protein quantification of VLPs was calculated according to this equation and the OD values.

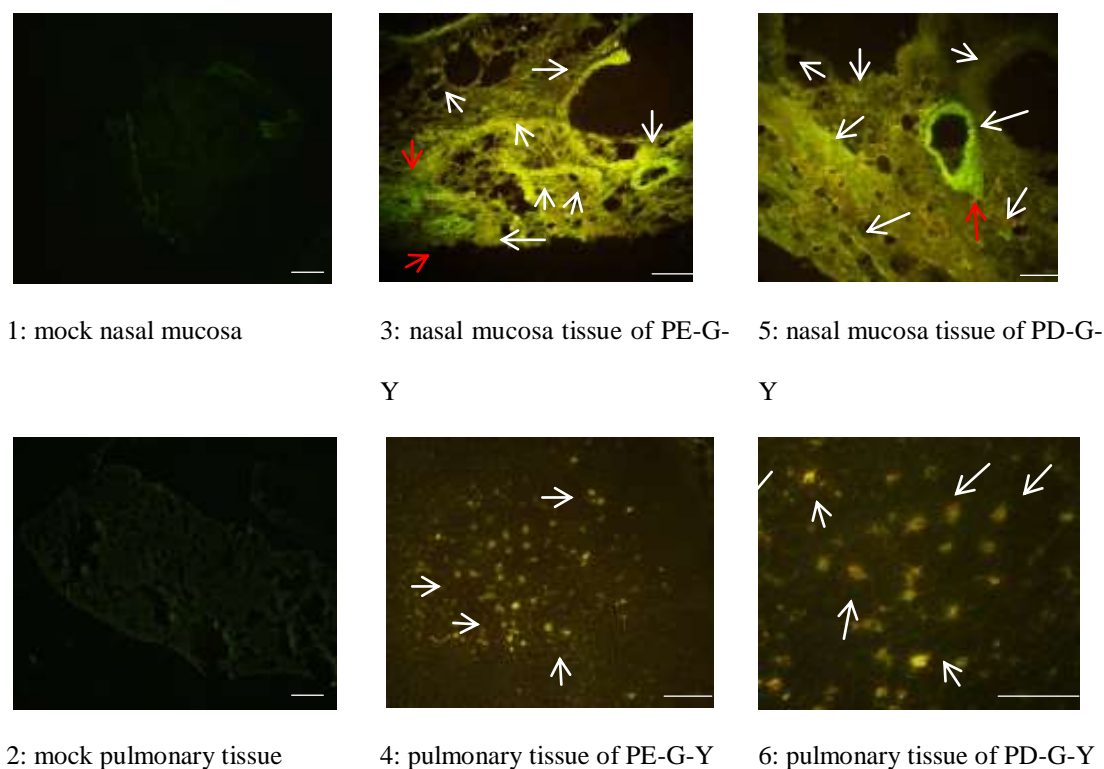


**Figure 30 - Detection of purified His-tagged L1 protein from transfected Sf9 cells.**

Lanes: 1, Protein marker (MagicMark™ XP, NuPAGE®); 2: Crude lysate of HEK293 cells that transfected with pcDNA3 L1. A non-specific protein band was apparent; 3, Crude cell lysate of untransfected Sf-9 cells; 4, Purified His-tagged L1 protein (20 µl); 5: Purified HPV-16 L1/L2 pseudovirions (PsV); Blue arrow depicts L1 protein approximately 55kDa. The antibody used was Mab CamVir-1 (1:5000, ab69, IgG2a, Abcam®).

HPV16 L1 specificity and protein purity of His-tagged protein required to be identified and estimated for further appropriate quantitative analysis. As described in the method section, the L1 protein fraction in self-assembled VLPs could be fully detected by Mab CamVir-1 antibody as Figure 30 demonstrated. The Western blot verified the two purified VLPs (Lane 4: His-tagged VLPs; Lane 5: PsVs) applied in this study were specifically HPV 16 L1 antigens by a specific and sensitive detection of monoclonal Mab CamVir-1 at 55kDa. VLPs were confirmed for further analysis and subcutaneously injection of positive controls.

### 4.5.3. Histological imaging to detect YFP protein expression



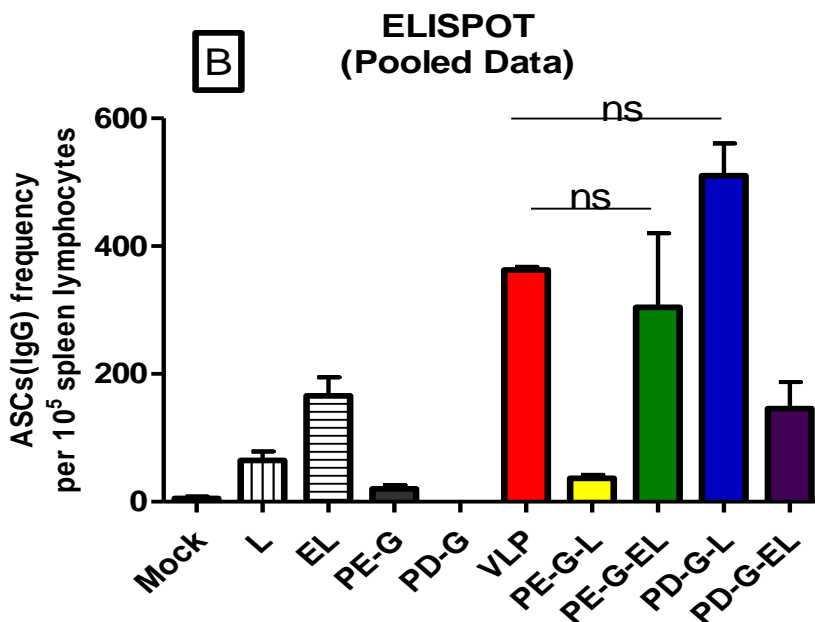
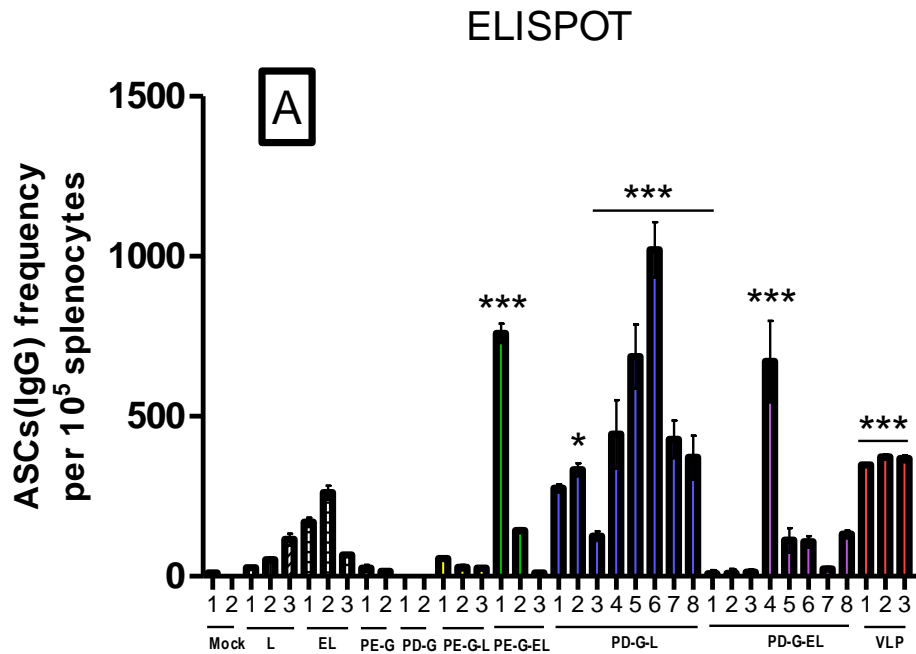
**Figure 31 - Fluorescent histological images of tissues from nasal mucosa and lung.** Tissues of nasal mucosa (1 & 3 & 5) and lung (2 & 4 & 6) were extracted from mice 2 days after immunization with water (1 & 2); PE-Gs-Y (3 & 4) and PD-G-Y (5 & 6). White arrows depict the cells or tissues with expressed fluorescence yellow proteins. Bar scale indicated 50  $\mu$ m. Red arrows pointed the area with cell accumulation.

The fluorescent images shown in Figure 31 illustrated the expression of YFP in nasal mucosa (22-3 and 22-5) and lungs (31-4 and 31-6) 2-day after immunization with PEI/PDDAC-GNRs-pcDNA3 YFP (PEG-Y and PDG-Y) complexes with high magnification. Remarkably, Yellow fluorescent proteins displayed at epithelium,

mucous glands and serous glands of lamina propria, thin walled venules in mucosa, as well as dust cells in pulmonary alveolus. Dust cells, which are depicted by white arrow in (Figure 31-4,6), are the major pulmonary macrophages involved in innate immune-response in lung tissues to engulf pathogens and activate the adaptive immune-response through present antigens to T or B cells in lung. In contrast, obvious fluorescence appeared in different regions of mucosa tissues, especially around the small venules.

There were certain infiltration sites of cells around the airways and blood vessels throughout the nasal tissues of mice immunized with PD-Gs or PE-Gs. This phenomenon was marked by red arrows indicating YFP accumulation. Possibly, inflammation might occur in nasal passage caused by the surface-coated GNRs. However, no histologic changes were observed in pulmonary sections for mice inoculated with naked YFP plasmid DNA alone.

#### **4.5.4. Immunological Assays after intranasal immunization of PEI/PDDAC-GNRs-HPV16 L1 vaccine**



**Figure 32 - Detection of IgG antibody secreting cells after intranasal immunization with GNRs-DNA.** A: Antibody secreting lymphocytes specific to L1 protein by enzyme-linked immunospot (ELISPOT) assay. B: Pooled data form ELISPOT assay for the comparison of ASCs (IgG) frequency. Female BALB/c mice (n = 3 or 8 per group) were immunized with various GNRs-DNA after three dose of immunization (30 $\mu$ l DNA-GNR suspension per dose) at day 0, 14 and 28. Positive VLP group was immunized with three

doses of 2ug purified His-tag VLPs each time. Spleen lymphocytes were isolated and pooled from mice. In each of the 96 wells, 105 lymphocytes were seeded in triplicate for the assay. Frequency of antibody IgG-secreting cells (ASCs) specific to HPV16 L1 VLP was detected by second antibody (IgG, HRP, Dako) and calculated according to the number of blue spots detected by chromogenic reaction. Data are presented as mean + SEM. Statistical analysis was performed with one-way ANOVO following Tukey test to compare all groups. Asterisks indicate statistical significance (\*:  $p < 0.05$ ; \*\*:  $p < 0.01$ ; \*\*\*  $p < 0.0001$ ).

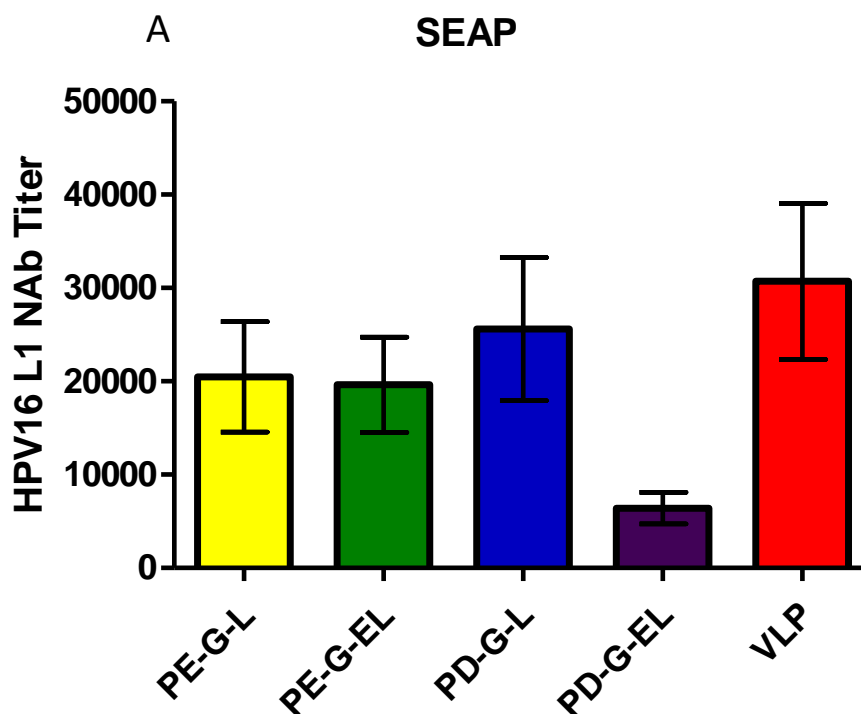
For the quantification of the number of IgG secreting cells specific to HPV16 L1, ELISPOT provided a sensitive tool. HPV16 L1-PDDAC-GNRs (PD-G-L) inoculated mice obtained a higher number (5/8 mice, No.4-8) significantly enhanced HPV16 L1 specific IgG secreting cells in spleen than L1 plasmid only group (L). One mouse in the groups (PE-G-L, PD-G-L, PD-G-EL) obtained significant higher IgG secreted APCs in spleen lymphocytes ( $p < 0.05$ ). PE-G-L performed with lowest IgG secreting efficiency than other three GNRs-DNA groups, especially significantly lower than PDG-YL ones (No.4-7,  $p < 0.001-0.05$ ). Except the extremely distinct mice in PE-G-EL and PD-G-EL group, there was no significant difference of IgG secreting in spleen lymphocytes by immunization with EL pDNA and PE-G-L, PE-G-EL and PD-G-EL.

Three mice in the pcDNA3 YFP-L1-*eltB* (EL) group inoculated with naked plasmid DNA encoding *E. coli* heat-labile cholera toxin B subunit. In contrast, mice immunized with EL plasmid received an increased IgG secreting cells in 1/3 mice by PE/PD-Gs adjuvant versus the EL plasmid control ( $p < 0.001$ ). However, PD-G-L performed stronger humoral immune-response than PD-G-EL group, which was out of expectation. Because, as a derivative of commonly used adjuvant – cholera toxin

for mucosal immunization with inactive vaccines<sup>438</sup>. There was about 2/3 mice of naked EL group still exhibited a slightly higher number of HPV16 L1-specific IgG-ASCs than naked L1 plasmid alone. But the difference was not significant ( $p > 0.05$ ). However, the increased IgG secretion in spleen lymphocytes is still parallel with the observable L1 expression *in vitro* 2-day after transfection of PD-G-L complexes in HEK293 (Figure 23 B).

In conclusion, based on the positive high HPV16 L1 specific IgG secreted ASCs provided by VLP via subcutaneous injection, PD-G-L vaccine formula performed promising adjuvant efficiency after conjugating with recombinant L1 plasmid DNA. Naked EL plasmids were unable to stimulate spleen lymphocytes secreting IgG antibodies against HPV16 L1. Tukey test demonstrated that 2-4 mice in PD-G-L group (No. 4-7) acquired significant high level of IgG-ASCs in spleen lymphocytes than EL group ( $p < 0.05$ ).





**B**

Observed	293TT PsV		
Animal ID	Number	Nab titer in plasma EC50 (SD)	No. of no titer
H <sub>2</sub> O	4	-	4/4
PE-G	4	-	4/4
PD-G	4	-	4/4
VLP	3	1:10240 - 1:40960	0/3
PE-G-L	7	1:10240 - 1:40960	1/7
PE-G-EL	11	1:2560 - 1:40960	2/11
PD-G-L	6	1:10240 - 1:40960	2/6
PD-G-EL	8	1:640 - 1:10240	1/8

**Figure 33 - Detection of HPV16L1 neutralizing antibody by SEAP assay.** Blood was drawn from same groups of mice used in Figure 32 (50  $\mu$ l serum/sample mixed with 50  $\mu$ l VLPs) before sacrifice for spleen isolation. A: The neutralizing activity of the neutralizing antibody (NAb) against HPV16. B: The range of Nab titer of the reciprocal dilutions yielding 50% SEAP inhibition for the neutralizing titers. The SEAP pseudovirus-based neutralization assay is to measure the neutralizing antibody specifically detected by purified SEAP HPV16 pseudoviruses (PsV) encapsidating a secreted alkaline phosphatase. Nab mediated HPV16 PsV was evaluated by a reduction in SEAP activity. The higher dilution titer indicates the

higher neutralizing activity. Data are presented as mean + SEM. In table B, the column of 'No. of no titer' records the number of mice in each group with no Nab titer in plasma against 50% SEAP inhibition. Neutralization SEAP assay was completed with the assistance of Depu Wang (Xi'an Jiaotong University, China). EC50: 50% neutralization titer. One-way ANOVA following Tukey test demonstrated there were no significant difference between each groups ( $p > 0.05$ ). No significance between each group according to Tukey's multiple comparison test.

The neutralizing ability of the antibodies against HPV VLPs HPV 16 L1/L2 pseudovirions is critical in type-specific qualitative and quantitative analysis of the capsid antigen, to investigate the immunogenicity of VLP and DNA vaccine <sup>444</sup>, which is more sensitive and specific than a standard VLP-based ELISA for vaccine evaluation <sup>447</sup>. The titers of HPV16L1-specific neutralizing antibodies IgG in serum were higher among groups treated with PDDAC-GNRs conjugated HPV16L1 (PDG-YL), but the difference between four GNRs-DNA complexes was not significant as a  $p$  value more than 0.05 (Figure 33). Compared with the spleen lymphocytes-specific IgG secretion test (Figure 31), both graph A and table B demonstrated a significant positive 50% neutralization titer of serum IgG for all GNRs-DNA samples. It is possible indicated an enhanced systemic humoral immune response of all samples, in addition to distinct IgG secretion status in different immune-functional organs.

## 4.6. Discussion

The most critical mechanism in preventing HPV infection hence preventing cervical cancer is the production of neutralizing antibody specific to HPV16 L1 IgG in systematic humoral responses. Nasal route vaccination has been found to stimulate mucosal immune responses in respiratory and genital tracts<sup>68</sup>. A spontaneous systematic humoral immunity in intranasal and cervicovaginal local mucosa has been the basis of the immunization strategy tested in this study. Eliciting sufficient HPV type-specific neutralizing IgG and IgA antibodies is essential to prevent HPV cervicovaginal infection<sup>440</sup>.

In the animal work, preparation begins VLP production and animal immunization. For the His-tagged HPV16 L1 VLP, several issues will influence the final quality and quantity of VLP yield. When Sf-9 was growing to 80% fluency, 100 µl of infection solution including baculovirus AcHPV16 L1 was added into the 25 cm<sup>2</sup> flask. It is noticeable that a 4-day post-infection period was the maximum time to maintain a high copy numbers of intracellular VLPs for further purification. As the micrograph of infected cells at the second day, observable VLPs could be found inside of the cells, which won't be seen in the first day. Long-time Infection over 4 days could cause loss of the VLPs due to cell death or detachment.

The purification of His-tagged L1 VLPs could be further influenced by the pH of each buffer used during the process. An early SDS-PAGE gel showed a substantial

amount of VLPs were washed away by native washing buffer. Following the troubleshooting suggestion on manufacturer's manual (ProBond™ Purification System, Invitrogen), increasing the pH of washing buffer to 7.5 during the high-stringency wash step highly decreased the VLP amount in the washing solution. As Dr Schiller recommended in his online protocol, the repeated freeze-thaw cycles could highly decrease the quality of VLPs, further work suggested the cell lysis procedure should try to avoid this step. Regarding the protein quality, proteinase K should be added earlier in the beginning of cell lysis process, to avoid the protein damage.

For the histological study, YFP expression was highly enhanced by the presence of surface-functionalized GNRs. The sections of nasal mucosa and lungs of BALB/c immunized with GNRs-DNA were analysed not only for the 2-day post-immunization, as well as one-days and three-days. Interestingly, YFP expression was hardly to be observed for the one-day post-immunization group, and was extremely higher in the 2-day post-immunization ones for both nasal mucosa and lung sites. A further interesting point is about the expression of our novel vaccines in nasal mucosa and lungs. Mice were grouped inoculated with the same dose as immunogenicity tests (480ng/dose.mouse) of 4 types of GNRs-DNA (PE-G-L, PE-G-EL, PD-G-L, PD-G-EL). Tissues were extracted for further histochemistry study by anti-L1 staining, to evaluate the L1 expression in the initial sites, which can directly document the recombinant viral DNA expression *in vivo* study. It is possibly further benefit the understanding about the effect of ELT insertion in the plasmid design.

Modification was demonstrated in the data of ELISPOT. The immunological efficiency of PE-G-EL was unstable in the production of HPV16 L1 specific IgG-APCs. This observation was distinct from the significantly induced L1 expression by PE-G-EL in in vitro study. Technically, it was possibly caused by the surface coating buffer used for the first trial, which was sodium carbonate buffer. This application may influence the result of mice labelled 1-3 in the 4 GNRs-DNA pooled data (PE-G-L, PE-G-EL, PD-G-L, PD-G-EL). Unlike traditional surface binding occurred via passive adsorption requiring an alkaline conditions, the U-bottom plates applied in this experiment were mainly designed with the inherent hydrophobicity of the capture Ab. Therefore, 1x phosphate-buffered saline (PBS, pH 7.4) was able to increase detective number, higher sensitivity and clear shape of blue spot <sup>448</sup>. This difference is observable on PD-G-L and PD-G-EL groups. Moreover, 5-8 additional mice were prepared for evaluation of 4 GNRs-DNA complexes on the second trial. However, it was failed to collect the ELISPOT data of PEI groups, due to the photo-bleaching of dye.

Comparing with the PD-G-L group, recombinant L1 DNA inserted with ELT gene did not enhance the immunogenicity of PD-Gs base construct. Previous studies histological micrograph showed a massive infiltration of mononuclear cells in pulmonary airways when ELT was used as adjuvant <sup>438</sup>. Therefore, ELISA study about IgA and IgG evaluation of nasal fluids and vaginal fluids may benefit the understanding of isotypes distribution of secreted antibodies after inoculation of these two recombinant DNA constructs. Negative controls of GNRs will help to

answer the effect of GNRs presence about antigen-specific immunoglobulin and inflammatory in the immunized site. As the strong adjuvant effect of cholera toxin illustrated, IgA response and IgG-associated inflammation by nasal vaccination, is possible to enhance the antibody development in these vaginal sites, but is possible influence the dosage matter regarding the inflammation conditions<sup>438</sup>.

SEAP analysis demonstrated the high HPV16 L1 NAb secreting in systemic humoral immune system after the GNRs-DNA vaccination. Although the HPV type-specific antibodies exhibited different quantity in splenic lymphocytes by ELISPOT, the neutralization activity elicited by these four types of vaccines still demonstrated a high systemic IgG-specific immune response but the positive titers in plasma samples. Especially for PE-Gs groups, both PE-G-L and PE-EL conjugates generated high and stable NAb titer in serum with low number of non-effective mice. This is extremely encouraging for PE-G-L vaccine, since the expression of L1 gene and the IgG excretion in spleen lymphocytes are both insufficient in the current ELISPOT data. The data variation among samples could be highly influenced by the aggregation of samples, especially for PE-G complexes according to the storage evaluation (Figure 12). This different distribution of antibody development in serum and spleen lead to a further interest about the antibody study in vaginal wash after immunization of these four types of vaccines.

To summarize, we have successfully immunized BALB/c mice with four types of GNRs-DNA prophylactic HPV16-L1 vaccine via intranasal route. All of them developed significant high neutralization titer against HPV 16 L1. Considering their

efficiency to develop HPV16 L1-specific IgG-secreting APCs in splenic lymphocytes, PDDAC-GNRs-L1 (PDG-YL) is more consistent potential to achieve strong immunogenicity.

.

## 4.7. Conclusion

GNRs-DNA led to expression of indicator YFP expression in the nasal and lung tissues. Thereafter, high IgG neutralizing antibodies (Nabs) were elicited after immunization with GNRs-DNA. The Nabs were produced as evidenced by SEAP assay. Consistent with previous studies, nasal mucosal immunization of GNRs-DNA constructs results in strong YFP expression in the nasal and lung tissues (Figure 31). Assessments of vaccine immunogenicity show production of neutralizing antibody IgG specific to HPV16 L1. According to previous studies, antibodies detected in genital tract were mainly coming from serum with a consistent isotype as systematic immune-response<sup>36,37</sup>. In this study, both ELISPOT and SEAP tests demonstrate production of antibody secreting cells in spleen lymphocytes and neutralizing antibodies in mice serum specifically against HPV16 L1. The most significant splenic level of HPV-L1 IgG secreting spleen cells was elicited by PDDAC-GNRs (6/8:  $p < 0.001$ ; 1/8:  $p < 0.05$ ). Among 4 types of GNRs-DNA, PD-G-L (PDDAC-GNRs conjugated with pDNA3 YFP-L1) appeared to be most potent one with EC50 of 1/10240 – 1/40960. PDDAC surface-coated GNRs offer most effective adjuvant activity to immunogenicity of L1 viral protein with an observable variation similar to other GNRs-DNA samples, as shown by significantly high levels of neutralizing IgG secreting in splenic APC. The variation was highly suspected to be one result of sample aggregation.



## 5. Conclusion and Future perspectives

It is noticeable that approximately 80% of cervical cancer caused by HPV occurs in developing countries. However, the screening system for monitoring HPV infection and prevention is not popularised in most of the developing countries. Especially, current licensed HPV vaccines, Gardasil<sup>®</sup> and Cervarix<sup>®</sup>, delivered by intramuscular injection requires well-trained medical personnel and special facilities. Therefore, An urge need to develop a cheap, convenient and effective DNA-based HPV vaccine, is concerned to reduce the cost from production, storage, delivery, to administration for the vaccination not only in developed countries, but also developing countries.

We targeted mucosal vaccination route because the immunisation of genital tracts is more efficiently potentiated when the vaccine is applied onto mucosal sites directly<sup>438</sup>. Therefore, we apply gold nanorods (GNRs) as an adjuvant to solve the difficulties of direct mucosal immunization.

This project has established four types of HPV GNRs-DNA vaccines and achieved high expression efficiency in cell culture. In BALB/c mouse model, excreted HPV type-specific IgG immunogenicity in systemic humoral system and APCs of spleen lymphocytes was significantly stimulated by our vaccination.

The DNA part is constructed in the backbone of mammalian expression vector, plasmid pcDNA3 YFP, from Addgene. Two versions of constructs were engineered for expression of HPV type 16 L1 VLP alone or together with E. coli heat labile toxin (ELT), which is a well-known adjuvant that enhance immunogenicity. Note that L1 or L1/ELT gene(s) were cloned up-stream of C/YFP gene, the expression of YFP offers a convenient way to monitor expression of L1 and ELT.

GNRs are nano-scaled gold colloid with a rod-shape. Application of surface modified GNRs has several advantages in DNA vaccination. As a nano-sized (<100nm) gold colloid, it was easily synthesized by the well-developed seed-growth method <sup>222</sup> and coated the nanorods with either polyethyleneimine (PEI) or poly diallyldimethylammonium chloride (PDDAC) polymers.

In our work, DNA molecules attach to GNRs through electrostatic interaction tightly, especially for PEI-coated GNRs. By a simple mixture comprised 10ng/μl GNRs with 16ng/ μl recombinant plasmid DNA, we have produced 4 types of the GNRs-DNA complexes: PEI coated GNR loaded with either pcDNA3 YFP-L1 (PE-G-L) or pcDNA3 YFP-L1-ELT (PE-G-EL); pDDAC coated GNR loaded with either pcDNA3 YFP-L1 (PD-G-L) or pcDNA3 YFP-L1-ELT (PD-G-EL).

Each type of the DNA was applied to human cell-lines HEK 293 (ATCC CRL-1573) and HeLa (ATCC CCL-2), and macrophage-like MΦ cell lines (ATCC® CRL1593.2™). *In vitro* analysis of GNRs-DNA complexes was to evaluate the cell

uptake and expression of VLP L1 genes. By Western blotting, the L1 proteins were detected in crude cell extracts of both HEK, and HeLa cell-lines. The results suggested that cells were readily uptake the GNRs-DNA complexes, and subsequently expressed HPV L1 proteins. The possible mechanisms have been revealed by Xu et al<sup>207</sup>; GNRs were up-taken by endocytosis and DNAs were released from endosomes and transferred to nuclei where gene transcription takes place due to the endosomal escape ability of cationic GNRs surface coating layer – PEI and PDDAC. The confocal imaging further demonstrated the expression of L1 proteins and YFP in HEK 293 cells as well as MΦ. The cytotoxicity was not significant, which was illustrated by the MTT analysis and PI viability assay in contrast with the mock controls (Figure 17 & 18,  $p > 0.05$ ).

The L1 GNRs-DNA vaccines were tested in mouse model in collaboration with Professor Yili Wang in Xi'an Jiao Tong University (XJTU) China. Each type of the GNRs-DNA conjugates was used to immunise 6-8 week BALB/c mice. BALB/c was inoculated via intranasal route on day 0, 14 and 28. Mice immunised via subcutaneous injection of purified VLP were served as controls; 3 mice were injected on day 0, 14, and 28. On day 33, all mice were sacrificed by cervical dislocation, which was approved experimental procedure by the Ethic Committee of XJTU. Spleens were isolated from each mouse for ELISPOT to detect antibody secreting cells specific to HPV 16 L1. Blood plasma and vaginal was collected for neutralization/inhibition ability against HPV 16 L1 specifically to detected IgG and IgA to HPV 16 L1. Blood plasma was also used for detecting neutralising antibodies against HPV 16 L1 VLP.

ELISPOT were carried out for all immunisation groups. Surprisingly inclusion of ELT genes suppressed PDDAC coated nanorods, and therefore, data for PDL (PD-G-L) are presented in Figure 33. On the other hand, exclusion ELT gene from PEI coated nanorods only elicited background of antibody secreting cells, and therefore data from PE-G-EL are presented in Figure 33. However, Western blot of in vitro gene expression assay demonstrated the adjuvant effect to boost DNA expression intracellularly and enhanced expression of both ELT contained GNRs-DNA constructs (Figure 23). One speculated reason is due to the variable cytotoxicity induced by different surface coated-GNRs observed in MTT analysis (Figure 17). As shown, mock control, plasmid control or coated GNRs (PD-G1 and PD-G2) did not produce any antibody secreting cells. The control VLP injection group produced consistent numbers of antibody secreting cells from all 3 mice (VLP1-3). Compared to VLP immunisation, immunisation with PDG-YL elicited equivalent or significantly more antibody secreting cells (PD-G-L-2 and 3; asterisks indicate statistical significance,  $p < 0.05$ ). PD-G-EL immunisation did not produce consistent results, 4/5 mice had low levels of antibody secreting cells whereas one individual (PD-G-EL 2) had significantly more antibody secreting cells compared to VLP control group. The unstable immunisation results varying among individual mice could be highly influenced by the dispersity of GNRs. Based on current results, we conclude that PD-G-L is the most suitable vaccine formula.

There are several limitations regarding current project discussed in each section. Firstly, the most ideal N/P ratio (Polymer/DNA ratio) was not evaluated in this project. The concentrations of GNRs and DNA selected was following the previous study of HIV DNA vaccine <sup>207</sup>. The zeta potential after GNP immobilised with DNA aptamers should be evaluated if the facility is available, because it is able to illustrate the electrostatic potential on the particle surface <sup>302</sup>, which shows the efficacy and stabilisation of vaccine samples were. As claimed in the discussion of sample preparation, changed structure and aggregation status of GNRs-DNA could highly affect the final immunisation result causing reduced and variable immunogenicity. Secondly, the techniques about handling GNR treated HEK293 cells brought a variable result for the DNA expression with a trouble of increased detached cells. Therefore, a sample collection including the medium should be taken into concern in the *in vitro* study. Due to the lab relocation during *in vivo* work, different concentrations of GNRs-DNA were not evaluated in this project. Therefore there is a promising potential to increase the immuno-responses by adjusting N/P ratio with low dosage of DNA-GNRs vaccines. Finally, Change of polymer/DNA concentration could provide a more saturated GNRs-DNA complexes, which could help the sample dispersity for a more stable immunisation. A whole profile of secreted local IgG, IgA, and factors stimulating cell-mediated immune response could be further discovered for an overall comprehension of intranasal GNRs-DNA vaccine against HPV infection.

To summarise, this project has successfully developed a new mucosal vaccination against human papillomavirus infection and cervical cancers. Currently, we

demonstrated enhanced immunogenicity of our designed vaccine by neutralisation assay and ELISPOT assay in a mouse immunisation model. Interestingly, the PEI-GNRs-DNA groups provided a strong humoral immunity with high neutralizing antibody IgG in serum. However the level of HPV16 L1-IgG secreting APCs developed by either PE-G-L or PE-G-EL was not consistent in the same group. However, considering the enhanced L1 expression of PE-G-EL complex, further study about IgG and IgA development at local mucosa (like cervicovaginal region) is recommended for a comprehensive understanding for PE-G-EL intranasal immunization.

These types of intranasal GNRs-DNA vaccines are particularly advantageous for vaccination in remote areas of the world. Especially pcDNA3 YFP-L1 conjugated with PDDAC-functionalised GNRs (PD-G-L) is more ideal for HPV prevention due to its significant immunogenicity to elicit HPV type-specific serum neutralization antibody IgG and higher level of HPV16-L1 specific IgG-secreting APC in spleen lymphocytes. The immunization strategy of our novel DNA vaccine was via nasal mucosa route. There is no need of supervision by medical professions for vaccination. As the male vaccination started to popularise in several developed countries, these advantages will further drive down the costs for vaccination and will make male vaccination affordable in the UK and other developed countries, and will likely persuade health authorities in resource-poor countries to implement vaccination.

## Bibliography

1. Kanodia S, Fahey LM, Kast WM. Mechanisms used by human papillomaviruses to escape the host immune response. *Curr Cancer Drug Targets*. 2007;7(1):79-89. doi:10.2174/156800907780006869.
2. Longworth MS, Laimins L a. Pathogenesis of Human Papillomaviruses in Differentiating Epithelia Pathogenesis of Human Papillomaviruses in Differentiating Epithelia. *Microbiol Mol Biol Rev*. 2004;68(2):362-372. doi:10.1128/MMBR.68.2.362.
3. Calleja-Macias IE, Kalantari M, Allan B, et al. Papillomavirus subtypes are natural and old taxa: phylogeny of human papillomavirus types 44 and 55 and 68a and -b. *J Virol*. 2005;79(10):6565-6569. doi:10.1128/JVI.79.10.6565-6569.2005.
4. Muñoz N, Bosch FX, de Sanjosé S, et al. Epidemiologic Classification of Human Papillomavirus Types Associated with Cervical Cancer. *N Engl J Med*. 2003;348(6):518-527. doi:10.1056/NEJMoa021641.
5. Molano M, Van den Brule A, Plummer M, et al. Determinants of clearance of human papillomavirus infections in Colombian women with normal cytology: A population-based, 5-year follow-up study. *Am J Epidemiol*. 2003;158(5):486-494. doi:10.1093/aje/kwg171.
6. Steenbergen RDM, De Wilde J, Wilting SM, Brink A a TP, Snijders PJF, Meijer CJLM. HPV-mediated transformation of the anogenital tract. *J Clin Virol*. 2005;32(SUPPL.). doi:10.1016/j.jcv.2004.11.019.
7. Syrjänen S. The role of human papillomavirus infection in head and neck cancers. *Ann Oncol*. 2010;21 Suppl 7:vii243-i245. doi:10.1093/annonc/mdq454.
8. Howley PM, Fields BN, Knipe D., Chanock RM. *Papillomavirinae: The Viruses and Their Replication*. 3rd ed.; 1996.
9. Human Papillomavirus ( HPV ) Vaccines For Australians : Information for Immunisation Providers. *NCIRS Fact sheet*. 2013;(March):1-7. <http://www.ncirs.edu.au/immunisation/fact-sheets/hpv-human-papillomavirus-fact-sheet.pdf>.
10. Tristram A, Flander A. Human papillomavirus ( including vaccines ). *Obstet Gynaecol Reprod Med*. 2007;17(11):324-329.
11. Doorbar J. Molecular biology of human papillomavirus infection and cervical cancer. *Clin Sci (Lond)*. 2006;110(5):525-541. doi:10.1042/CS20050369.
12. Chaturvedi AK. Beyond Cervical Cancer: Burden of Other HPV-Related Cancers Among Men and Women. *J Adolesc Heal*. 2010;46(4 SUPPL.):S20-S26. doi:10.1016/j.jadohealth.2010.01.016.
13. Reis A, Cruz A. The Impact of Human Papillomavirus on Cancer Risk in Penile Cancer. In: *Human Papillomavirus and Related Diseases - From Bench to Bedside - A Clinical Perspective.*; 2010.
14. Forman D, de Martel C, Lacey CJ, et al. Global burden of human papillomavirus and related diseases. *Vaccine*. 2012;30 Suppl 5:F12-23.

doi:10.1016/j.vaccine.2012.07.055.

15. Shuyama K, Castillo a, Aguayo F, et al. Human papillomavirus in high- and low-risk areas of oesophageal squamous cell carcinoma in China. *Br J Cancer*. 2007;96(10):1554-1559.
16. Castillo A. Human Papillomavirus and Carcinogenesis in the Upper Aero-Digestive Tract. In: *Carcinogenesis*. doi:http://dx.doi.org/10.5772/54800.
17. Clifford GM, Smith JS, Plummer M, Muñoz N, Franceschi S. Human papillomavirus types in invasive cervical cancer worldwide: a meta-analysis. *Br J Cancer*. 2003;88(1):63-73.  
<http://www.pubmedcentral.nih.gov/articlerender.fcgi?artid=2376782&tool=pmcentrez&rendertype=abstract>.
18. Torre L a, Bray F, Siegel RL, Ferlay J, Lortet-tieulent J, Jemal A. Global Cancer Statistics, 2012. 2015;0(0):1-22. doi:10.3322/caac.21262.
19. Giuliano AR, Lee J-H, Fulp W, et al. Incidence and clearance of genital human papillomavirus infection in men (HIM): a cohort study. *Lancet*. 2011;377(9769):932-940. doi:10.1016/S0140-6736(10)62342-2.
20. Clifford G, Franceschi S, Diaz M, Muñoz N, Villa LL. Chapter 3: HPV type-distribution in women with and without cervical neoplastic diseases. *Vaccine*. 2006;24(SUPPL. 3):26-34. doi:10.1016/j.vaccine.2006.05.026.
21. Baseman JG, Koutsky L a. The epidemiology of human papillomavirus infections. *J Clin Virol*. 2005;32(SUPPL.):16-24. doi:10.1016/j.jcv.2004.12.008.
22. Munoz N, Castellsagu X, Gonz AB De. Chapter 1 : HPV in the etiology of human cancer. *J vaccine*. 2006;3:1-10. doi:10.1016/j.vaccine.2006.05.115.
23. Cróquer ZDG. Development of Vaccines and Gene Therapy Against HPV Infection and Cervical Cancer. 2009.
24. Louie KS, de Sanjose S, Mayaud P. Epidemiology and prevention of human papillomavirus and cervical cancer in sub-Saharan Africa: a comprehensive review. *Trop Med Int Health*. 2009;14(10):1287-1302. doi:10.1111/j.1365-3156.2009.02372.x.
25. Huang S, Afonina I, Miller BA, Beckmann AM. Human papillomavirus types 52 and 58 are prevalent in cervical cancers from Chinese women. *Int J cancer*. 1997;411(October 1996):408-411.
26. HPV Information Center. *China - Human Papillomavirus and Related Cancers - Fact Sheet 2016*. Barcelona, Spain; 2016. [www.hpvcentre.net](http://www.hpvcentre.net).
27. Li Z, Liu F, Cheng S, et al. Prevalence of HPV infection among 28,457 Chinese women in Yunnan Province, southwest China. *Sci Rep*. 2016;6(February):21039. doi:10.1038/srep21039.
28. Liu X-X, Fan X-L, Yu Y-P, Ji L, Yan J, Sun A-H. Human papillomavirus prevalence and type-distribution among women in Zhejiang Province, Southeast China: a cross-sectional study. *BMC Infect Dis*. 2014;14(1):708. doi:10.1186/s12879-014-0708-8.
29. Bosch F, Manos M. Prevalence of human papillomavirus in cervical cancer: a worldwide perspective. *J ....* 1995;87(11).  
<http://jnci.oxfordjournals.org/content/87/11/796.short>.
30. Frazer IH. Prevention of cervical cancer through papillomavirus vaccination. *Nat Rev*



- Immunol.* 2004;4(1):46-54. doi:10.1038/nri1260.
31. Stanley M a. Immune responses to human papilloma viruses. *Indian J Med Res.* 2009;130(3):266-276.
  32. Roberts JN, Buck CB, Thompson CD, et al. Genital transmission of HPV in a mouse model is potentiated by nonoxynol-9 and inhibited by carrageenan. *Nat Med.* 2007;13(7):857-861.  
[http://www.ncbi.nlm.nih.gov/entrez/query.fcgi?cmd=Retrieve&db=PubMed&dopt=Citation&list\\_uids=17603495](http://www.ncbi.nlm.nih.gov/entrez/query.fcgi?cmd=Retrieve&db=PubMed&dopt=Citation&list_uids=17603495).
  33. Nelson LM, Rose RC, Moroianu J. Nuclear import strategies of high risk HPV16 L1 major capsid protein. *J Biol Chem.* 2002;277(26):23958-23964.  
doi:10.1074/jbc.M200724200.
  34. Florin L, Sapp C, Streeck RE, Sapp M. Assembly and translocation of papillomavirus capsid proteins. *J Virol.* 2002;76(19):10009-10014. doi:10.1128/JVI.76.19.10009-10014.2002.
  35. Stanley M. Immune responses to human papillomavirus. *Vaccine.* 2006;24(SUPPL. 1):16-22. doi:10.1016/j.vaccine.2005.09.002.
  36. Lowe RS, Brown DR, Bryan JT, et al. Human papillomavirus type 11 (HPV-11) neutralizing antibodies in the serum and genital mucosal secretions of African green monkeys immunized with HPV-11 virus-like particles expressed in yeast. *J Infect Dis.* 1997;176(5):1141-1145. <http://www.ncbi.nlm.nih.gov/pubmed/9359711>.
  37. Nardelli-Haeffliger D, Wirthner D, Schiller JT, et al. Specific Antibody Levels at the Cervix During the Menstrual Cycle of Women Vaccinated With Human Papillomavirus 16 Virus-Like Particles. *JNCI J Natl Cancer Inst.* 2003;95(15):1128-1137. doi:10.1093/jnci/djg018.
  38. Opalka D, Lachman CE, MacMullen SA, et al. Simultaneous quantitation of antibodies to neutralizing epitopes on virus-like particles for human papillomavirus types 6, 11, 16, and 18 by a multiplexed luminex assay. *Clin Diagn Lab Immunol.* 2003;10(1):108-115.  
<http://www.pubmedcentral.nih.gov/articlerender.fcgi?artid=145272&tool=pmcentrez&rendertype=abstract>.
  39. Stanley M, Lowy DR, Frazer I. Chapter 12: Prophylactic HPV vaccines: underlying mechanisms. *Vaccine.* 2006;24 Suppl 3:S3/106-13.  
doi:10.1016/j.vaccine.2006.05.110.
  40. Smith PD, Macdonald TT, Blumberg RS. *Principles of Mucosal Immunology.*; 2012.  
<http://www.nature.com/doifinder/10.1038/mi.2013.8>.
  41. Van Ginkel FW, Nguyen HH, McGhee JR. Vaccines for mucosal immunity to combat emerging infectious diseases. *Emerg Infect Dis.* 2000;6(2):123-132.  
doi:10.3201/eid0602.000204.
  42. Lee SJ, Cho YS, Cho MC, et al. Both E6 and E7 oncoproteins of human papillomavirus 16 inhibit IL-18-induced IFN-gamma production in human peripheral blood mononuclear and NK cells. *J Immunol.* 2001;167(1):497-504.  
doi:10.4049/jimmunol.167.1.497.
  43. Gravitt PE. The known unknowns of HPV natural history. *J Clin Invest.* 2011;121(12):4593-4599. doi:10.1172/JCI57149.

44. Amador-Molina A, Hernández-Valencia JF, Lamoyi E, Contreras-Paredes A, Lizano M. Role of innate immunity against human papillomavirus (HPV) infections and effect of adjuvants in promoting specific immune response. *Viruses*. 2013;5(11):2624-2642. doi:10.3390/v5112624.
45. Ho. G, R. B, L. B, C. C, Burk R. Natural History of Cervicovaginal Papillomavirus Infection in Young Women. *Nat Hist cervicovaginal papillomavirus Infect young women*. 1998;338(7):423-428.
46. Gariglio P, Gutiérrez J, Cortés E, Vázquez J. The Role of Retinoid Deficiency and Estrogens as Cofactors in Cervical Cancer. *Arch Med Res*. 2009;40(6):449-465. doi:10.1016/j.arcmed.2009.08.002.
47. Schiffman MH, Bauer HM, Hoover RN, et al. Epidemiologic evidence showing that human papillomavirus infection causes most cervical intraepithelial neoplasia. *J Natl Cancer Inst*. 1993;85(12):958-964.
48. Franco EL, Villa LL, Sobrinho JP, et al. Epidemiology of acquisition and clearance of cervical human papillomavirus infection in women from a high-risk area for cervical cancer. *J Infect Dis*. 1999;180(5):1415-1423. doi:10.1086/315086.
49. Munoz N, Franceschi S, Bosetti C, et al. Role of parity and human papillomavirus in cervical cancer: The IARC multicentric case-control study. *Lancet*. 2002;359(9312):1093-1101.
50. Arbeit JM, Howley PM, Hanahan D. Chronic estrogen-induced cervical and vaginal squamous carcinogenesis in human papillomavirus type 16 transgenic mice. *PNAS*. 1996;93(7):2930-2935.
51. Autierl P, Coibion ' M, Huet ' F, Grivegneel A. Transformation zone location and intraepithelial neoplasia of the cervix uteri. *Bridsh J Cancer*. 1996;74:488-490.
52. Akira S, Hemmi H. Recognition of pathogen-associated molecular patterns by TLR family. *Immunol Lett*. 2003;85(2):85-95. doi:10.1016/S0165-2478(02)00228-6.
53. Hausen H Zur. Papillomavirus infections — a major cause of human cancers. *Biochim Biophys Acta - Rev Cancer*. 1996;1288(2):F55-F78. doi:10.1016/0304-419X(96)00020-0.
54. Tindle RW. Immune evasion in human papillomavirus-associated cervical cancer. *Nat Rev Cancer*. 2002;2(1):59-65. <http://www.ncbi.nlm.nih.gov/pubmed/11902586>.
55. Wang K. H UMAN P APILLOMAVIRUS AND V ACCINATION IN C ERVICAL C ANCKER. 2007;46(4):15-20.
56. zur Hausen H. Papillomaviruses causing cancer: evasion from host-cell control in early events in carcinogenesis. *J Natl Cancer Inst*. 2000;92(9):690-698. doi:10.1093/jnci/92.9.690.
57. Cason J, Patel D, Naylor J, et al. Identification of immunogenic regions of the major coat protein of human papillomavirus type 16 that contain type-restricted epitopes. *J Gen Virol*. 1989;70(11):2973-2987.
58. Rudolf MP, Nieland JD, DaSilva DM, et al. Induction of HPV16 capsid protein-specific human T cell responses by virus-like particles. *Biol Chem*. 1999;380(3):335-340. <http://www.ncbi.nlm.nih.gov/pubmed/10223336>.
59. Carter JJ, Koutsky L a, Hughes JP, et al. Comparison of human papillomavirus types 16, 18, and 6 capsid antibody responses following incident infection. *J Infect Dis*.

- 2000;181(6):1911-1919. doi:10.1086/315498.
60. Moerman-Herzog A, Nakagawa M. Early Defensive Mechanisms against Human Papillomavirus Infection. *Clin Vaccine Immunol*. 2015;22(8):850-857. doi:10.1128/CVI.00223-15.
  61. Appay V, Rowland-Jones SL. RANTES: A versatile and controversial chemokine. *Trends Immunol*. 2001;22(2):83-87.
  62. Caux C, It-Yahia S, Chemin K, et al. Dendritic cell biology and regulation of dendritic cell trafficking by chemokines. *Springer Semin*. 2000;4(22):345-369. doi:10.1007/s002810000053.
  63. Charbonnier AS, Kohrgruber N, Kriehuber E, Stingl G, Rot A, Maurer D. Macrophage inflammatory protein 3alpha is involved in the constitutive trafficking of epidermal langerhans cells. *J Exp Med*. 1999;190(12):1755-1768. <http://www.ncbi.nlm.nih.gov/pubmed/10601351> <http://www.pubmedcentral.nih.gov/articlerender.fcgi?artid=PMC2195721>.
  64. Bonecchi R, Bianchi G, Bordignon PP, et al. Differential expression of chemokine receptors and chemotactic responsiveness of type 1 T helper cells (Th1s) and Th2s. *J Exp Med*. 1998;187(1):129-134. doi:10.1084/jem.187.1.129.
  65. Kleine-Lowinski K, Rheinwald JG, Fichorova RN, et al. Selective suppression of monocyte chemoattractant protein-1 expression by human papillomavirus E6 and E7 oncoproteins in human cervical epithelial and epidermal cells. *Int J Cancer*. 2003;107(3):407-415. doi:10.1002/ijc.11411.
  66. Karim R, Meyers C, Backendorf C, et al. Human papillomavirus deregulates the response of a cellular network comprising of chemotactic and proinflammatory genes. *PLoS One*. 2011;6(3).
  67. Deligeoroglou E, Giannouli A, Athanasopoulos N, et al. HPV infection: Immunological aspects and their utility in future therapy. *Infect Dis Obstet Gynecol*. 2013;2013. doi:10.1155/2013/540850.
  68. Smith PD, MacDonald TT, Blumberg RS. Cellular Constituents of mucosal immune systems and their function in mucosal homeostasis. In: *Principles of Mucosal Immunology*.; 2013:55-68.
  69. Mestecky J, Amm ME, Ogra PL, Strober W. Cellular and Molecular Basis for Antigen Transport Across Epithelial Barriers. In: *Mucosal Immunology*. 2nd ed.; 1999:111-130.
  70. Vinther J, Norrild B. Clearance of cervical human papillomavirus infections. *Int J Cancer*. 2003;104(2):255-256. doi:10.1002/ijc.10922.
  71. Scott M, Stites DP, Moscicki a B. Th1 cytokine patterns in cervical human papillomavirus infection. *Clin Diagn Lab Immunol*. 1999;6(5):751-755.
  72. Scott M, Nakagawa M, Moscicki AB. Cell-Mediated Immune Response to Human Papillomavirus Infection. *Clin Diagn Lab Immunol*. 2001;8(2):209-220. doi:10.1128/CDLI.8.2.209.
  73. Kyo S, Inoue M, Hayasaka N, et al. Regulation of early gene expression of human papillomavirus type 16 by inflammatory cytokines. *Virology*. 1994;200(1):130-139. doi:10.1006/viro.1994.1171.
  74. Rösl F, Lengert M, Albrecht J, et al. Differential regulation of the JE gene encoding the monocyte chemoattractant protein (MCP-1) in cervical carcinoma cells and

- derived hybrids. *J Virol*. 1994;68(4):2142-2150.
75. Stetson DB, Medzhitov R. Type I Interferons in Host Defense. *Immunity*. 2006;25(3):373-381.
  76. Fensterl V, Sen GC. Interferons and viral infections. *BioFactors*. 2009;35(1):14-20.
  77. Stanley M a. Epithelial cell responses to infection with human papillomavirus. *Clin Microbiol Rev*. 2012;25(2):215-222. doi:10.1128/CMR.05028-11.
  78. Oldak M, Majewski S, Grzela T, et al. Natural cell-mediated cytotoxicity of peripheral blood lymphocytes against target cells transfected with epidermodysplasia verruciformis-specific human papillomavirus type 8 L1 DNA sequences. *Int J Mol Med*. 2004;13(1):187-191.
  79. Gulino a V. WHIM syndrome: a genetic disorder of leukocyte trafficking. *Curr Opin Allergy Clin Immunol*. 2003;3(6):443-450. doi:10.1097/00130832-200312000-00005.
  80. Connor JP, Ferrer K, Kane JP, Goldberg JM. Evaluation of Langerhans' cells in the cervical epithelium of women with cervical intraepithelial neoplasia. *Gynecol Oncol*. 1999;75(1):130-135. <http://www.ncbi.nlm.nih.gov/pubmed/10502439>.
  81. Fausch SC, Fahey LM, Da Silva DM, Kast WM. Human papillomavirus can escape immune recognition through Langerhans cell phosphoinositide 3-kinase activation. *J Immunol*. 2005;174(11):7172-7178. doi:10.4049/jimmunol.174.11.7172.
  82. O'Brien PM, Saveria Campo M. Evasion of host immunity directed by papillomavirus-encoded proteins. *Virus Res*. 2002;88(1-2):103-117. doi:10.1016/S0168-1702(02)00123-5.
  83. Viscidi RP, Schiffman M, Hildesheim A, et al. Seroreactivity to human papillomavirus (HPV) types 16, 18, or 31 and risk of subsequent HPV infection: results from a population-based study in Costa Rica. *Cancer Epidemiol Biomarkers Prev*. 2004;13(2):324-327. doi:10.1158/1055-9965.EPI-03-0166.
  84. Day PM, Thompson CD, Buck CB, Pang Y-YS, Lowy DR, Schiller JT. Neutralization of human papillomavirus with monoclonal antibodies reveals different mechanisms of inhibition. *J Virol*. 2007;81(16):8784-8792. doi:10.1128/JVI.00552-07.
  85. Suzich JA, Ghim SJ, Palmer-Hill FJ, et al. Systemic immunization with papillomavirus L1 protein completely prevents the development of viral mucosal papillomas. *Proc Natl Acad Sci U S A*. 1995;92(25):11553-11557. doi:10.1073/pnas.92.25.11553.
  86. Dillner J. The serological response to papillomaviruses. *Semin Cancer Biol*. 1999;9(6):423-430. [http://www.ncbi.nlm.nih.gov/entrez/query.fcgi?cmd=Retrieve&db=PubMed&dopt=Citation&list\\_uids=10712889](http://www.ncbi.nlm.nih.gov/entrez/query.fcgi?cmd=Retrieve&db=PubMed&dopt=Citation&list_uids=10712889).
  87. Combita A-L, Touzé A, Bousarghin L, Christensen ND, Coursaget P. Identification of two cross-neutralizing linear epitopes within the L1 major capsid protein of human papillomaviruses. *J Virol*. 2002;76(13):6480-6486. doi:10.1128/JVI.76.13.6480.
  88. Harper DM, Franco EL, Wheeler CM, et al. Sustained efficacy up to 4-5 years of a bivalent L1 virus-like particle vaccine against human papillomavirus types 16 and 18: follow-up from a randomised control trial. *Lancet*. 2006;367(9518):1247-1255.
  89. Koshiol J, Kovacic MB. Cytokines and Markers of Immune Response to HPV Infection. *Recent Adv Immunol to target cancer, Inflamm Infect*. 2011:520.
  90. Pett MR, Herdman MT, Palmer RD, et al. Selection of cervical keratinocytes

- containing integrated HPV16 associates with episome loss and an endogenous antiviral response. *Proc Natl Acad Sci U S A*. 2006;103(10):3822-3827. <http://www.ncbi.nlm.nih.gov/pubmed/16505361>.
91. Parr MB, Parr EL. Mucosal immunity in the female and male reproductive tract. In: *Handbook of Mucosal Immunology*. San Diego: Academy Press; 1996:677-689.
  92. Greslin I, Mouglin C, Seilles E. Biologie des infections à papillomavirus. II. Réponse immunitaire. *Ann Biol Clin*. 1998;56:267-276.
  93. Roncalli M, Sideri M, Gie P. Immunophenotypic analysis of the transformation zone of human cervix. *Lab Investigations*. 1988;58:141-149.
  94. Pett M, Coleman N. Integration of high-risk human papillomavirus - a key event in cervical carcinogenesis? *J Pathol*. 2007;212(June):356-367. doi:10.1002/path.
  95. Ashrafi GH, Brown DR, Fife KH, Campo MS. Down-regulation of MHC class I is a property common to papillomavirus E5 proteins. *Virus Res*. 2006;120(1-2):208-211. doi:10.1016/j.virusres.2006.02.005.
  96. Kadaja M, Sumerina A, Verst T, Ojarand M, Ustav E, Ustav M. Genomic instability of the host cell induced by the human papillomavirus replication machinery. *EMBO J*. 2007;26(8):2180-2191. doi:10.1038/sj.emboj.7601665.
  97. Bernard B a, Bailly C, Lenoir MC, Darmon M, Thierry F, Yaniv M. The human papillomavirus type 18 (HPV18) E2 gene product is a repressor of the HPV18 regulatory region in human keratinocytes. *J Virol*. 1989;63(10):4317-4324.
  98. Stenlund a, Botchan MR. The E2 trans-activator can act as a repressor by interfering with a cellular transcription factor. *Genes Dev*. 1990;4(1):123-36.
  99. Dowhanick JJ, McBride a a, Howley PM. Suppression of cellular proliferation by the papillomavirus E2 protein. *J Virol*. 1995;69(12):7791-7799.
  100. Herdman TM, Pett MR, Roberts I, et al. Interferon- $\beta$  treatment of cervical keratinocytes naturally infected with human papillomavirus 16 episomes promotes rapid reduction in episome numbers and emergence of latent integrants. *Carcinogenesis*. 2006;27(11):2341-2353.
  101. Cone RW, Minson AC, Smith MR, McDougall JK. Conservation of HPV-16 E6/E7 ORF sequences in a cervical carcinoma. *J Med Virol*. 1992;37(2):99-107.
  102. Schwarz E, Freese UK, Gissmann L, et al. Structure and transcription of human papillomavirus sequences in cervical carcinoma cells. *Nature*. 1985;314(6006):111-114. doi:10.1038/314111a0.
  103. Wagatsuma M, Hashimoto K, Matsukura T. Analysis of integrated human papillomavirus type 16 DNA in cervical cancers: amplification of viral sequences together with cellular flanking sequences. *J Virol*. 1990;64(2):813-821. <http://www.pubmedcentral.nih.gov/articlerender.fcgi?artid=249176&tool=pmcentrez&rendertype=abstract>.
  104. Choo K, Pan C, SH H. Integration of human papillomavirus type 16 into cellular DNA of cervical carcinoma: preferential deletion of the E2 gene and invariable retention of the long control region and the E6/E7 open reading frames. *Virology*. 1987;161:259-261.
  105. Southern SA, Evans MF, Herrington CS. Basal cell tetrasomy in low-grade cervical squamous intraepithelial lesions infected with high-risk human papillomaviruses.

- Cancer Res.* 1997;57:4210-4213.
106. Jeon S, Lambert PF. Integration of human papillomavirus type 16 DNA into the human genome leads to increased stability of E6 and E7 mRNAs: implications for cervical carcinogenesis. *Proc Natl Acad Sci U S A.* 1995;92(5):1654-1658. doi:10.1073/pnas.92.5.1654.
  107. Francis D a, Schmid SI, Howley PM. Repression of the integrated papillomavirus E6/E7 promoter is required for growth suppression of cervical cancer cells. *J Virol.* 2000;74(6):2679-2686. doi:10.1128/JVI.74.6.2679-2686.2000.
  108. Solinas-Toldo S, Dürst M, Lichter P. Specific chromosomal imbalances in human papillomavirus-transfected cells during progression toward immortality. *Proc Natl Acad Sci U S A.* 1997;94(8):3854-3859. <http://www.pubmedcentral.nih.gov/articlerender.fcgi?artid=20531&tool=pmcentrez&rendertype=abstract>.
  109. Duensing S, Munger K. The human papillomavirus type 16 E6 and E7 oncoproteins independently induce numerical and structural chromosomal instability. *Cancer Res.* 2002;62:7075-82.
  110. Liu X, Han S, Baluda M a, Park NH. HPV-16 oncogenes E6 and E7 are mutagenic in normal human oral keratinocytes. *Oncogene.* 1997;14(19):2347-2353. <http://www.ncbi.nlm.nih.gov/pubmed/9178911>.
  111. Song S, Gulliver G a, Lambert PF. Human papillomavirus type 16 E6 and E7 oncogenes abrogate radiation-induced DNA damage responses in vivo through p53-dependent and p53-independent pathways. *Proc Natl Acad Sci U S A.* 1998;95(5):2290-2295. doi:10.1073/pnas.95.5.2290.
  112. Kesis TD, Slebos RJ, Nelson WG, et al. Human papillomavirus 16 E6 expression disrupts the p53-mediated cellular response to DNA damage. *Proc Natl Acad Sci U S A.* 1993;90(9):3988-3992. <http://www.pubmedcentral.nih.gov/articlerender.fcgi?artid=46431&tool=pmcentrez&rendertype=abstract>.
  113. Moody C a, Laimins L a. Human papillomavirus oncoproteins: pathways to transformation. *Nat Rev Cancer.* 2010;10(8):550-560. doi:10.1038/nrc2886.
  114. Duensing S, Lee LY, Duensing A, et al. The human papillomavirus type 16 E6 and E7 oncoproteins cooperate to induce mitotic defects and genomic instability by uncoupling centrosome duplication from the cell division cycle. *Proc Natl Acad Sci U S A.* 2000;97(18):10002-10007. doi:10.1073/pnas.170093297.
  115. Duensing S, Duensing A, Crum CP, Münger K. Human papillomavirus type 16 E7 oncoprotein-induced abnormal centrosome synthesis is an early event in the evolving malignant phenotype. *Cancer Res.* 2001;61(6):2356-2360.
  116. Crum CP, Ikenberg H, Richart RM, Gissman L. Human papillomavirus type 16 and early cervical neoplasia. *N Engl J Med.* 1984;310:880-883.
  117. Salisbury JL, Whitehead CM, Lingle WL, Barrett SL. Centrosomes and cancer. *Biol Cell.* 1999;91(6):451-460.
  118. zur Hausen H. Papillomaviruses and cancer: from basic studies to clinical application. *Nat Rev Cancer.* 2002;2(5):342-350. doi:10.1038/nrc798.
  119. Soto U, Denk C, Finzer P, Hutter KJ, Zur Hausen H, Rösl F. Genetic complementation

- to non-tumorigenicity in cervical-carcinoma cells correlates with alterations in AP-1 composition. *Int J Cancer*. 2000;86(6):811-817.
120. Bosch FX, Schwarz E, Boukamp P, Fusenig NE, Bartsch D, zur Hausen H. Suppression in vivo of human papillomavirus type 18 E6-E7 gene expression in nontumorigenic HeLa X fibroblast hybrid cells. *J Virol*. 1990;64(10):4743-4754. [/pmc/articles/PMC247961/?report=abstract](https://pubmed.ncbi.nlm.nih.gov/100000000/).
  121. Talora C, Sgroi DC, Crum CP, Paolo Dotto G. Specific down-modulation of Notch1 signaling in cervical cancer cells is required for sustained HPV-E6/E7 expression and late steps of malignant transformation. *Genes Dev*. 2002;16(17):2252-2263. doi:10.1101/gad.988902.
  122. Rush M, Zhao X, Schwartz S. A splicing enhancer in the E4 coding region of human papillomavirus type 16 is required for early mRNA splicing and polyadenylation as well as inhibition of premature late gene expression. *J Virol*. 2005;79(18):12002-12015. doi:10.1128/JVI.79.18.12002-12015.2005.
  123. Klymenko T, Graham S. Human papillomavirus gene expression is controlled by host cell splicing factors. 2012:773-777. doi:10.1042/BST20120079.
  124. Zheng Z-M, Baker CC. Papillomavirus Genome Structure, Expression, and Post-transcriptional Regulation. *Front Biosci*. 2006;11:2286-2302.
  125. Johansson C, Schwartz S. Regulation of human papillomavirus gene expression by splicing and polyadenylation. *Nat Rev Microbiol*. 2013;11(4):239-251. <http://www.ncbi.nlm.nih.gov/pubmed/23474685>.
  126. Krieg AM. CpG motifs in bacterial DNA and their immune effects. *Annu Rev Immunol*. 2002;20:709-760. doi:10.1146/annurev.immunol.20.100301.064842.
  127. Tokunaga T, Yamamoto H, Shimada S, et al. Antitumor activity of deoxyribonucleic acid fraction from Mycobacterium bovis BCG. I. Isolation, physicochemical characterization, and antitumor activity. *J Natl Cancer Inst*. 1984;72(4):955-962. <http://eutils.ncbi.nlm.nih.gov/entrez/eutils/elink.fcgi?dbfrom=pubmed&id=6200641&retmode=ref&cmd=prlinks%5Cnpapers2://publication/uuid/276FC7B9-EBD8-4C73-97FD-84B511F7A9F8>.
  128. Verthelyi D, Ishii KJ, Gursel M, Takeshita F, Klinman DM. Human peripheral blood cells differentially recognize and respond to two distinct CPG motifs. *J Immunol*. 2001;166(4):2372-2377.
  129. Lin K, Doolan K, Hung CF, Wu TC. Perspectives for Preventive and Therapeutic HPV Vaccines. *J Formos Med Assoc*. 2010;109(1):4-24. doi:10.1016/S0929-6646(10)60017-4.
  130. von Knebel Doeberitz M. The dawn of prophylactic vaccines against human papillomaviruses and cervical cancer. *Int J Cancer*. 2006;119(11):xi-xii. doi:10.1002/ijc.22445.
  131. Jansen KU, Shar AR. Human papillomavirus vaccines and prevention of cervical cancer. *Annu Rev Med*. 2004;55:319.
  132. Adurthi S, Krishna S, Mukherjee G, Bafna UD, Devi U, Jayshree RS. Regulatory T cells in a spectrum of HPV-induced cervical lesions: Cervicitis, cervical intraepithelial neoplasia and squamous cell carcinoma. *Am J Reprod Immunol*. 2008;60(1):55-65.
  133. Kobayashi A, Greenblatt RM, Anastos K, et al. Functional attributes of mucosal

- immunity in cervical intraepithelial neoplasia and effects of HIV infection. *Cancer Res.* 2004;64(18):6766-6774.
134. Hammitt LL, Hennessy TW, Fiore AE, et al. Hepatitis B immunity in children vaccinated with recombinant hepatitis B vaccine beginning at birth: A follow-up study at 15 years. *Vaccine.* 2007;25(39-40):6958-6964.
  135. Kols A, Sherris J, Ph D. HPV Vaccines : 2000;(July).
  136. Lowy DR, Schiller JT. Papillomaviruses: prophylactic vaccine prospects. *Biochim Biophys Acta.* 1999;1423(1):M1-8. <http://www.ncbi.nlm.nih.gov/pubmed/9989208>.
  137. Frazer IH. Interaction of human papillomaviruses with the host immune system : A well evolved relationship. *Virology.* 2009;384(2):410-414. doi:10.1016/j.virol.2008.10.004.
  138. Kawana K, Yasugi T, Taketani Y. Human papillomavirus vaccines: current issues & future. *Indian J Med Res.* 2009;130(3):341-347.
  139. García-Piñeres A, Hildesheim A, Dodd L, et al. Cytokine and chemokine profiles following vaccination with human papillomavirus type 16 L1 Virus-like particles. *Clin Vaccine Immunol.* 2007;14(8):984-989. doi:10.1128/CVI.00090-07.
  140. Yang R, Murillo FM, Cui H, et al. Papillomavirus-Like Particles Stimulate Murine Bone Marrow-Derived Dendritic Cells To Produce Alpha Interferon and Th1 Immune Responses via MyD88 Papillomavirus-Like Particles Stimulate Murine Bone Marrow-Derived Dendritic Cells To Produce Alpha Interfero. 2004;78(20):11152-11160. doi:10.1128/JVI.78.20.11152.
  141. Nordenvall C, Chang ET, Adami HO. Cancer risk among patients with condylomata acuminata. *Int J Cancer.* 2006;119(4):888-893.
  142. Stanley M. HPV - immune response to infection and vaccination. *Infect Agent Cancer.* 2010;5(1):19. doi:10.1186/1750-9378-5-19.
  143. Bryan JT, Jasen KU, Lowe RS, et al. Human papillomavirus type 11 neutralization in the athymic mouse xenograft system: Correlation with virus-like particle IgG concentration. *J Medi Viro.* 1997;53(3):185-188.
  144. Lin YL, Borenstein LA, Selvakumar R, Ahmed R, Wettstein FO. Effective vaccination against papilloma development by immunization with L1 or L2 structural protein of cottontail rabbit papillomavirus. *Virology.* 1992;187(2):612-619.
  145. Jansen KU, Rosolowsky M, Schultz LD, et al. Vaccination with yeast-expressed cottontail rabbit papillomavirus (CRPV) virus-like particles protects rabbits from CRPV-induced papilloma formation. *Vaccine.* 1995;13(16):1509-1514. doi:10.1016/0264-410X(95)00103-8.
  146. Christensen ND, Reed C a, Cladel NM, Han R, Kreider JW. Immunization with viruslike particles induces long-term protection of rabbits against challenge with cottontail rabbit papillomavirus. *J Virol.* 1996;70(2):960-965. <http://www.pubmedcentral.nih.gov/articlerender.fcgi?artid=189900&tool=pmcentrez&rendertype=abstract>.
  147. Collins S, Mazloomzadeh S, Winter H, et al. High incidence of cervical human papillomavirus infection in women during their first sexual relationship. *BJOG.* 2002;109(1):96-98. <http://www.ncbi.nlm.nih.gov/pubmed/11845815>.
  148. Roden R, Wu T-C. How will HPV vaccines affect cervical cancer? *Nat Rev Cancer.*



- 2006;6(10):753-763.  
<http://www.pubmedcentral.nih.gov/articlerender.fcgi?artid=3181152&tool=pmcentrez&rendertype=abstract>.
149. Barnabas R V., Laukkanen P, Koskela P, Kontula O, Lehtinen M, Garnett GP. Epidemiology of HPV 16 and cervical cancer in Finland and the potential impact of vaccination: Mathematical modelling analyses. *PLoS Med.* 2006;3(5):624-632.
  150. Reiter PL, Brewer NT, McRee AL, Gilbert P, Smith JS. Acceptability of HPV Vaccine Among a National Sample of Gay and Bisexual Men. *Sex Transm Dis.* 2010;37(3):197-203. doi:10.1097/OLQ.0b013e3181bf542c.
  151. Palefsky JM. Human Papillomavirus-Related Disease in Men: Not Just a Women's Issue. *J Adolesc Heal.* 2010;46(4 SUPPL.).
  152. Ferris DG, Waller JL, Miller J, et al. Variables Associated With Human Papillomavirus (HPV) Vaccine Acceptance by Men. *J Am Board Fam Med.* 2009;22(1):34-42. doi:10.3122/jabfm.2009.01.080008.
  153. *FactSheet - Human Papillomavirus (HPV) Vaccines for Australians: Information for Immunisation Providers.*; 2016.
  154. American Cancer Society. American Cancer Society Recommendations for Human Papilloma Virus (HPV) Vaccine Use. 2016.  
<http://www.cancer.org/cancer/cancercauses/othercarcinogens/infectiousagents/hpv/acs-recommendations-for-hpv-vaccine-use>.
  155. Saslow D, Andrews KS, Manassaram-Baptiste D, et al. Human papillomavirus vaccination guideline update: American Cancer Society guideline endorsement. *CA Cancer J Clin.* 2016.
  156. McKie R. Give HPV Vaccine to Boys to Protect against Cancer, Experts Say. *theGuardian.* 2016. <https://www.theguardian.com/science/2016/jul/09/vaccine-boys-cancer-men-hpv>.
  157. Yang R, Murillo FM, Lin KY, et al. Human papillomavirus type-16 virus-like particles activate complementary defense responses in key dendritic cell subpopulations. *J Immunol.* 2004;173(4):2624-2631.  
[http://www.ncbi.nlm.nih.gov/entrez/query.fcgi?cmd=Retrieve&db=PubMed&dopt=Citation&list\\_uids=15294979%5Cnhttp://www.jimmunol.org/cgi/reprint/173/4/2624.pdf](http://www.ncbi.nlm.nih.gov/entrez/query.fcgi?cmd=Retrieve&db=PubMed&dopt=Citation&list_uids=15294979%5Cnhttp://www.jimmunol.org/cgi/reprint/173/4/2624.pdf).
  158. Yan M, Peng J, Jabbar IA, et al. Activation of dendritic cells by human papillomavirus-like particles through TLR4 and NF-kappaB-mediated signalling, moderated by TGF-beta. *Immunol Cell Biol.* 2005;83(1):83-91. doi:10.1111/j.1440-1711.2004.01291.x.
  159. Olsson SE, Villa LL, Costa RLR, et al. Induction of immune memory following administration of a prophylactic quadrivalent human papillomavirus (HPV) types 6/11/16/18 L1 virus-like particle (VLP) vaccine. *Vaccine.* 2007;25(26):4931-4939.
  160. Giannini SL, Hanon E, Moris P, et al. Enhanced humoral and memory B cellular immunity using HPV16/18 L1 VLP vaccine formulated with the MPL/aluminium salt combination (AS04) compared to aluminium salt only. *Vaccine.* 2006;24(33-34):5937-5949.
  161. Breitburd F, Kirnbauer R, Hubbert NL, et al. Immunization with viruslike particles from cottontail rabbit papillomavirus (CRPV) can protect against experimental CRPV infection. *J Virol.* 1995;69(6):3959-3963.

<http://www.scopus.com/inward/record.url?eid=2-s2.0-0029025444&partnerID=tZOtx3y1>.

162. Ghim S, Newsome J, Bell J, Sundberg JP, Schlegel R, Jenson AB. Spontaneously regressing oral papillomas induce systemic antibodies that neutralize canine oral papillomavirus. *Exp Mol Pathol*. 2000;68(3):147-151. doi:10.1006/exmp.1999.2298.
163. Keam SJ, Harper DM. Human Papillomavirus types 16 and 18 vaccine (recombinant, AS04 adjuvanted, adsorbed)[Cervarix]. *Drugs*. 2008;68(3):359-372.
164. Siddiqui MA, Perry CM. Human papillomavirus quadrivalent (types 6, 11, 16, 18) recombinant vaccine (Gardasil). *Drugs*. 2006;66(9):1263-1271.
165. Ronco G, Dillner J, Elfström KM, et al. Efficacy of HPV-based screening for prevention of invasive cervical cancer: follow-up of four European randomised controlled trials. *Lancet*. 2014;383(9916):524-532. doi:10.1016/S0140-6736(13)62218-7.
166. Giuliano AR, Palefsky JM, Goldstone S, et al. Efficacy of quadrivalent HPV vaccine against HPV Infection and disease in males. *N Engl J Med*. 2011;364(5):401-411. <http://www.pubmedcentral.nih.gov/articlerender.fcgi?artid=3495065&tool=pmcentrez&rendertype=abstract>.
167. Palefsky JM, Giuliano AR, Goldstone S, et al. HPV vaccine against anal HPV infection and anal intraepithelial neoplasia. *N Engl J Med*. 2011;365(17):1576-1585. [http://www.ncbi.nlm.nih.gov/entrez/query.fcgi?cmd=Retrieve&db=PubMed&dopt=Citation&list\\_uids=22029979](http://www.ncbi.nlm.nih.gov/entrez/query.fcgi?cmd=Retrieve&db=PubMed&dopt=Citation&list_uids=22029979).
168. The FUTURE II Study Group. Quadrivalent Vaccine against Human Papillomavirus to Prevent High-Grade Cervical Lesions. *N Engl J Med*. 2007;356(19):1915-1927. doi:10.1056/NEJMoa061741.
169. Villa LL, Ault K a., Giuliano AR, et al. Immunologic responses following administration of a vaccine targeting human papillomavirus Types 6, 11, 16, and 18. *Vaccine*. 2006;24(27-28):5571-5583. doi:10.1016/j.vaccine.2006.04.068.
170. Einstein MH, Baron M, Levin MJ, et al. Comparison of the immunogenicity and safety of Cervarix™ and Gardasil® human papillomavirus (HPV) cervical cancer vaccines in healthy women aged 18–45 years. *Hum Vaccin*. 2009;5(10):705-719. doi:10.4161/hv.5.10.9518.
171. Didierlaurent a. M, Morel S, Lockman L, et al. AS04, an Aluminum Salt- and TLR4 Agonist-Based Adjuvant System, Induces a Transient Localized Innate Immune Response Leading to Enhanced Adaptive Immunity. *J Immunol*. 2009;183(10):6186-6197. doi:10.4049/jimmunol.0901474.
172. Smith JF, Brownlow M, Brown M, et al. Antibodies from Women Immunized with Gardasil® Cross-Neutralize HPV 45 Pseudovirions. *Hum Vaccin*. 2014;3(4):109-115. <http://www.tandfonline.com/doi/abs/10.4161/hv.3.4.4058#>.
173. Kavanagh K, Pollock KGJ, Potts A, et al. Introduction and sustained high coverage of the HPV bivalent vaccine leads to a reduction in prevalence of HPV 16/18 and closely related HPV types. *Br J Cancer*. 2014;110(11):2804-2811. <http://www.scopus.com/inward/record.url?eid=2-s2.0-84901636857&partnerID=tZOtx3y1>.
174. Hong K, Greer CE, Ketter N, Van Nest G, Paliard X. Isolation and characterization of human papillomavirus type 6-specific T cells infiltrating genital warts. *J Virol*. 1997;71(9):6427-6432.

175. Kondo K, Ochi H, Matsumoto T, Yoshikawa H, Kanda T. Modification of human papillomavirus-like particle vaccine by insertion of the cross-reactive L2-epitopes. *J Med Virol*. 2008;80(5):841-846. doi:10.1002/jmv.
176. Greenstone HL, Nieland JD, de Visser KE, et al. Chimeric papillomavirus virus-like particles elicit antitumor immunity against the E7 oncoprotein in an HPV16 tumor model. *Proc Natl Acad Sci U S A*. 1998;95(4):1800-1805. doi:10.1073/pnas.95.4.1800.
177. U.S. Clinical Trials. V503. 2015.
178. Tsu VD, Pollack a E. Preventing cervical cancer in low-resource settings: how far have we come and what does the future hold? *Int J Gynaecol Obstet*. 2005;89 Suppl 2:S55-S59. doi:10.1016/j.ijgo.2005.01.011.
179. Franco EL, Cuzick J, Hildesheim A, de Sanjos?? S. Chapter 20: Issues in planning cervical cancer screening in the era of HPV vaccination. *Vaccine*. 2006;24(SUPPL. 3).
180. *Human Papillomavirus Vaccine Supply & Demand Update.*; 2015.
181. Leary NW, Seattle W. Current and Future HPV Vaccines : Promise and Challenges. 2006.
182. Maclean J, Rybicki EP, Williamson A-L. Vaccination strategies for the prevention of cervical cancer. *Expert Rev Anticancer Ther*. 2005;5:97-107. doi:10.1586/14737140.5.1.97.
183. Jochmus-Kudielka I, Schneider A, Braun R, et al. Antibodies against the human papillomavirus type 16 early proteins in human sera: correlation of anti-E7 reactivity with cervical cancer. *J Natl Cancer Inst*. 1989;81(22):1698-1704. <http://www.ncbi.nlm.nih.gov/pubmed/2553991>.
184. Höpfl R, Heim K, Christensen N, et al. Spontaneous regression of CIN and delayed-type hypersensitivity to HPV-16 oncoprotein E7. *Lancet*. 2000;356(9246):1985-1986. doi:10.1016/S0140-6736(00)03315-8.
185. Cheng S, Murrant DST, Broker TR, Chow LT. Differentiation-dependent up-regulation of the human papillomavirus E7 gene reactivates cellular DNA replication in suprabasal differentiated keratinocytes. 1995:2335-2349.
186. Morrison M a., Morreale RJ, Akunuru S, Kofron M, Zheng Y, Wells SI. Targeting the Human Papillomavirus E6 and E7 Oncogenes through Expression of the Bovine Papillomavirus Type 1 E2 Protein Stimulates Cellular Motility. *J Virol*. 2011;85(20):10487-10498. doi:10.1128/JVI.05126-11.
187. Stanley M. Chapter 17: Genital human papillomavirus infections--current and prospective therapies. *J Natl Cancer Inst Monogr*. 2003;6(31):117-124.
188. Venuti A, Paolini F, Nasir L, et al. Papillomavirus E5: the smallest oncoprotein with many functions. *Mol Cancer*. 2011;10:140. doi:10.1186/1476-4598-10-140.
189. Tang D, Devit M, Johnston S a. Genetic immunization is a simple method for eliciting an immune response. *Nature*. 1992;356:152-154.
190. Kutzler M a., Weiner DB. DNA vaccines: ready for prime time? *Nat Rev Genet*. 2008;9(10):776-788. doi:10.1038/nrg2432.
191. Ulmer JB, Donnelly JJ, Parker SE, et al. Heterologous protection against influenza by injection of DNA encoding a viral protein. *Science*. 1993;259(5102):1745-1749. doi:10.1126/science.8456302.

192. Shedlock DJ, Weiner DB. DNA vaccination: antigen presentation and the induction of immunity. *J Leukoc Biol.* 2000;68(6):793-806.
193. Wilson KD, Lall R, Hope MJ, Cullis PR, Tam YK. The combination of stabilized plasmid lipid particles and lipid nanoparticle encapsulated CpG containing oligodeoxynucleotides as a systemic genetic vaccine. 2009;(November 2008):14-25. doi:10.1002/jgm.
194. Edelman R. An update on vaccine adjuvants in clinical trial. *AIDS Res Hum Retroviruses.* 1992;8(8):1409-1411.
195. Davies L. Human papillomavirus vaccines— a review of advances in the development of HPV vaccines. *HIV Treat Bull.* 2005;6(7).
196. Ling M, Kanayama M, Roden R, Wu TC. Preventive and therapeutic vaccines for human papillomavirus-associated cervical cancers. *J Biomed Sci.* 2000;7(5):341-356.
197. Peng S, Trimble C, Ji H, et al. Characterization of HPV-16 E6 DNA vaccines employing intracellular targeting and intercellular spreading strategies. *J Biomed Sci.* 2005;12(5):689-700.
198. Kim SJ, Lee C, Lee SY, et al. Enhanced immunogenicity of human papillomavirus 16 L1 genetic vaccines fused to an ER-targeting secretory signal peptide and RANTES. *Gene Ther.* 2003;10(15):1268-1273. <http://www.ncbi.nlm.nih.gov/pubmed/12858192>.
199. Tobery TW, Smith JF, Kuklin N, et al. Effect of vaccine delivery system on the induction of HPV16L1-specific humoral and cell-mediated immune responses in immunized rhesus macaques. *Vaccine.* 2003;21(13-14):1539-1547.
200. Kowalczyk DW, Wlazlo a P, Shane S, Ertl HC. Vaccine regimen for prevention of sexually transmitted infections with human papillomavirus type 16. *Vaccine.* 2001;19(25-26):3583-3590. <http://www.ncbi.nlm.nih.gov/pubmed/11348726>.
201. Johns Hopkins Medicine. *Cervical Cancer SPORE Program Description.* Baltimore, Md.: Johns Hopkins University.; 2004.
202. Locher CP, Sykes KF, Blackburn DJ, Johnston SA. Immune responses in baboons vaccinated with HIV-2 genetic expression libraries. *JMedPrimatol.* 2002;31(0047-2565 (Print)):323-329. doi:doi:10.1034/j.1600-0684.2002.01035.x.
203. Fuller DH, Loudon P, Schmaljohn C. Preclinical and clinical progress of particle-mediated DNA vaccines for infectious diseases. *Methods.* 2006;40(1):86-97. doi:10.1016/j.ymeth.2006.05.022.
204. Tiwari PM, Vig K, Dennis V a., Singh SR. Functionalized Gold Nanoparticles and Their Biomedical Applications. *Nanomaterials.* 2011;1(1):31-63. doi:10.3390/nano1010031.
205. Lévy R, Shaheen U, Cesbron Y, Sée V. Gold nanoparticles delivery in mammalian live cells: a critical review. *Nano Rev.* 2010;1:1-18. doi:10.3402/nano.v1i0.4889.
206. Lewinski N, Colvin V, Drezek R. Cytotoxicity of nanoparticles. *Small.* 2008;4(1):26-49. doi:10.1002/sml.200700595.
207. Xu L, Liu Y, Chen Z, et al. Surface-engineered gold nanorods: promising DNA vaccine adjuvant for HIV-1 treatment. *Nano Lett.* 2012;12(4):2003-2012. doi:10.1021/nl300027p.
208. Ge C, Du J, Zhao L, et al. Binding of blood proteins to carbon nanotubes reduces

- cytotoxicity. *Proc Natl Acad Sci*. 2011;108(41):16968-16973.  
<http://www.pnas.org/content/108/41/16968>.
209. Rea JC, Gibly RF, Barron AE, Shea LD. Self-assembling peptide-lipoplexes for substrate-mediated gene delivery. *Acta Biomater*. 2009;5(3):903-912.
  210. Chen C-C, Lin Y-P, Wang C-W, et al. DNA-gold nanorod conjugates for remote control of localized gene expression by near infrared irradiation. *J Am Chem Soc*. 2006;128(11):3709-3715. doi:10.1021/ja0570180.
  211. Huang XG, Xu JQ, Qiu C, Ren L, Liu L, Wan Y. Mucosal priming with PEI/DNA complex and systemic boosting with recombinant TianTan vaccinia stimulate vigorous mucosal and systemic immune responses. *Vaccine*. 2007;25:2620-2629.
  212. Stone JW, Thornburg NJ, Blum DL, Kuhn SJ, Wright DW, Crowe JE. Gold nanorod vaccine for respiratory syncytial virus. *Nanotechnology*. 2013;24(29):295102.  
<http://www.pubmedcentral.nih.gov/articlerender.fcgi?artid=3754908&tool=pmcentrez&rendertype=abstract>.
  213. Holmgren J, Czerkinsky C. Mucosal immunity and vaccines. *Nat Med*. 2005;11(4 Suppl):S45-53. doi:10.1038/nm1213.
  214. Sonavane G, Tomoda K, Makino K. Biodistribution of colloidal gold nanoparticles after intravenous administration: effect of particle size. *Colloids Surf B Biointerfaces*. 2008;66(2):274-280. doi:10.1016/j.colsurfb.2008.07.004.
  215. Eustis S, el-Sayed M a. Why gold nanoparticles are more precious than pretty gold: noble metal surface plasmon resonance and its enhancement of the radiative and nonradiative properties of nanocrystals of different shapes. *Chem Soc Rev*. 2006;35(3):209-217. doi:10.1039/b514191e.
  216. Rosi NL, Giljohann D a, Thaxton CS, Lytton-Jean AKR, Han MS, Mirkin C a. Oligonucleotide-modified gold nanoparticles for intracellular gene regulation. *Science*. 2006;312(5776):1027-1030. doi:10.1126/science.1125559.
  217. Shenhar R, Rotello VM. Nanoparticles: scaffolds and building blocks. *Acc Chem Res*. 2003;36(7):549-561. <http://www.ncbi.nlm.nih.gov/pubmed/12859216>.
  218. Choi CHJ, Hao L, Narayan SP, Auyeung E, Mirkin C a. Mechanism for the endocytosis of spherical nucleic acid nanoparticle conjugates. *Proc Natl Acad Sci U S A*. 2013;110(19):7625-7630. doi:10.1073/pnas.1305804110.
  219. Parak WJ. Complex Colloidal Assembly. *Science (80- )*. 2011;334(DECEMBER):1359-1360.
  220. Huang X, Neretina S, El-Sayed M a. Gold Nanorods: From Synthesis and Properties to Biological and Biomedical Applications. *Adv Mater*. 2009;21(48):4880-4910. doi:10.1002/adma.200802789.
  221. Chen PC, Mwakwari SC, Oyelere AK. Gold nanoparticles : From nanomedicine to nanosensing. 2008:45-66.
  222. Murphy CJ, Sau TK, Gole AM, et al. Anisotropic Metal Nanoparticles : Synthesis , Assembly , and Optical Applications. *J Physical Chem*. 2005;109:13857-13870.
  223. Jana NR, Gearheart L, Murphy CJ. Seed-Mediated Growth Approach for Shape-Controlled Synthesis of Spheroidal and Rod-like Gold Nanoparticles Using a Surfactant Template. *Adv Mater*. 2001;13(18):1389-1393. doi:10.1002/1521-4095(200109)13:18<1389::AID-ADMA1389>3.0.CO;2-F.

224. Nikoobakht B, El-sayed MA. Preparation and Growth Mechanism of Gold Nanorods ( NRs ) Using Seed-Mediated Growth Method. 2003;(16):1957-1962.
225. Rayavarapu RG, Petersen W, Ungureanu C, Post JN, van Leeuwen TG, Manohar S. Synthesis and bioconjugation of gold nanoparticles as potential molecular probes for light-based imaging techniques. *Int J Biomed Imaging*. 2007;2007:29817. doi:10.1155/2007/29817.
226. Huang X, El-sayed IH, El-sayed MA. Gold nanoparticles : interesting optical properties and recent applications in cancer diagnostics and therapy. *Nanomedicine*. 2007;2(5):681-693.
227. Niidome Y, Nakamura Y, Honda K, et al. Characterization of silver ions absorbed on gold nanorods: surface analysis by using surface-assisted laser desorption/ionization time-of-flight mass spectrometry. *Chem Commun (Camb)*. 2009;(13):1754-1756. doi:10.1039/b821402f.
228. Link S, El-sayed MA. Size and Temperature Dependence of the Plasmon Absorption of Colloidal Gold Nanoparticles. *J Phys Chem B*. 1999;103:4212-4217.
229. Link S, Wang ZL, El-sayed MA. How Does a Gold Nanorod Melt? *J Phys Chem*. 2000;104(33):0-3.
230. Jain PK, Lee KS, El-sayed IH, El-sayed MA. Calculated Absorption and Scattering Properties of Gold Nanoparticles of Different Size , Shape , and Composition : Applications in Biological Imaging and Biomedicine. 2006:7238-7248.
231. Nikoobakht B, El-sayed M a. Evidence for Bilayer Assembly of Cationic Surfactants on the Surface of Gold Nanorods Evidence for Bilayer Assembly of Cationic Surfactants on the Surface of Gold Nanorods. *Assembly*. 2001;(18):6368-6374. doi:10.1021/la010530o.
232. Smith DK, Miller NR, Korgel B a. Iodide in CTAB Prevents Gold Nanorod Formation. *Langmuir*. 2009;25(16):9518-9524. doi:10.1021/la900757s.
233. Sun Y, Xia Y. Shape-controlled synthesis of gold and silver nanoparticles. *Science*. 2002;298(5601):2176-2179. doi:10.1126/science.1077229.
234. Mie G. Beiträge zur Optik trüber Medien, speziell kolloidaler Metallösun. *Ann Phys*. 1908;330(3):377-445.
235. Kreibig U, Vollmer M. Optical Properties of Metal Clusters. *Springer Ser Mater Sci*. 1995;25:117.
236. Pavassiliou GC. Optical properties of small inorganic and organic metal particles. *Prog Solid-State Chem*. 1980;12:185-271.
237. Ng LN. Chapter 3: Manipulation of particles on optical waveguides. 2000.
238. Lopatynskiy AM, Lopatynska OG, Guo LJ, Chegel VI. Localized Surface Plasmon Resonance Biosensor — Part I : Theoretical Study of Sensitivity — Extended Mie Approach. *IEEE Sens J*. 2011;11(2):361-369.
239. Patching SG. Surface plasmon resonance spectroscopy for characterisation of membrane protein-ligand interactions and its potential for drug discovery. *Biochim Biophys Acta*. 2014;1838(1 Pt A):43-55. doi:10.1016/j.bbamem.2013.04.028.
240. Pedersen DB, Duncan EJ. *Surface Plasmon Resonance Spectroscopy of Gold Nanoparticle- Coated Substrates.*; 2005. doi:TR2005-09.

241. Smitha SL, Gopchandran KG, Ravindran TR, Prasad VS. Gold nanorods with finely tunable longitudinal surface plasmon resonance as SERS substrates. *Nanotechnology*. 2011;22(26):265705. doi:10.1088/0957-4484/22/26/265705.
242. Smith DK, Korgel BA. The importance of the CTAB surfactant on the colloidal seed-mediated synthesis of gold nanorods. *Langmuir*. 2008;24(3):644-649. doi:10.1021/la703625a.
243. Stone J, Jackson S, Wright D. Biological applications of gold nanorods. *Wiley Interdiscip Rev Nanomed Nanobiotechnol*. 2011;3(1):100-109. doi:10.1002/wnan.120.
244. Oldenburg S., Averitt R., Westcott S., Halas N. Nanoengineering of optical resonances. *Chem Phys Lett*. 1998;288(2-4):243-247. doi:10.1016/S0009-2614(98)00277-2.
245. Gole A, Murphy CJ. Polyelectrolyte-coated gold nanorods: Synthesis, characterization and immobilization. *Chem Mater*. 2005;17(c):1325-1330. doi:10.1021/cm048297d.
246. Murphy CJ, Gole AM, Hunyadi SE, et al. Chemical sensing and imaging with metallic nanorods. *Chem Commun (Camb)*. 2008;(5):544-557. doi:10.1039/b711069c.
247. Thomas KG, Barazzouk S, Ipe BI, Joseph STS, Kamat P V. Uniaxial plasmon coupling through longitudinal self-assembly of gold nanorods. *J Phys Chem B*. 2004;108(35):13066-13068.
248. Jain PK, Eustis S, El-Sayed MA. Plasmon coupling in nanorod assemblies: Optical absorption, discrete dipole approximation simulation, and exciton-coupling model. *J Phys Chem B*. 2006;110(37):18243-18253. doi:10.1021/jp063879z.
249. Gluodenis M, Foss CA. The Effect of Mutual Orientation on the Spectra of Metal Nanoparticle Rod-Rod and Rod-Sphere Pairs. *J Phys Chem B*. 2002;106:9484.
250. Zhang Y, Xu D, Li W, Yu J, Chen Y. Effect of Size, Shape, and Surface Modification on Cytotoxicity of Gold Nanoparticles to Human HEp-2 and Canine MDCK Cells. *J Nanomater*. 2012;2012:1-7. doi:10.1155/2012/375496.
251. Leung A, Trau M, Nielsen LK. Assembly of multilayer PSS/PAH membrane on coherent alginate/PLO microcapsule for long-term graft transplantation. *J Biomed Mater Res A*. 2009;88(1):226-237. doi:10.1002/jbm.a.31891.
252. Yoffe AD. Low-dimensional systems: Quantum size effects and electronic properties of semiconductor microcrystallites (zero- dimensional systems) and some quasi-two-dimensional systems. *Adv Phys*. 2002;51(2):799-890. doi:10.1080/00018730110117451.
253. Suryajaya, Nabok A, Davis F, Hassan A, Higson SPJ, Evans-Freeman J. Optical and AFM study of electrostatically assembled films of CdS and ZnS colloid nanoparticles. *Appl Surf Sci*. 2008;254(15):4891-4898. doi:10.1016/j.apsusc.2008.01.134.
254. Ling T, Wei Q, Wei A, Cheng J-X. Gold Nanorods as Contrast Agents for Biological Imaging : Optical Properties , Surface Conjugation and Photothermal Effects. *Photochem Photobiol*. 2009;85:21-32.
255. Huang X, El-sayed IH, Qian W, El-sayed MA. Cancer Cell Imaging and Photothermal Therapy in the Near-Infrared Region by Using Gold Nanorods. 2006;(2):2115-2120.
256. Huang X, Jain PK, El-Sayed IH, El-Sayed M a. Plasmonic photothermal therapy (PPTT)

- using gold nanoparticles. *Lasers Med Sci.* 2008;23(3):217-228. doi:10.1007/s10103-007-0470-x.
257. Sapsford KE, Berti L, Medintz IL. Materials for fluorescence resonance energy transfer analysis: beyond traditional donor-acceptor combinations. *Angew Chem Int Ed Engl.* 2006;45(28):4562-4589. doi:10.1002/anie.200503873.
  258. Yang X, Stein EW, Ashkenazi S, Wang L V. Nanoparticles for photoacoustic imaging. 2009;(2). doi:10.1002/wnan.042.
  259. Wang Y, Xie X, Wang X, et al. Photoacoustic Tomography of a Nanoshell Contrast Agent in the in Vivo Rat Brain. *Nano Lett.* 2004;4(9):1689-1692. doi:10.1021/nl049126a.
  260. Katz E, Willner I. Integrated nanoparticle-biomolecule hybrid systems: synthesis, properties, and applications. *Angew Chem Int Ed Engl.* 2004;43(45):6042-6108. doi:10.1002/anie.200400651.
  261. Weissleder R, Mahmood U. Molecular Imaging. *Radiology.* 2001;219(2):316-333. doi:10.1148/radiology.219.2.r01ma19316.
  262. Oheim M, Michael DJ, Geisbauer M, Madsen D, Chow RH. Principles of two-photon excitation fluorescence microscopy and other nonlinear imaging approaches. *Adv Drug Deliv Rev.* 2006;58(7):788-808. doi:10.1016/j.addr.2006.07.005.
  263. Manuscript A, Oval M, Gold S, Based N, Sensitive H, Assay TS. Multifunctional Oval Shape Gold Nanoparticle Based Selective Detection of Breast Cancer Cells Using Simple Colorimetric and Highly Sensitive Two-Photon Scattering Assay. *ACS Nano.* 2010;4(3):1739-1749. doi:10.1021/nn901742q.Multifunctional.
  264. Durr NJ, Larson T, Smith DK, Korgel BA, Ben-yakar A. Two-Photon Luminescence Imaging of Cancer Cells using Molecularly Targeted Gold nanorods. *Nano Lett.* 2007;7(4):941-945. doi:10.1021/nl062962v.Two-Photon.
  265. Li J-L, Gu M. Surface plasmonic gold nanorods for enhanced two-photon microscopic imaging and apoptosis induction of cancer cells. *Biomaterials.* 2010;31(36):9492-9498. doi:10.1016/j.biomaterials.2010.08.068.
  266. Wang H, Huff TB, Zweifel DA, et al. In vitro and in vivo two-photon luminescence imaging of single gold nanorods. 2005;2005.
  267. Rubart M. Two-photon microscopy of cells and tissue. *Circ Res.* 2004;95(12):1154-1166. doi:10.1161/01.RES.0000150593.30324.42.
  268. Arnida, Janát-Amsbury MM, Ray a, Peterson CM, Ghandehari H. Geometry and surface characteristics of gold nanoparticles influence their biodistribution and uptake by macrophages. *Eur J Pharm Biopharm.* 2011;77(3):417-423. doi:10.1016/j.ejpb.2010.11.010.
  269. Ghosh P, Han G, De M, Kim CK, Rotello VM. Gold nanoparticles in delivery applications. *Adv Drug Deliv Rev.* 2008;60(11):1307-1315. doi:10.1016/j.addr.2008.03.016.
  270. Mahapatro A, Singh DK. Biodegradable Nanoparticles are Excellent Vehicle for Site Directed in-vivo Delivery of Drugs and Vaccines. *J Nanobiotechnology.* 2011;9(1):55. doi:10.1186/1477-3155-9-55.
  271. Horisberger M, Clerc M-F. Labelling of colloidal gold with protein A. *Histochemistry.* 1985;82:219-223.



272. Hermanson GT. *Bioconjugate Techniques*. 2nd Editio. New York; 2008.
273. Bastús NG, Sánchez-Tilló E, Pujals S, et al. Homogeneous conjugation of peptides onto gold nanoparticles enhances macrophage response. *ACS Nano*. 2009;3(6):1335-1344. <http://www.ncbi.nlm.nih.gov/pubmed/19489561>.
274. Higuchi M, Ushiba K, Kawaguchi M. Structural control of peptide-coated gold nanoparticle assemblies by the conformational transition of surface peptides. *J Colloid Interface Sci*. 2007;308(2):356-363.
275. Javier DJ, Castellanos-Gonzalez A, Weigum SE, White a C, Richards-Kortum R. Oligonucleotide-gold nanoparticle networks for detection of *Cryptosporidium parvum* heat shock protein 70 mRNA. *J Clin Microbiol*. 2009;47(12):4060-4066. doi:10.1128/JCM.00807-09.
276. Dobrovolskaia M a, Patri AK, Zheng J, et al. Interaction of colloidal gold nanoparticles with human blood: effects on particle size and analysis of plasma protein binding profiles. *Nanomedicine*. 2009;5(2):106-117. doi:10.1016/j.nano.2008.08.001.
277. Niidome T, Yamagata M, Okamoto Y, et al. PEG-modified gold nanorods with a stealth character for in vivo applications. *J Control Release*. 2006;114(3):343-347. doi:10.1016/j.jconrel.2006.06.017.
278. Akiyama Y, Mori T, Katayama Y, Niidome T. The effects of PEG grafting level and injection dose on gold nanorod biodistribution in the tumor-bearing mice. *J Control Release*. 2009;139(1):81-84. doi:10.1016/j.jconrel.2009.06.006.
279. Paciotti GF, Myer L, Weinreich D, et al. Colloidal gold: a novel nanoparticle vector for tumor directed drug delivery. *Drug Deliv*. 2004;11(3):169-183. doi:10.1080/10717540490433895.
280. Fan Z, Yang X, Li Y, et al. Deciphering an underlying mechanism of differential cellular effects of nanoparticles: An example of Bach-1 dependent induction of HO-1 expression by gold nanorod. *Biointerphases*. 2012;7(1-4):1-8. doi:10.1007/s13758-011-0010-x.
281. Gregory AE, Titball R, Williamson D. Vaccine delivery using nanoparticles. *Front Cell Infect Microbiol*. 2013;3(March):13. doi:10.3389/fcimb.2013.00013.
282. Regnstrom K, Ragnarsson EG, Koping-Hoggard M, Torstensson E, Nyblom H, Artursson P. PEI - a potent, but not harmless, mucosal immuno-stimulator of mixed T-helper cell response and FasL-mediated cell death in mice. *Gene Ther*. 2003;10(18):1575-1583. doi:10.1038/sj.gt.3302054.
283. Densmore CL, Orson FM, Xu B, et al. Aerosol delivery of robust polyethyleneimine-DNA complexes for gene therapy and genetic immunization. *Mol Ther*. 2000;1(2):180-188. doi:10.1006/mthe.1999.0021.
284. Regnström K, Ragnarsson E., Rydell N, Sjöholm I, Artursson P. Tetanus antigen modulates the gene expression profile of aluminum phosphate adjuvant in spleen lymphocytes in vivo. *Pharmacogenomics J*. 2002;2(1):57-64.
285. Tiyaboonchai W. Chitosan Nanoparticles : A Promising System for Drug Delivery. *Naresuan Univ J*. 2003;11(3):51-66.
286. Lashuel H a, Hartley D, Petre BM, Walz T, Lansbury PT. Neurodegenerative disease: amyloid pores from pathogenic mutations. *Nature*. 2002;418(6895):291.
287. Bolhassani A, Javanad S, Saleh T, Hashemi M, Aghasadeghi MR, Sadat SM.

- Polymeric nanoparticles Potent vectors for vaccine delivery targeting cancer and infectious diseases. *Hum Vaccines Immunother.* 2014;10(2):321-323. doi:10.4161/hv.26796.
288. Lycke N. Targeted vaccine adjuvants based on modified cholera toxin. *Curr Mol Med.* 2005;5(6):591-597. [http://www.ncbi.nlm.nih.gov/entrez/query.fcgi?cmd=Retrieve&db=PubMed&dopt=Citation&list\\_uids=16178769](http://www.ncbi.nlm.nih.gov/entrez/query.fcgi?cmd=Retrieve&db=PubMed&dopt=Citation&list_uids=16178769).
289. Holmgren J, Adamsson J, Anjuère F, et al. Mucosal adjuvants and anti-infection and anti-immunopathology vaccines based on cholera toxin, cholera toxin B subunit and CpG DNA. *Immunol Lett.* 2005;97(2 SPEC. ISS.):181-188. doi:10.1016/j.imlet.2004.11.009.
290. Hur J, Lee JH. Enhancement of Immune Responses by an Attenuated Salmonella enterica Serovar Typhimurium Strain Secreting an Escherichia coli Heat-Labile Enterotoxin B Subunit Protein as an Adjuvant for a Live Salmonella Vaccine Candidate. *Clin Vaccine Immunol.* 2011;18(2):203-209.
291. Wang X, Liu J, Wu X, et al. Oral immunisation of mice with a recombinant rabies virus vaccine incorporating the heat-labile enterotoxin B subunit of Escherichia coli in an attenuated Salmonella strain. *Res Vet Sci.* 2012;93(2):675-681. doi:10.1016/j.rvsc.2011.09.015.
292. Fensterle J, Bergmann B, Yone CLRP, et al. Cancer immunotherapy based on recombinant Salmonella enterica serovar Typhimurium aroA strains secreting prostate-specific antigen and cholera toxin subunit B. *Cancer Gene Ther.* 2008;15(2):85-93. doi:10.1038/sj.cgt.7701109.
293. Sadeghi H, Bregenholt S, Wegmann D, Petersen JS, Holmgren J, Lebens M. Genetic fusion of human insulin B-chain to the B-subunit of cholera toxin enhances in vitro antigen presentation and induction of bystander suppression in vivo. *Immunology.* 2002;106(2):237-245. doi:10.1046/j.1365-2567.2002.01413.x.
294. Yuki Y, Byun Y, Fujita M, et al. Production of a recombinant hybrid molecule of cholera toxin-B-subunit and proteolipid-protein-peptide for the treatment of experimental encephalomyelitis. *Biotechnol Bioeng.* 2001;74(1):62-69. <http://www.ncbi.nlm.nih.gov/pubmed/11353411>.
295. Arakawa T, Yu J, Chong DK, Hough J, Engen PC, Langridge WH. A plant-based cholera toxin B subunit-insulin fusion protein protects against the development of autoimmune diabetes. *Nat Biotechnol.* 1998;16(10):934-938. doi:10.1038/nbt1098-934.
296. Gole A, Murphy CJ. Seed-Mediated Synthesis of Gold Nanorods : Role of the Size and Nature of the Seed. 2004;(21):3633-3640.
297. Zhang Y, Yu J, Birch DJS, Chen Y. Gold nanorods for fluorescence lifetime imaging in biology. *J Biomed Opt.* 2012;15(2):20504. doi:10.1117/1.3366646.
298. Xu D, Wang D, Yang X, Cao M, Yu J, Wang Y. Fusion of HPV L1 into Shigella surface IcsA: a new approach in developing live attenuated Shigella-HPV vaccine. *Antiviral Res.* 2014;102(October 2015):61-69. doi:10.1016/j.antiviral.2013.12.003.
299. Abdelhalim MAK, M. Mady M. Physical Properties of Different Gold Nanoparticles: Ultraviolet-Visible and Fluorescence Measurements. *J Nanomed Nanotechnol.* 2012;3(3):1-5. doi:10.4172/2157-7439.1000133.

300. Khlebtsov NG. Determination of size and concentration of gold nanoparticles from extinction spectra. *Anal Chem.* 2008;80(17):6620–6625. doi:10.1007/s00216-007-1768-z.
301. Li L, Chen Y, Lu Q, et al. Electrochemiluminescence energy transfer-promoted ultrasensitive immunoassay using near-infrared-emitting CdSeTe/CdS/ZnS quantum dots and gold nanorods. *Sci Rep.* 2013;3:1529. <http://www.pubmedcentral.nih.gov/articlerender.fcgi?artid=3607123&tool=pmcentrez&rendertype=abstract>.
302. Wang S-H, Lee C-W, Chiou A, Wei P-K. Size-dependent endocytosis of gold nanoparticles studied by three-dimensional mapping of plasmonic scattering images. *J Nanobiotechnology.* 2010;8(1):33. doi:10.1186/1477-3155-8-33.
303. Giljohann DA, Seferos DS, Patel PC, Millstone JE, Rosi NL, Mirkin CA. Oligonucleotide loading determines cellular uptake of DNA-modified gold nanoparticles. *Nano Lett.* 2007;7(12):3818-3821.
304. Yang SY, Rubner MF. Micropatterning of polymer thin films with pH-sensitive and cross-linkable hydrogen-bonded polyelectrolyte multilayers. *J Am Chem Soc.* 2002;124(10):2100-2101. doi:10.1021/ja017681y.
305. Ladam G, Schaad P, Voegel JC, et al. In Situ Determination of the Structural Properties of Initially Deposited Polyelectrolyte Multilayers. *Langmuir.* 1999;16(3):1249-1255. doi:10.1021/la990650k.
306. Lavalle P, Gergely C, Cuisinier FJG, et al. Comparison of the structure of polyelectrolyte multilayer films exhibiting a linear and an exponential growth regime: An in situ atomic force microscopy study. *Macromolecules.* 2002;35(11):4458-4465. doi:10.1021/ma0119833.
307. Mendelsohn JD, Yang SY, Hiller J a., Hochbaum AI, Rubner MF. Rational design of cytophilic and cytophobic polyelectrolyte multilayer thin films. *Biomacromolecules.* 2003;4(1):96-106. doi:10.1021/bm0256101.
308. Buron CC, Filiâtre C, Membrey F, Perrot H, Foissy a. Mass and charge balance in self-assembled multilayer films on gold. Measurements with optical reflectometry and quartz crystal microbalance. *J Colloid Interface Sci.* 2006;296(2):409-418. doi:10.1016/j.jcis.2005.09.034.
309. Burke SE, Barrett CJ. pH-responsive properties of multilayered poly(L-lysine)/hyaluronic acid surfaces. *Biomacromolecules.* 2003;4(6):1773-1783. doi:10.1021/bm034184w.
310. Ren K, Wang Y, Ji J, Lin Q, Shen J. Construction and deconstruction of PLL/DNA multilayered films for DNA delivery: Effect of ionic strength. *Colloids Surfaces B Biointerfaces.* 2005;46(2):63-69. doi:10.1016/j.colsurfb.2005.09.004.
311. Westwood M, Roberts D, Parker R. Enzymatic degradation of poly-L-lysine-polygalacturonic acid multilayers. *Carbohydr Polym.* 2011;84(3):960-969. doi:10.1016/j.carbpol.2010.12.051.
312. Mironava T, Hadjiargyrou M, Simon M, Jurukovski V, Rafailovich MH. Gold nanoparticles cellular toxicity and recovery: effect of size, concentration and exposure time. *Nanotoxicology.* 2010;4(1):120-137. doi:10.3109/17435390903471463.
313. Basu S, Ghosh SK, Kundu S, et al. Biomolecule induced nanoparticle aggregation :

- Effect of particle size on interparticle coupling. 2007;313:724-734.  
doi:10.1016/j.jcis.2007.04.069.
314. Conner SD, Schmid SL. Regulated portals of entry into the cell. *Nature*. 2003;422(6927):37-44. doi:10.1038/nature01451.
  315. Kneipp J, Kneipp H, McLaughlin M, Brown D, Kneipp K. In vivo molecular probing of cellular compartments with gold nanoparticles and nanoaggregates. *Nano Lett*. 2006;6(10):2225-2231. doi:10.1021/nl061517x.
  316. Shukla R, Bansal V, Chaudhary M, Basu A, Bhonde RR, Sastry M. Biocompatibility of gold nanoparticles and their endocytotic fate inside the cellular compartment: a microscopic overview. *Langmuir Acs J Surfaces Colloids*. 2005;21(23):10644-10654. <http://www.ncbi.nlm.nih.gov/pubmed/16262332>.
  317. Chithrani BD, Ghazani A a, Chan WCW. Determining the size and shape dependence of gold nanoparticle uptake into mammalian cells. *Nano Lett*. 2006;6(4):662-668. doi:10.1021/nl052396o.
  318. Rejman J, Oberle V, Zuhorn IS, Hoekstra D. Size-dependent internalization of particles via the pathways of clathrin- and caveolae-mediated endocytosis. *Biochem J*. 2004;377(Pt 1):159-169. doi:10.1042/BJ20031253.
  319. Gao W, Ji L, Li L, et al. Bifunctional combined Au-Fe(2)O(3) nanoparticles for induction of cancer cell-specific apoptosis and real-time imaging. *Biomaterials*. 2012;33(14):3710-3718. doi:10.1016/j.biomaterials.2012.01.047.
  320. Chithrani BD, Chan WCW. Elucidating the mechanism of cellular uptake and removal of protein-coated gold nanoparticles of different sizes and shapes. *Nano Lett*. 2007;7(6):1542-1550. <http://www.ncbi.nlm.nih.gov/pubmed/17465586>.
  321. Paulo CSO, Pires das Neves R, Ferreira LS. Nanoparticles for intracellular-targeted drug delivery. *Nanotechnology*. 2011;22(49):494002. doi:10.1088/0957-4484/22/49/494002.
  322. Trischler M, Stoorvogel W, Ullrich O. Biochemical analysis of distinct Rab5- and Rab11-positive endosomes along the transferrin pathway. *J Cell Sci*. 1999;112 ( Pt 2:4773-4783. <http://www.ncbi.nlm.nih.gov/pubmed/10574724>.
  323. Eskelinen E-L, Saftig P. Autophagy: a lysosomal degradation pathway with a central role in health and disease. *Biochim Biophys Acta*. 2009;1793(4):664-673. doi:10.1016/j.bbamcr.2008.07.014.
  324. Eskelinen EL, Tanaka Y, Saftig P. At the acidic edge: Emerging functions for lysosomal membrane proteins. *Trends Cell Biol*. 2003;13(3):137-145. doi:10.1016/S0962-8924(03)00005-9.
  325. Razi M, Chan EYW, Tooze S a. Early endosomes and endosomal coatomer are required for autophagy. *J Cell Biol*. 2009;185(2):305-321. doi:10.1083/jcb.200810098.
  326. Aoyama Y, Kanamori T, Nakai T, et al. Artificial viruses and their application to gene delivery. Size-controlled gene coating with glycocluster nanoparticles. *J Am Chem Soc*. 2003;125:3455-3457. doi:10.1021/ja029608t.
  327. Osaki F, Kanamori T, Sando S, Sera T, Aoyama Y. A quantum dot conjugated sugar ball and its cellular uptake. On the size effects of endocytosis in the subviral region. *J Am Chem Soc*. 2004;126(21):6520-6521. doi:10.1021/ja048792a.
  328. Fernando LP, Kandel PK, Yu J, McNeill J, Ackroyd PC, Christensen KA. Mechanism of

- cellular uptake of highly fluorescent conjugated polymer nanoparticles. *Biomacromolecules*. 2010;11(10):2675-2682. doi:10.1021/bm1007103.
329. Cui W, Li J, Zhang Y, Rong H, Lu W, Jiang L. Effects of aggregation and the surface properties of gold nanoparticles on cytotoxicity and cell growth. *Nanomedicine*. 2012;8(1):46-53. doi:10.1016/j.nano.2011.05.005.
  330. Malugin A, Ghandehari H. Cellular uptake and toxicity of gold nanoparticles in prostate cancer cells: a comparative study of rods and spheres. *J Appl Toxicol*. 2010;30(3):212-217. doi:10.1002/jat.1486.
  331. Takahashi H, Niidome T, Kawano T, Yamada S, Niidome Y. Surface modification of gold nanorods using layer-by-layer technique for cellular uptake. *J Nanoparticle Res*. 2007;10(1):221-228. doi:10.1007/s11051-007-9227-5.
  332. Champion J a, Mitragotri S. Shape induced inhibition of phagocytosis of polymer particles. *Pharm Res*. 2009;26(1):244-249. doi:10.1007/s11095-008-9626-z.
  333. Chithrani DB, Dunne M, Stewart J, Allen C, Jaffray D a. Cellular uptake and transport of gold nanoparticles incorporated in a liposomal carrier. *Nanomedicine*. 2010;6(1):161-169. doi:10.1016/j.nano.2009.04.009.
  334. Fromen CA, Dunn SS, DeSimone JM. Biomedical Nanopreparations with Controlled Geometry. In: *Handbook of Nanobiomedical Research: Fundamentals, Applications and Recent Developments.*; 2014:349-398.
  335. Lee C-W, Lin E-H, Cheng J-Y, Wei P-K. Study of gold nanoparticles and live cells interactions by using planar evanescent wave excitation. *J Biomed Opt*. 2009;14(2):21005.
  336. Carmona-Ribeiro AM. Interactions between cationic liposomes and drugs or biomolecules. *An Acad Bras Cienc*. 2000;72(1):39-43. doi:10.1590/S0001-37652000000100005.
  337. Carmona-Ribeiro AM. Biomimetic Systems in Nanomedicine. In: Torchilin V, ed. *Handbook of Nanobiomedical Research: Fundamentals, Applications and Recent Developments.*; 2014:400-454.
  338. Stylianopoulos T, Poh M-Z, Insin N, et al. Diffusion of Particles in the Extracellular Matrix: The Effect of Repulsive Electrostatic Interactions. *Biophys J*. 2010;99(5):1342-1349. doi:10.1016/j.bpj.2010.06.016.
  339. Wang JW, Roden RBS. Virus-like particles for the prevention of human papillomavirus-associated malignancies. *Expert Rev Vaccines*. 2013;12(2):129-141. doi:10.1586/erv.12.151.
  340. Baltazar GC, Guha S, Lu W, et al. Acidic nanoparticles are trafficked to lysosomes and restore an acidic lysosomal pH and degradative function to compromised ARPE-19 cells. *PLoS One*. 2012;7(12):e49635. doi:10.1371/journal.pone.0049635.
  341. Bieber T, Meissner W, Kostin S, Niemann A, Elsasser HP. Intracellular route and transcriptional competence of polyethylenimine-DNA complexes. *J Control Release*. 2002;82:441-454. doi:10.1016/S0168-3659(02)00129-3.
  342. Hou S, Xiebacz N, Wiczorek SA, et al. Formation and structure of PEI/DNA complexes: quantitative analysis. *Soft Matter*. 2011;7:6967-6972. doi:10.1039/b000000x.
  343. Rodrigo Garzón M, Berraondo P, Crettaz J, et al. Induction of gp120-specific

- protective immune responses by genetic vaccination with linear polyethylenimine-plasmid complex. *Vaccine*. 2005;23(11):1384-1392. doi:10.1016/j.vaccine.2004.09.009.
344. Pyshnaya I a, Razum K V, Poletaeva JE, Pyshnyi D V, Zenkova M a, Ryabchikova EI. Comparison of behaviour in different liquids and in cells of gold nanorods and spherical nanoparticles modified by linear polyethyleneimine and bovine serum albumin. *Biomed Res Int*. 2014;2014:908175. doi:10.1155/2014/908175.
  345. Nel AE, Mädler L, Velegol D, et al. Understanding biophysicochemical interactions at the nano-bio interface. *Nat Mater*. 2009;8(7):543-557. doi:10.1038/nmat2442.
  346. Breunig M, Hozsa C, Lungwitz U, et al. Mechanistic investigation of poly(ethylene imine)-based siRNA delivery: Disulfide bonds boost intracellular release of the cargo. *J Control Release*. 2008;130:57-63. doi:10.1016/j.jconrel.2008.05.016.
  347. Zhou X, Yu T, Zhang Y, et al. Nanozeolite-assembled interface towards sensitive biosensing. *Electrochem commun*. 2007;9(7):1525-1529. doi:10.1016/j.elecom.2007.02.018.
  348. Pei RJ, Cui XQ, Yang XR, Wang EK. Assembly of alternating polycation and DNA multilayer films by electrostatic layer-by-layer adsorption. *Biomacromolecules*. 2001;2(2):463-468. doi:10.1021/bm0001289.
  349. Morais T, Soares ME, Duarte JA, et al. Effect of surface coating on the biodistribution profile of gold nanoparticles in the rat. *Eur J Pharm Biopharm*. 2012;80(1):185-193. doi:10.1016/j.ejpb.2011.09.005.
  350. Qiu Y, Liu Y, Wang L, et al. Surface chemistry and aspect ratio mediated cellular uptake of Au nanorods. *Biomaterials*. 2010;31(30):7606-7619. <http://www.ncbi.nlm.nih.gov/pubmed/20656344>.
  351. El Ouahabi a, Thiry M, Pector V, Fuks R, Ruyschaert JM, Vandenbranden M. The role of endosome destabilizing activity in the gene transfer process mediated by cationic lipids. *FEBS Lett*. 1997;414(2):187-192. doi:10.1016/S0014-5793(97)00973-3.
  352. Maurer B, Untener E, Hyssain S. *Bioeffects of Gold Nanorods as a Function of Aspect Ratio and Surface Chemistry 711th Human Performance Wing Human Effectiveness Directorate Bioeffects Division Molecular Bioeffects Branch.*; 2012. <http://www.dtic.mil/dtic/tr/fulltext/u2/a583577.pdf>.
  353. Panyam J, Zhou W-Z, Prabha S, Sahoo SK, Labhasetwar V. Rapid endo-lysosomal escape of poly(DL-lactide-co-glycolide) nanoparticles: implications for drug and gene delivery. *FASEB J*. 2002;16(10):1217-1226. doi:10.1096/fj.02-0088com.
  354. Shen H, Ackerman AL, Cody V, et al. Enhanced and prolonged cross-presentation following endosomal escape of exogenous antigens encapsulated in biodegradable nanoparticles. *Immunology*. 2006;117(1):78-88. doi:10.1111/j.1365-2567.2005.02268.x.
  355. Ogris M, Carlisle RC, Bettinger T, Seymour LW. Melittin Enables Efficient Vesicular Escape and Enhanced Nuclear Access of Nonviral Gene Delivery Vectors. *J Biol Chem*. 2001;276(50):47550-47555. doi:10.1074/jbc.M108331200.
  356. Helander IM, Latva-Kala K, Lounatmaa K. Permeabilizing action of polyethyleneimine on *Salmonella typhimurium* involves disruption of the outer membrane and interactions with lipopolysaccharide. *Microbiology*. 1998;144(2):385-390. doi:10.1099/00221287-144-2-385.

357. Elbakry A, Zaky A, Liebl R, Rachel R, Goepferich A, Breunig M. Layer-by-Layer Assembled Gold Nanoparticles for siRNA Delivery 2009. 2009.
358. Oh YK, Kim JP, Yoon H, Kim JM, Yang JS, Kim CK. Prolonged organ retention and safety of plasmid DNA administered in polyethylenimine complexes. *Gene Ther.* 2001;8:1587-1592.
359. Cho W-S, Cho M, Jeong J, et al. Acute toxicity and pharmacokinetics of 13 nm-sized PEG-coated gold nanoparticles. *Toxicol Appl Pharmacol.* 2009;236(1):16-24. doi:10.1016/j.taap.2008.12.023.
360. De Jong WH, Hagens WI, Krystek P, Burger MC, Sips AJ a M, Geertsma RE. Particle size-dependent organ distribution of gold nanoparticles after intravenous administration. *Biomaterials.* 2008;29(12):1912-1919. doi:10.1016/j.biomaterials.2007.12.037.
361. Semmler-Behnke M, Kreyling WG, Lipka J, et al. Biodistribution of 1.4- and 18-nm gold particles in rats. *Small.* 2008;4(12):2108-2111. doi:10.1002/smll.200800922.
362. Tkachenko AG, Xie H, Coleman D, et al. Multifunctional gold nanoparticle-peptide complexes for nuclear targeting. *J Am Chem Soc.* 2003;125(16):4700-4701. doi:10.1021/ja0296935.
363. Paciotti GF, Kingston D, Tamarkin L. Colloidal Gold Nanoparticles: A Novel Nanoparticle Platform for Developing Multifunctional Tumor-Targeted Drug Delivery Vectors. *DRUG Dev Res.* 2006;67(2 SUPPL.):47-54. doi:10.1002/ddr.
364. Visaria RK, Griffin RJ, Williams BW, et al. Enhancement of tumor thermal therapy using gold nanoparticle-assisted tumor necrosis factor-alpha delivery. *Mol Cancer Ther.* 2006;5:1014-1020. doi:10.1158/1535-7163.MCT-05-0381.
365. El-Sayed IH, Huang X, El-Sayed M a. Selective laser photo-thermal therapy of epithelial carcinoma using anti-EGFR antibody conjugated gold nanoparticles. *Cancer Lett.* 2006;239(1):129-135. doi:10.1016/j.canlet.2005.07.035.
366. Di Bonito P, Grasso F, Mochi S, et al. Anti-tumor CD8+ T cell immunity elicited by HIV-1-based virus-like particles incorporating HPV-16 E7 protein. *Virology.* 2009;395:45-55. doi:10.1016/j.virol.2009.09.012.
367. Jebali A, Kalantar SM, Hekmatimoghaddam S, Saffarzadeh N, Sheikha MH, Ghasemi N. Surface modification of tri-calcium phosphate nanoparticles by DOPE and/or anti-E6 antibody to enhance uptake of antisense of E6 mRNA. *Colloids Surfaces B Biointerfaces.* 2015;126:297-302. doi:10.1016/j.colsurfb.2014.12.040.
368. Buzea C, Pacheco II, Robbie K. Nanomaterials and nanoparticles: sources and toxicity. *Biointerphases.* 2007;2(4):MR17-71. <http://www.ncbi.nlm.nih.gov/pubmed/20419892>.
369. Connor EE, Mwamuka J, Gole A, Murphy CJ, Wyatt MD. Gold nanoparticles are taken up by human cells but do not cause acute cytotoxicity. *Small Weinheim an der Bergstrasse Ger.* 2005;1(3):325-327. <http://www.ncbi.nlm.nih.gov/pubmed/17193451>.
370. Yen H-J, Hsu S-H, Tsai C-L. Cytotoxicity and immunological response of gold and silver nanoparticles of different sizes. *Small.* 2009;5(13):1553-1561. doi:10.1002/smll.200900126.
371. Hwang JH, Kim SJ, Kim Y-H, et al. Susceptibility to gold nanoparticle-induced

- hepatotoxicity is enhanced in a mouse model of nonalcoholic steatohepatitis. *Toxicology*. 2012;294(1):27-35. doi:10.1016/j.tox.2012.01.013.
372. Nan A, Bai X, Son SJ, Lee SB, Ghandehari H. Cellular uptake and cytotoxicity of silica nanotubes. *Nano Lett*. 2008;8(8):2150-2154. <http://www.ncbi.nlm.nih.gov/pubmed/18624386>.
373. Pan Y, Leifert A, Ruau D, et al. Gold nanoparticles of diameter 1.4 nm trigger necrosis by oxidative stress and mitochondrial damage. *Small*. 2009;5(18):2067-2076. doi:10.1002/smll.200900466.
374. Kang B, Mackey MA, El-sayed MA. Nuclear Targeting of Gold Nanoparticles in Cancer Cells Induces DNA Damage , Causing Cytokinesis Arrest and Apoptosis. 2010:1517-1519.
375. Gu Y-J, Cheng J, Lin C-C, Lam YW, Cheng SH, Wong W-T. Nuclear penetration of surface functionalized gold nanoparticles. *Toxicol Appl Pharmacol*. 2009;237(2):196-204. doi:10.1016/j.taap.2009.03.009.
376. Nixon R a. Endosome function and dysfunction in Alzheimer's disease and other neurodegenerative diseases. *Neurobiol Aging*. 2005;26(3):373-382. doi:10.1016/j.neurobiolaging.2004.09.018.
377. Goodman CM, McCusker CD, Yilmaz T, Rotello VM. Toxicity of gold nanoparticles functionalized with cationic and anionic side chains. *Bioconjug Chem*. 2004;15(4):897-900. doi:10.1021/bc049951i.
378. Murphy CJ, Gole AM, Stone JW, et al. Gold nanoparticles in biology: beyond toxicity to cellular imaging. *Acc Chem Res*. 2008;41(12):1721-1730. <http://www.ncbi.nlm.nih.gov/pubmed/18712884>.
379. Johnson CJ, Dujardin E, Davis SA, Murphy CJ, Mann S. Growth and form of gold nanorods prepared by seed-mediated, surfactant-directed synthesis. *J Mater Chem*. 2002;12(6):1765-1770. doi:10.1039/b200953f.
380. Jana NR, Gearheart L, Murphy CJ. Wet-Chemical Synthesis of High Aspect Ratio Cylindrical Gold Nanorods. *J Phys Chem B*. 2001;105:4065-4067. doi:10.
381. Wang S, Lu W, Tovmachenko O, Rai US, Yu H, Ray PC. Challenge in understanding size and shape dependent toxicity of gold nanomaterials in human skin keratinocytes. *Chem Phys Lett*. 2008;463(1-3):145-149. doi:10.1016/j.cplett.2008.08.039.
382. Alkilany AM, Nagaria PK, Hexel CR, Shaw TJ, Murphy CJ, Wyatt MD. Cellular uptake and cytotoxicity of gold nanorods: molecular origin of cytotoxicity and surface effects. *Small*. 2009;5(6):701-708. doi:10.1002/smll.200801546.
383. Boca SC, Astilean S. Detoxification of gold nanorods by conjugation with thiolated poly(ethylene glycol) and their assessment as SERS-active carriers of Raman tags. *Nanotechnology*. 2010;21(23):235601. <http://www.ncbi.nlm.nih.gov/pubmed/20463383>.
384. Grabinski C, Schaeublin N, Wijaya A, et al. Effect of Gold Nanorod Surface Chemistry on Cellular Response. *ACS Nano*. 2010. 10.1021/nn103476x.
385. Brunot C, Ponsonnet L, Lagneau C, Farge P, Picart C, Grosogeat B. Cytotoxicity of polyethyleneimine (PEI), precursor base layer of polyelectrolyte multilayer films. *Biomaterials*. 2007;28(4):632-640. doi:10.1016/j.biomaterials.2006.09.026.



386. Liu C, Zhu Q, Wu W, et al. Degradable copolymer based on amphiphilic N-octyl-N-quaternary chitosan and low-molecular weight polyethylenimine for gene delivery. *Int J Nanomedicine*. 2012;7:5339-5350. doi:10.2147/IJN.S36179.
387. Takemoto H, Nishiyama N. Design of functional polymers for intracellular nucleic acids delivery. In: Prokop A, Iwasaki Y, Harada A, eds. *Intracellular Delivery II: Fundamentals and Applications*. Springer; 2014:208-217.
388. Godbey WT, Wu KK, Hirasaki GJ, Mikos G. Improved packing of poly(ethylenimine)/DNA complexes increases transfection efficiency. *Gene Ther*. 1999;6(8):1380-1388. doi:10.1038/sj.gt.3300976.
389. Alkilany AM, Murphy CJ. Toxicity and cellular uptake of gold nanoparticles: what we have learned so far? *J Nanopart Res*. 2010;12(7):2313-2333. doi:10.1007/s11051-010-9911-8.
390. Rao DD, Vorhies JS, Senzer N, Nemunaitis J. siRNA vs. shRNA: similarities and differences. *Adv Drug Deliv Rev*. 2009;61(9):746-759. doi:10.1016/j.addr.2009.04.004.
391. Frier M. Derivatives of 4-Amino-Quinaldinium and 8-Hydroxyquinolone. In: *Inhibition and Destruction of the Microbial Cell*. London, UK: Academic Press, Ltd; 1971:107-120.
392. Merianos JJ. Quaternary Ammonium Antimicrobial Compounds. In: *Disinfection, Sterilization, and Preservation*. 4th ed. Philadelphia, PA, USA: Lea & Febiger; 1991:225-255.
393. Fu Y, Kao WJ. Drug release kinetics and transport mechanisms of non-degradable and degradable polymeric delivery systems. *Expert Opin Drug Deliv*. 2010;7(4):429-444. doi:10.1517/17425241003602259.
394. van der Zee M, Stoutjesdijk JH, van der Heijden P a a W, de Wit D. Structure-biodegradation relationships of polymeric materials. 1. Effect of degree of oxidation on biodegradability of carbohydrate polymers. *J Environ Polym Degrad*. 1995;3(4):235-242. doi:10.1007/BF02068678.
395. Fritz HG, SEIDENSTÜCKER T, BÖLZ U, Juza M, Schroeter J, Enders HJ. *Study on Production of Thermoplastics and Fibers Based Mainly on Biological Materials*. Agro Ind Research Division; 1994.
396. Siepmann J, Siepmann F. Mathematical modeling of drug delivery. *Int J Pharm*. 2008;364(2):328-343. doi:10.1016/j.ijpharm.2008.09.004.
397. Demeneix B, Behr JP. Polyethylenimine (PEI). *Adv Genet*. 2005;53:215-230.
398. Jäger M, Schubert S, Ochrimenko S, Fischer D, Schubert US. Branched and linear poly(ethylene imine)-based conjugates: synthetic modification, characterization, and application. *Chem Soc Rev*. 2012;41(13):4755-4767.
399. Suh J, Paik H-J, Hwang BK. Ionization of Poly(ethylenimine) and Poly(allylamine) at Various pH's. *Bioorg Chem*. 1994;22:318-327. doi:10.1006/bioo.1994.1025.
400. Oishi M, Nagatsugi F, Sasaki S, Nagasaki Y, Kataoka K. Smart polyion complex micelles for targeted intracellular delivery of PEGylated antisense oligonucleotides containing acid-labile linkages. *ChemBioChem*. 2005;6:718-725. doi:10.1002/cbic.200400334.
401. Peng Q, Zhong Z, Zhuo R. Disulfide cross-linked polyethylenimines (PEI) prepared via

- thiolation of low molecular weight PEI as highly efficient gene vectors. *Bioconjug Chem.* 2008;19(2):499-506. doi:10.1021/bc7003236.
402. Diogo MM, Ribeiro SC, Queiroz JA, et al. Production, purification and analysis of an experimental DNA vaccine against rabies. *J Gene Med.* 2001;3(6):577-584.
403. Mahmoud RY, Stones DH, Li W, et al. The Multivalent Adhesion Molecule SSO1327 plays a key role in *Shigella sonnei* pathogenesis. *Mol Microbiol.* 2015:n/a-n/a. doi:10.1111/mmi.13255.
404. Tummers B, Goedemans R, Jha V, et al. CD40-Mediated Amplification of Local Immunity by Epithelial Cells is Impaired by HPV. *J Invest Dermatol.* 2014;134(January):1-36. doi:10.1038/jid.2014.262.
405. Davy C. Papillomavirus Research: from Natural History to Vaccines and Beyond. *Future Virol.* 2006;1(4):423-424.
406. Buck CB, Cheng N, Thompson CD, et al. Arrangement of L2 within the papillomavirus capsid. *J Virol.* 2008;82(11):5190-5197. doi:10.1128/JVI.02726-07.
407. Hagensee M, Yaegashi N, Galloway DA. Self-Assembly of Human Papillomavirus Type 1 Capsids by of the L1 and L2 Capsid Proteins. *Journay Virol.* 1993;67(1):315-322.
408. Baker TS, Newcomb WW, Olson NH, Cowser LM, Olson C, Brown JC. Structures of bovine and human papillomaviruses. Analysis by cryoelectron microscopy and three-dimensional image reconstruction. *Biophys J.* 1991;60(6):1445-1456. doi:10.1016/S0006-3495(91)82181-6.
409. Wang Z, Christensen N, Schiller JT, Dillner J. A monoclonal antibody against intact human papillomavirus type 16 capsids blocks the serological reactivity of most human sera. *J Gen Virol.* 1997;78 ( Pt 9):2209-2215. <http://www.ncbi.nlm.nih.gov/pubmed/9292008>.
410. Christensen ND, Kreider JW, Cladel NM, Patrick SD, Welsh P a. Monoclonal antibody-mediated neutralization of infectious human papillomavirus type 11. *J Virol.* 1990;64(11):5678-5681. <http://www.pubmedcentral.nih.gov/articlerender.fcgi?artid=248629&tool=pmcentrez&rendertype=abstract>.
411. Chen XS, Garcea RL, Goldberg I, Casini G, Harrison SC. Structure of small virus-like particles assembled from the L1 protein of human papillomavirus 16. *Mol Cell.* 2000;5(3):557-567. doi:10.1016/S1097-2765(00)80449-9.
412. Fleury MJJ, Touzé a, Alvarez E, et al. Identification of type-specific and cross-reactive neutralizing conformational epitopes on the major capsid protein of human papillomavirus type 31. *Arch Virol.* 2006;151(8):1511-1523. doi:10.1007/s00705-006-0734-y.
413. Christensen ND, Reed C a, Cladel NM, Hall K, Leiserowitz GS. Monoclonal antibodies to HPV-6 L1 virus-like particles identify conformational and linear neutralizing epitopes on HPV-11 in addition to type-specific epitopes on HPV-6. *Virology.* 1996;224(2):477-486. doi:10.1006/viro.1996.0554.
414. Schädlich L, Senger T, Gerlach B, et al. Analysis of modified human papillomavirus type 16 L1 capsomeres: the ability to assemble into larger particles correlates with higher immunogenicity. *J Virol.* 2009;83(15):7690-7705. doi:10.1128/JVI.02588-08.
415. Fernández-San Millán A, Ortigosa SM, Hervás-Stubbs S, et al. Human papillomavirus

- L1 protein expressed in tobacco chloroplasts self-assembles into virus-like particles that are highly immunogenic. *Plant Biotechnol J*. 2008;6(5):427-441. doi:10.1111/j.1467-7652.2008.00338.x.
416. WHO. Human papillomavirus and HPV vaccines: technical information for policy-makers and health professionals. *WHO*. 2007.
  417. Kirnbauer R, Booy F, Cheng N, Lowy DR, Schiller JT. Papillomavirus L1 major capsid protein self-assembles into virus-like particles that are highly immunogenic. *Proc Natl Acad Sci U S A*. 1992;89(24):12180-12184. doi:10.1073/pnas.89.24.12180.
  418. Roden RB, Kirnbauer R, Jensen a B, Lowy DR, Schiller JT. Interaction of papillomaviruses with the cell surface. *J Virol*. 1994;68(11):7260-7266.
  419. Roden R, Yutzy W, Fallon R, Inglis S, Lowy D, Schiller J. Minor capsid protein of human genital papillomaviruses contains subdominant, cross-neutralizing epitopes. *Virology*. 2000;270(2):254-257. doi:10.1006/viro.2000.0272.
  420. Faust H, Dillner J. Mutations in human papillomavirus type 16 L1 hypervariable surface-exposed loops affect L2 binding and DNA encapsidation. *J Gen Virol*. 2013;94(Pt 8):1841-1849. doi:10.1099/vir.0.054205-0.
  421. Thönes N, Herreiner A, Schädlich L, Piuko K, Müller M. A direct comparison of human papillomavirus type 16 L1 particles reveals a lower immunogenicity of capsomeres than viruslike particles with respect to the induced antibody response. *J Virol*. 2008;82(11):5472-5485. doi:10.1128/JVI.02482-07.
  422. Villa LL, Denny L. Methods for detection of HPV infection and its clinical utility. *Int J Gynecol Obstet*. 2006;94:71-80. doi:10.1016/S0020-7292(07)60013-7.
  423. Buonaguro L, Tornesello ML, Gallo RC, Marincola FM, Lewis GK, Buonaguro FM. Th2 polarization in peripheral blood mononuclear cells from human immunodeficiency virus (HIV)-infected subjects, as activated by HIV virus-like particles. *J Virol*. 2009;83(1):304-313. doi:10.1128/JVI.01606-08.
  424. Yang R, Murillo FM, Delannoy MJ, et al. B lymphocyte activation by human papillomavirus-like particles directly induces Ig class switch recombination via TLR4-MyD88. *J Immunol*. 2005;174(12):7912-7919. <http://www.ncbi.nlm.nih.gov/pubmed/15944297>.
  425. Woo MK, Hur SJ, Park S, Kim HJ. Study of cell-mediated response in mice by HPV16 L1 virus-like particles expressed in *Saccharomyces cerevisiae*. *J Microbiol Biotechnol*. 2007;17(10):1738-1741. doi:7038 [pii].
  426. Palker TJ, Monteiro JM, Martin MM, et al. Antibody, cytokine and cytotoxic T lymphocyte responses in chimpanzees immunized with human papillomavirus virus-like particles. *Vaccine*. 2001;19(27):3733-3743. doi:10.1016/S0264-410X(01)00093-7.
  427. Kushnir N, Streatfield SJ, Yusibov V. Virus-like particles as a highly efficient vaccine platform: Diversity of targets and production systems and advances in clinical development. *Vaccine*. 2012;31(1):58-83. doi:10.1016/j.vaccine.2012.10.083.
  428. Guillén G, Aguilar JC, Dueñas S, et al. Virus-Like Particles as vaccine antigens and adjuvants: Application to chronic disease, cancer immunotherapy and infectious disease preventive strategies. *Procedia Vaccinol*. 2010;2(2):128-133. doi:10.1016/j.provac.2010.07.004.
  429. Zheng J, Ma J, Yang X-F, et al. Highly efficient and economical baculovirus expression

- system for preparing human papillomavirus type16 virus-like particle. *Acta Biochim Biophys Sin (Shanghai)*. 2004;36(8):548-552.  
<http://www.ncbi.nlm.nih.gov/pubmed/15295647>.
430. Kirnbauer R, Taub J, Greenstone H, et al. Efficient self-assembly of human papillomavirus type 16 L1 and L1-L2 into virus-like particles. *J Virol*. 1993;67(12):6929-6936.  
<http://www.pubmedcentral.nih.gov/articlerender.fcgi?artid=238150&tool=pmcentrez&rendertype=abstract>.
  431. Schwarz TF, Leo O. Immune response to human papillomavirus after prophylactic vaccination with AS04-adjuvanted HPV-16/18 vaccine: Improving upon nature. *Gynecol Oncol*. 2008;110(3 SUPPL.1):1-10. doi:10.1016/j.ygyno.2008.05.036.
  432. Zhang W, Carmichael J, Ferguson J, Inglis S, Ashrafian H, Stanley M. Expression of human papillomavirus type 16 L1 protein in Escherichia coli: Denaturation, renaturation, and self-assembly of virus-like particles in vitro. *Virology*. 1998;243(2):423-431. doi:DOI 10.1006/viro.1998.9050.
  433. Pastrana D V., Buck CB, Pang YYS, et al. Reactivity of human sera in a sensitive, high-throughput pseudovirus-based papillomavirus neutralization assay for HPV16 and HPV18. *Virology*. 2004;321(2):205-216. doi:10.1016/j.virol.2003.12.027.
  434. Ali SH, DeCaprio J a. Cellular transformation by SV40 large T antigen: interaction with host proteins. *Semin Cancer Biol*. 2001;11(1):15-23. doi:10.1006/scbi.2000.0342.
  435. Dessy FJ, Giannini SL, Bougelet C a, et al. Correlation between direct ELISA, single epitope-based inhibition ELISA and pseudovirion-based neutralization assay for measuring anti-HPV-16 and anti-HPV-18 antibody response after vaccination with the AS04-adjuvanted HPV-16/18 cervical cancer vaccine. *Hum Vaccin*. 2008;4(6):425-434. doi:10.4161/hv.4.6.6912.
  436. Takamura S, Niikura M, Li T-C, et al. DNA vaccine-encapsulated virus-like particles derived from an orally transmissible virus stimulate mucosal and systemic immune responses by oral administration. *Gene Ther*. 2004;11(7):628-635.  
doi:10.1038/sj.gt.3302193.
  437. Noriega FR, Losonsky G, Wang JY, Formal SB, Levine MM. Further characterization of delta aroA delta virG Shigella flexneri 2a strain CVD 1203 as a mucosal shigella vaccine and as a live-vector vaccine for delivering antigens of enterotoxigenic escherichia coli. *Infect Immun*. 1996;64(1):23-27.
  438. Hodge LM, Marinaro M, Jones HP, McGhee JR, Kiyono H, Simecka JW. Immunoglobulin A (IgA) responses and IgE-associated inflammation along the respiratory tract after mucosal but not systemic immunization. *Infect Immun*. 2001;69(4):2328-2338. doi:10.1128/IAI.69.4.2328.
  439. Mutsch M, Zhou W, Rhodes P, et al. Use of the inactivated intranasal influenza vaccine and the risk of Bell's palsy in Switzerland. *N Engl J Med*. 2004;350(9):896-903. doi:10.1056/NEJMoa030595.
  440. Holmgren JAN, Johansson E, Wasse L, Jertborn M, Rudin A. Nasal and Vaginal Vaccinations Have Differential Effects on Antibody Responses in Vaginal and Cervical Secretions in Humans. 2001;69(12):7481-7486. doi:10.1128/IAI.69.12.7481.
  441. Mestecky J, Fultz PN. Mucosal immune system of the human genital tract. *J Infect Dis*. 1999;179 Suppl(Suppl 3):S470-4. doi:10.1086/314806.

442. Thapar MA, Parr EL, Bozzola JJ, Parr MB. Secretory immune responses in the mouse vagina after parenteral or intravaginal immunization with an immunostimulating complex (ISCOM). *Vaccine*. 1991;9(2):129-133.
443. Le Cann P, Coursaget P, lochmann S, Touze A. Self-assembly of human papillomavirus type 16 capsids by expression of the L1 protein in insect cells. *FEMS Microbiol Lett*. 1994;117(3):269-274. doi:10.1016/0378-1097(94)90570-3.
444. Vidyasagar P, Sridevi VN, Rajan S, et al. Generation and characterization of neutralizing monoclonal antibodies against baculo-expressed HPV 16 VLPs. *Eur J Microbiol Immunol (Bp)*. 2014;4:56-64. doi:10.1556/EuJMI.4.2014.1.5.
445. McLean CS, Churcher MJ, Meinke J, et al. Production and characterisation of a monoclonal antibody to human papillomavirus type 16 using recombinant vaccinia virus. *J Clin Pathol*. 1990;43(6):488-492.  
<http://www.pubmedcentral.nih.gov/articlerender.fcgi?artid=502503&tool=pmcentrez&rendertype=abstract>.
446. Czerkinsky CC, Nilsson L-Å, Nygren H, Ouchterlony Ö, Tarkowski A. A solid-phase enzyme-linked immunospot (ELISPOT) assay for enumeration of specific antibody-secreting cells. *J Immunol Methods*. 1983;65(1-2):109-121. doi:10.1016/0022-1759(83)90308-3.
447. Pastrana D V., Buck CB, Lowy DR, Schiller JT. *Papillomavirus Neutralization Assay*. Bethesda, MD <http://home.ccr.cancer.gov/Lco/neutralizationassay.htm>.
448. Merck Millipore. Elispot assays : state-of-the-art tools for functional analysis of cellular immunology. *Merck Millipore - White Pap*. 2012.